NASA TECHNICAL NOTE

NASA TN D-5770

c. 1

NASA TN D-5770

WIND-TUNNEL INVESTIGATION OF A VTOL JET-TRANSPORT MODEL WITH POWERED LIFT ENGINES IN PODS AT WING MIDSPAN OR INBOARD

by Raymond D. Vogler

Langley Research Center
Langley Station, Hampton, Va.

NATIONAL AERONAUTICS AND SPACE ADMINISTRATION • WASHINGTON, D. C. • APRIL 1970

1. Report No. NASA TN D-5770	2. Government Accession No.	3. Recipient's Catalog No.
4. Title and Subtitle WIND-TUNNEL INVESTIGATION OF A VTOL JET-TRANSPORT MODEL WITH POWERED LIFT ENGINES IN PODS AT WING MIDSPAN OR INBOARD		5. Report Date April 1970 6. Performing Organization Code
7. Author(s) Raymond D. Vogler		8. Performing Organization Report No. L-6962
9. Performing Organization Name and Address NASA Langley Research Center Hampton, Va. 23365		10. Work Unit No. 721-01-11-05-23 11. Contract or Grant No.
12. Sponsoring Agency Name and Address National Aeronautics and Space Administration Washington, D.C. 20546		13. Type of Report and Period Covered Technical Note 14. Sponsoring Agency Code

15. Supplementary Notes

16. Abstract

Four ejectors mounted in each pod under each wing and powered with compressed air were used to simulate vertical-lift, fan-type jet engines. Data were obtained through an angle-of-attack range to show the effects of engine-pod location, ground-plane movement, flaps, tail size and location, and 10^{o} of sideslip on the aerodynamic characteristics of the model, and the effects of configuration changes on the jet and free-stream interference increments.

17. Key Words (Suggested by Author(s)) VTOL model Ejector lift engines Interference effects Ground effects Moving ground plane	18. Distribution Statement Unclassified – Unlimited

19. Security Classif. (of this report) Unclassified	20. Security Classif. (of this page) Unclassified	21. No. of Pages 151	22. Price* $3.00

*For sale by the Clearinghouse for Federal Scientific and Technical Information
Springfield, Virginia 22151

WIND-TUNNEL INVESTIGATION OF A VTOL JET-TRANSPORT MODEL WITH POWERED LIFT ENGINES IN PODS AT WING MIDSPAN OR INBOARD

By Raymond D. Vogler
Langley Research Center

SUMMARY

A wind-tunnel investigation was made to determine the aerodynamic characteristics of a VTOL jet-transport model with lift engines mounted under the wings in pods located either at midspan or adjacent to the fuselage (inboard). Cruise engines were not on the model. Eight lift engines were simulated by ejectors powered with compressed air. The scope of the investigation included the determination of the effects of engine-pod location, ground-plane movement, flaps, tail size and location, and sideslip on the aerodynamic characteristics, and the effects of configuration changes on the jet and free-stream interference increments.

Comparison of engine-pod locations shows that the inboard location gives lower minimum drag in the cruise condition and higher lift coefficients with flaps and power before inboard wing stall occurs. The midspan location gives more stability, less downwash at the tail, and smaller undesirable interference increments. For the model with power on and pods at midspan, the ground generally produces increments of negative pitch, negative drag, positive lift, and large upwash angles. Results over still ground and moving ground show little difference except with power at the higher free-stream velocities and with the model nearest the ground plane. For such conditions, the model over the moving ground plane has more lift and more negative pitching moments than the model over the still ground plane. Lateral forces and moments produced by sideslip are generally in the desired direction, and the vertical tail is much more effective when the engine pods are inboard than when they are at the wing midspan.

INTRODUCTION

Considerable research is being done toward the development of jet-powered airplanes capable of vertical or short take-off and landing (V/STOL). Such airplanes at very low speeds get negligible lift from the wings and must be supported by direct lift from the jets. This lift may be obtained by deflecting the jet efflux of cruise engines with vanes or flaps (refs. 1 and 2) or by using lift engines set vertically in the wing or

fuselage (ref. 3). In wind-tunnel testing of small-scale models, the engines are often simulated with nozzles and compressed air. Previous investigations (refs. 4, 5, and 6) of jet models have shown that lift losses occur when the model is hovering near the ground and that jet-induced lift losses and nose-up pitching moments occur at transition speeds. These jet-induced lift losses and moment changes result from interference effects between the jet, free stream, and model and are in addition to the ground effects when the model is near the ground. The magnitude of these ground and interference effects varies with such factors as the thrust of the jet, the locations and geometric arrangement of the jets, and the surface area adjacent to the jet exit, especially the area behind the jet.

The effects mentioned so far are associated primarily with the jet exit, but in full-scale airplanes the jet inlet conditions not only have an effect on engine operation, but the inlet air momentum may account for sizable effects on the forces and moments of the airplane. Reference 7 indicates that the ejectors used in this investigation may simulate turbojet or fan-type jet engines based on the ratio of jet thrust to mass rate of inlet flow. The two ratios of jet thrust to mass rate of inlet flow used in this investigation were 150 and 340 $\frac{N}{kg/sec}$. Reference 7 indicates that a ratio of 340 $\frac{N}{kg/sec}$ is sufficient to represent some fan-type jet engines. Simulation of turbojet engines requiring larger ratios was prevented by the limited capacity of the air lines operating the ejector engines.

The purposes of this investigation were to determine aerodynamic characteristics of the model in and out of ground effect, flap effectiveness, horizontal-tail effectiveness, downwash angles at the tail, and interference effects. The results were obtained with the four-engine pods on each wing at the midspan or the inboard location. In addition, longitudinal aerodynamic characteristics were obtained for the model with the pods at midspan and in ground effect over a still and a moving ground plane. The effects of 10° of sideslip were also obtained out of ground effect and with the engine pods at both locations.

SYMBOLS

The force and moment data are presented about the stability axes with the origin at the moment center shown in figure 1. The units of measure used in this report are given in the International System of Units (SI). (See ref. 8.) The power-off data are given in conventional aerodynamic force and moment coefficients based on free-stream dynamic pressure. In order to avoid unusually large coefficients, the power-on data have been nondimensionalized by the thrust or the product of the thrust and an appropriate length $\left(\text{for examples, } L/T \text{ and } M_Y/T\bar{c}\right)$.

A jet exit area (0.01621467 m^2 total for eight engines)

b	wing span, centimeters
C_D	drag coefficient, $\frac{D}{qS}$
C_L	lift coefficient, $\frac{L}{qS}$
C_m	pitching-moment coefficient, $\frac{M_Y}{qS\bar{c}}$
C_T	engine thrust coefficient, $\frac{T}{qS}$
c	wing local chord, centimeters
$\bar{c}$	wing mean aerodynamic chord, centimeters
D	drag, newtons
F_Y	side force, newtons
h	height from ground plane to lower surface of fuselage at $\alpha = 0^o$, centimeters
i_t	incidence of horizontal tail with respect to wing chord plane, degrees
L	lift, newtons
M_X	rolling moment, centimeter-newtons
M_Y	pitching moment, centimeter-newtons
$(M_Y)_T$	static pitching moment for given jet thrust, centimeter-newtons
M_Z	yawing moment, centimeter-newtons
$\Delta L, \Delta D, \Delta F_Y$	increment of lift, drag, and side force, newtons
$\Delta M_X, \Delta M_Y, \Delta M_Z$	increment of rolling moment, pitching moment, and yawing moment, centimeter-newtons

q	free-stream dynamic pressure, newtons/meter^2
q_j	jet-exit dynamic pressure, newtons/meter^2
$\sqrt{\frac{q}{q_j}}$	effective velocity ratio
S	wing area, meters^2
T	engine jet thrust, newtons
α	wing or fuselage angle of attack, degrees
β	angle of sideslip, degrees
δ_j	jet deflection angle, degrees

MODEL AND APPARATUS

A three-view drawing of the general research model of a VTOL transport is shown in figure 1. Additional geometry of the model is presented in table I, and photographs of the model mounted on the tunnel sting are presented in figure 2. The model was made of aluminum, wood, and fiber glass. Provision was made for locating either the large or the small horizontal tail surfaces at three positions vertically, as indicated in figure 1.

The lift-engine pods were located either next to the fuselage or at the midspan of the wing. Cruise engines were not on the model for this investigation. When the pods were located at midspan, the untapered flap extended from the fuselage to the inboard side of the engine pod. When the pods were inboard, the same flap abutted the outboard side of the engine pod. (See fig. 1.) Each flap had a span of 0.366 b/2, and the inboard ends were located at 0.125 b/2 for the midspan pods and at 0.225 b/2 for the inboard pods. When the flaps were on the model, the deflection was 60°. Each engine pod housed four ejector nozzles with 5.08-cm-diameter exits. The ejectors used compressed air for operation. Details of the ejector units and some of their characteristics are discussed in reference 7. High-pressure air was brought to a plenum in the fuselage through a tube inside the sting mount. From the plenum, the air was carried to each pair of ejectors through a smaller tube. Each of the four smaller tubes had a throttle to help equalize the flow between pairs. Flow in each pair was adjusted by inserting orifice plates between the tubes and ejectors at the point of attachment. Near each ejector exit there were several total-pressure tubes and one static-pressure tube for determining dynamic pressure in the exit.

The model was attached to a six-component strain-gage balance on the end of the mounting sting over a movable ground plane in the 5.18-meter test section of the Langley 300-mph 7- by 10-foot tunnel. The moving ground plane was a fabric belt between two rollers driven by an electric motor. Details of the ground belt showing a typical model installation are given in reference 9. The purpose of the moving belt is to prevent boundary-layer buildup on the ground plane.

TEST CONDITIONS AND ACCURACY

Tests were made through a range of low speeds representing the transition flight regime of the model with the engine pods located at either the inboard position or the midspan position of the wing. In addition, in-ground-effect tests were made in hovering and at transition speeds with the engine pods located at only the midspan of the wing. In transition, the angle of attack, measured with an electronic angle-of-attack meter, was -4° to 24° unless restricted by the ground plane. Except for a few tests made for comparison of data obtained over a still and a moving ground plane, all tests at forward speed with the model in ground effect were made with the ground-plane velocity approximately equal to free-stream velocity. Some tests were made through an angle-of-attack range with the model in 10° of sideslip to determine the effect of various model components on the lateral aerodynamic characteristics.

Thrust settings of 245 and 690 newtons and free-stream dynamic pressures of 93 and 474 N/m^2 were combined to give a range of tunnel-to-jet dynamic-pressure ratios, or effective velocity or momentum ratios $\left(\sqrt{q/q_j} \approx \text{Free-stream velocity/Jet velocity}\right)$. The effective velocity ratio has been found (ref. 3) to be a primary correlating factor to aid in the analysis of the interference effects of the jet efflux on the aerodynamic characteristics of the airplane during transition flight. The relationship between effective velocity ratio $\sqrt{q/q_j}$ and thrust coefficient C_T for this investigation is given in figure 3.

Each engine had static- and total-pressure orifices inside the jet exit. A static calibration of balance-measured thrust against dynamic pressure in the jet exit was made for each engine before installing it in the model. The installed model thrust for each data point during testing was the sum of the individual engine thrusts, based on the static calibration, and the measured dynamic pressure in each engine exit. The average jet-exit dynamic pressure used for determining effective velocity ratio $\sqrt{q/q_j}$ was obtained from the total thrust and total exit area $\left(q_j = T/2A\right)$.

When an air line is attached to the model, movement of the model is restrained by the air line and the balance beams. If the air line is firmly anchored to the sting, the restraints it produces are small and repeatable and are included in the balance

calibration. Temperature changes in the sting and air lines may cause zero shifts in balance readings unless the temperature stabilizes before data are recorded. In order to reduce the air-line restraint in the drag direction, the air line was coiled around the rear of the sting. Pressure in the coil expanded the coil and produced a negative drag force. Consequently, the power-on drag-thrust ratios D/T of the basic data as presented are estimated to be about 0.03 to 0.04 too low. Although the drag measurements are not sufficiently accurate for precise performance calculations because of the errors that may be present in the drag levels, the changes in drag with primary variables are valid and provide adequate insight into their effects. In the computations of the interference increments, the drag-thrust ratios were corrected for coil pressure.

RESULTS AND DISCUSSION

Presentation of Results

The basic data figures (figs. 4 to 39) are presented in tables II and III. Figures 40 to 44, presented in table IV, give a summary of some of the results from the basic data. Out-of-ground-effect data were obtained with the model near the center line of the tunnel, or 1.3 wing spans above the ground plane. In-ground-effect data were obtained with the model height ranging from 0.10 to 0.40 wing spans. Flap deflection is 60^{o} when the flaps are on the model.

Model Characteristics Out of Ground Effect

Longitudinal, power off.- The power-off longitudinal aerodynamic characteristics of the model with the large horizontal tail and without flaps are shown in figure 4 for the engine pods at the inboard location and in figure 15 for the engine pods at the midspan location. A comparison of these figures indicates that the model with the engine pods inboard shows a little higher maximum lift and lower minimum drag than the model with the engine pods at midspan. Both configurations show good stability for the three vertical tail positions, but the mid position gives a little lower level of stability than the high or low position because the tail in the mid position is more directly behind the pods and fuselage at positive model angles of attack. With flaps on (figs. 5 and 16), pitching moments are more sensitive to tail position when the engine pods are located at midspan than at the inboard position, and drag differences owing to pod locations are less than with flaps off. (Compare figs. 4 and 15 with figs. 5 and 16.)

Additional results for the two pod locations and with the flaps on are presented in figures 6 and 17, and the tail-off curves indicate large negative pitching moments resulting from addition of the flaps and the rather forward model moment-center location. Addition of the tail at zero incidence shows lift reductions and positive moments, which

would indicate a rather large downwash angle at the low tail position. Partial wing stall and increased stability occur at an angle of attack of about 8° with the pods at midspan (fig. 17) and at a higher angle of attack (10°) with the pods at the inboard location (fig. 6). Partial stall in the region of the flaps would result in reduced downwash and increased stability, as indicated.

Longitudinal, power on.- The longitudinal characteristics of the model with power on and flaps off are given in figures 7 and 18 for the engine pods at the inboard and midspan locations, respectively, for a range of effective velocity ratios. The corresponding data for the model with flaps on are given in figures 8 and 19. The power-on data are presented as force and moment ratios, which are equivalent to conventional aerodynamic force and moment coefficients divided by the thrust coefficient $\left(\text{e.g., } \frac{L}{T} = \frac{C_L}{C_T}\right)$. At low velocity ratios, the power effects predominate the data; but, as the velocity ratios increase, the aerodynamic effects increase, and the force and moment ratios become more comparable with power-off data or conventional coefficients.

With power on and flaps on (figs. 8 and 9), the model generally has poor stability except at the higher effective velocity ratios with the pods at the inboard location as was the case with flaps off (fig. 7). With the engine pods at the midspan location, the model is stable with the flaps off (fig. 18) or on (figs. 19 and 20) for all tail positions through the effective-velocity-ratio range except at the lowest velocity ratio, where neutral stability is indicated.

The power-on drag of the model with flaps on is lower at small angles of attack for the model with engine pods at the midspan location (fig. 19) than for the model with pods at the inboard location (fig. 8). The pod locations show little difference in drag for the power-on, flaps-off condition. (See figs. 7 and 18.)

Sharp breaks occur early ($\alpha = 8^{\circ}$ to 14°) in the lift curves at the higher velocity ratios with flaps and power on for either engine-pod location. (See figs. 8, 9, 19, and 20.) Breaks also occur with pods at either location for flaps on and power off (figs. 5, 6, 16, and 17), but no early breaks occur with the flaps off (figs. 4, 7, and 15). Evidently the flap or that part of the wing ahead of the flap partially stalls as a result of flow disturbance on top of the wing from vortices from the engine pods as the angle of attack is increased. Power delays the stall 2° when the pods are at the inboard location (figs. 5, 8, and 9) but has no effect when the pods are at midspan (figs. 16 and 19). The stall break occurs at an angle of attack of approximately 8° when the engine pods are at the midspan location and at angles 2° to 4° higher when the pods are at the inboard location.

Downwash angles.- Data for several horizontal-tail deflections through an effective-velocity-ratio range are given in figures 10 and 21 for inboard and midspan

locations, respectively. The tail at an incidence of -15° is apparently stalled at low model angles of attack. At low velocity ratios, the downwash values as determined by the pitching moments are more subject to error because of the small moments and flatness of the curves; but, at velocity ratios of 0.15 (high jet velocity) and 0.25 (low jet velocity), downwash angles as high as 28° (fig. 10(c)) and 17° (fig. 10(d)), respectively, are indicated for the inboard pod location. For the midspan pod location, the downwash angles are about 12° for corresponding conditions. (See figs. 21(c) and 21(d).)

Lateral, power on.- The lateral aerodynamic characteristics of the model at 0° and 10° of sideslip are given in figures 11 to 14 for the engine pods at the inboard location and in figures 22 to 25 for the engine pods at the midspan location. In addition to the effects of engine-pod location, the effects of flaps and vertical tail are shown by the data. The positive shift in the rolling-moment level for the model with pods at midspan compared with the result with pods inboard is due to more asymmetrical pod thrust in the former case, which accounts for part (0.08 to 0.10) of the positive rolling moment of the model with pods at the midspan position. This thrust difference between pods would have little or no effect on the incremental results produced by 10° of sideslip. These increments are discussed in a subsequent section.

Model Characteristics in Ground Effect

Only longitudinal data were obtained in ground effect for the model with the small horizontal tail and with the engine pods at the midspan location.

Power off.- The aerodynamic characteristics of the model without flaps and with power off (fig. 26(b)) are very similar to the out-of-ground-effect characteristics (fig. 15) except for the effects resulting from the difference in horizontal-tail area. At a horizontal-tail incidence of 15°, tail stall at lower angles of attack noted for the flaps-off condition (fig. 26(c)) is prevented in the flaps-on condition (fig. 27(c)) as a result of the large downwash from the flaps. The tail in the high position (fig. 28) is more effective and shows more linear moment curves and less moment variations with model height than the tail in the low position (fig. 27) for conditions below stall.

Power on.- The aerodynamic characteristics of the model without flaps and with power on are presented in figures 29 to 31. The characteristics of the model with flaps and power on are presented in figures 32 to 36. Flow conditions over the model were observed by means of tufts on the model for several heights and power-on conditions. Tufts on the fuselage just ahead of the tail indicated very large upwash angles. The increased lift and stability at low angles of attack (e.g., figs. 30(c) and 33(c)) result from the jet upwash after the efflux impinges against the ground plane. The stall breaks in the lift curves (figs. 32, 33, and 35) mentioned previously are similar to the breaks occurring out of ground effect (figs. 20(d), 20(a), and 20(c), respectively) but occur at lower angles

of attack as the model approaches the ground plane. The effect of height and velocity ratio on the forces and moments of the model at $\alpha = 0^{o}$ with flaps on and off is shown in figure 37.

Effects of ground-plane movement.- Comparison of the longitudinal aerodynamic characteristics of the flaps-off model over a still and over a moving ground plane is shown in figure 38 for power off and in figure 39 for power on. Any differences shown for the power-off condition are probably within the repeatability of the data. With a few exceptions, the same can be said for the flaps-off, power-on data. (See fig. 39.) When the model is nearest the ground plane (h/b = 0.10) and at the higher effective velocity ratios (figs. 39(i) and 39(l)), more lift and more negative pitching moments are indicated for the moving ground plane than for the still ground plane. At some heights and at the lower velocity ratios (figs. 39(c) and 39(f)), the pitching moments tend to become more positive with the moving ground plane.

Incremental Effects

Interference effects.- If the total measured forces and moments on the model are the forces and moments of the jet, plus the aerodynamic forces and moments without the jet, plus the mutual interference effects of the jet, model, and free stream (for example, $L = T\cos(\delta_j - \alpha) + C_L qS + \Delta L$), then the nondimensional interference increments may be expressed as follows:

$$\frac{\Delta L}{T} = \frac{L}{T} - \cos(\delta_j - \alpha) - \frac{C_L qS}{T}$$

$$\frac{\Delta D}{T} = \frac{D}{T} + \sin(\delta_j - \alpha) - \frac{C_D qS}{T}$$

$$\frac{\Delta M_Y}{T\bar{c}} = \frac{M_Y}{T\bar{c}} - \frac{(M_Y)_T}{T\bar{c}} - \frac{C_m qS\bar{c}}{T\bar{c}}$$

These equations were used in determining the interference increments given in figures 40 and 41.

The results show that the interference between the jet, model, and free stream increases the drag and pitching moments and reduces the lift. These interference increments are much larger for the model with the engine pods in the inboard location (fig. 40) than in the midspan location (fig. 41) because the inboard jets are closer to the larger surface areas of the model, the fuselage and tail. Figure 40(a) shows the tail to have an effect on these increments when the engine pods are inboard, but when the pods are at midspan (fig. 41(a)), the tail has little effect on the increments. When the angle of attack is increased from 0^{o} to 10^{o}, the lift and drag interference increments generally decrease

and the pitching increments generally increase. The effect of angle of attack on the increments is related to early wing stall, which occurs below an angle of attack of 10°. (See figs. 19 and 20.)

Effects of sideslip.- The increments of rolling and yawing moments and side force produced by 10° of positive sideslip are shown in figure 42 for the engine pods inboard and in figure 43 for the pods at midspan for various model components. Except for small negative yawing moments with the vertical tail off, the forces and moments are in the desired direction. The vertical tail was much more effective with engine pods inboard than at midspan. Flaps reduced the rolling moments with pods inboard but usually gave somewhat larger moments with the pods at midspan. The sharp break in the rolling-moment curves (fig. 43) at high angle of attack and the higher velocity ratios probably results from asymmetrical stall caused by the pods.

Ground-plane effects.- Figure 44 shows the variation with model height of the incremental forces and moments due to the ground plane for the power range with the model at three angles of attack. Some general effects of the ground plane may be noted. With engine pods at midspan and the small horizontal tail in the low position (fig. 44(a)), the ground plane generally produces increments of negative pitch, negative drag, and positive lift which increases in magnitude with effective velocity ratio and ground proximity especially at the higher velocity ratios. Placing the tail in the high position (fig. 44(b)) or removing the tail (fig. 44(c)) did not substantially change the lift and drag increments except for a few conditions. With the tail high or off, the pitching-moment increments were positive in most instances.

SUMMARY OF RESULTS

An investigation was made at low forward velocities to determine the aerodynamic characteristics of a VTOL jet transport with lift engines mounted under the wings in pods located either at midspan or adjacent to the fuselage. Cruise engines were not on the model. Eight lift engines were simulated by ejectors powered with compressed air with most of the inlets on the top surface of the wing. The scope of the investigation included the determination of the effects of engine-pod location, ground-plane movement, flaps, tail size and location, and sideslip on the aerodynamic characteristics, and the effects of configuration changes on the jet and free-stream interference increments. Some of the results as indicated by the data are as follows:

1. With power off and flaps off, the model has a little higher maximum lift and lower minimum drag when the engine pods are inboard than when they are at midspan, but with power on and flaps on, the model has less drag at small angles of attack when the pods are at midspan.

2. With flaps on and power on or off, sharp breaks in the lift curves resulting from inboard wing stall occur at lower angles of attack (as low as 8^{o}) when the engine pods are at midspan than when they are inboard.

3. With power on and flaps on or off, the model is more stable when the engine pods are at midspan than when they are inboard.

4. With power on, the indicated downwash angles at the low tail position are as high as 17^{o} or 28^{o}, depending on the jet velocity, when the engine pods are inboard and are about 12^{o} when the pods are at midspan.

5. Interference between the jet, free stream, and model increases the drag and pitching moments and reduces the lift. These interference increments are much larger when engine pods are inboard than when they are at midspan.

6. With power on and engine pods at midspan, the ground plane generally produces increments of negative pitch, negative drag, and positive lift which increases in magnitude with effective ratio of free-stream velocity to jet velocity and with ground proximity. The ground-reflected jet upwash causes mixed flows over the wing, fuselage, and tail. There is little ground effect with flaps off and power off.

7. Without flaps and power, results differ little between the moving and the still ground plane. With power on and the model nearest the ground plane and at the higher effective velocity ratios, the model over the moving ground plane shows more lift and more negative pitching moments than the model over the still ground plane.

8. Lateral forces and moments produced by sideslip are generally in the desired direction, and the vertical tail is much more effective when the engine pods are inboard than when they are at midspan.

Langley Research Center,
National Aeronautics and Space Administration,
Langley Station, Hampton, Va., February 9, 1970.

REFERENCES

1. Vogler, Raymond D.; and Kuhn, Richard E.: Longitudinal and Lateral Stability Characteristics of Two Four-Jet VTOL Models in the Transition Speed Range. NASA TM X-1092, 1965.

2. Spreemann, Kenneth P.: Investigation of Interference of a Deflected Jet With Free Stream and Ground on Aerodynamic Characteristics of a Semispan Delta-Wing VTOL Model. NASA TN D-915, 1961.

3. Williams, John; and Wood, Maurice N.: Aerodynamic Interference Effects With Jet-Lift V/STOL Aircraft Under Static and Forward-Speed Conditions. Tech. Rep. No. 66403, Brit. R.A.E., Dec. 1966.

4. Vogler, Raymond D.: Interference Effects of Single and Multiple Round or Slotted Jets on a VTOL Model in Transition. NASA TN D-2380, 1964.

5. Otis, James H., Jr.: Induced Interference Effects on a Four-Jet VTOL Configuration With Various Wing Planforms in the Transition Speed Range. NASA TN D-1400, 1962.

6. Vogler, Raymond D.: Ground Effects on Single- and Multiple-Jet VTOL Models at Transition Speeds Over Stationary and Moving Ground Planes. NASA TN D-3213, 1966.

7. Margason, Richard J.; and Gentry, Garl L.: Static Calibration of an Ejector Unit for Simulation of Jet Engines in Small-Scale Wind-Tunnel Models. NASA TN D-3867, 1967.

8. Mechtly, E. A.: The International System of Units – Physical Constants and Conversion Factors. NASA SP-7012, 1964.

9. Turner, Thomas R.: A Moving-Belt Ground Plane for Wind-Tunnel Ground Simulation and Results for Two Jet-Flap Configurations. NASA TN D-4228, 1967.

TABLE I.- MODEL GEOMETRY

Characteristic	Wing	Vertical tail	Horizontal tail	
			Large	Small
Airfoil	NACA 4415	NACA 0015	Modified NACA 0015	NACA 0015
Root chord, cm	27.08	37.59	18.80	18.80
Tip chord, cm	13.54	18.80	9.40	9.40
Span, cm	162.56	45.72	81.30	60.96
$\bar{c}$, cm	21.06	29.23	14.60	14.60
Sweep of c/2, deg	0	10.08	2.05	0
Area, m^2	0.3301	0.1282	0.1146	0.0859

Flaps:
- Airfoil . . . . . NACA 4415
- Length (each), cm 29.72
- Chord, cm 7.37

Fuselage length, cm 152.4

Fuselage maximum diameter, cm 20.32

Tail length, cm:
- With small horizontal tail 72.2
- With large horizontal tail 72.9

Jet exit area total for eight engines, m^2 . . . . . 0.01621467

Engine pods:
- Width, cm 11.18
- Depth, cm 15.75
- Length, cm 70.10

TABLE II.- INDEX TO FIGURES FOR OUT-OF-GROUND-EFFECT DATA FOR MODEL WITH ENGINE PODS LOCATED INBOARD OR AT MIDSPAN

Figure	Data description	Power	Flaps (*)	Horizontal tail		i_t, deg
				Size	Location	
	Inboard					
4	Longitudinal data showing effects of tail position	Off	Off	Large	Low, mid, and high	0
5	Longitudinal data showing effects of tail size and position	Off	On	Large and small	Low, mid, and high	0
6	Longitudinal data showing effects of tail incidence	Off	On	Large	Low	Tail off 0, 15, and -15
7	Longitudinal data showing effects of tail position	On	Off	Large	Low, mid, and high	0
8	Longitudinal data showing effects of tail position	On	On	Large	Low, mid, and high	0
9	Longitudinal data showing effects of tail position	On	On	Small	Low, mid, and high	Tail off 0
10	Longitudinal data showing effects of tail incidence	On	On	Large	Low	Tail off 0, 15, and -15
11	Lateral data showing effects of wing, fuselage	On	Off	Large	Low	0
12	Lateral data showing effects of wing, fuselage, flaps	On	On	Large	Low	0
13	Lateral data showing effects of wing, fuselage, vertical tail	On	Off	Large	Low	0
14	Lateral data showing effects of complete model	On	On	Large	Low	0
	Midspan					
15	Longitudinal data showing effects of tail position	Off	Off	Large	Low, mid, and high	0
16	Longitudinal data showing effects of tail size and position	Off	On	Large and small	Low, mid, and high	0
17	Longitudinal data showing effects of tail incidence	Off	On	Large	Low	Tail off 0, 15, and -15
18	Longitudinal data showing effects of tail position	On	Off	Large	Low, mid, and high	0
19	Longitudinal data showing effects of tail position	On	On	Large	Low, mid, and high	0
20	Longitudinal data showing effects of tail position	On	On	Small	Low, mid, and high	Tail off 0
21	Longitudinal data showing effects of tail incidence	On	On	Large	Low	Tail off 0, 15, and -15
22	Lateral data showing effects of wing, fuselage	On	Off	Large	Low	0
23	Lateral data showing effects of wing, fuselage, flaps	On	On	Large	Low	0
24	Lateral data showing effects of wing, fuselage, vertical tail	On	Off	Large	Low	0
25	Lateral data showing effects of complete model	On	On	Large	Low	0

*Flap deflection 60^{o} when the flaps are on the model.

TABLE III.- INDEX TO FIGURES FOR IN-GROUND-EFFECT DATA FOR MODEL WITH ENGINE PODS LOCATED AT MIDSPAN

Figure	Data description	Power	Flaps	Horizontal tail		i_t, deg
				Size	Location	
26	Longitudinal data showing effects of model height range	Off	Off	Small	Low	Tail off 0 and 15
27	Longitudinal data showing effects of model height range	Off	On	Small	Low	Tail off 0 and 15
28	Longitudinal data showing effects of model height range	Off	On	Small	High	0 and 15
29	Longitudinal data showing effects of model height range	On	Off	-----	----	Tail off
30	Longitudinal data showing effects of model height range	On	Off	Small	Low	0
31	Longitudinal data showing effects of model height range	On	Off	Small	Low	15
32	Longitudinal data showing effects of model height range	On	On	-----	----	Tail off
33	Longitudinal data showing effects of model height range	On	On	Small	Low	0
34	Longitudinal data showing effects of model height range	On	On	Small	Low	15
35	Longitudinal data showing effects of model height range	On	On	Small	High	0
36	Longitudinal data showing effects of model height range	On	On	Small	High	15
37	Comparison at hovering and transition speeds	On	On and off	Small	Low	0
38	Comparison over still and moving ground planes	Off	Off	Small	Low	0
39	Comparison over still and moving ground planes	On	Off	Small	Low	0

TABLE IV.- SUMMARY FIGURES

Figure	Data description	Engine-pod location	Ground proximity
40	Interference increments	Inboard	Out
41	Interference increments	Midspan	Out
42	Effect of model components on lateral characteristics in sideslip	Inboard	Out
43	Effect of model components on lateral characteristics in sideslip	Midspan	Out
44	Incremental effects of ground proximity and effective velocity ratio	Midspan	In

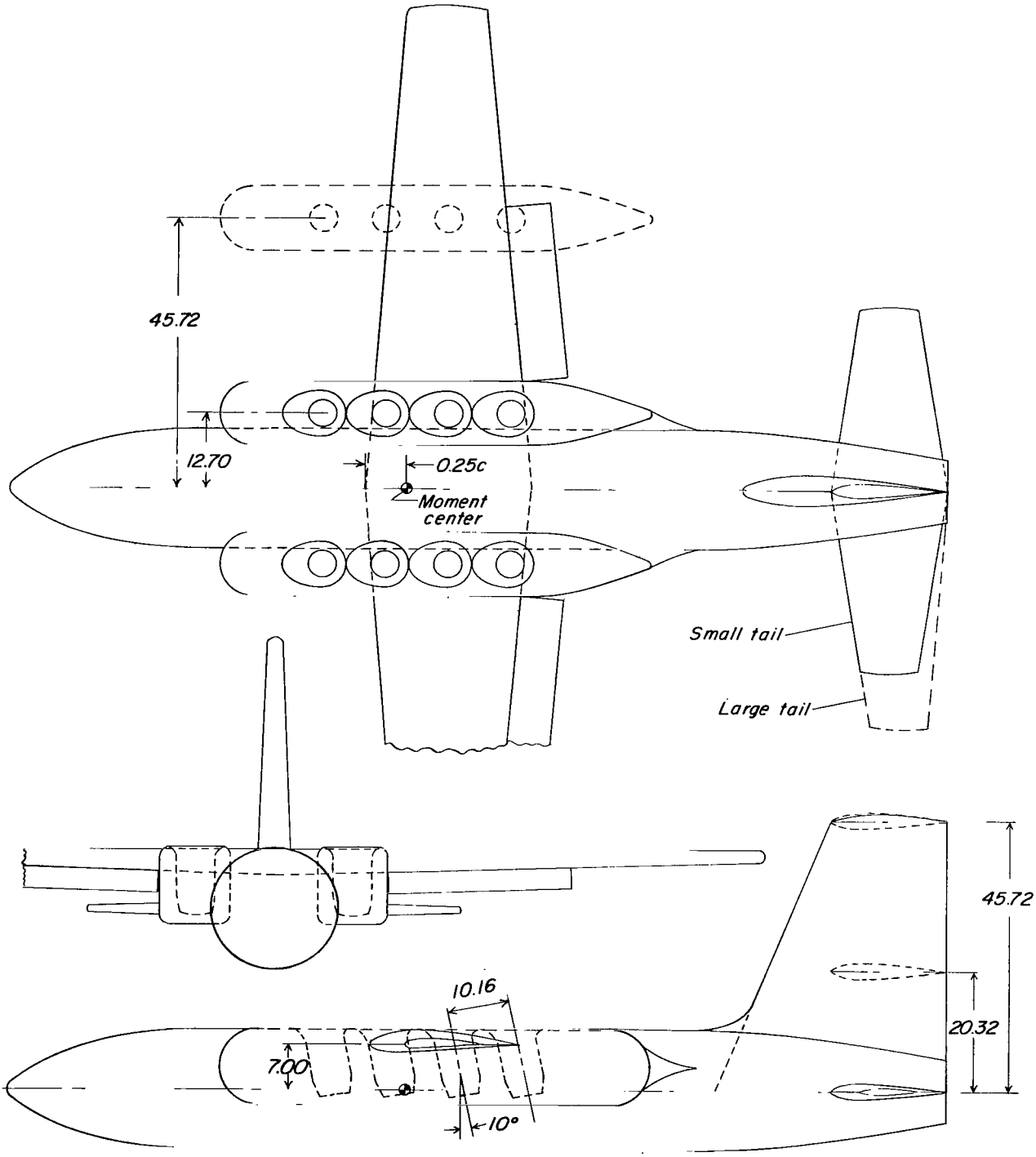

Figure 1.- Three-view drawing of model showing alternate engine-pod and horizontal-tail locations. Dimensions in centimeters.

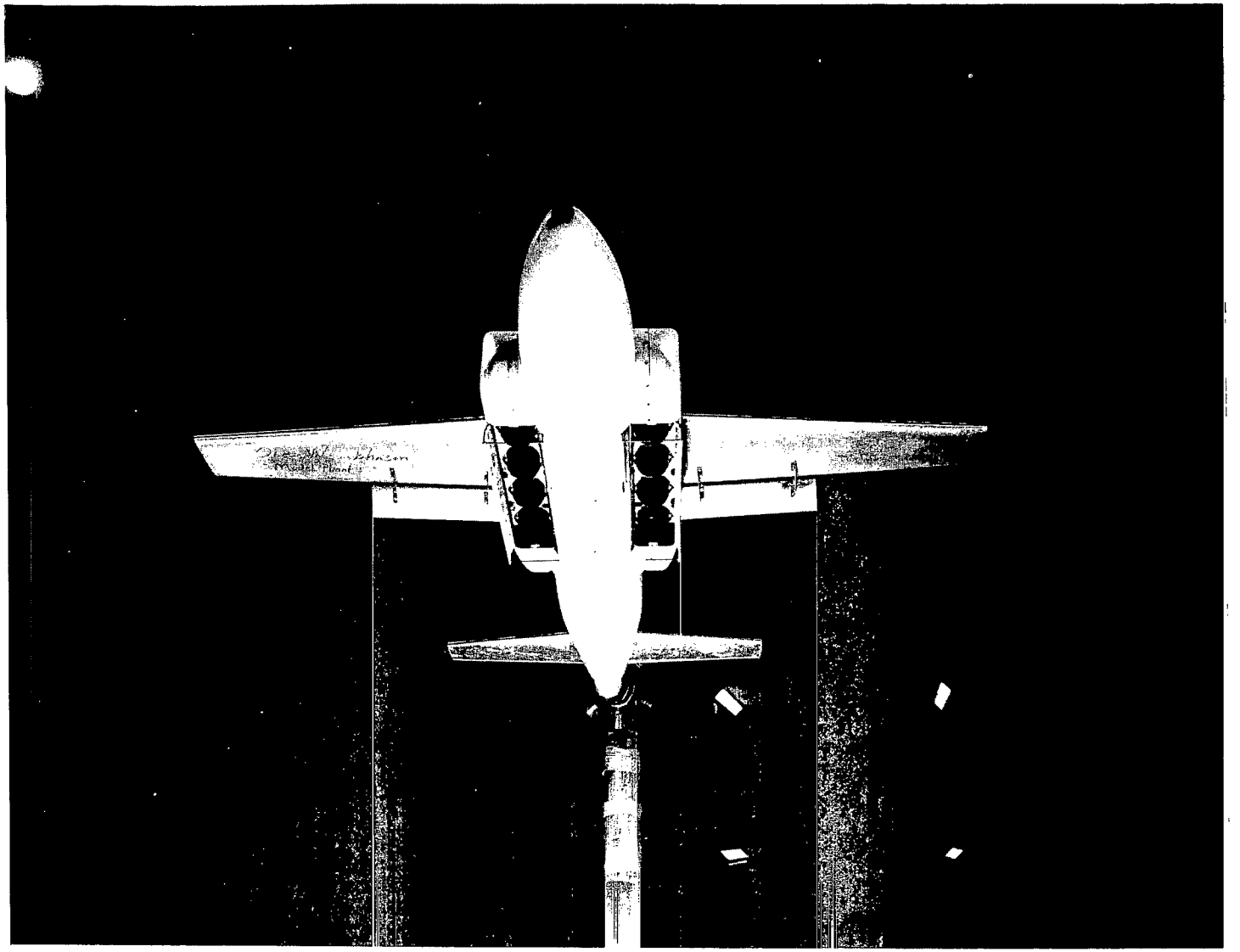

(a) Bottom view.

L-66-10042

Figure 2.- Photographs of model in tunnel.

L-66-10043

(b) Three-quarter front view.

Figure 2.- Continued.

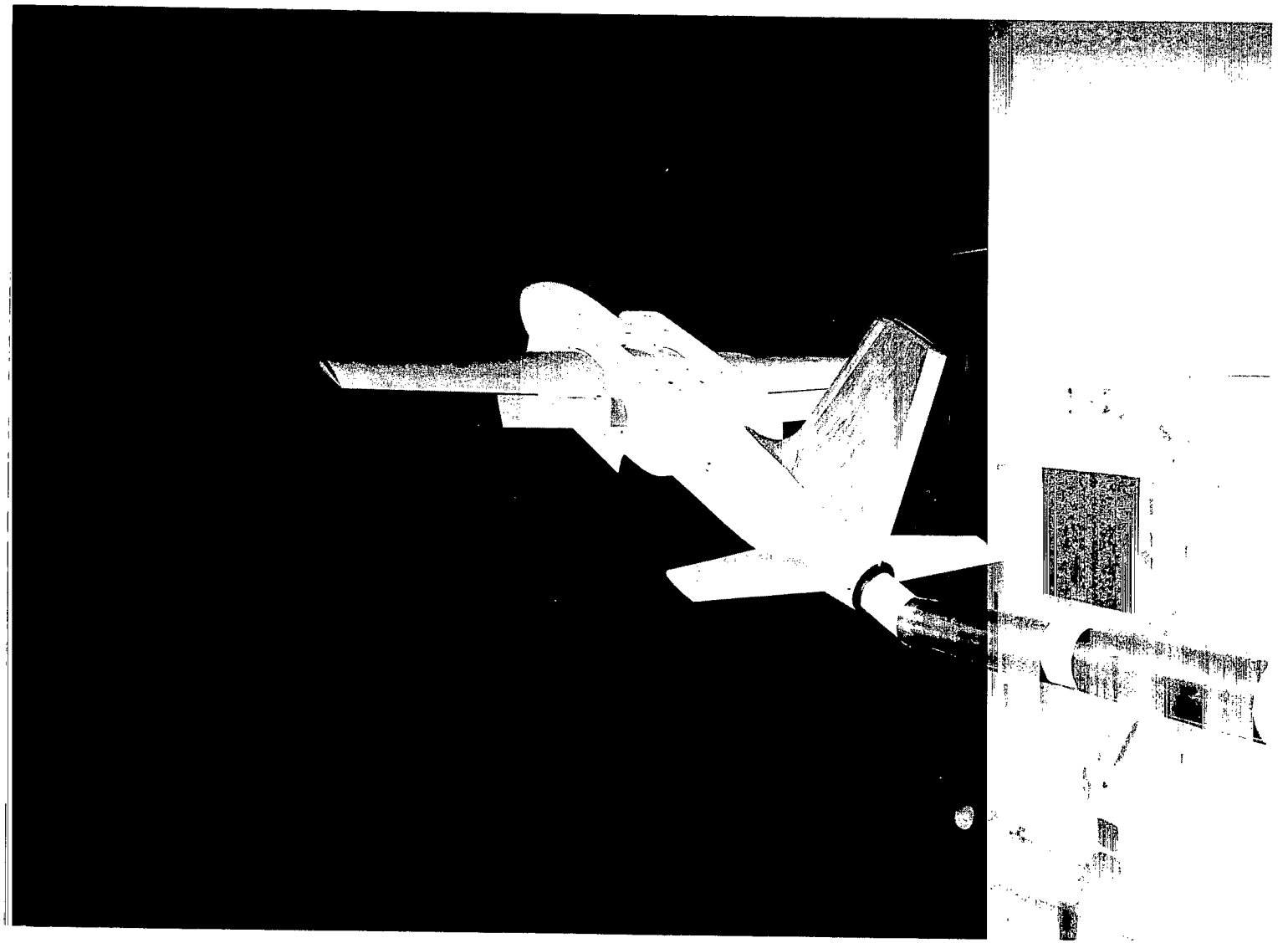

(c) Three-quarter rear view.

L-66-10044

Figure 2.- Concluded.

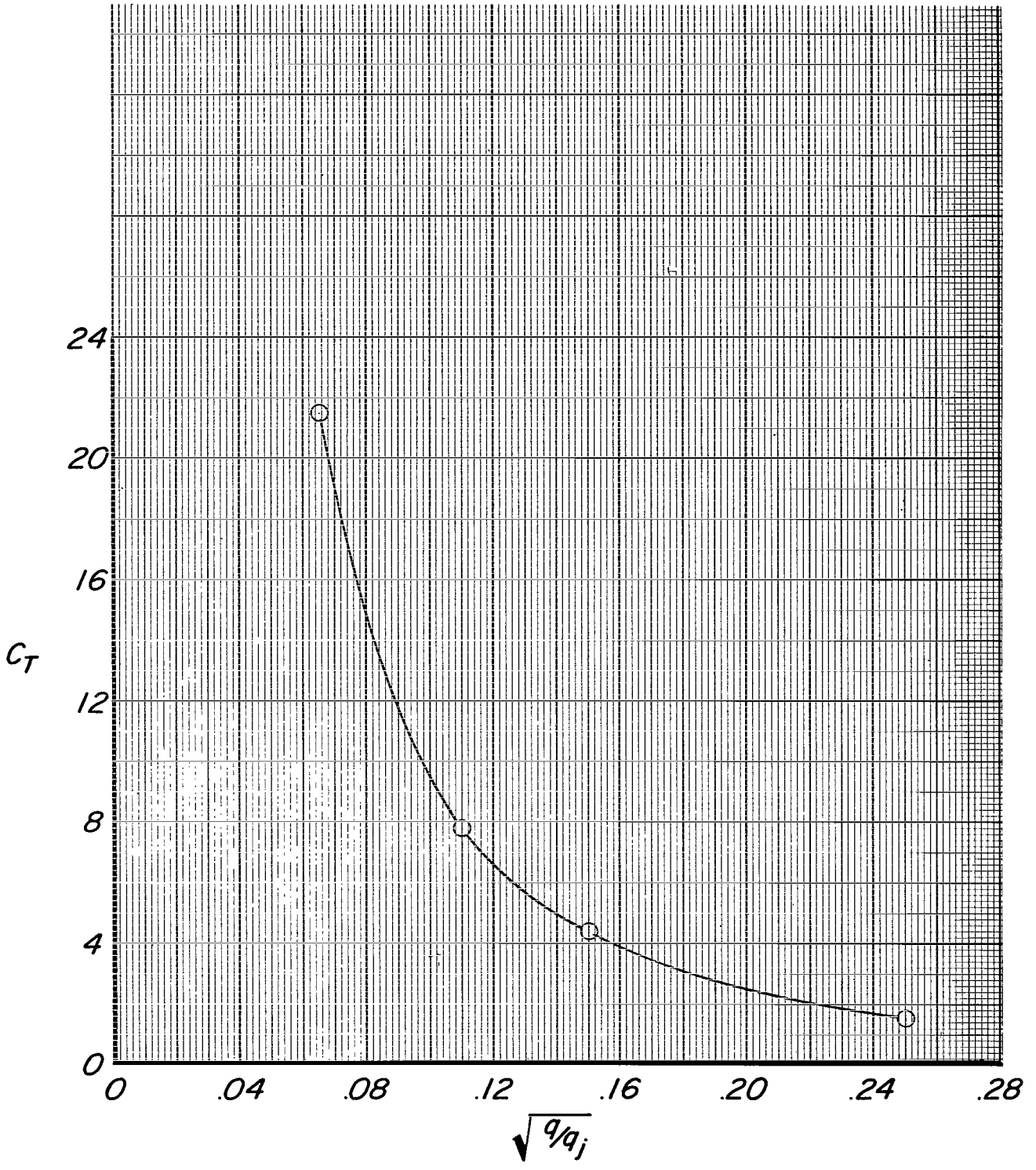

Figure 3.- Thrust coefficient as a function of effective velocity ratio.

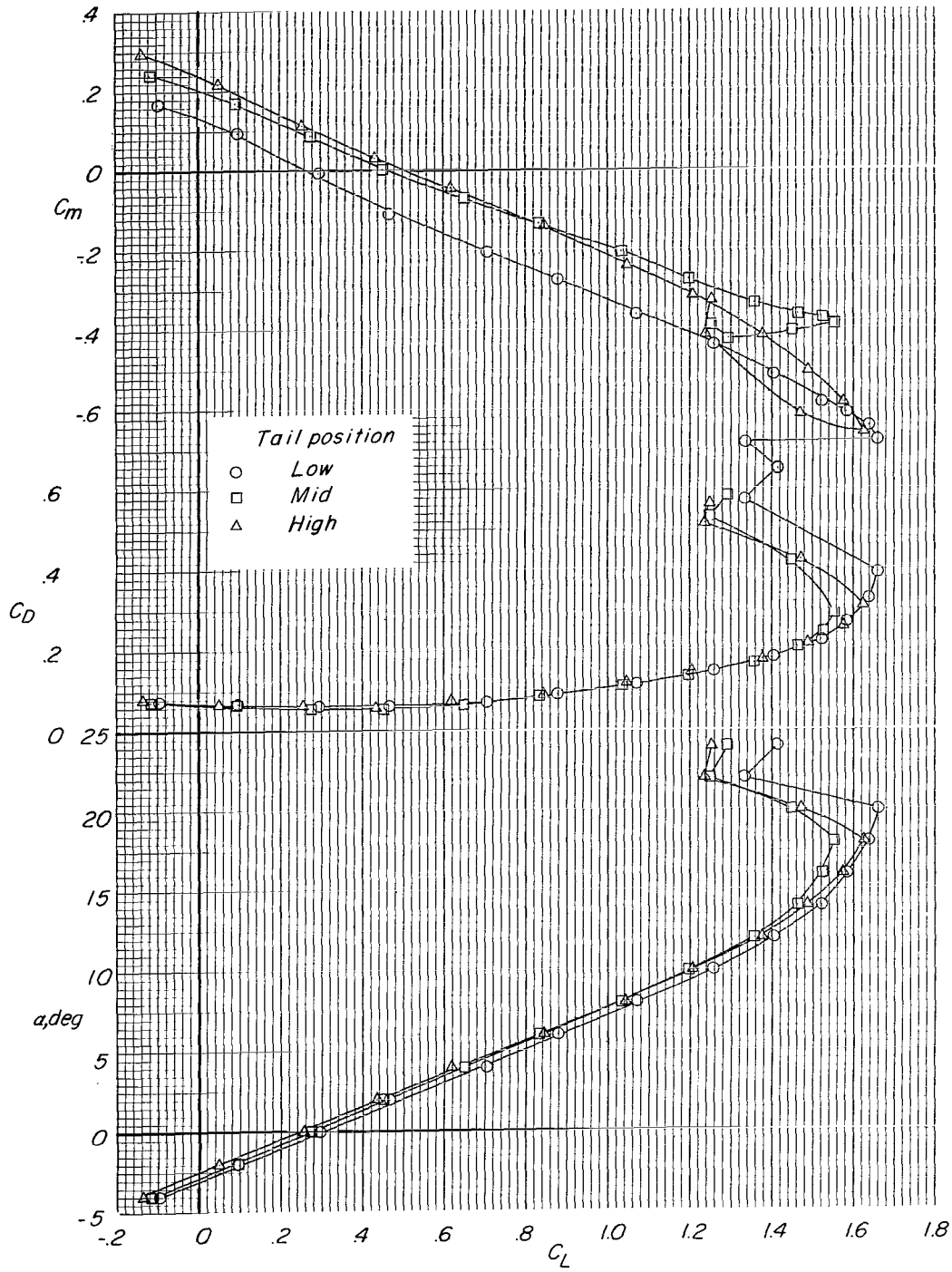

Figure 4.- Longitudinal aerodynamic characteristics of model with large horizontal tail at three locations. Flaps off; power off; $i_t = 0^o$; engine pods inboard.

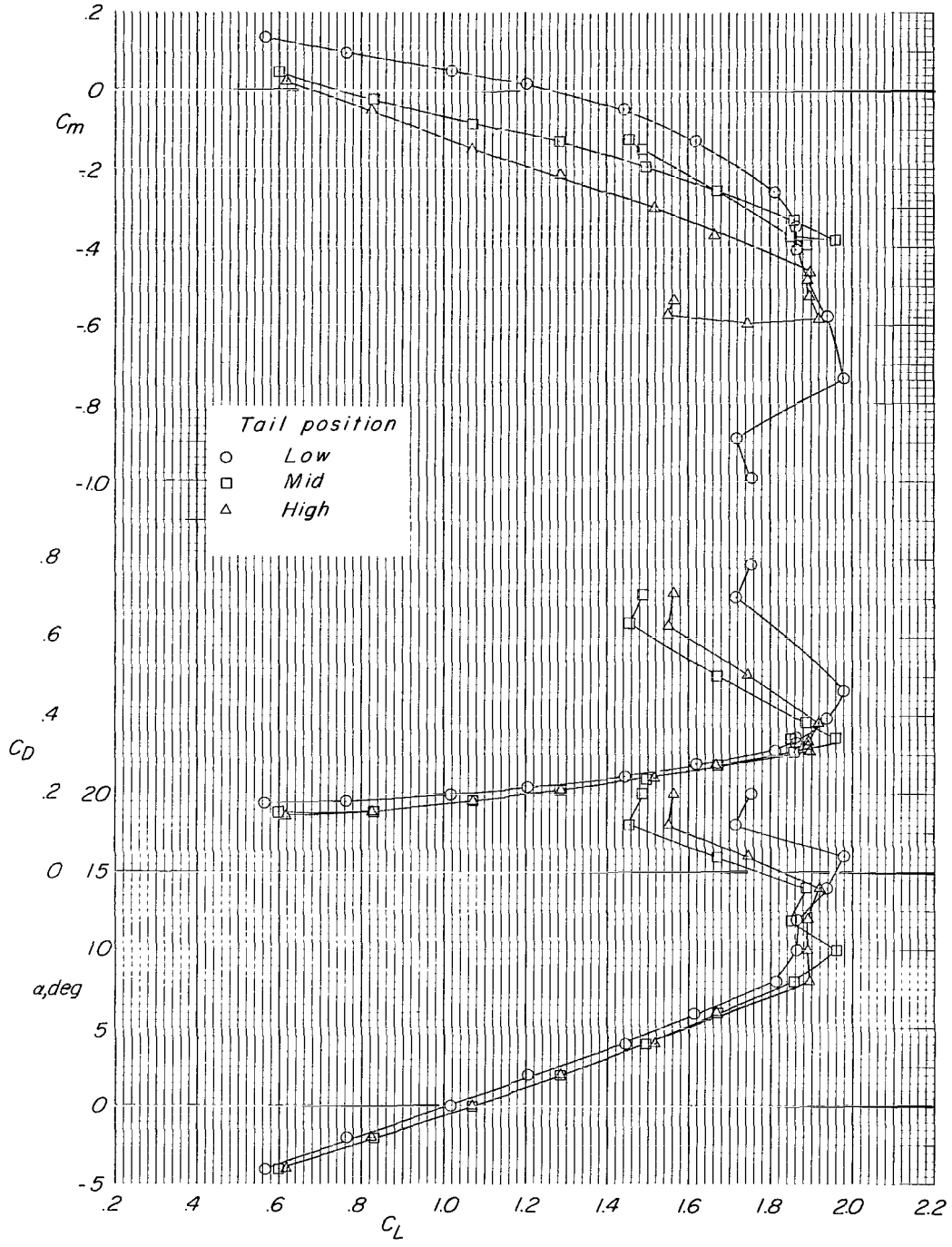

(a) Large tail.

Figure 5.- Longitudinal aerodynamic characteristics of model with small and large tails at three locations. Flaps on; power off; $i_t = 0^0$; engine pods inboard.

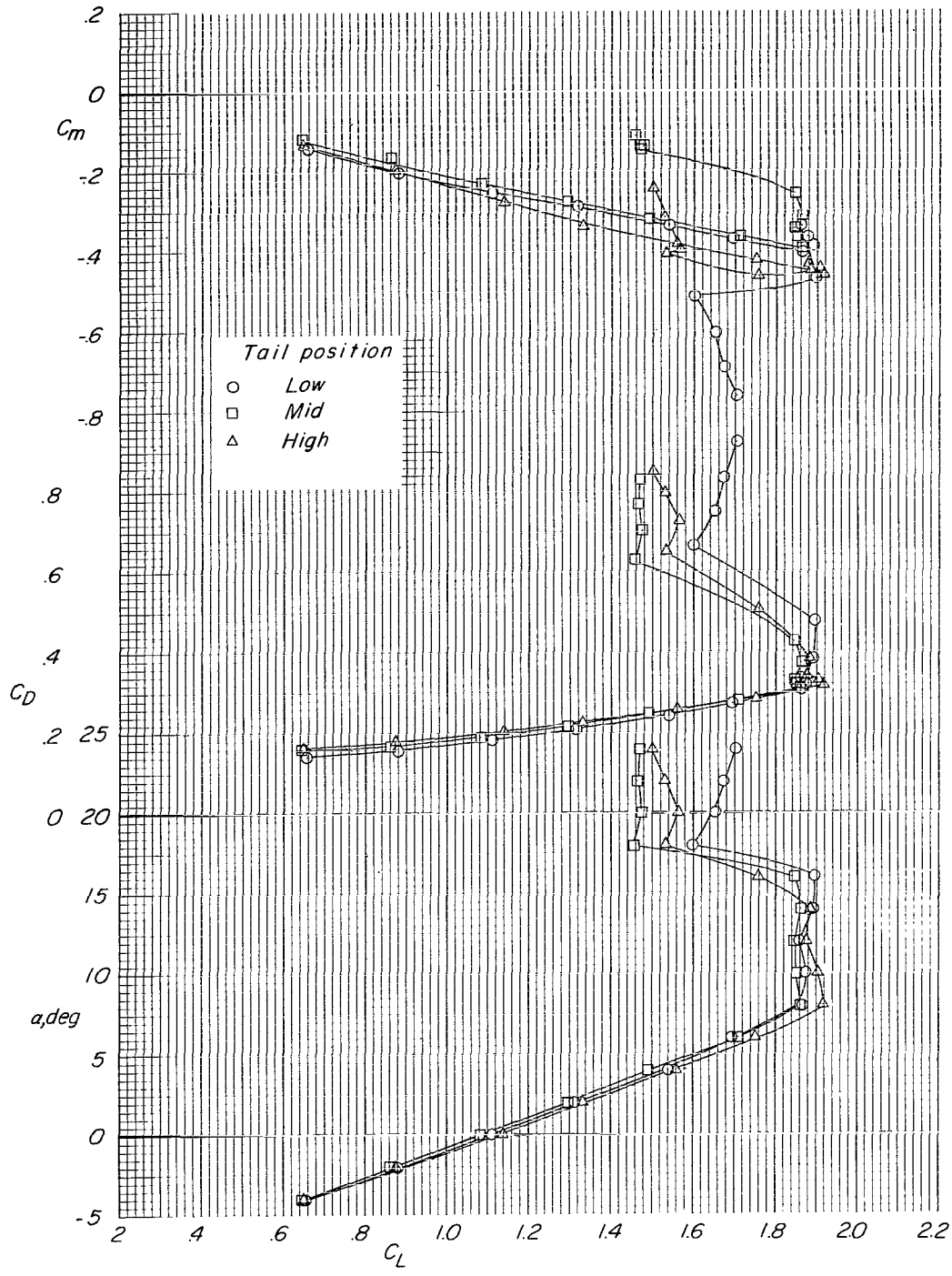

(b) Small tail.

Figure 5.- Concluded.

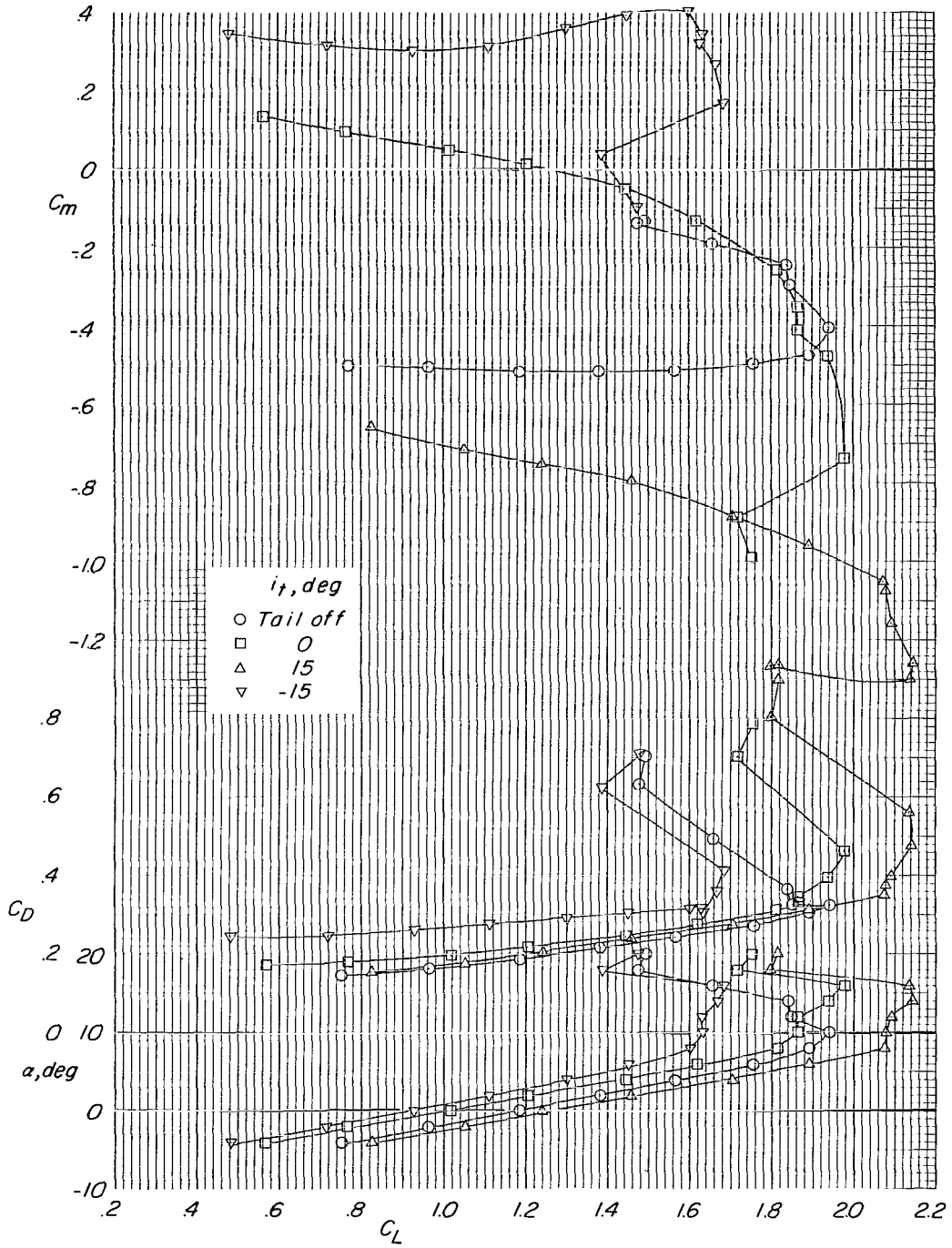

Figure 6.- Effect of horizontal-tail incidence on longitudinal aerodynamic characteristics of model with large tail in low position. Flaps on; power off; engine pods inboard.

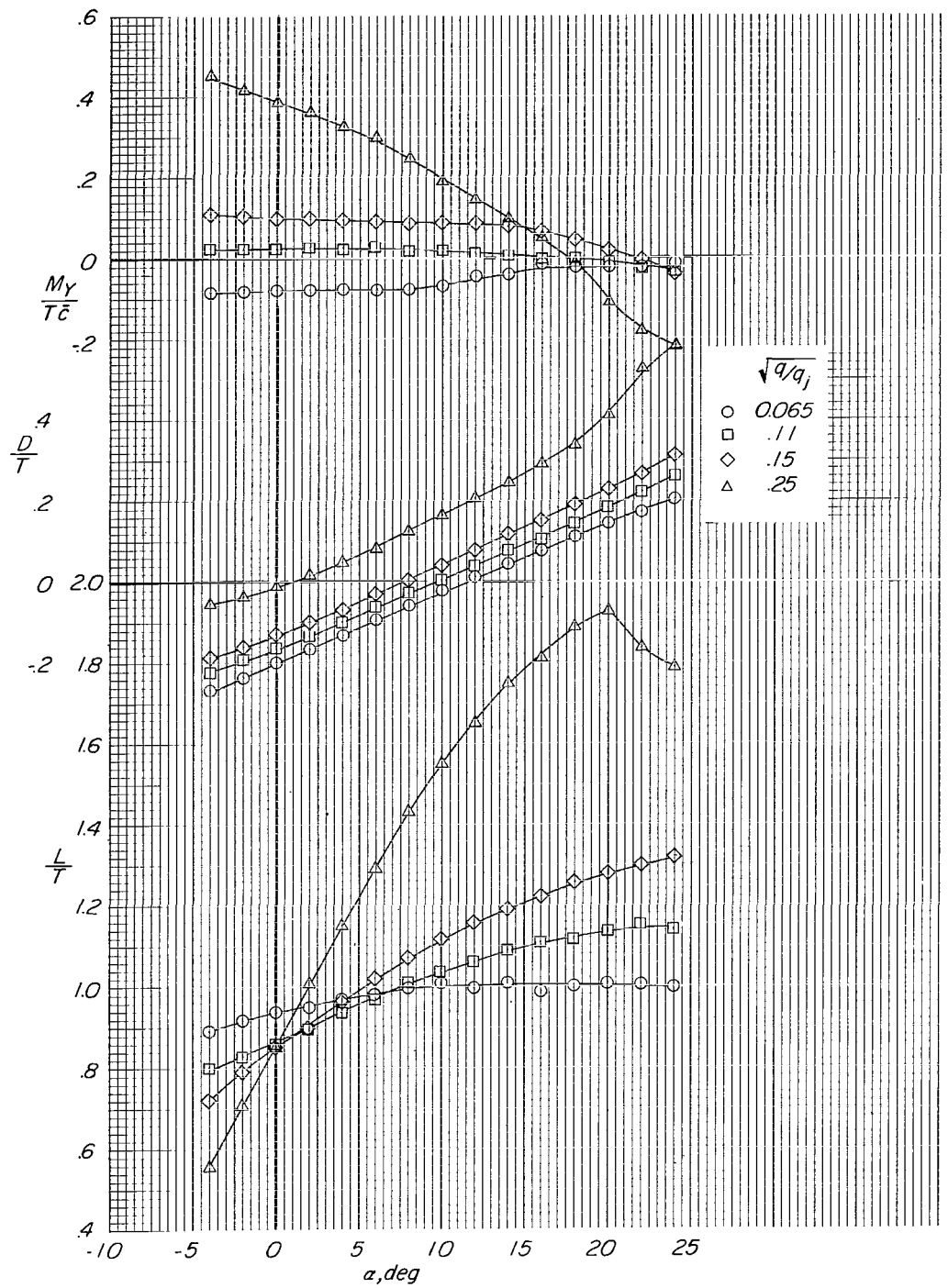

(a) Tail in low position.

Figure 7.- Longitudinal aerodynamic characteristics of model with large horizontal tail at three locations. Flaps off; power on; $i_t = 0^0$; engine pods inboard.

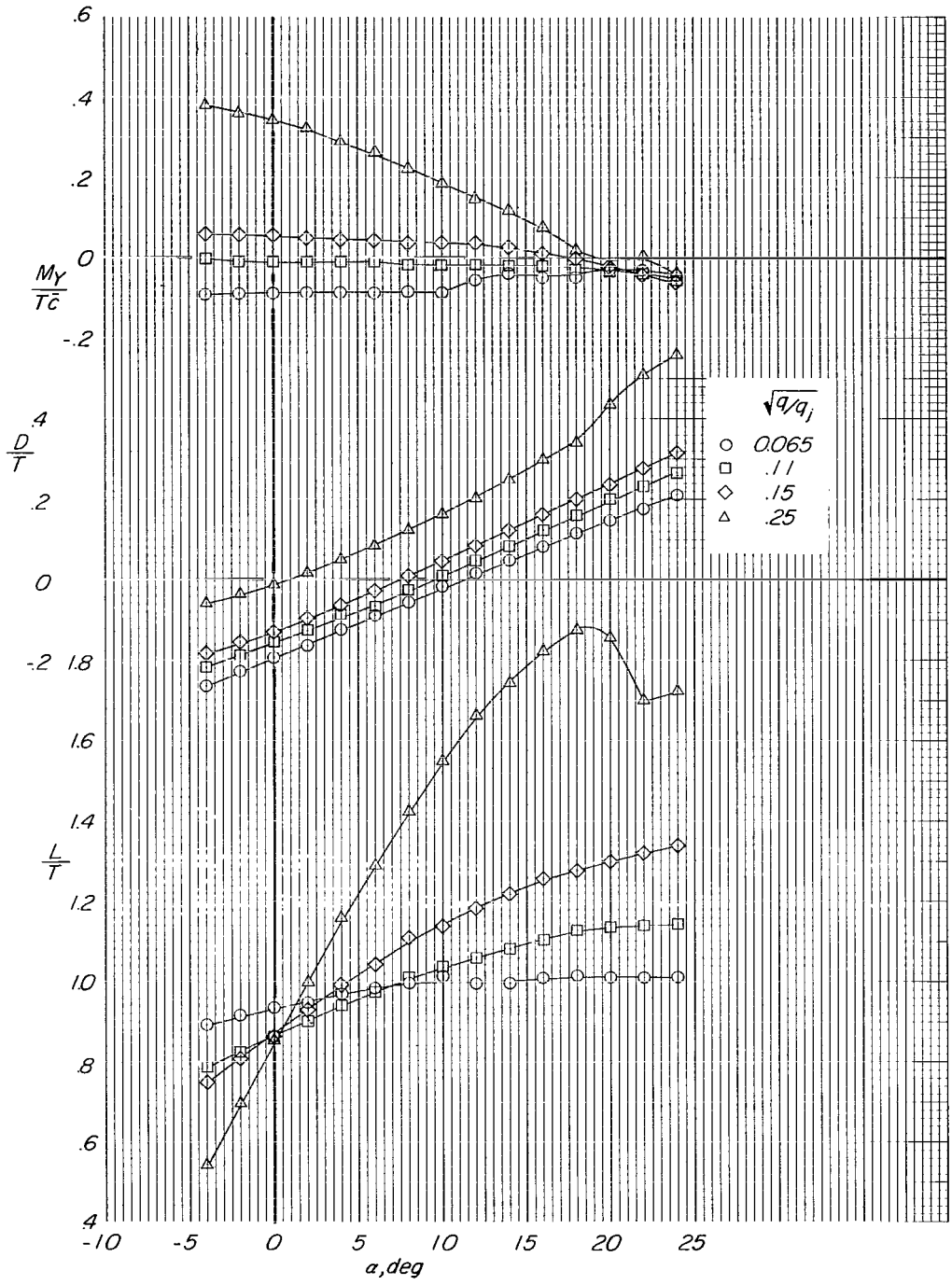

(b) Tail in mid position.

Figure 7.- Continued.

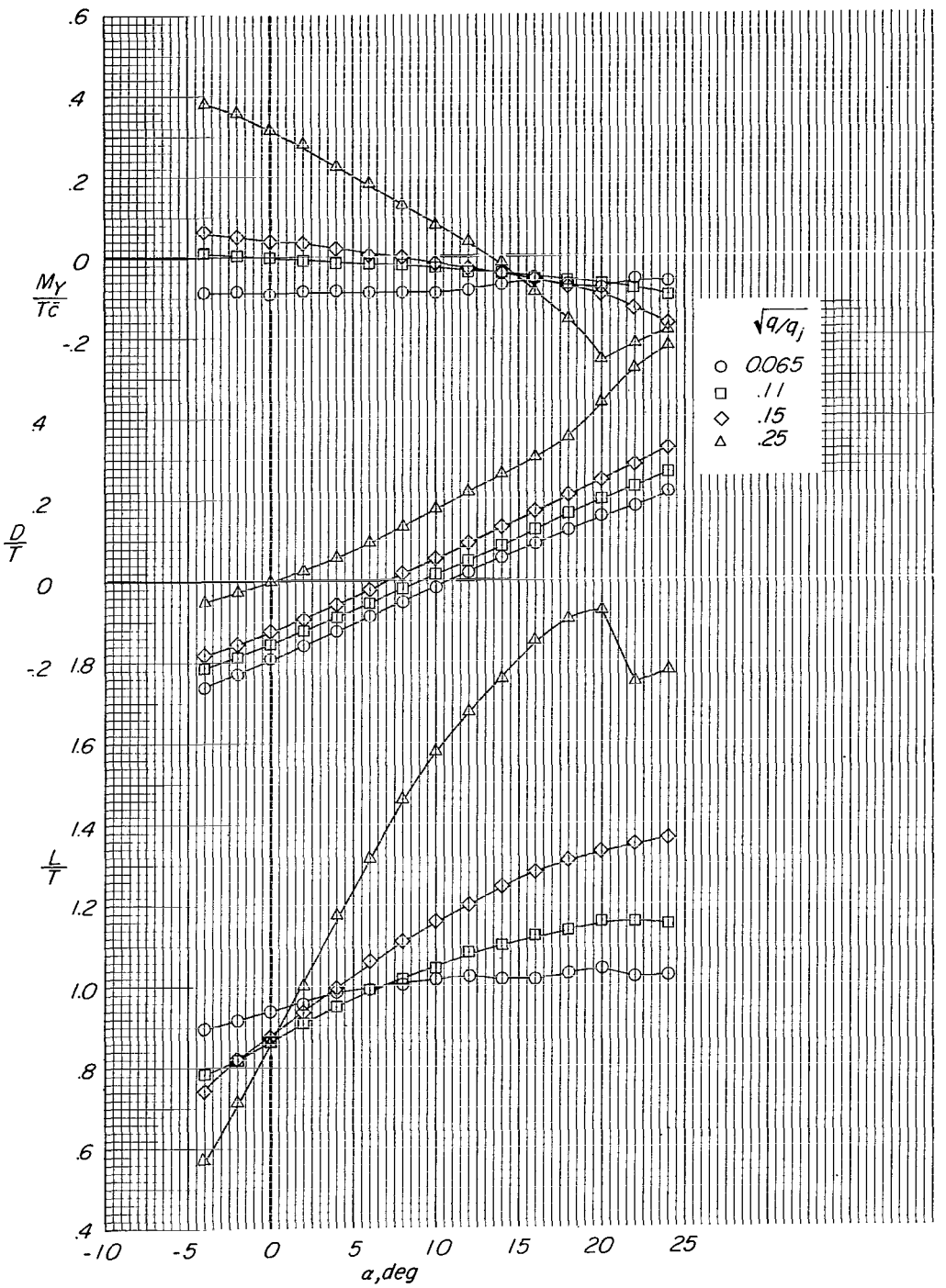

(c) Tail in high position.

Figure 7.- Concluded.

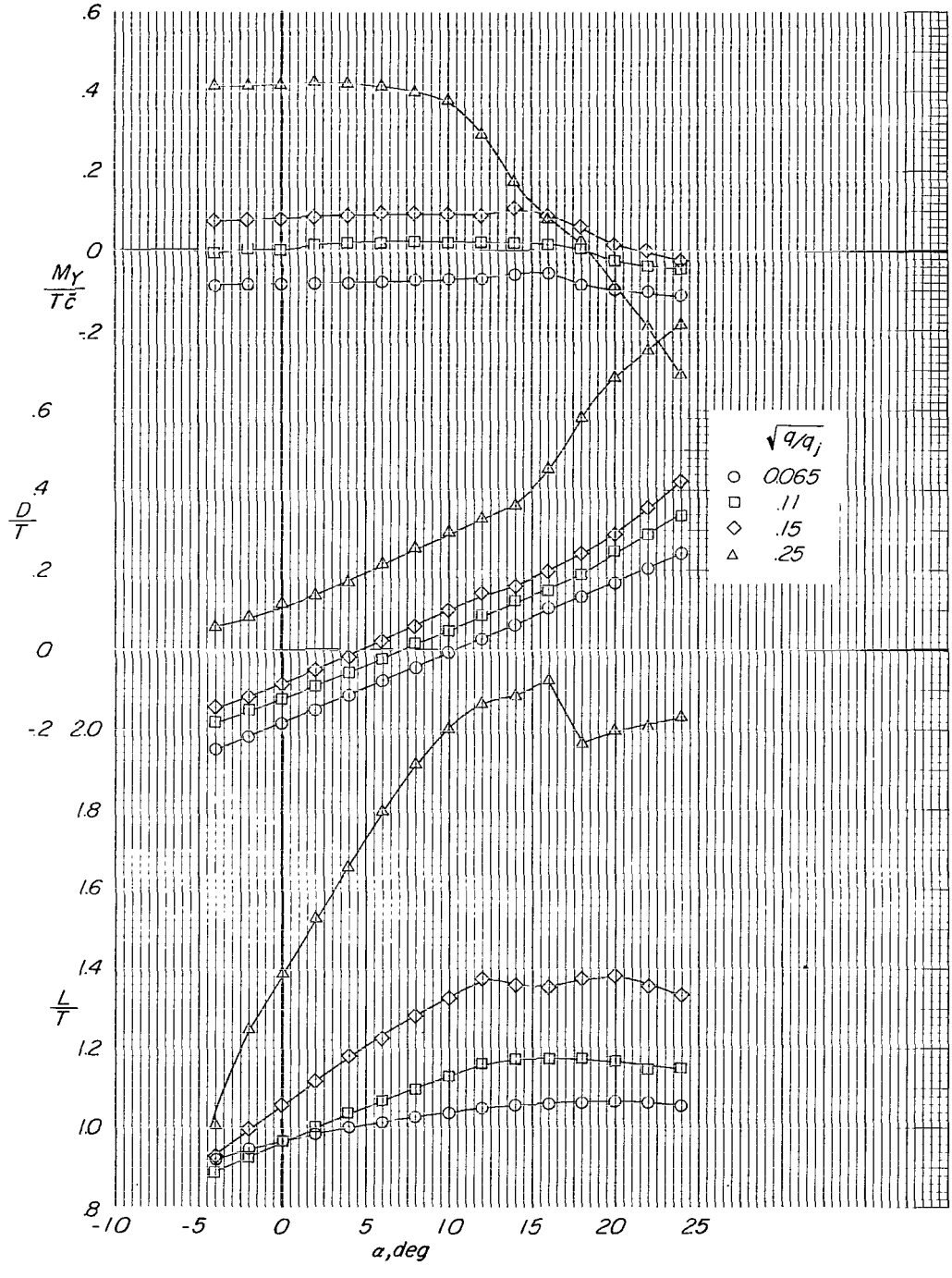

(a) Tail in low position.

Figure 8.- Longitudinal aerodynamic characteristics of model with large horizontal tail at three locations. Flaps on; power on; $i_t = 0^0$; engine pods inboard.

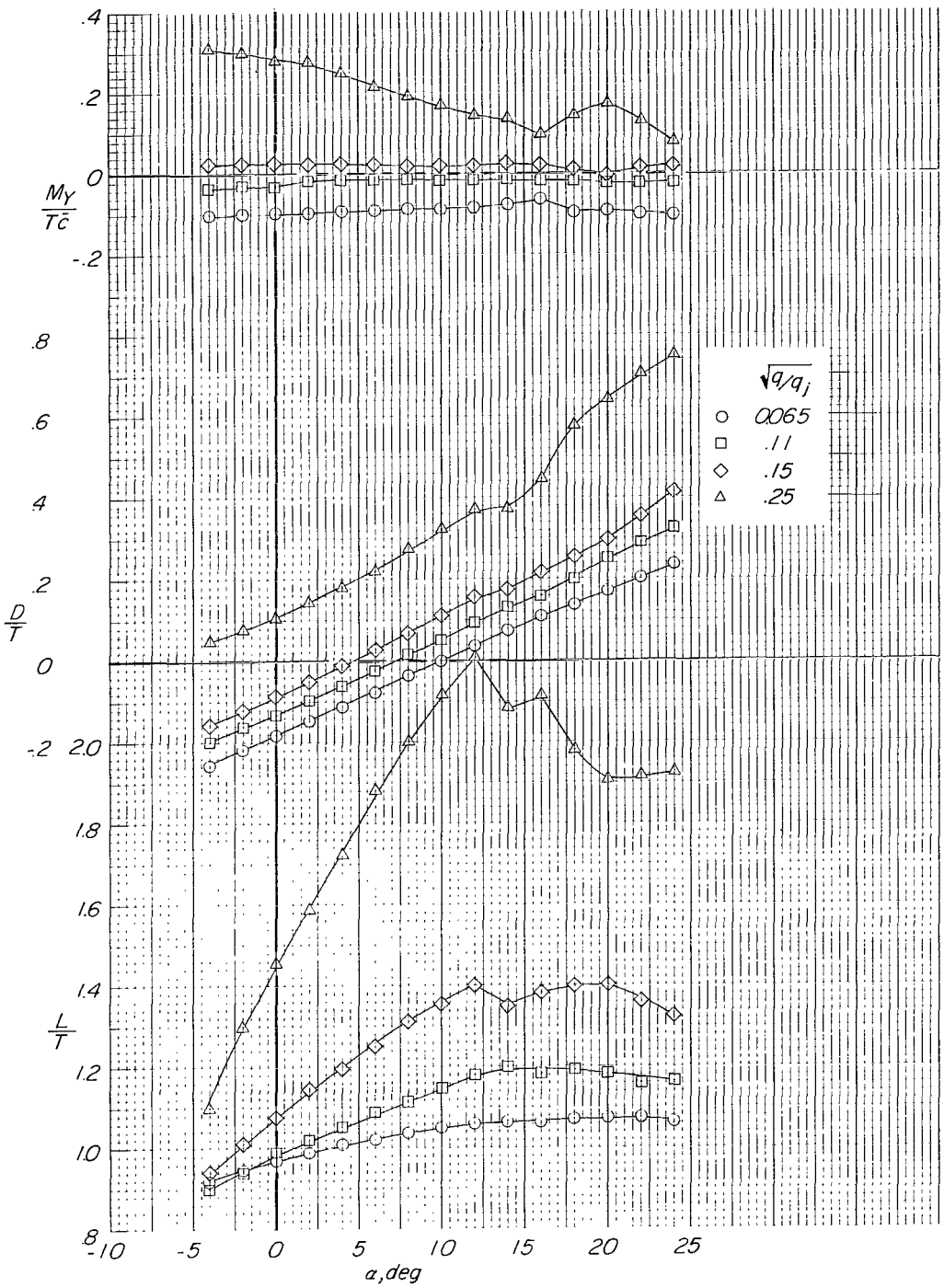

(b) Tail in mid position.

Figure 8.- Continued.

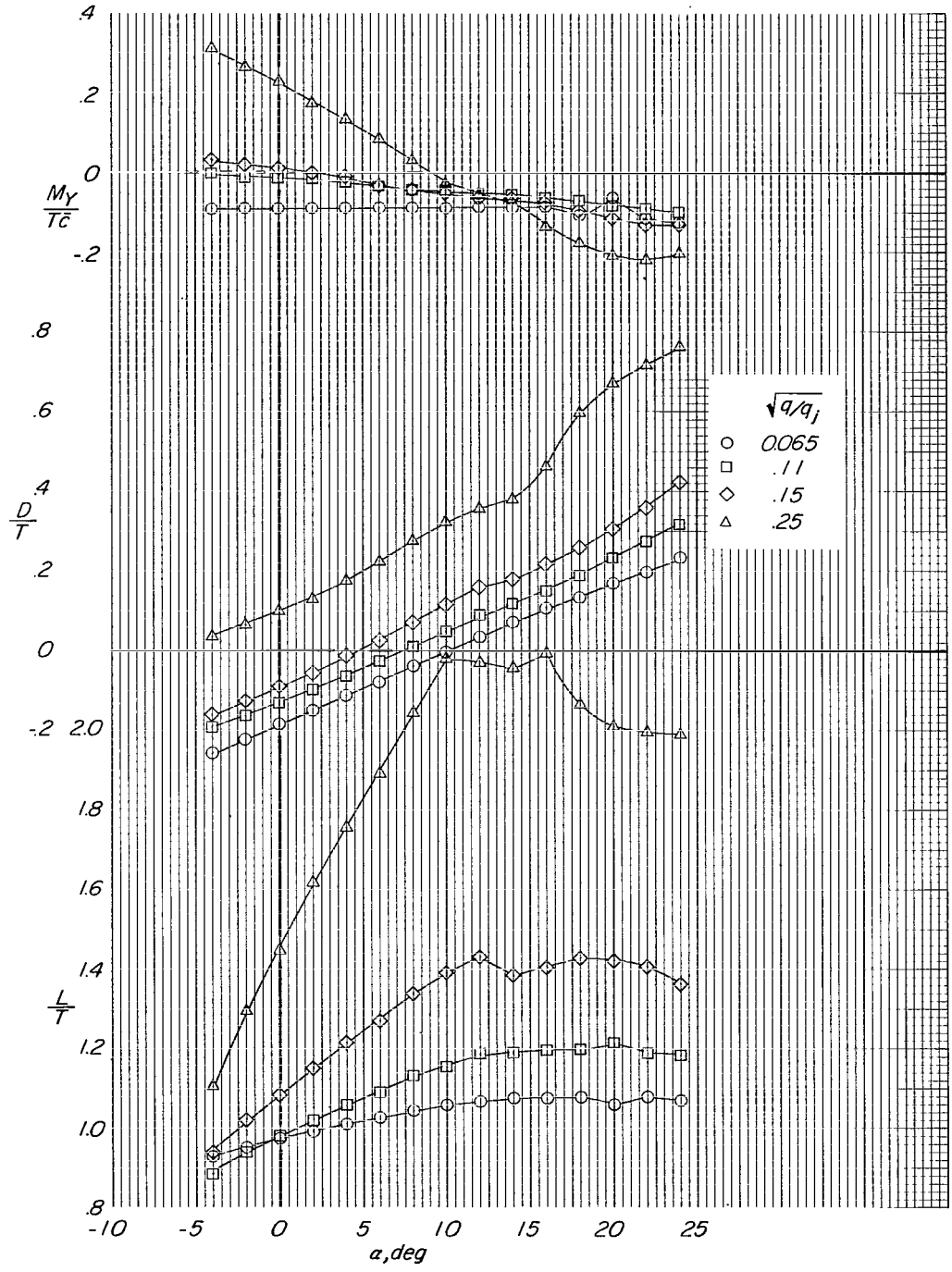

(c) Tail in high position.

Figure 8.- Concluded.

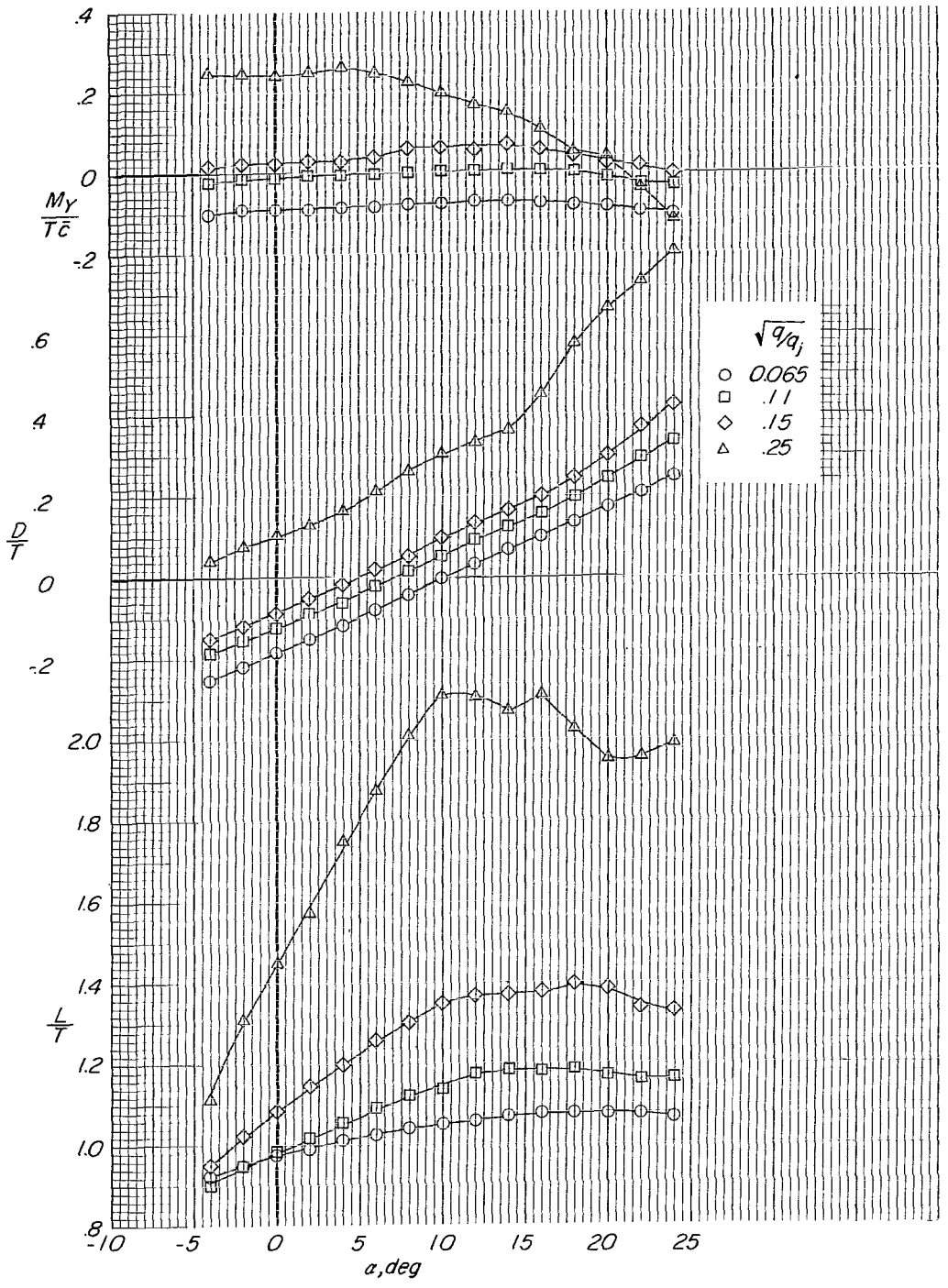

(a) Tail in low position.

Figure 9.- Longitudinal aerodynamic characteristics of model with small horizontal tail at three locations and with tail off. Flaps on; power on; $i_t = 0^o$ if tail on engine pods inboard.

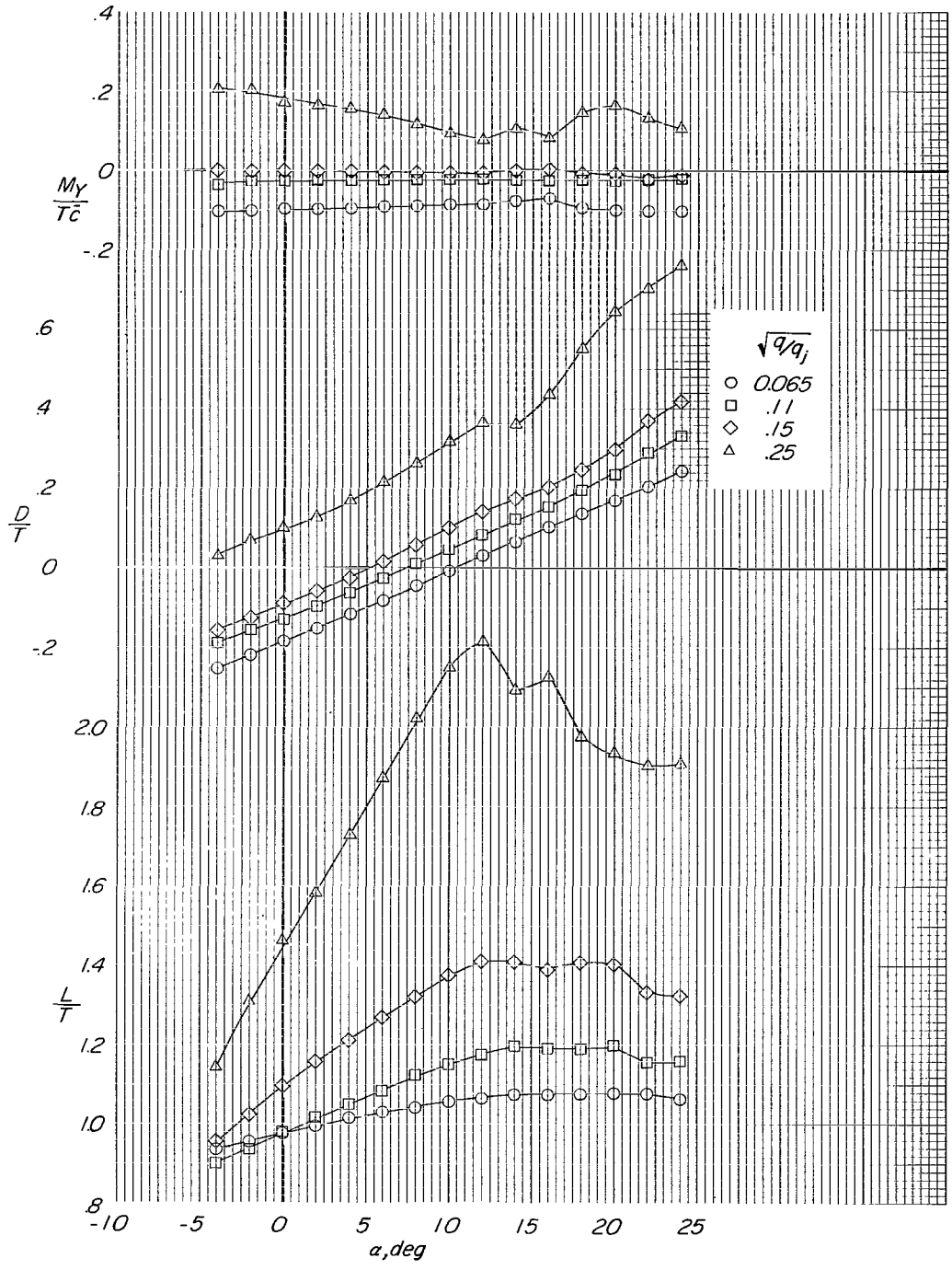

(b) Tail in mid position.

Figure 9.- Continued.

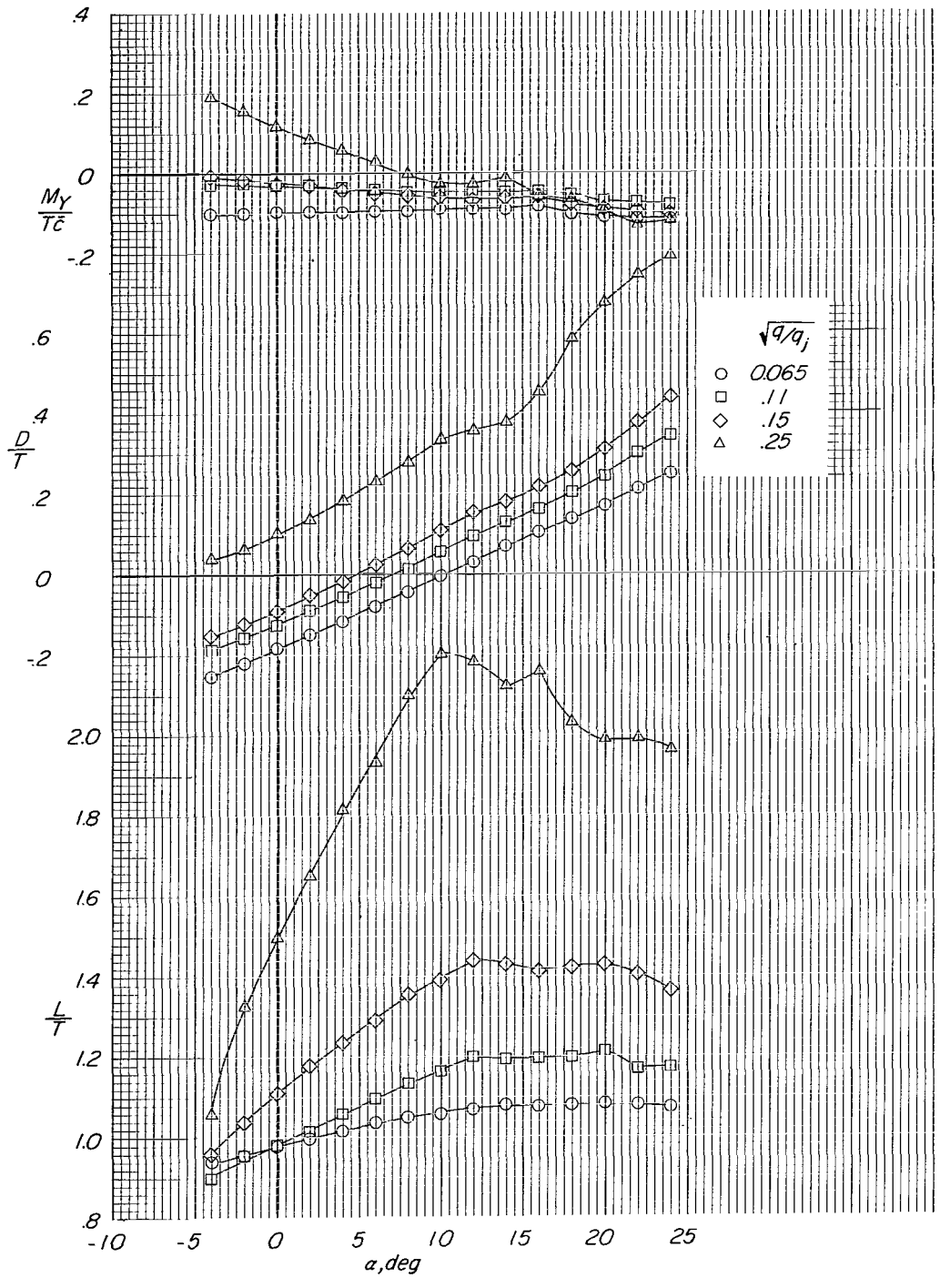

(c) Tail in high position.

Figure 9.- Continued.

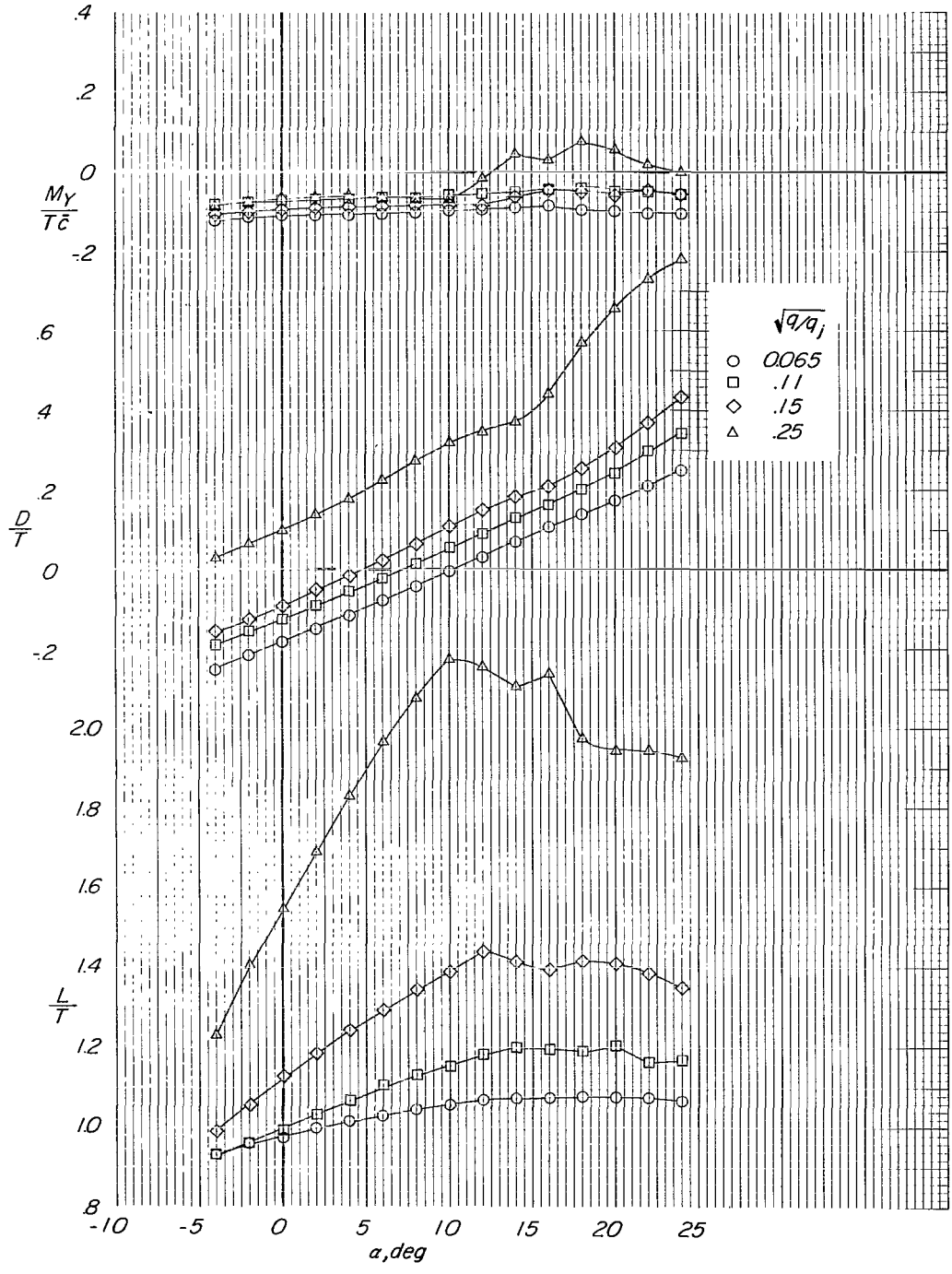

(d) Tail off.

Figure 9.- Concluded.

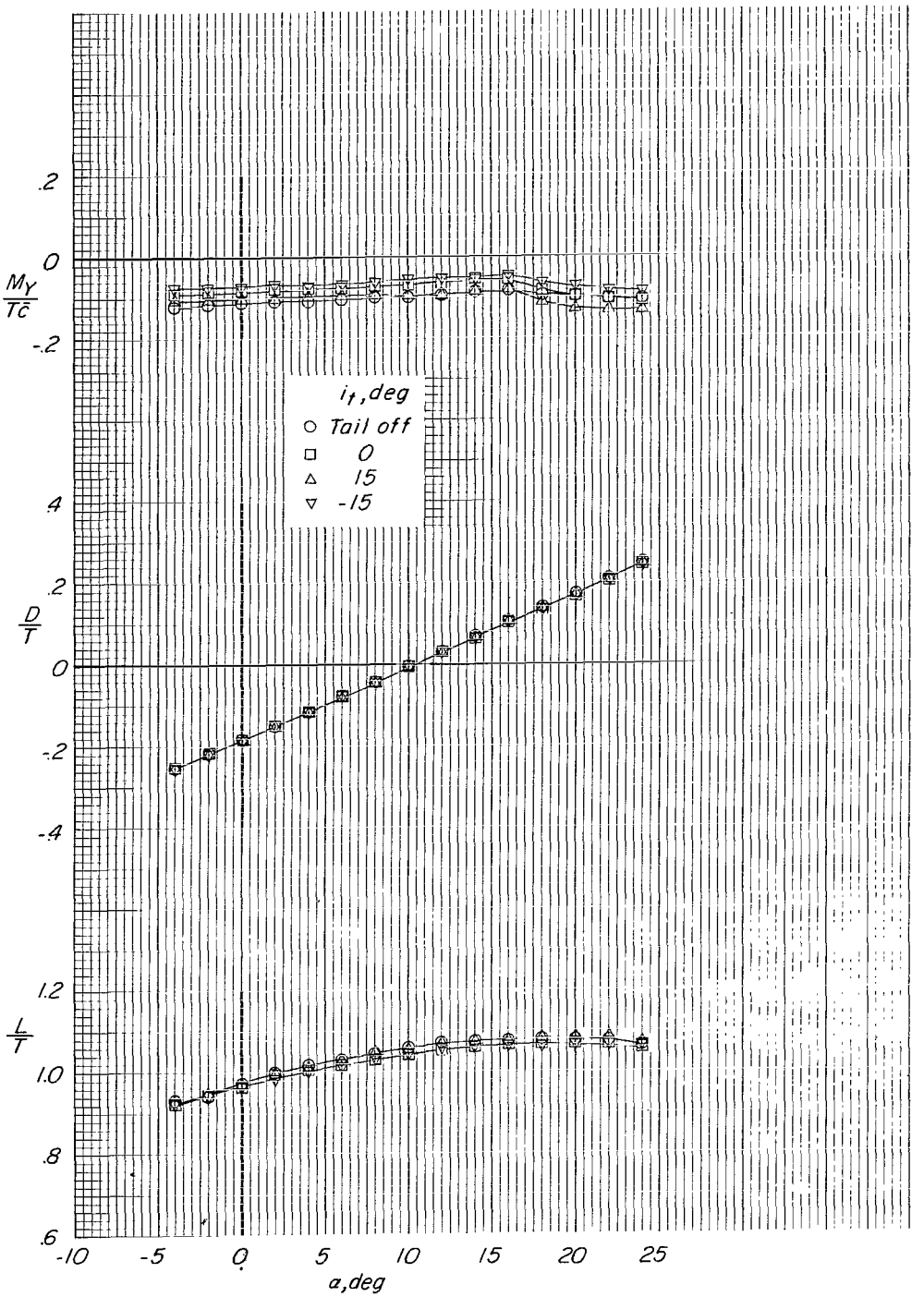

(a) $\sqrt{q/q_j} = 0.065$.

Figure 10.- Effect of horizontal-tail incidence on longitudinal aerodynamic characteristics of model with large tail in low position. Flaps on; power on; engine pods inboard.

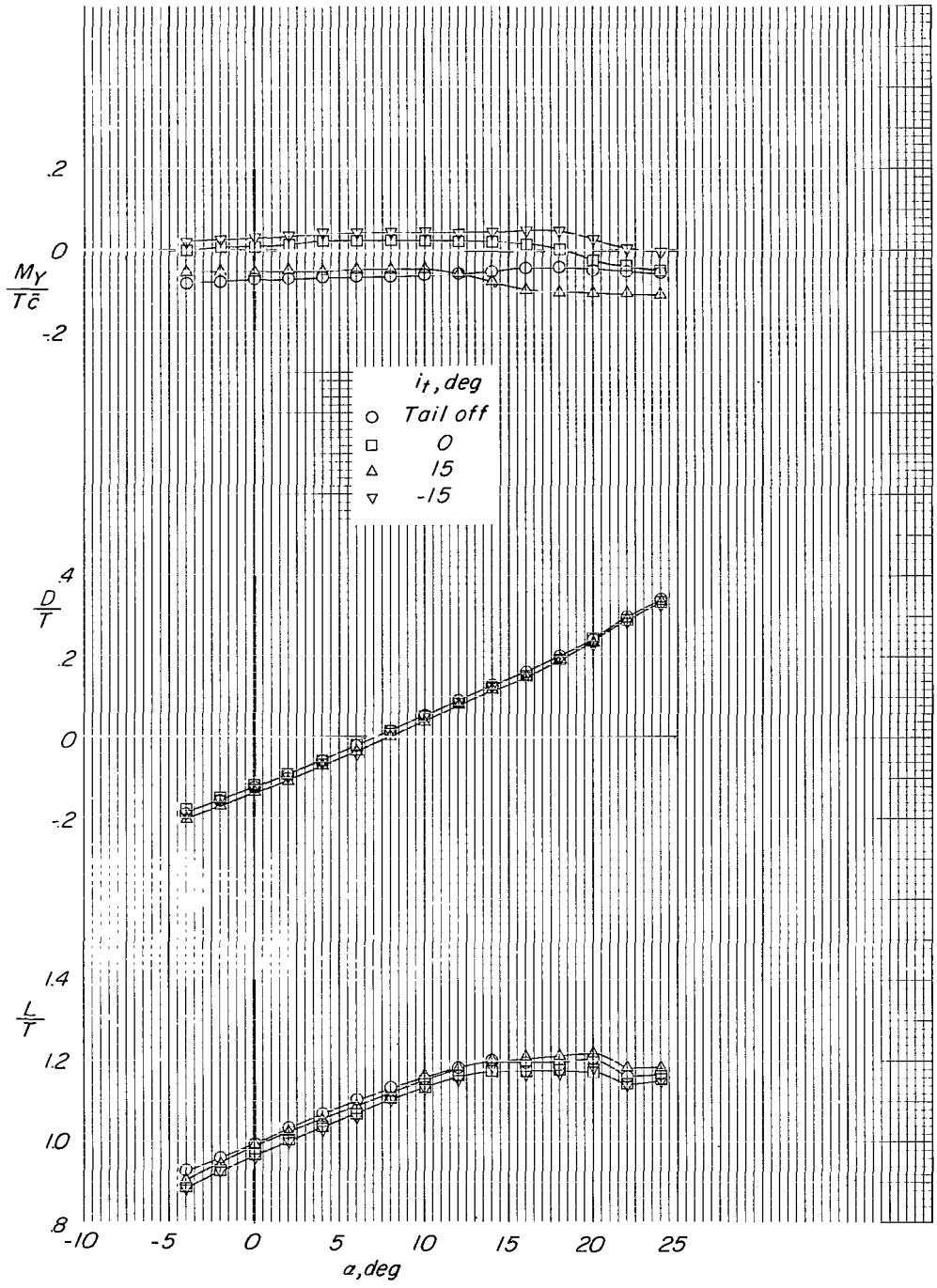

(b) $\sqrt{q/q_j} = 0.11$.

Figure 10.- Continued.

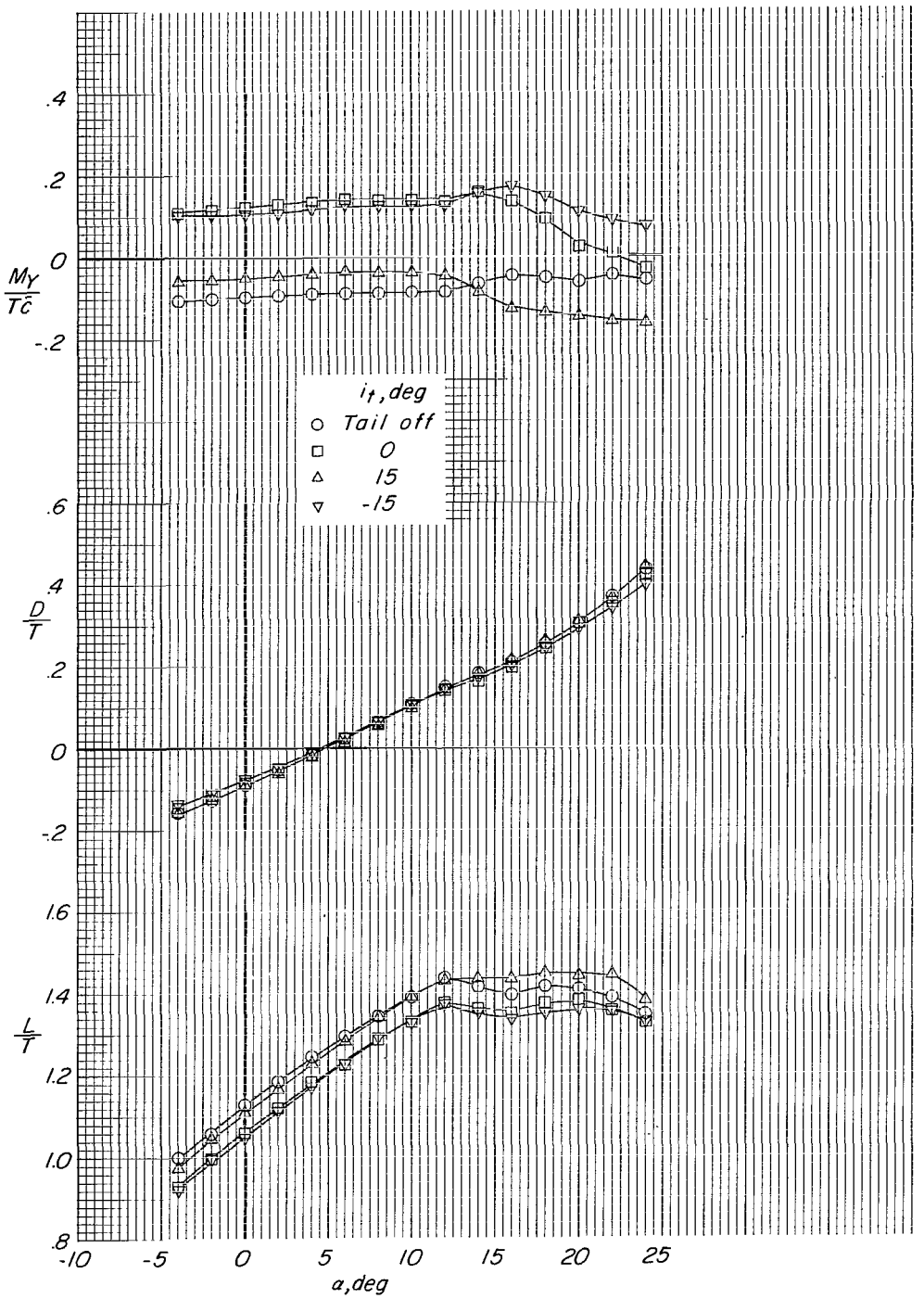

(c) $\sqrt{q/q_j} = 0.15$.

Figure 10.- Continued.

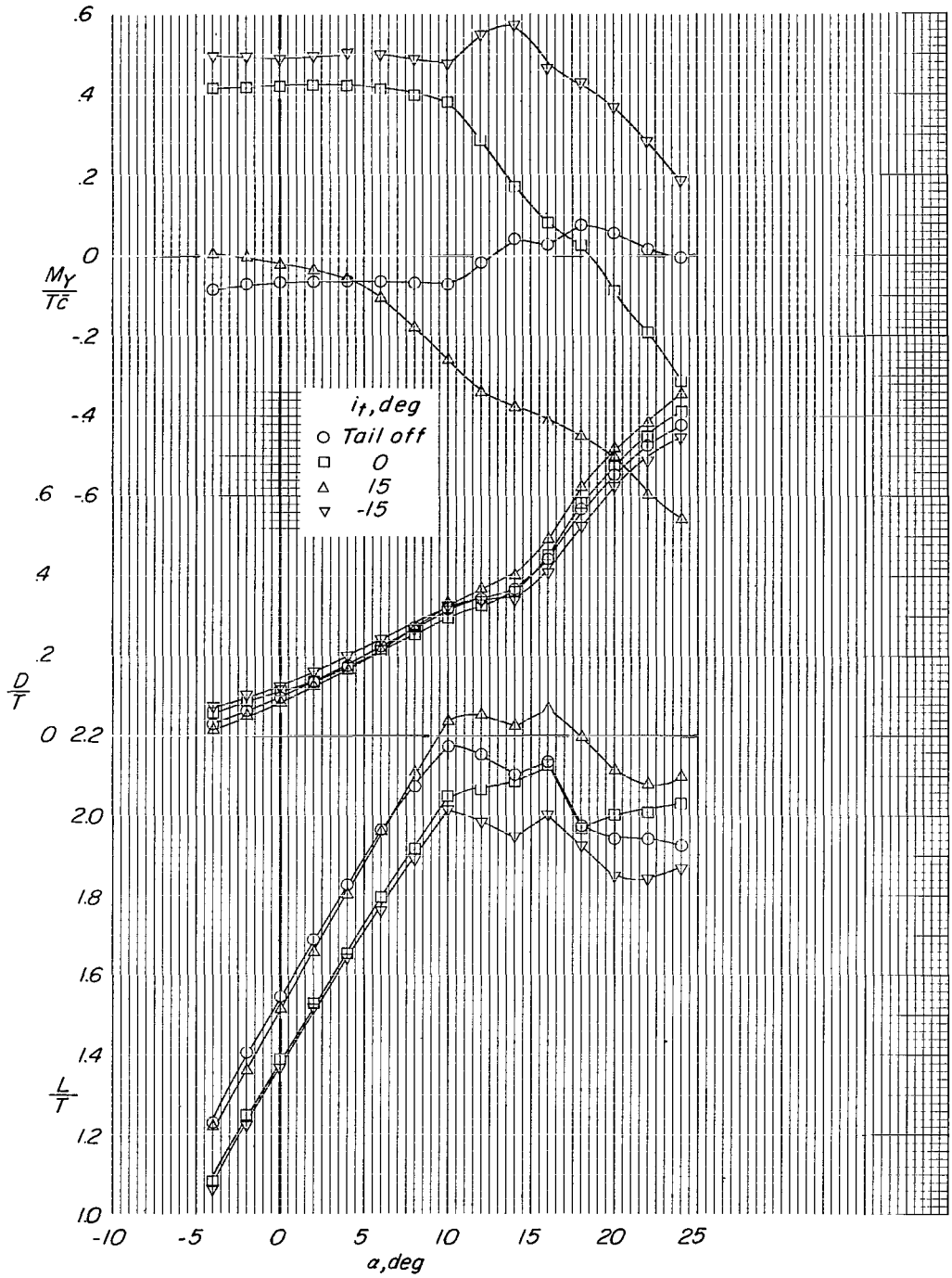

(d) $\sqrt{q/q_j} = 0.25$.

Figure 10.- Concluded.

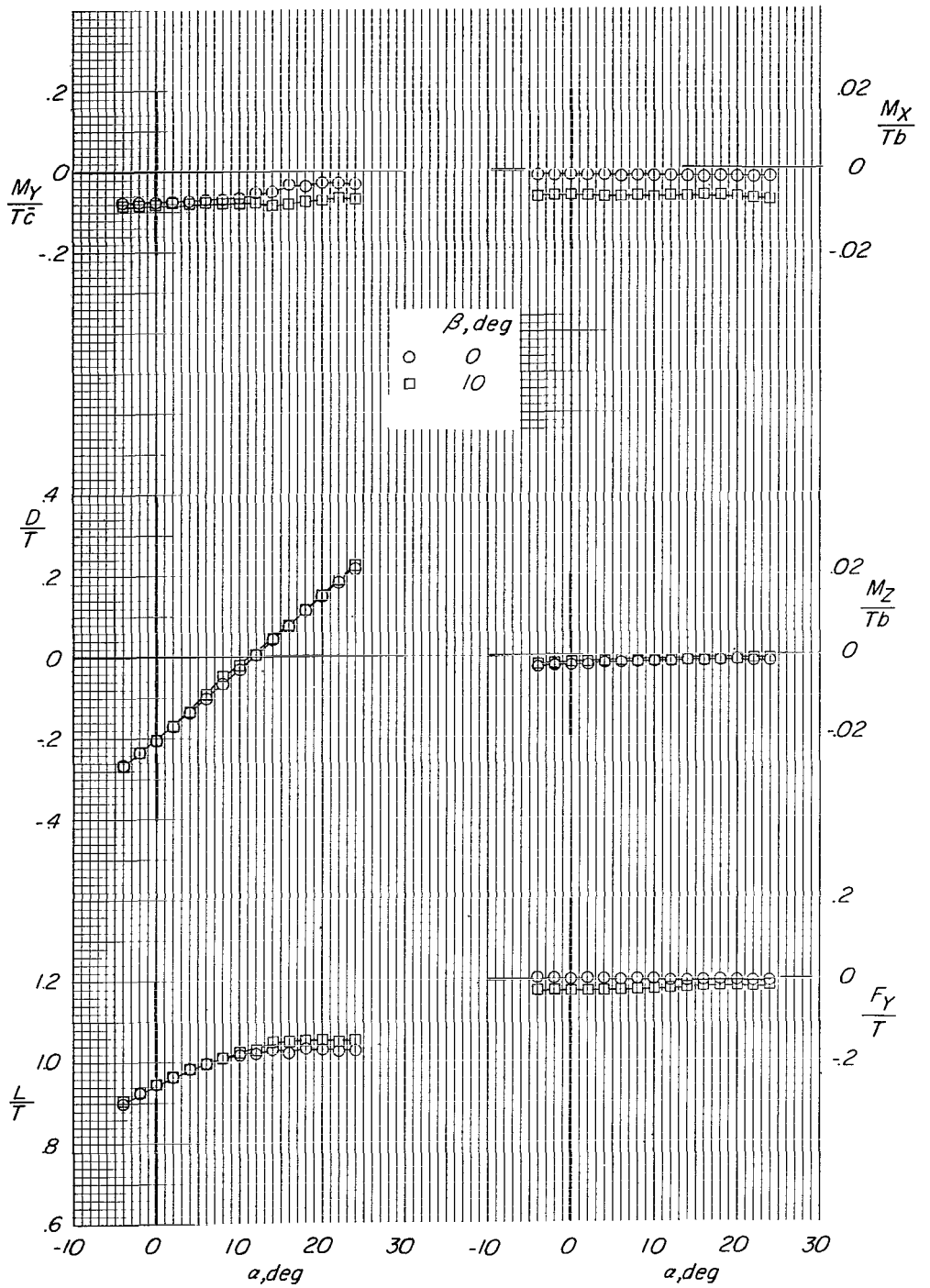

(a) $\sqrt{q/q_j} = 0.065$.

Figure 11.- Effect of 10^0 of sideslip on aerodynamic characteristics of model with large tail in low position and with flaps off and vertical tail removed. Power on; $i_t = 0^0$; engine pods inboard.

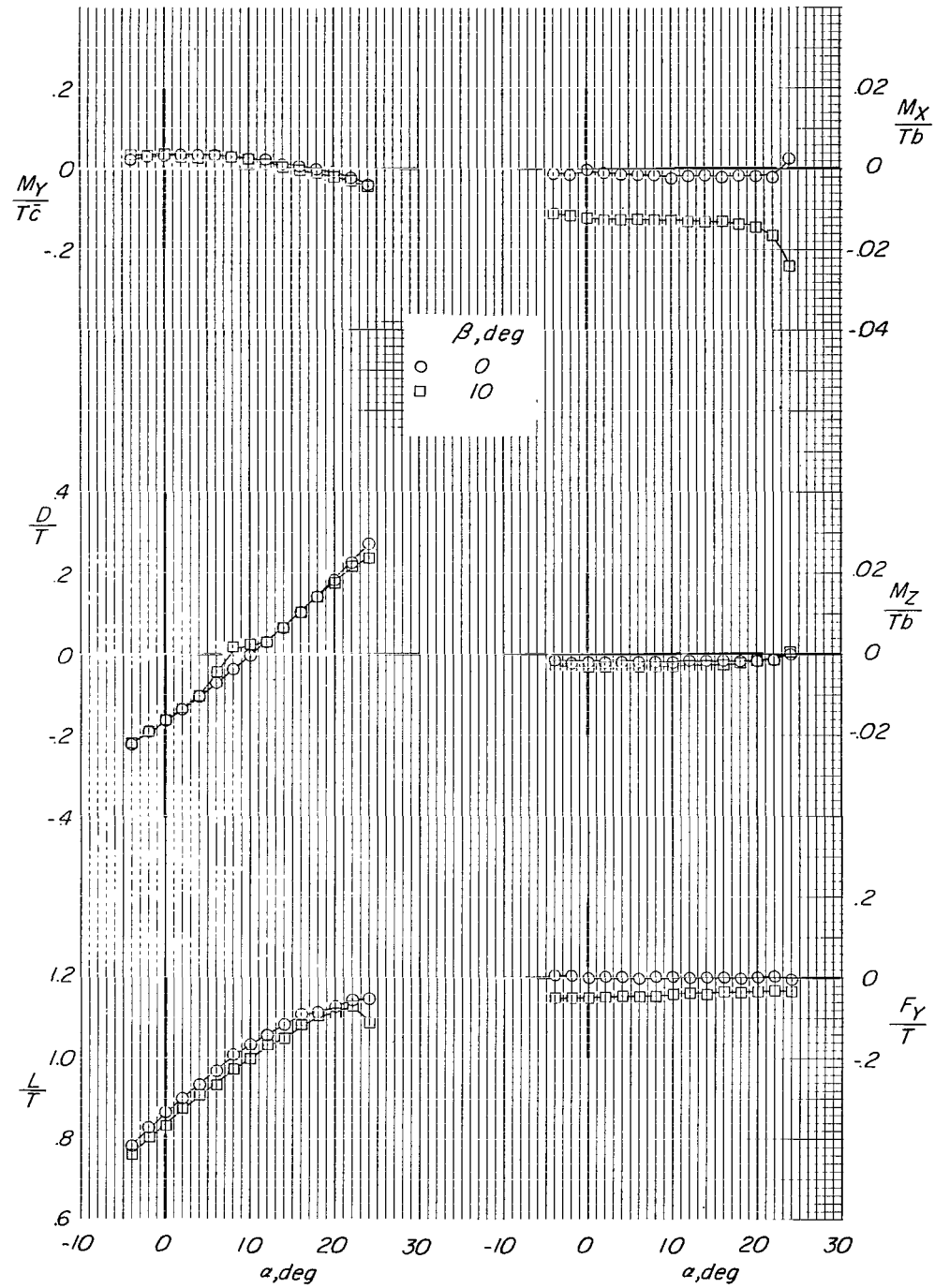

(b) $\sqrt{q/q_j} = 0.11$.

Figure 11.- Continued.

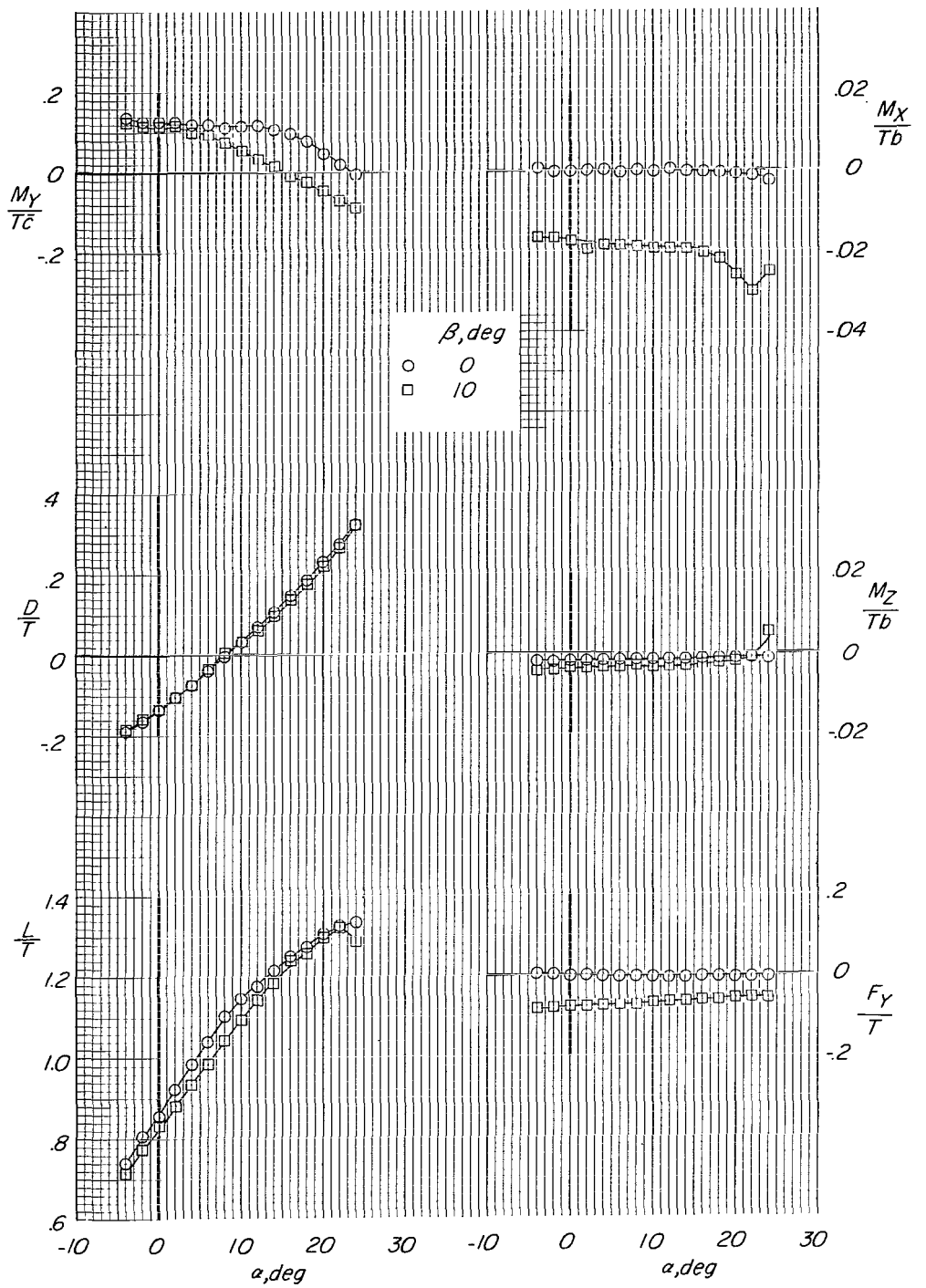

(c) $\sqrt{q/q_j} = 0.15$.

Figure 11.- Continued.

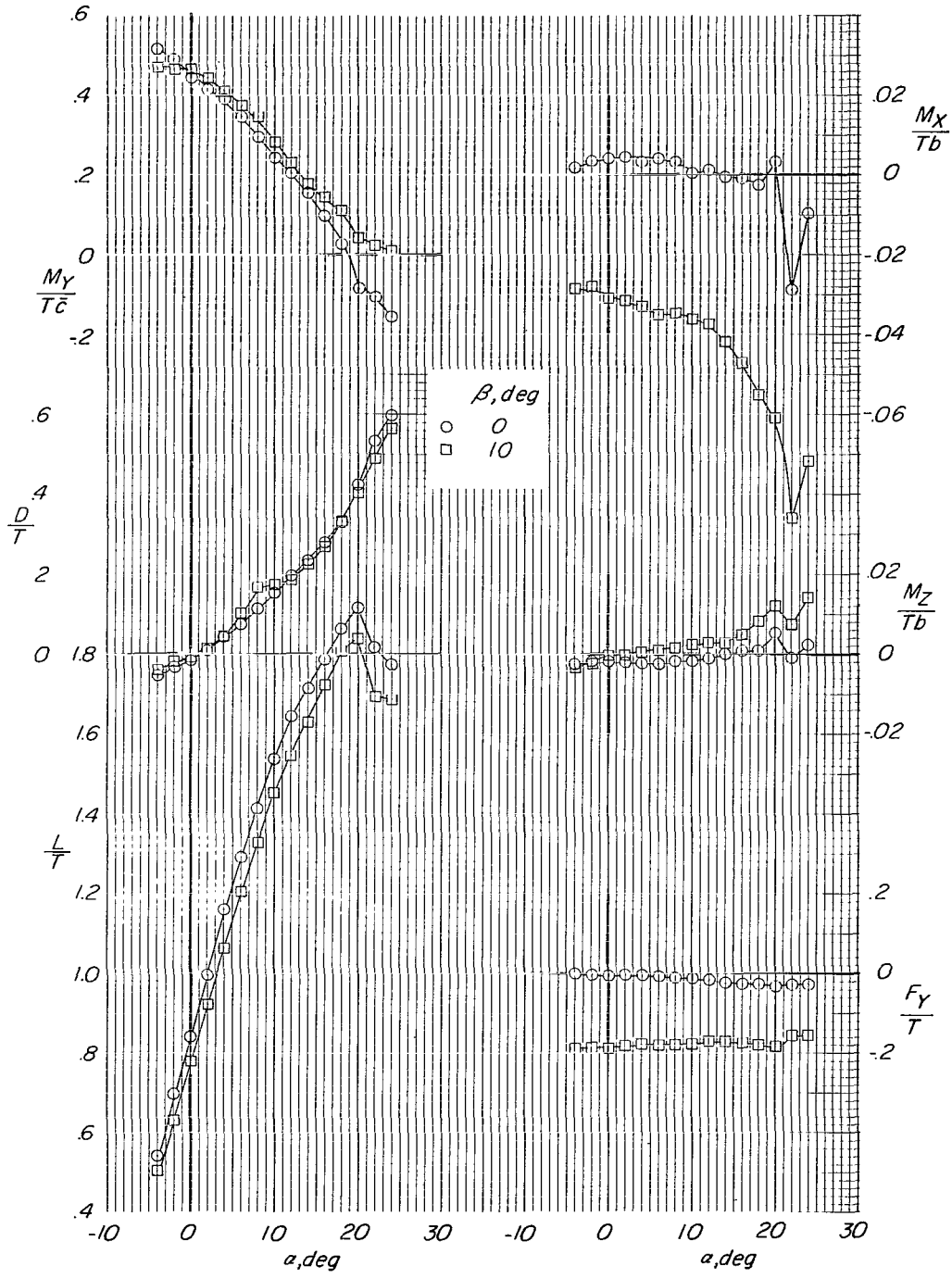

(d) $\sqrt{q/q_j} = 0.25$.

Figure 11.- Concluded.

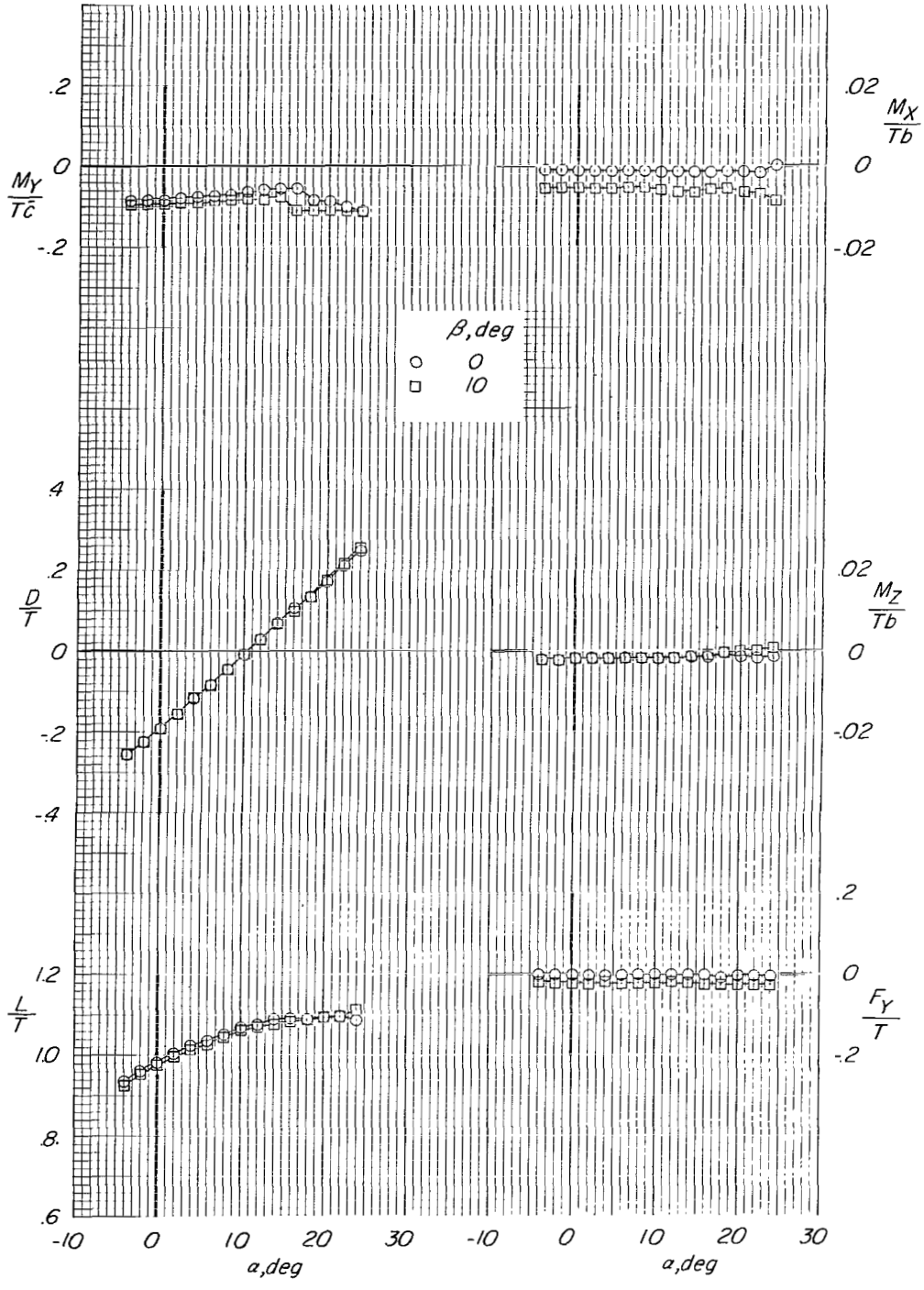

(a) $\sqrt{q/q_j}$ = 0.065.

Figure 12.- Effect of 10^0 of sideslip on aerodynamic characteristics of model with large tail in low position with flaps on and vertical tail removed. Power on; $i_t = 0^0$; engine pods inboard.

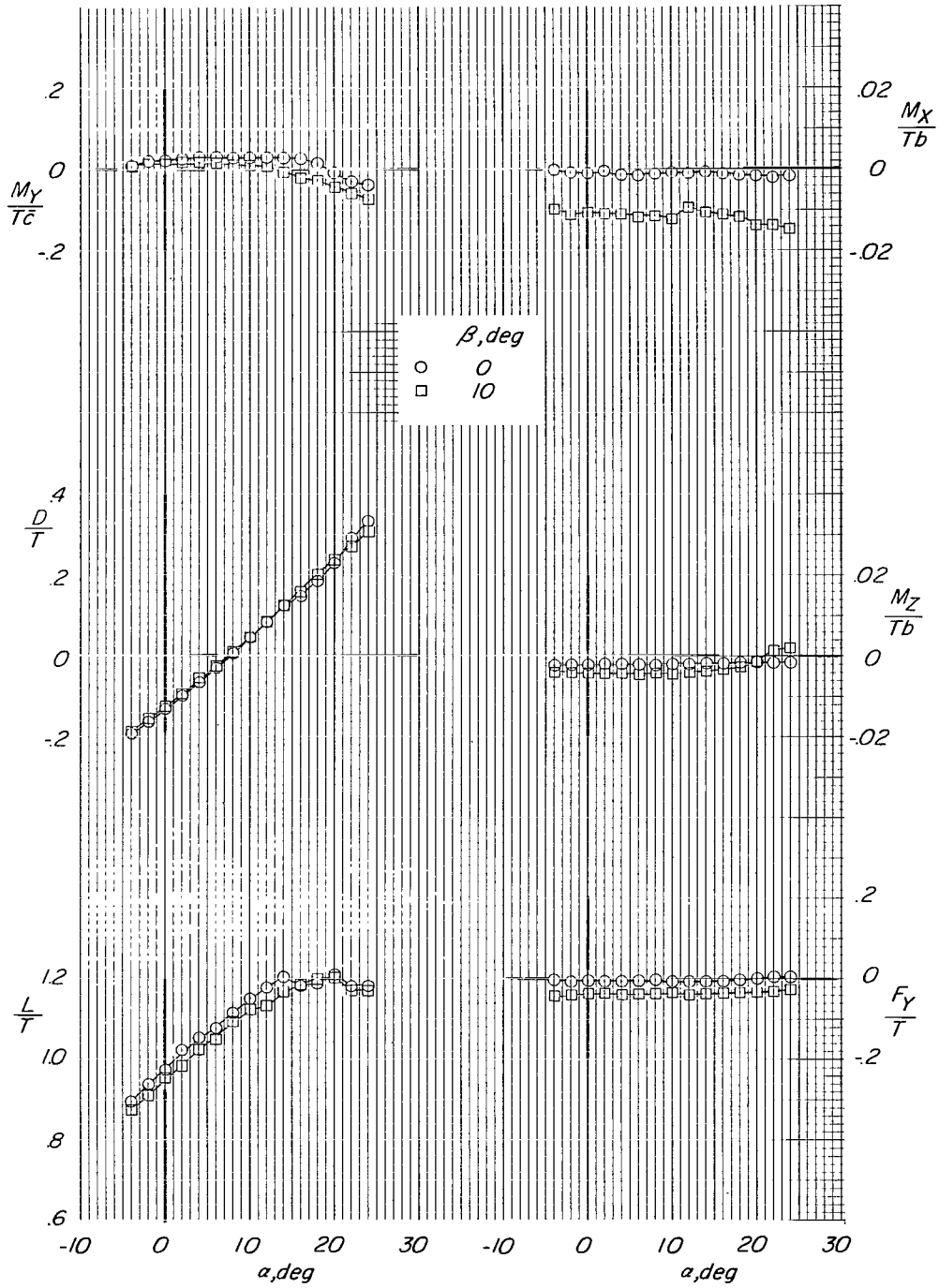

(b) $\sqrt{q/q_j} = 0.11$.

Figure 12.- Continued.

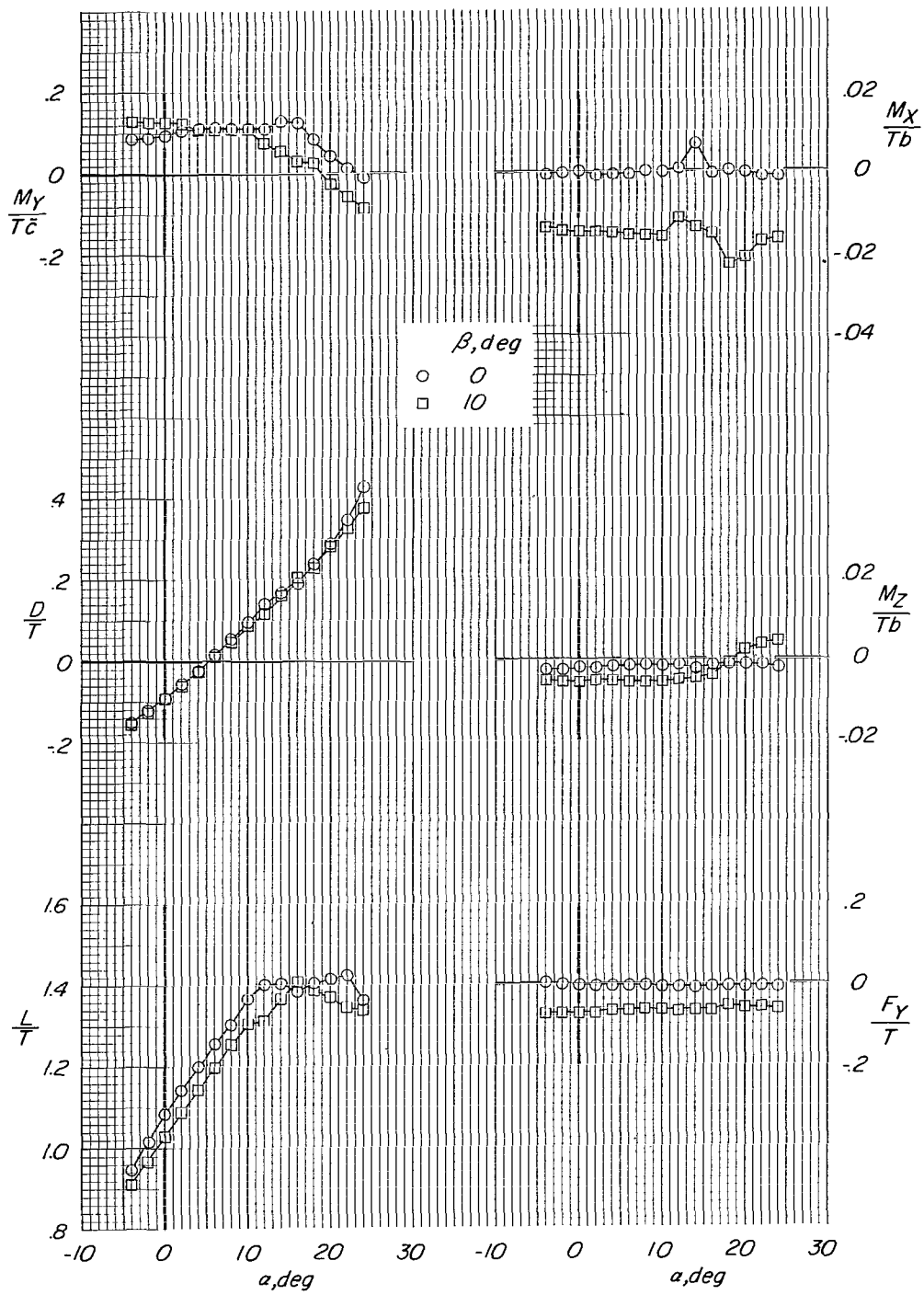

(c) $\sqrt{q/q_j} = 0.15$.

Figure 12.- Continued.

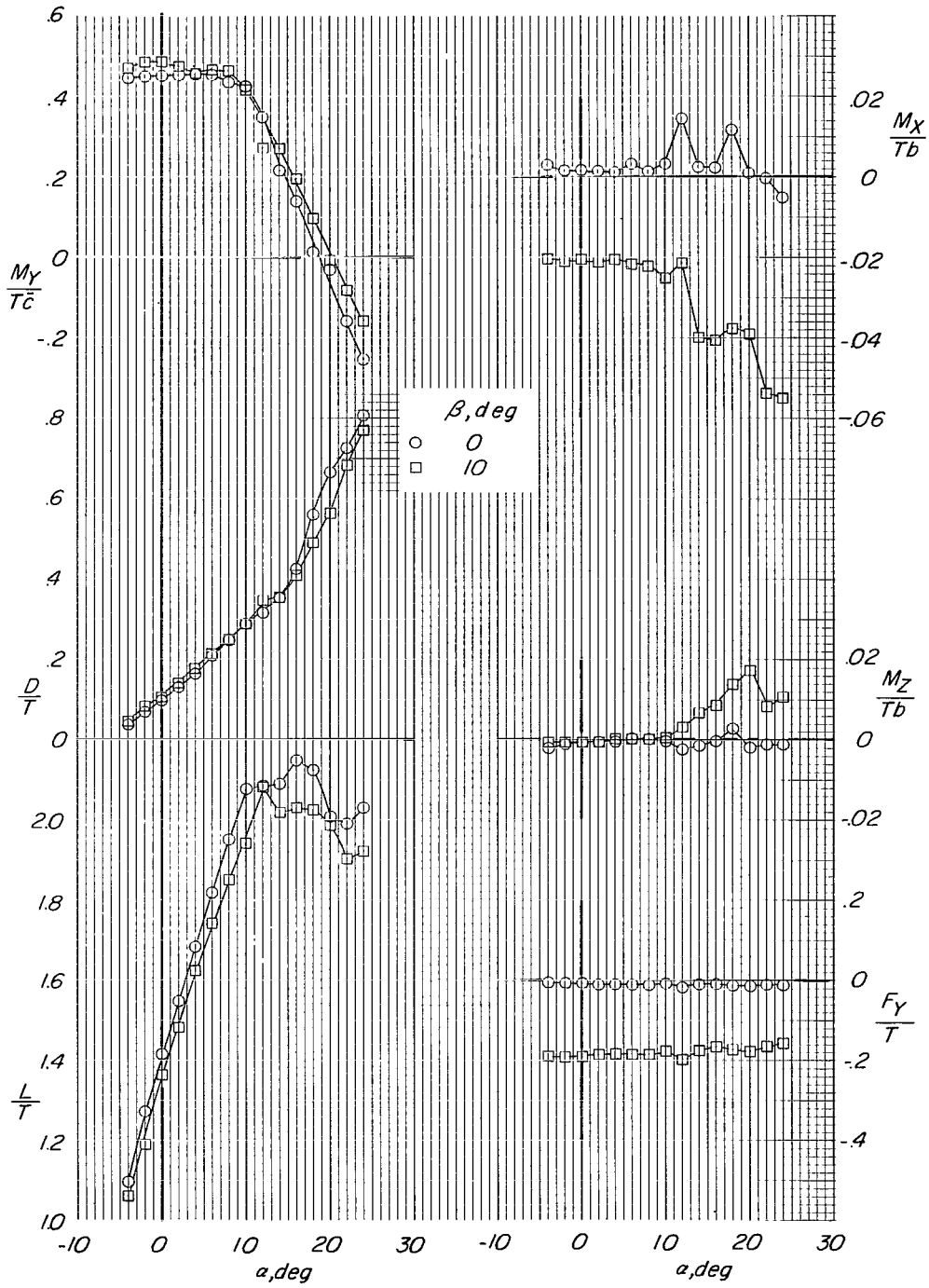

(d) $\sqrt{q/q_j} = 0.25$.

Figure 12.- Concluded.

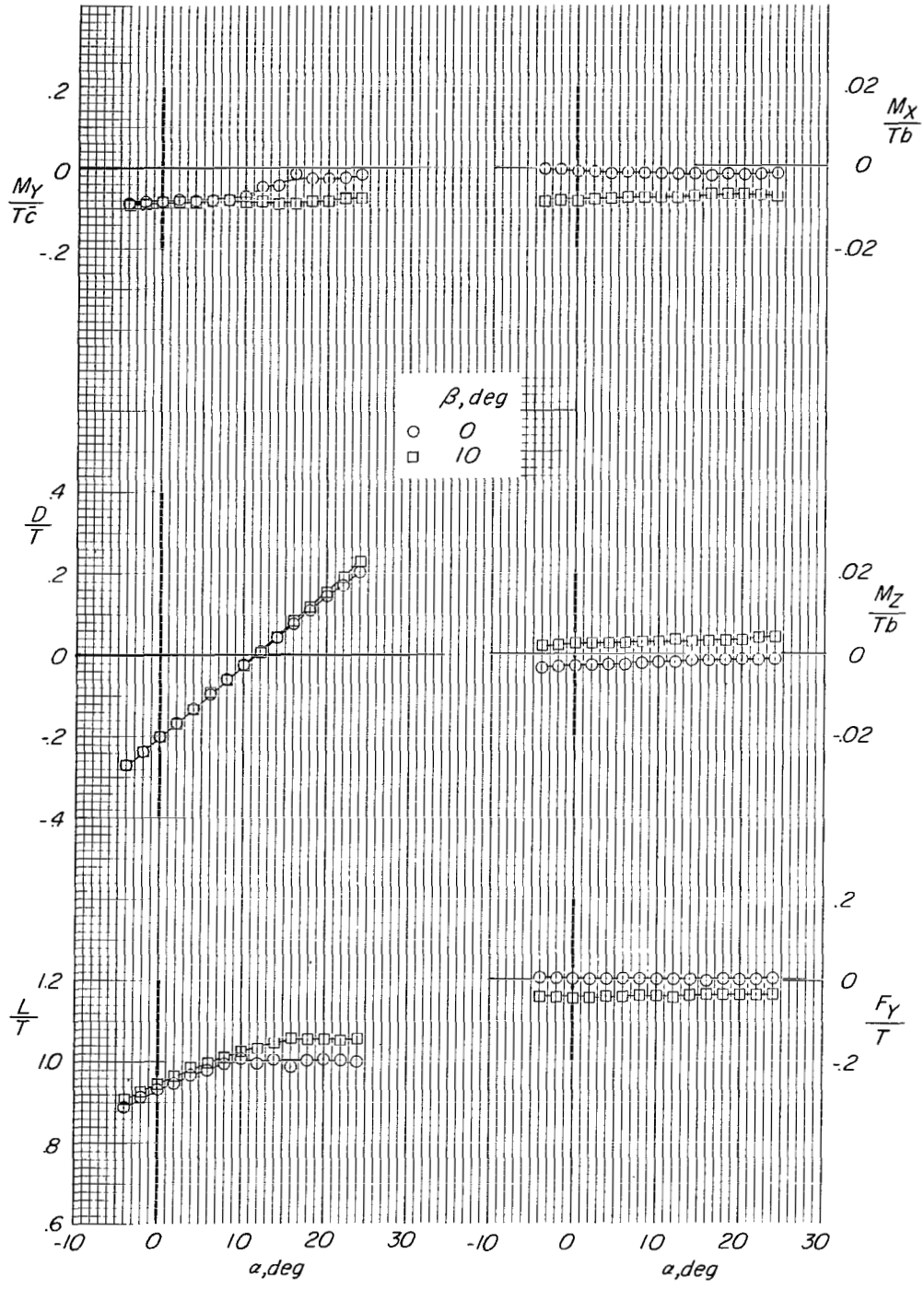

(a) $\sqrt{q/q_j} = 0.065$.

Figure 13.- Effect of 10^0 of sideslip on model aerodynamic characteristics with large tail in low position. Flaps off; power on; $i_t = 0^0$; engine pods inboard.

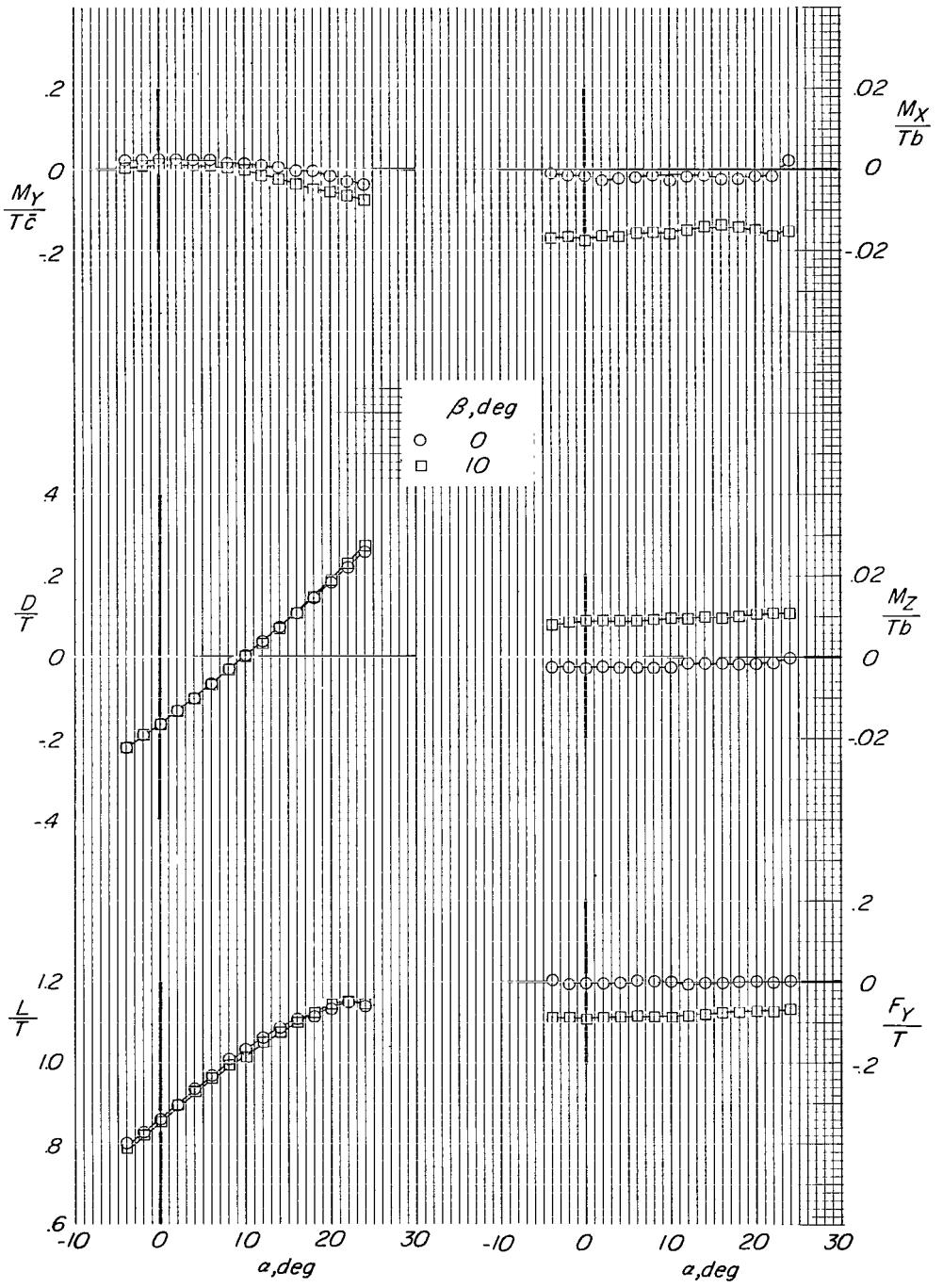

(b) $\sqrt{q/q_j} = 0.11$.

Figure 13.- Continued.

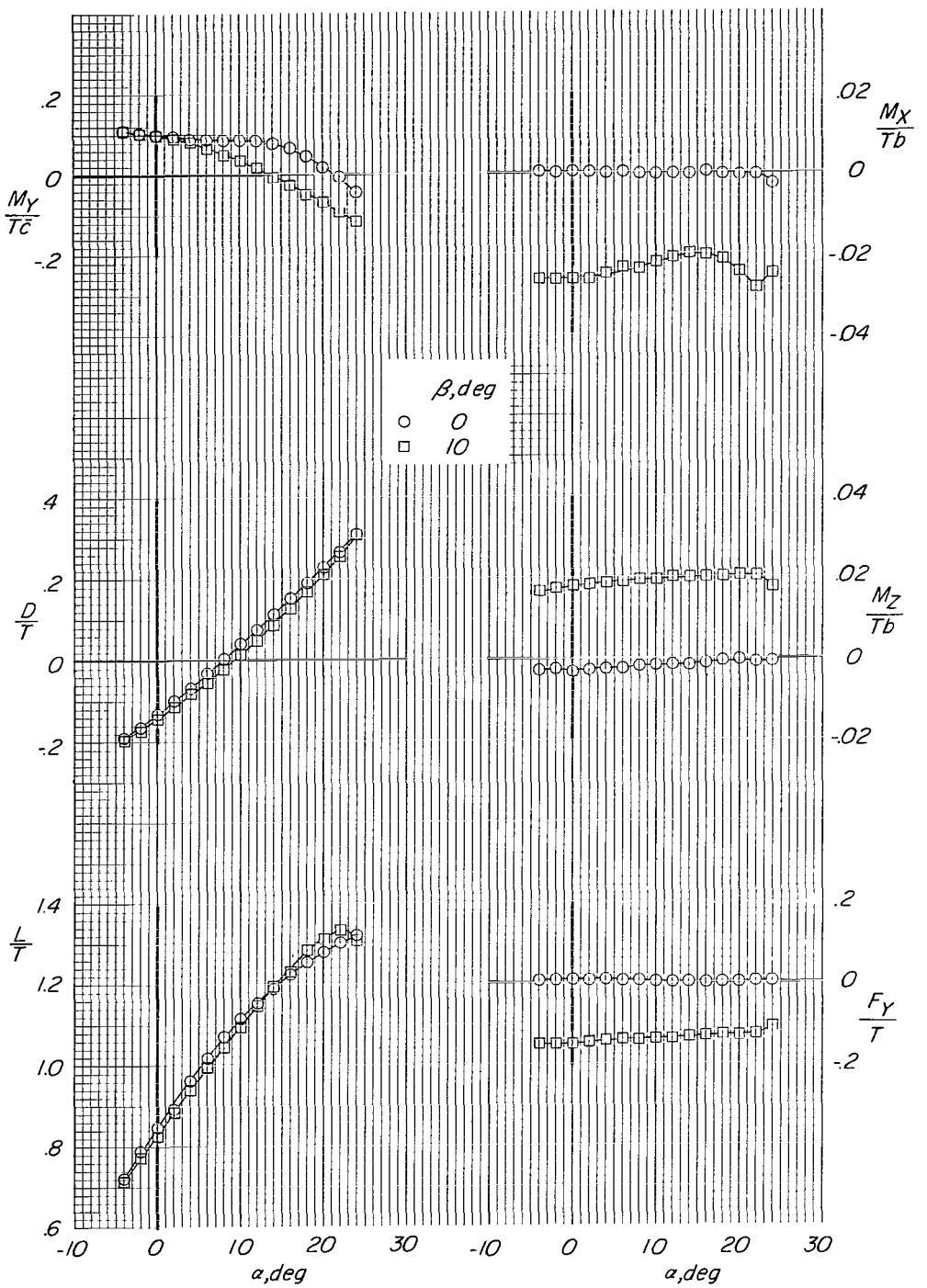

(c) $\sqrt{q/q_j} = 0.15$.

Figure 13.- Continued.

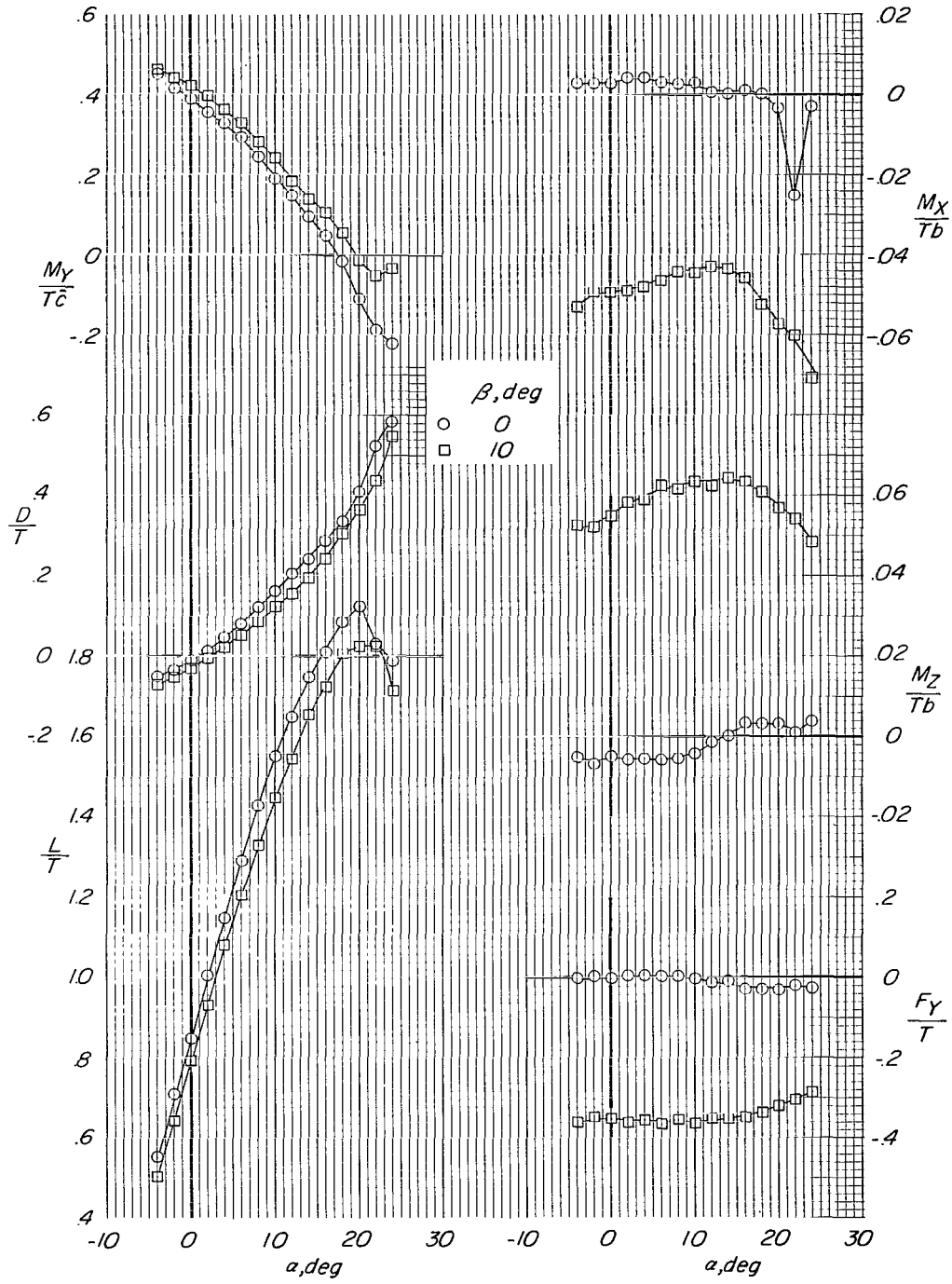

(d) $\sqrt{q/q_j} = 0.25$.

Figure 13.- Concluded.

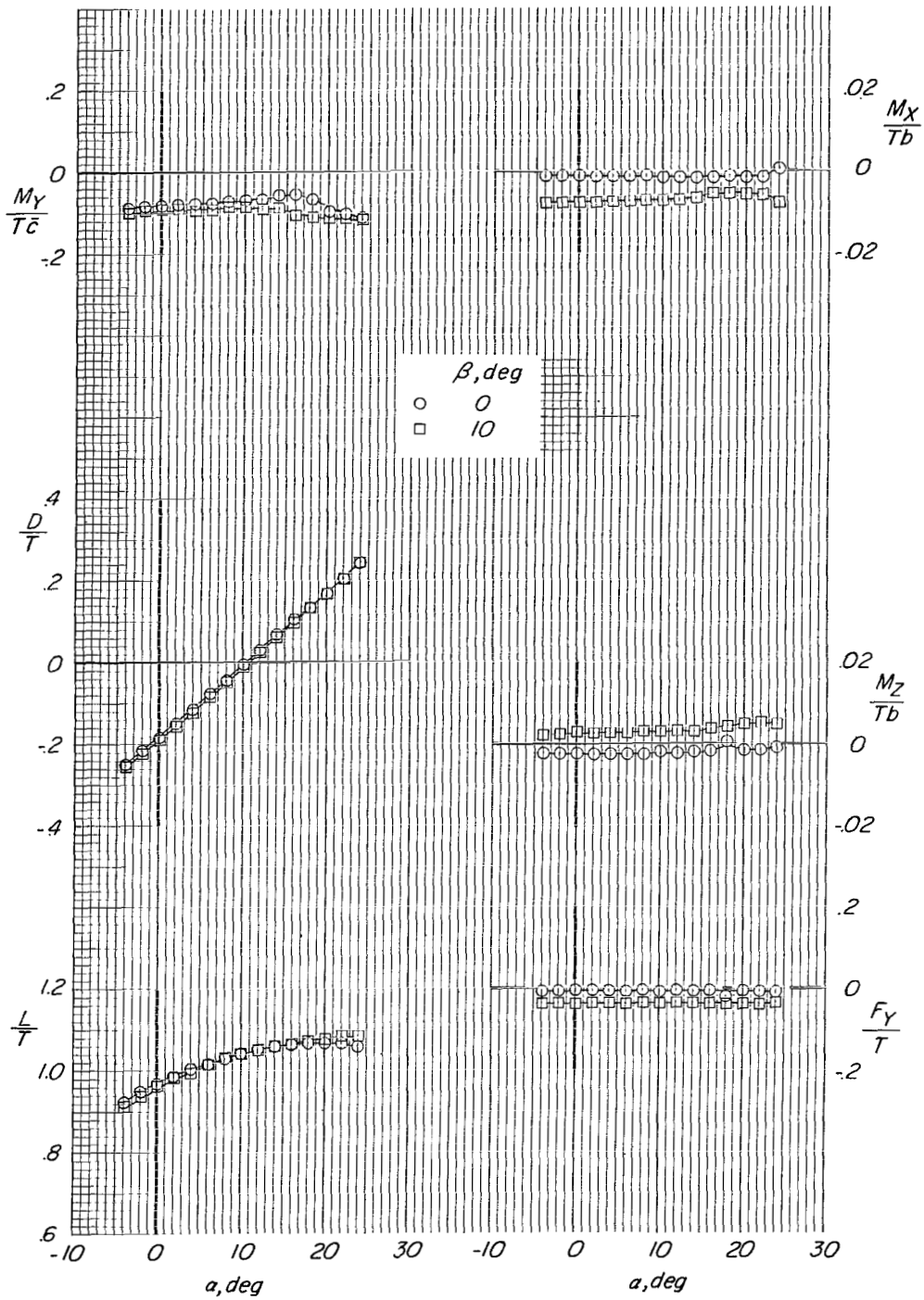

(a) $\sqrt{q/q_j} = 0.065$.

Figure 14.- Effect of 10^0 of sideslip on model aerodynamic characteristics with large tail in low position. Flaps on; power on; $i_t = 0^0$; engine pods inboard.

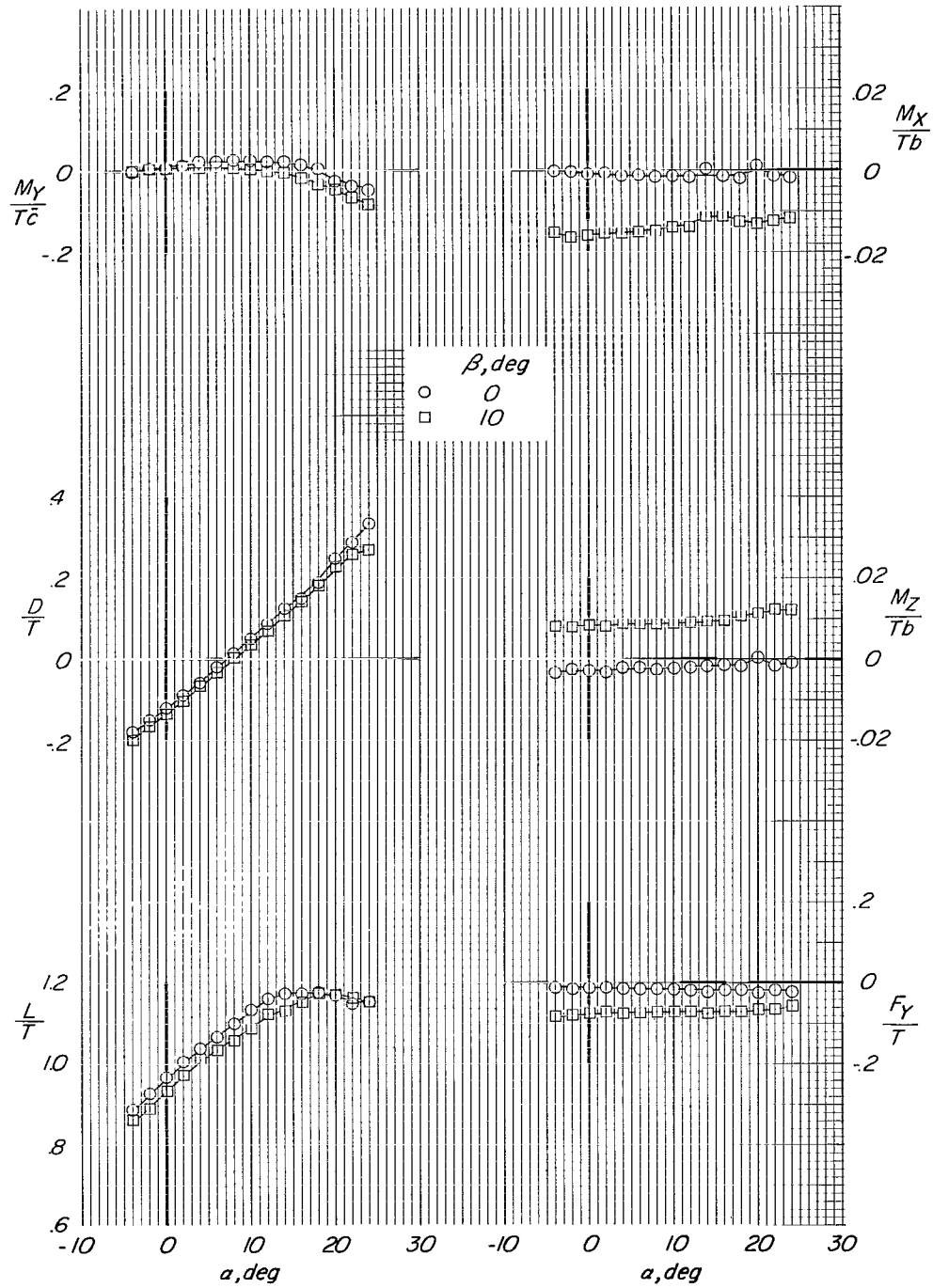

(b) $\sqrt{q/q_j} = 0.11$.

Figure 14.- Continued.

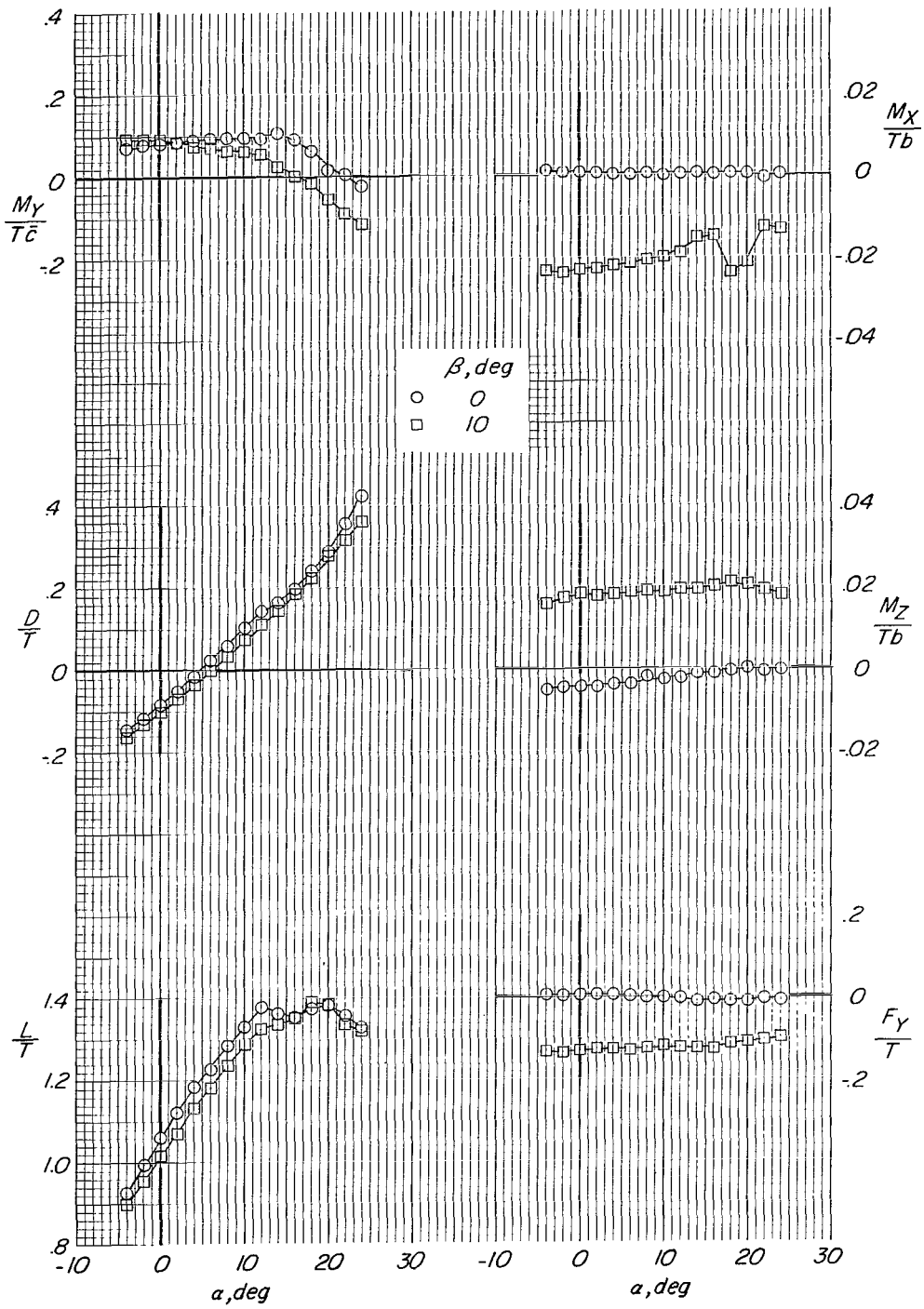

(c) $\sqrt{q/q_j} = 0.15$.

Figure 14.- Continued.

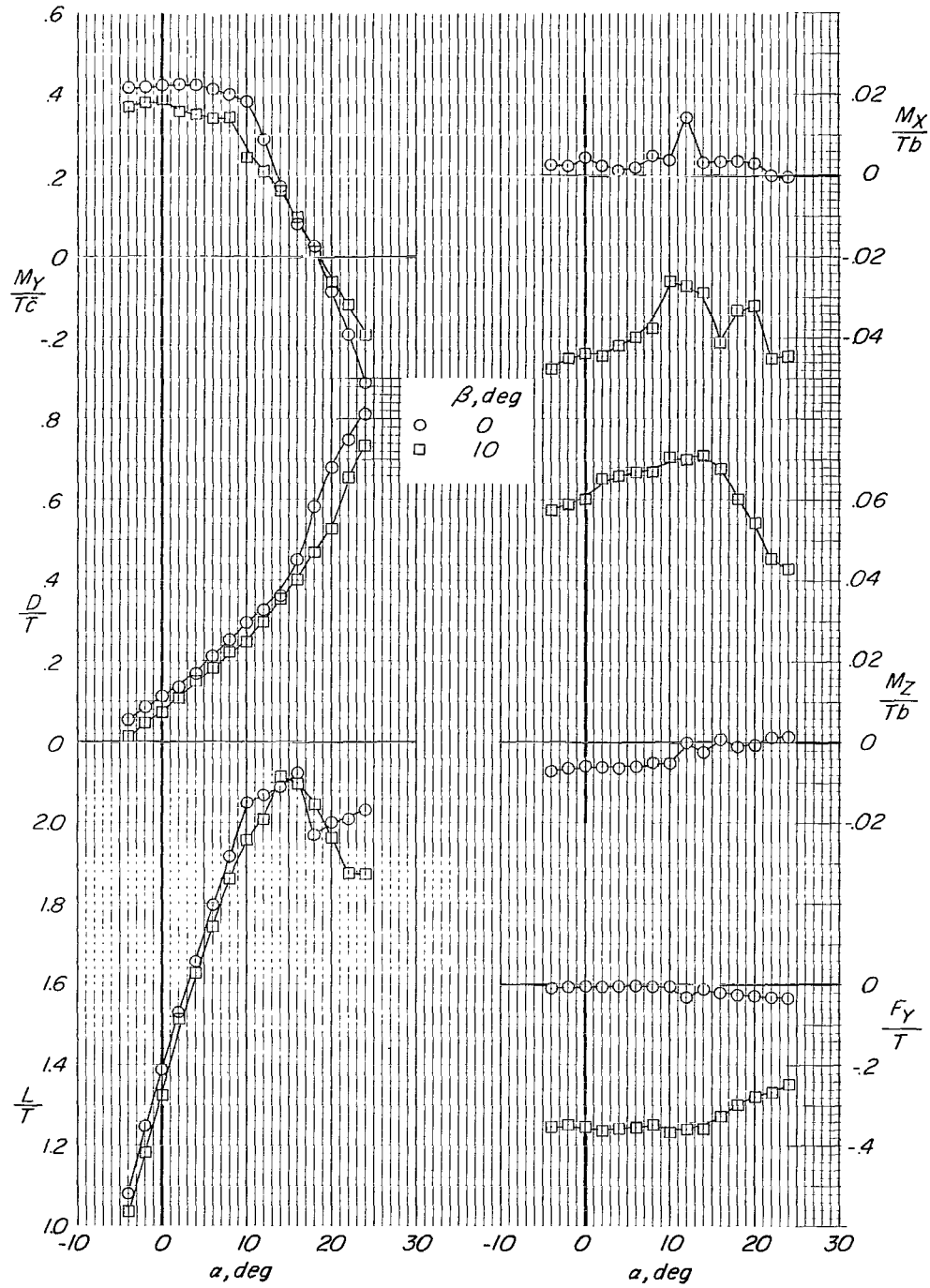

(d) $\sqrt{q/q_j} = 0.25$.

Figure 14.- Concluded.

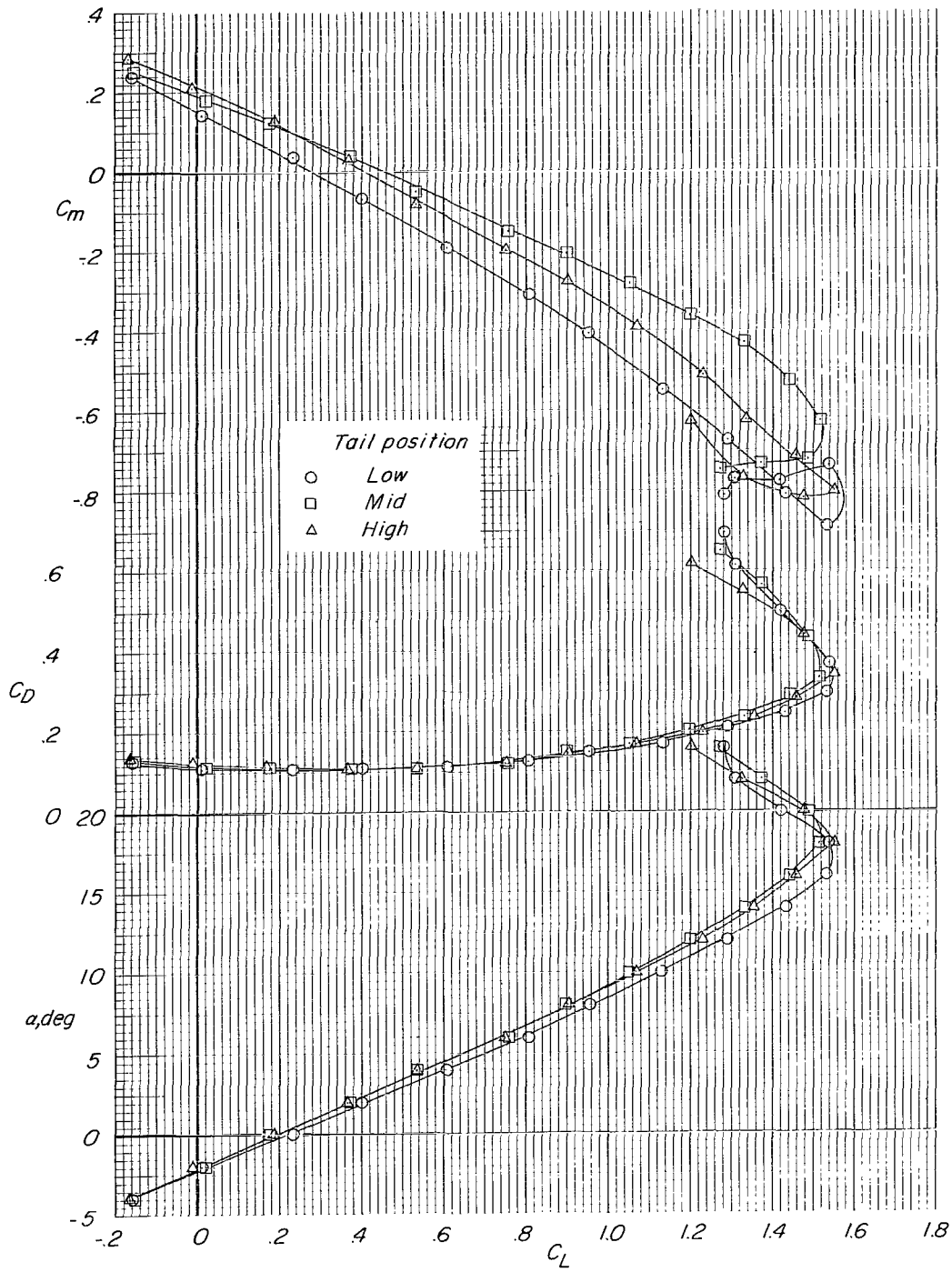

Figure 15.- Longitudinal aerodynamic characteristics of model with large horizontal tail at three locations. Flaps off; power off; $i_t = 0^0$; engine pods at midspan.

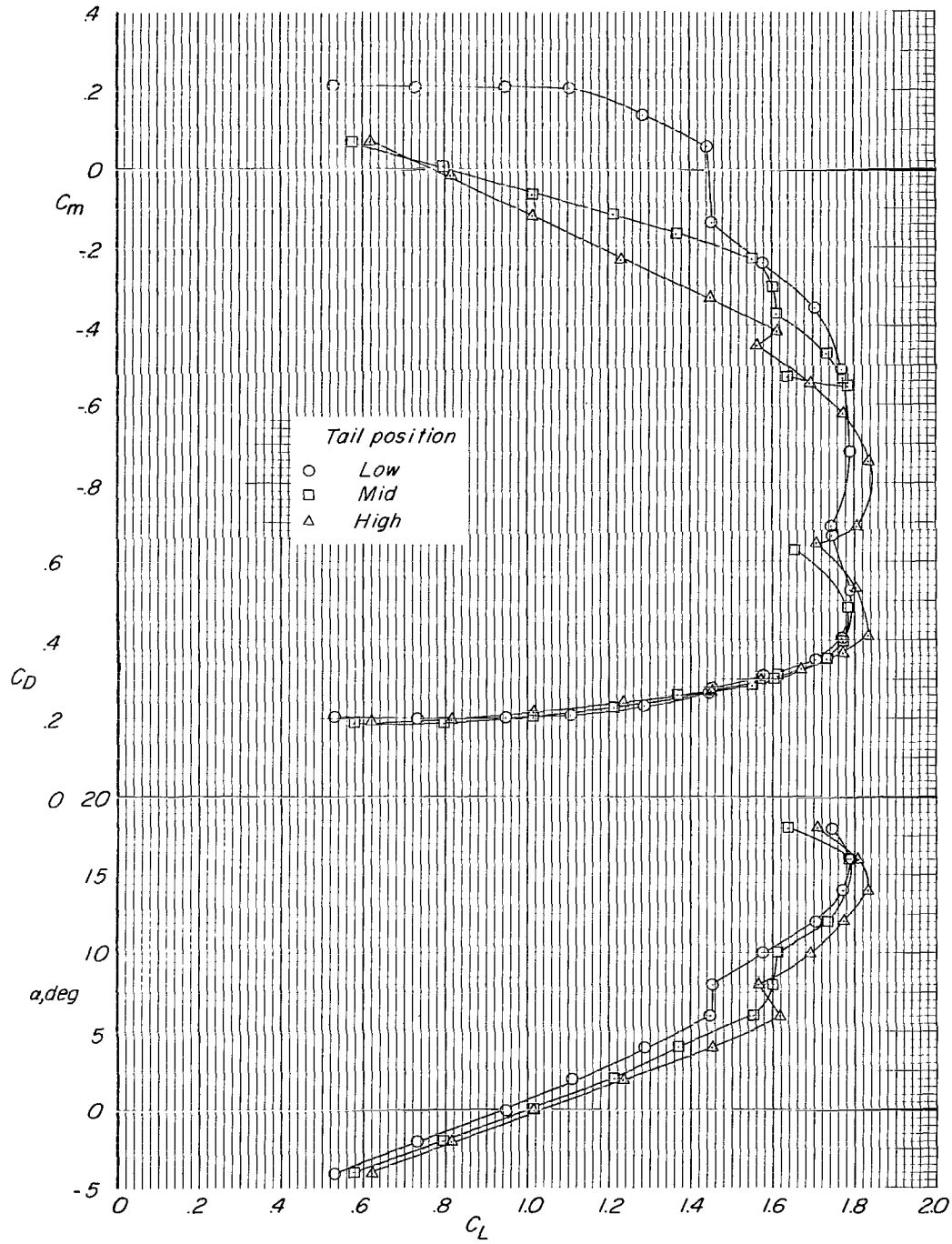

(a) Large tail.

Figure 16.- Longitudinal aerodynamic characteristics of model with small and large tail at three locations. Flaps on; power off; $i_t = 0^0$; engine pods at midspan.

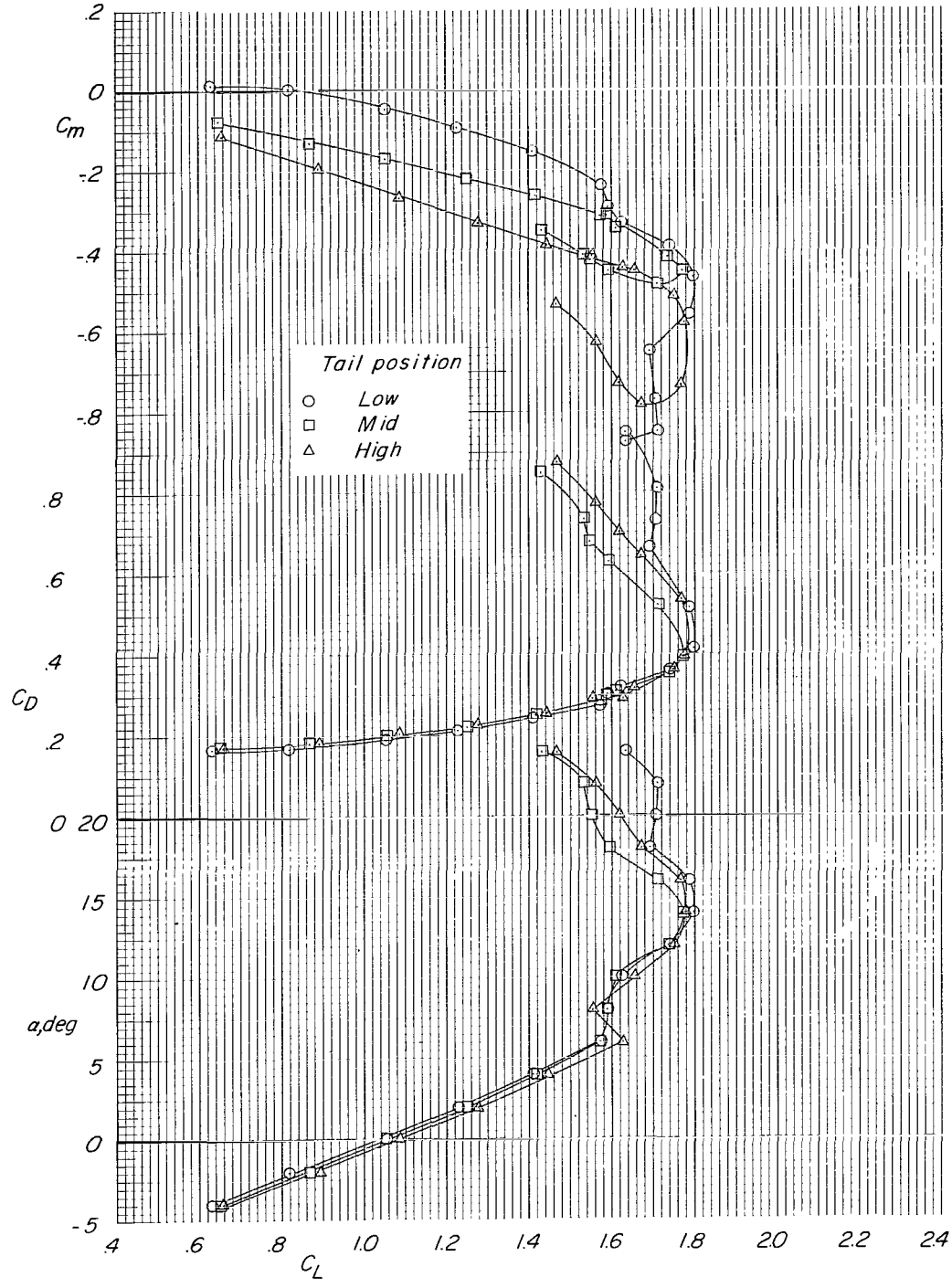

(b) Small tail.

Figure 16.- Concluded.

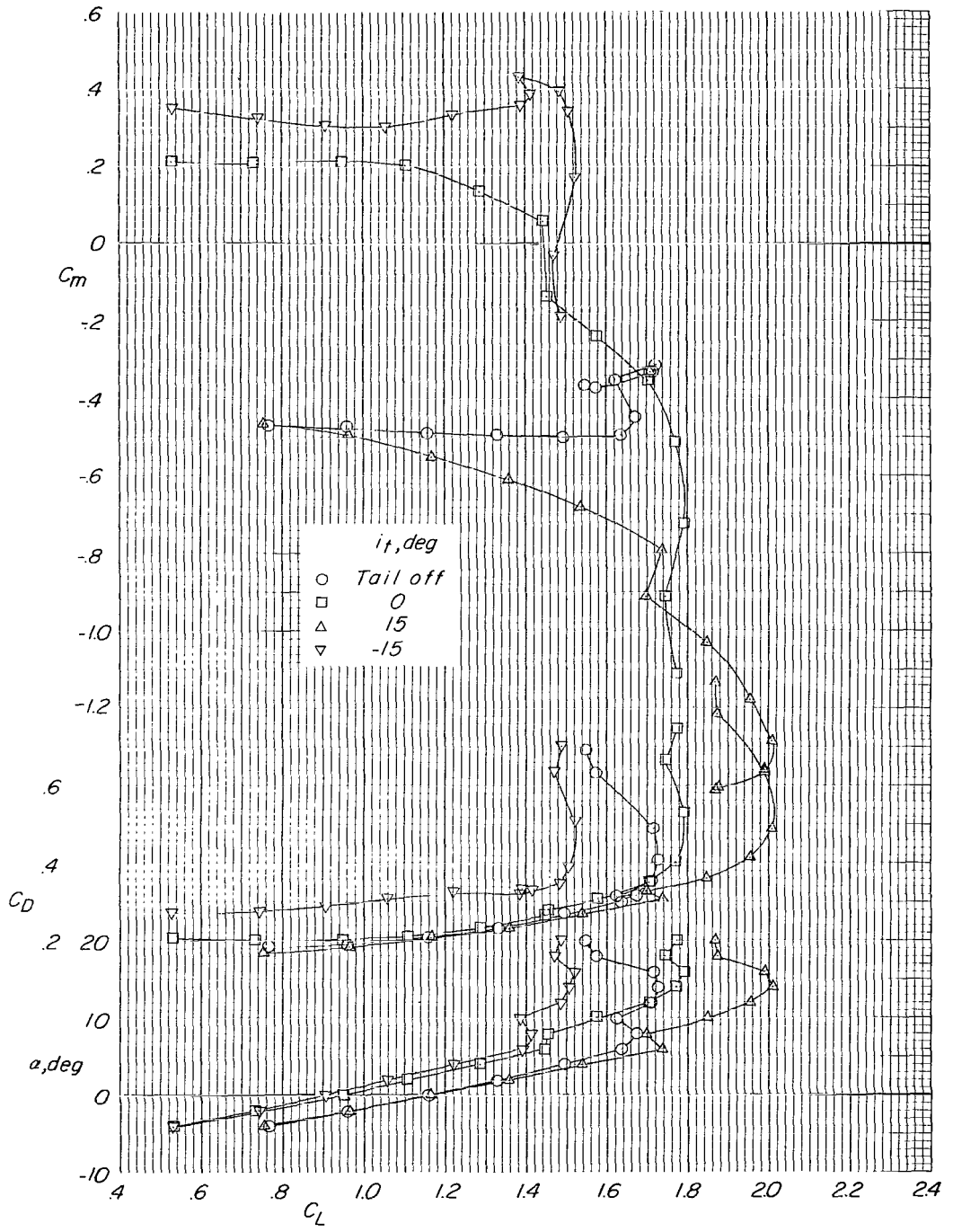

Figure 17.- Effect of horizontal-tail incidence on longitudinal aerodynamic characteristics of model with large tail in low position. Flaps on; power off; engine pods at midspan.

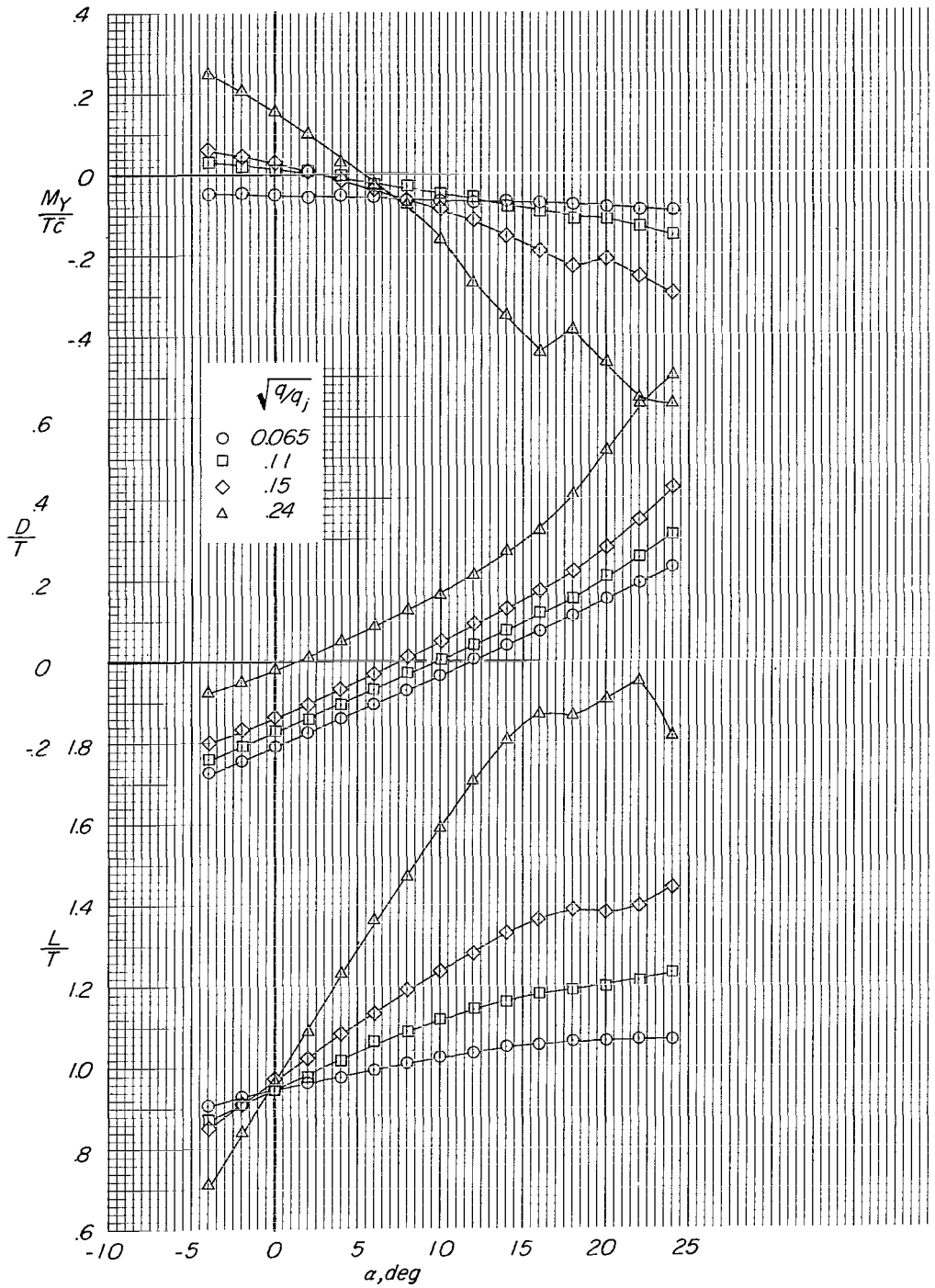

(a) Tail in low position.

Figure 18.- Longitudinal aerodynamic characteristics of model with large horizontal tail at three locations. Flaps off; power on; $i_t = 0^o$; engine pods at midspan.

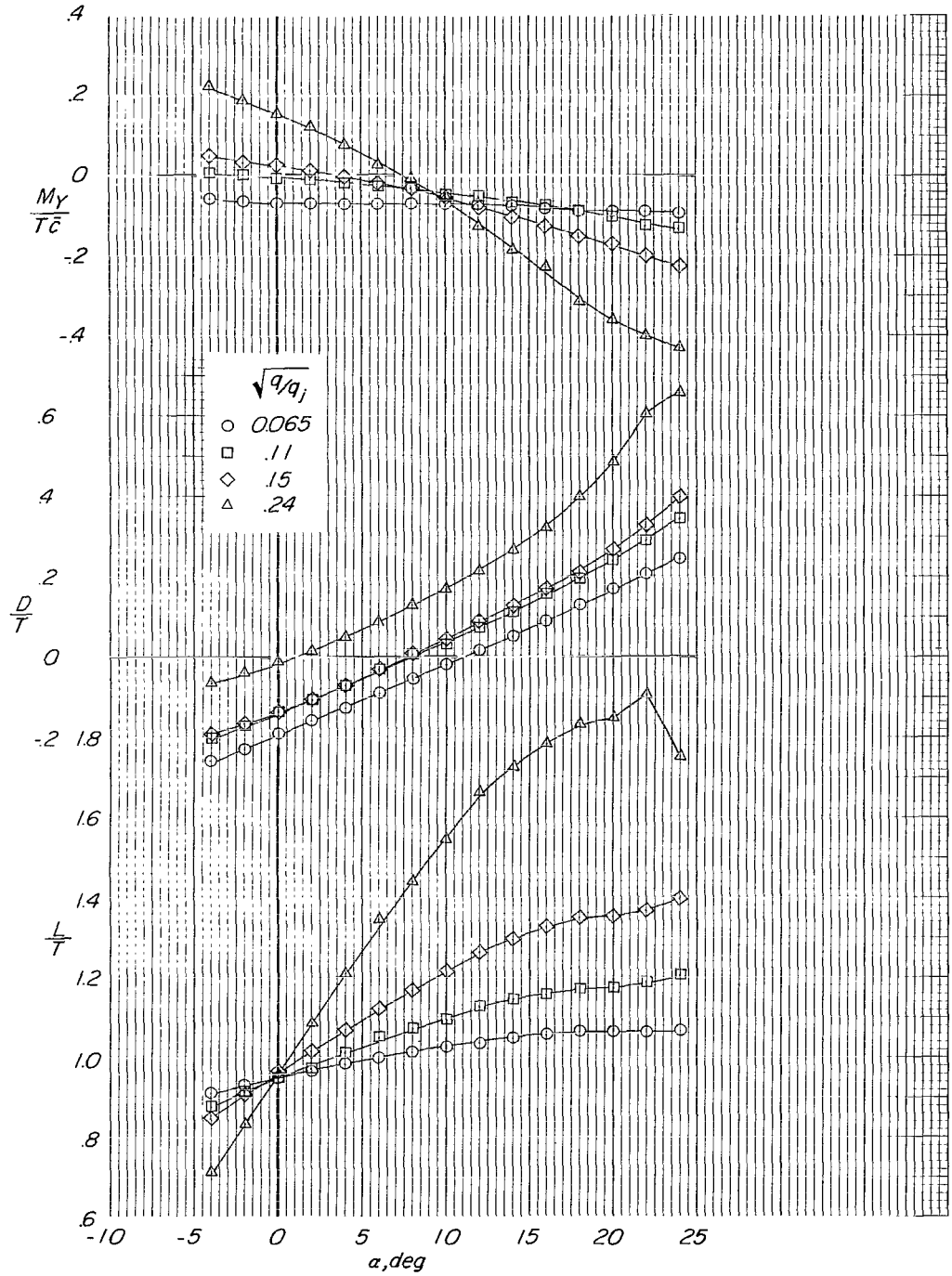

(b) Tail in mid position.

Figure 18.- Continued.

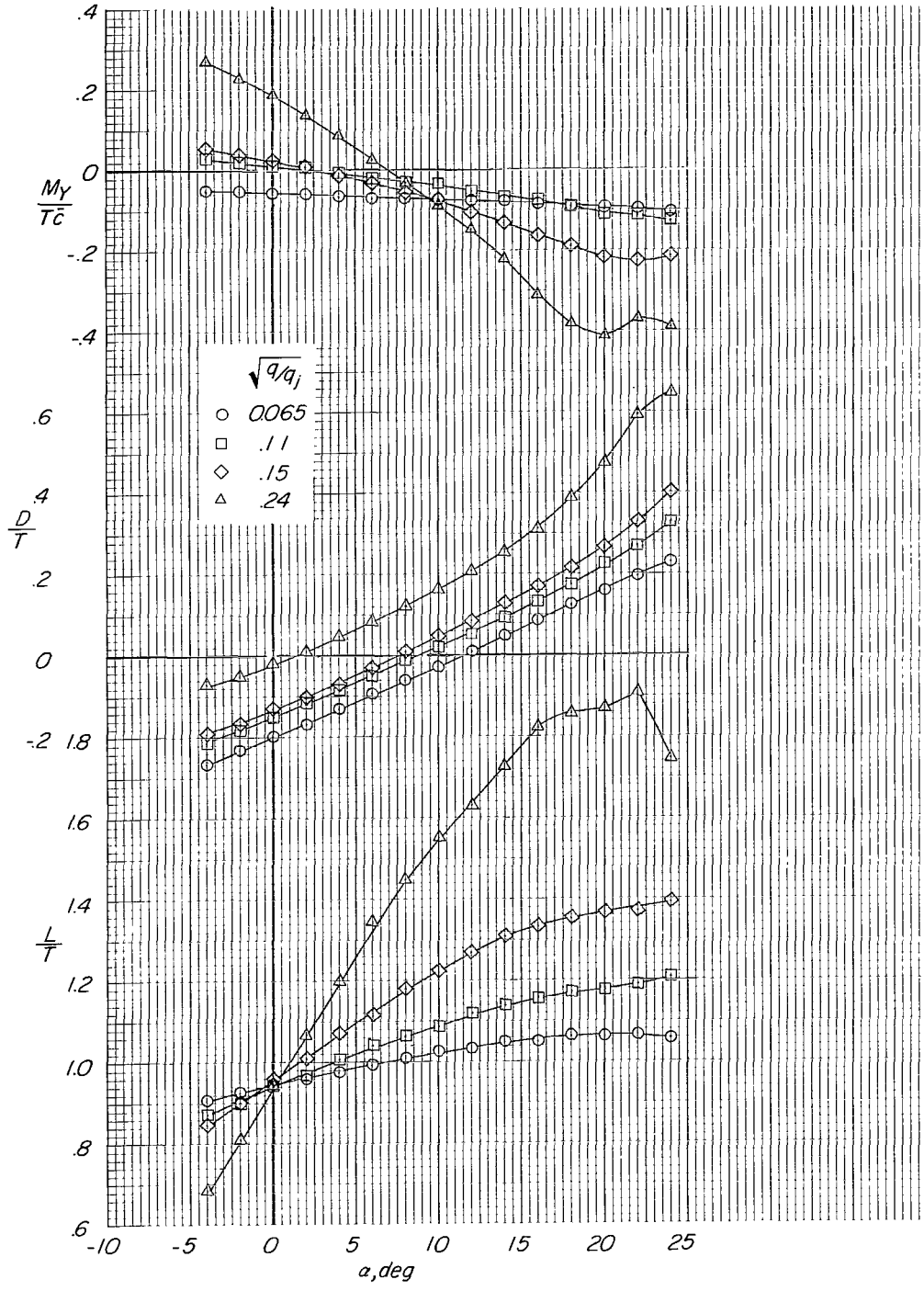

(c) Tail in high position.

Figure 18.- Concluded.

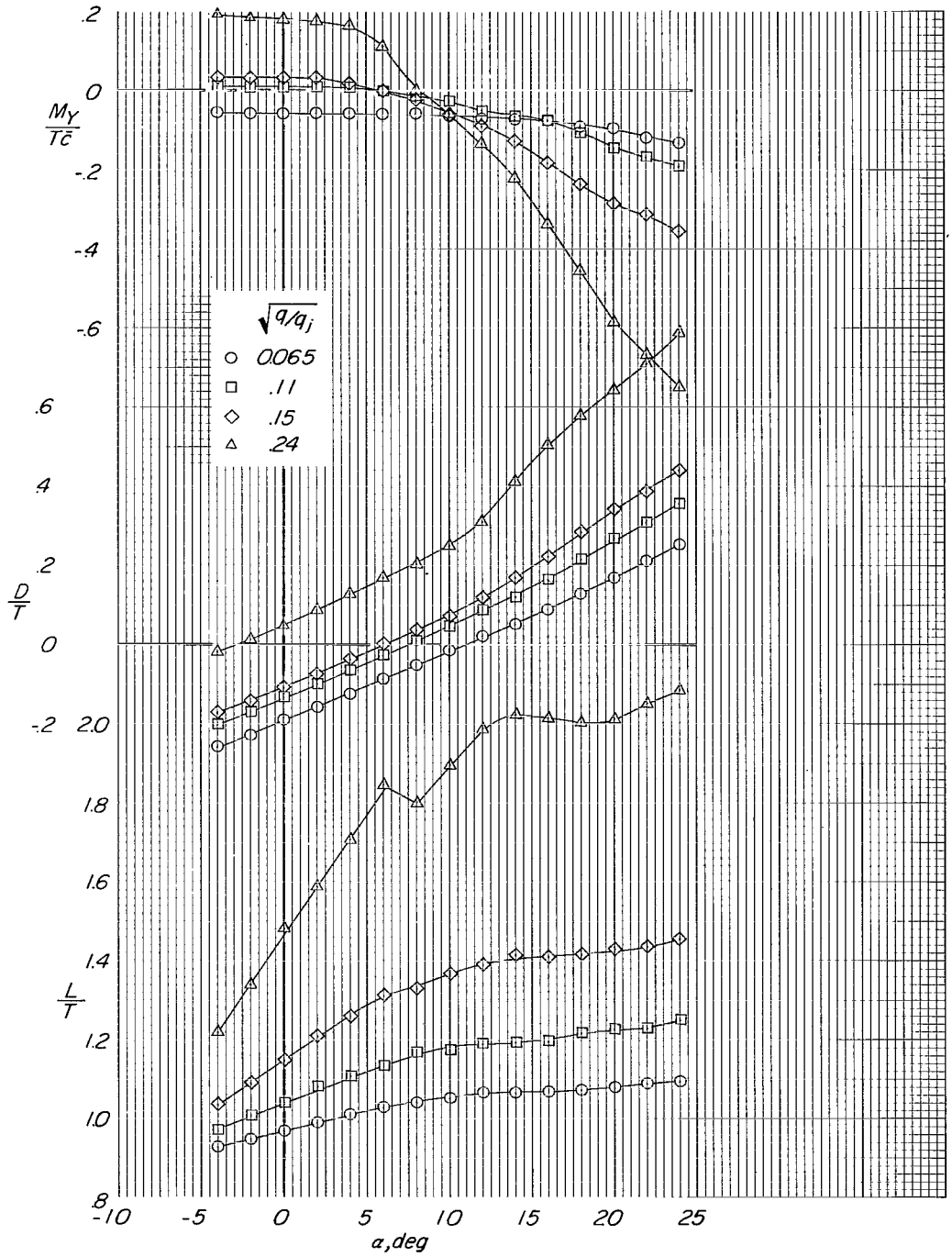

(a) Tail in low position.

Figure 19.- Longitudinal aerodynamic characteristics of model with large horizontal tail at three locations. Flaps on; power on; $i_t = 0^0$; engine pods at midspan.

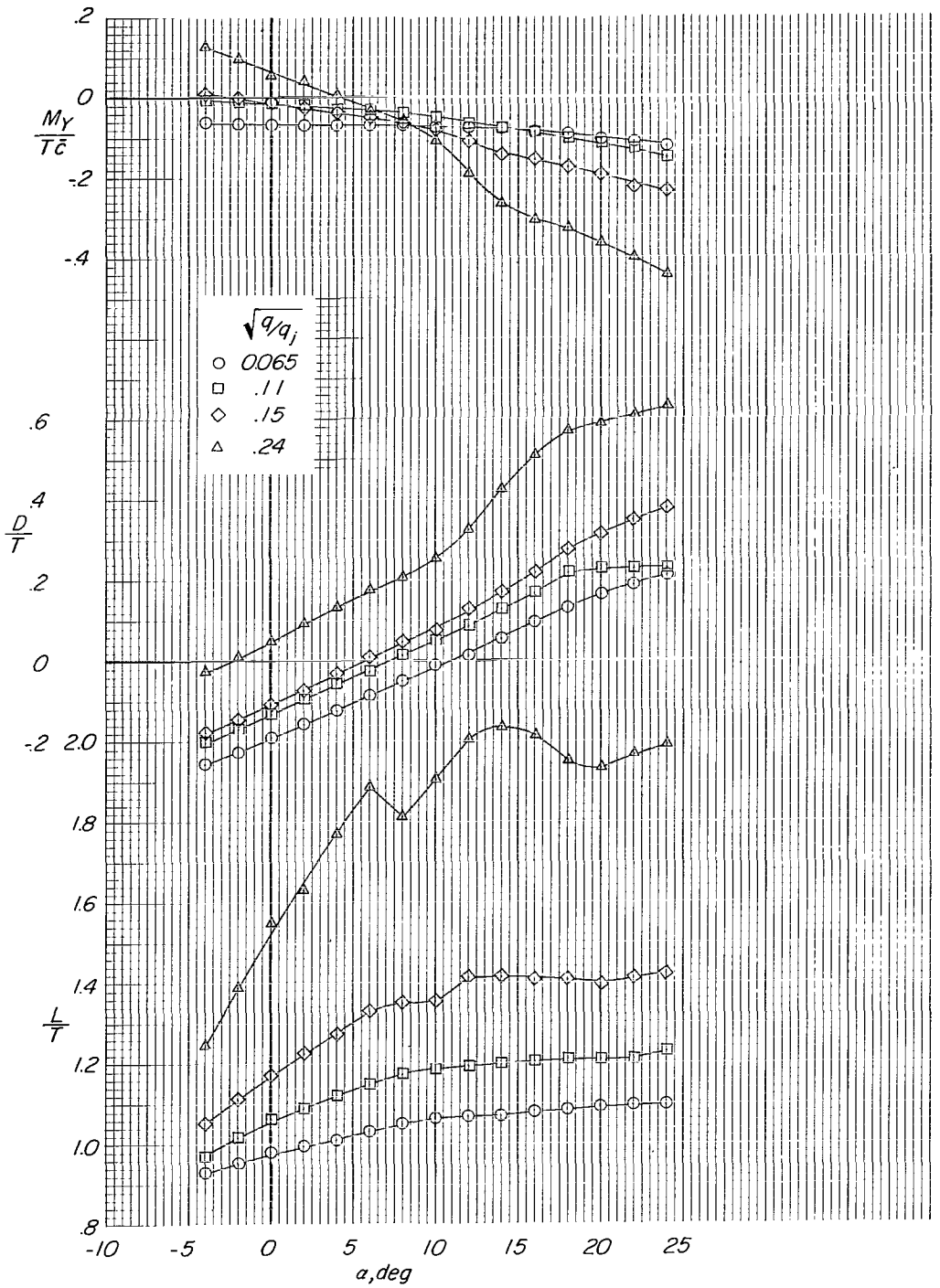

(b) Tail in mid position.

Figure 19.- Continued.

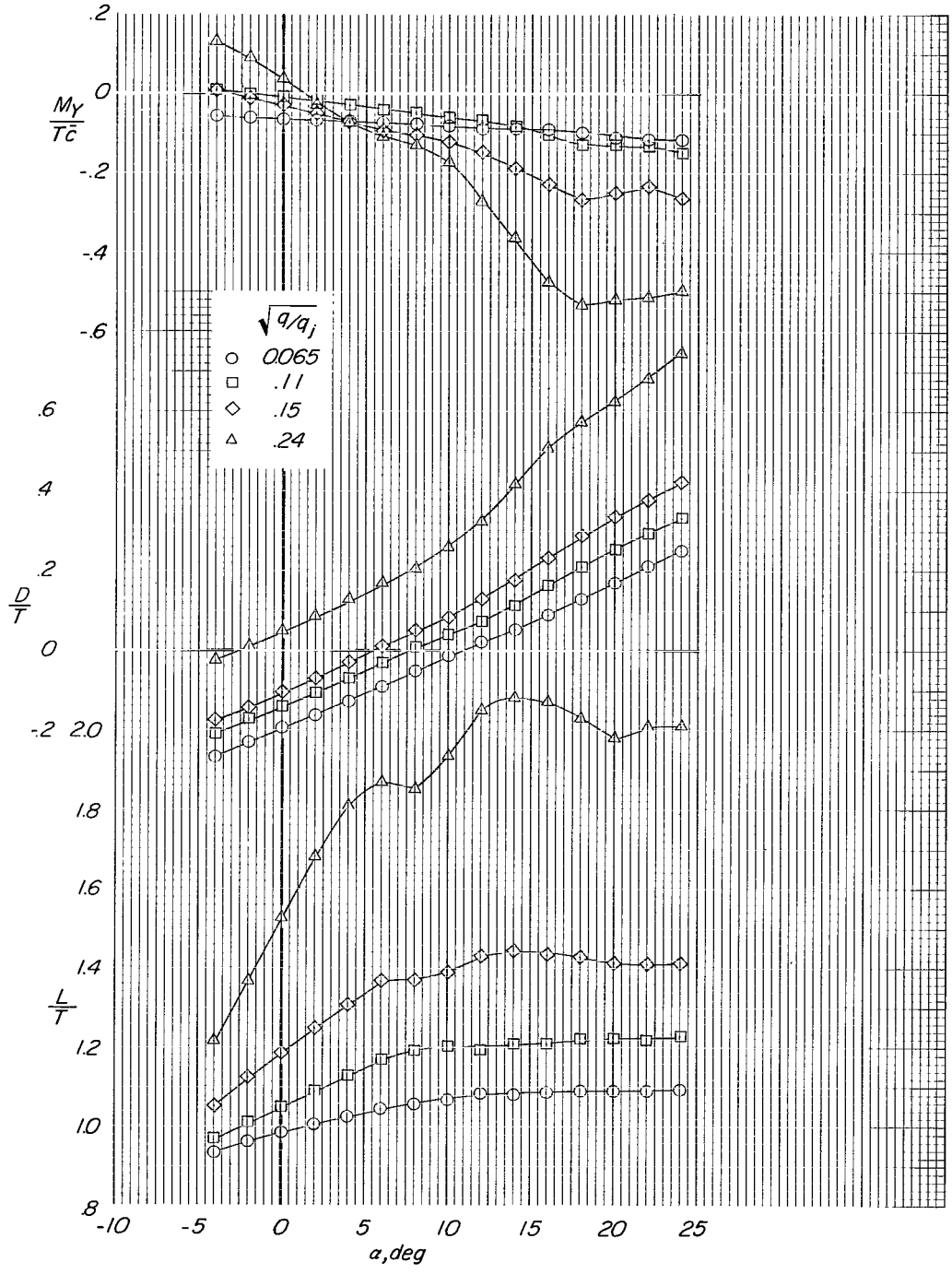

(c) Tail in high position.

Figure 19.- Concluded.

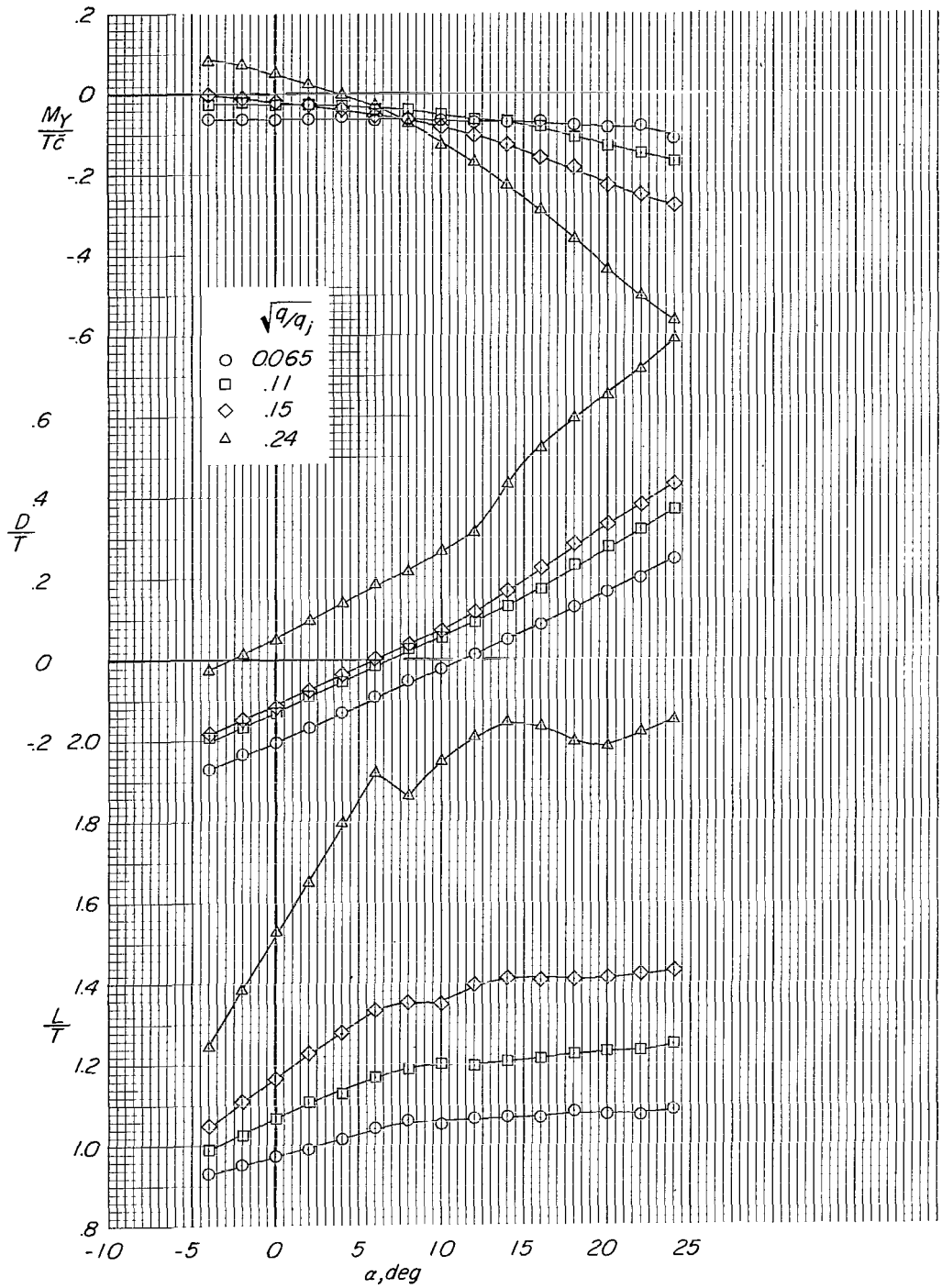

(a) Tail in low position.

Figure 20.- Longitudinal aerodynamic characteristics of model with small horizontal tail at three locations and with tail off. Flaps on; power on; $i_t = 0^0$ if tail on; engine pods at midspan.

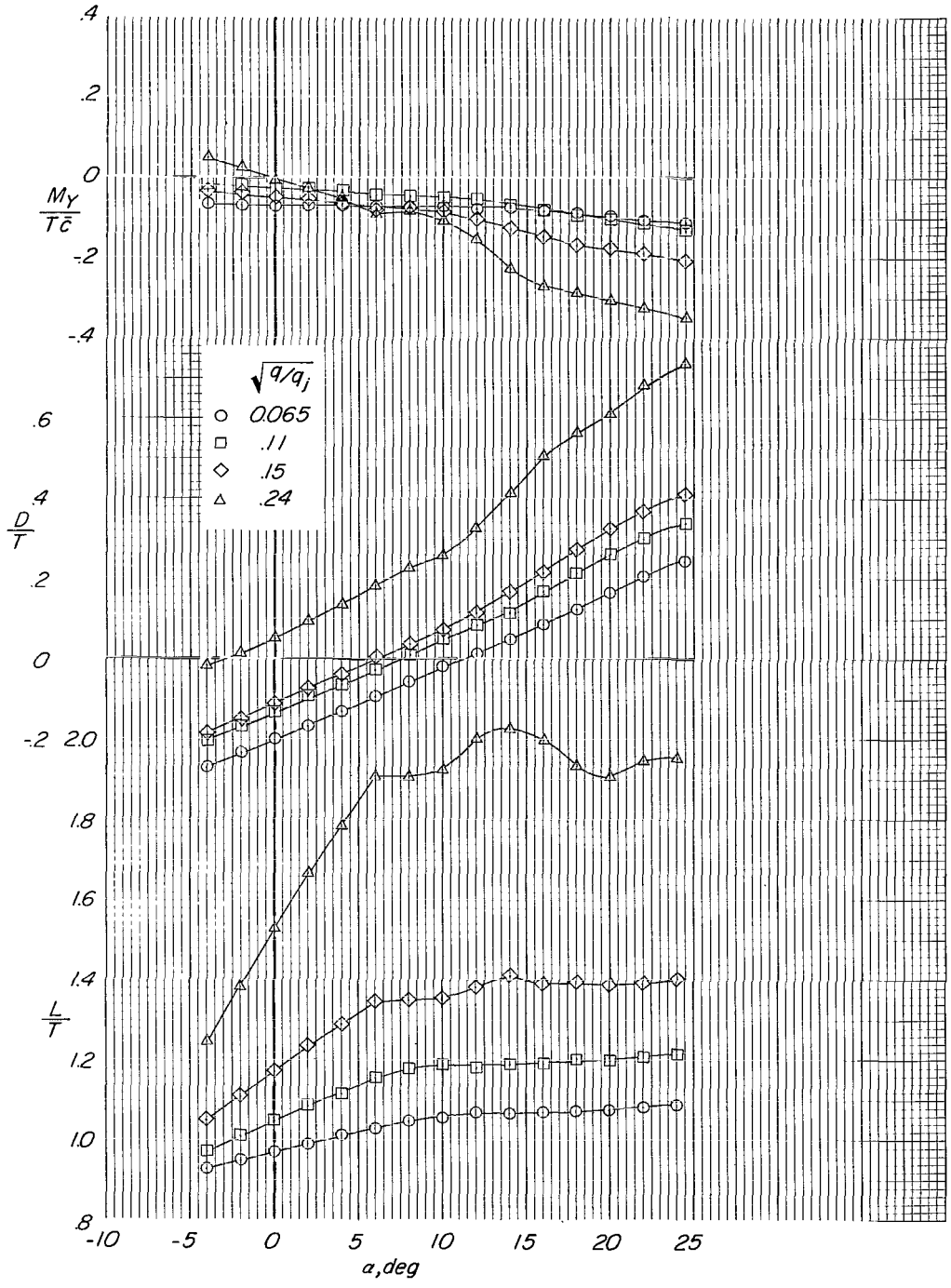

(b) Tail in mid position.

Figure 20.- Continued.

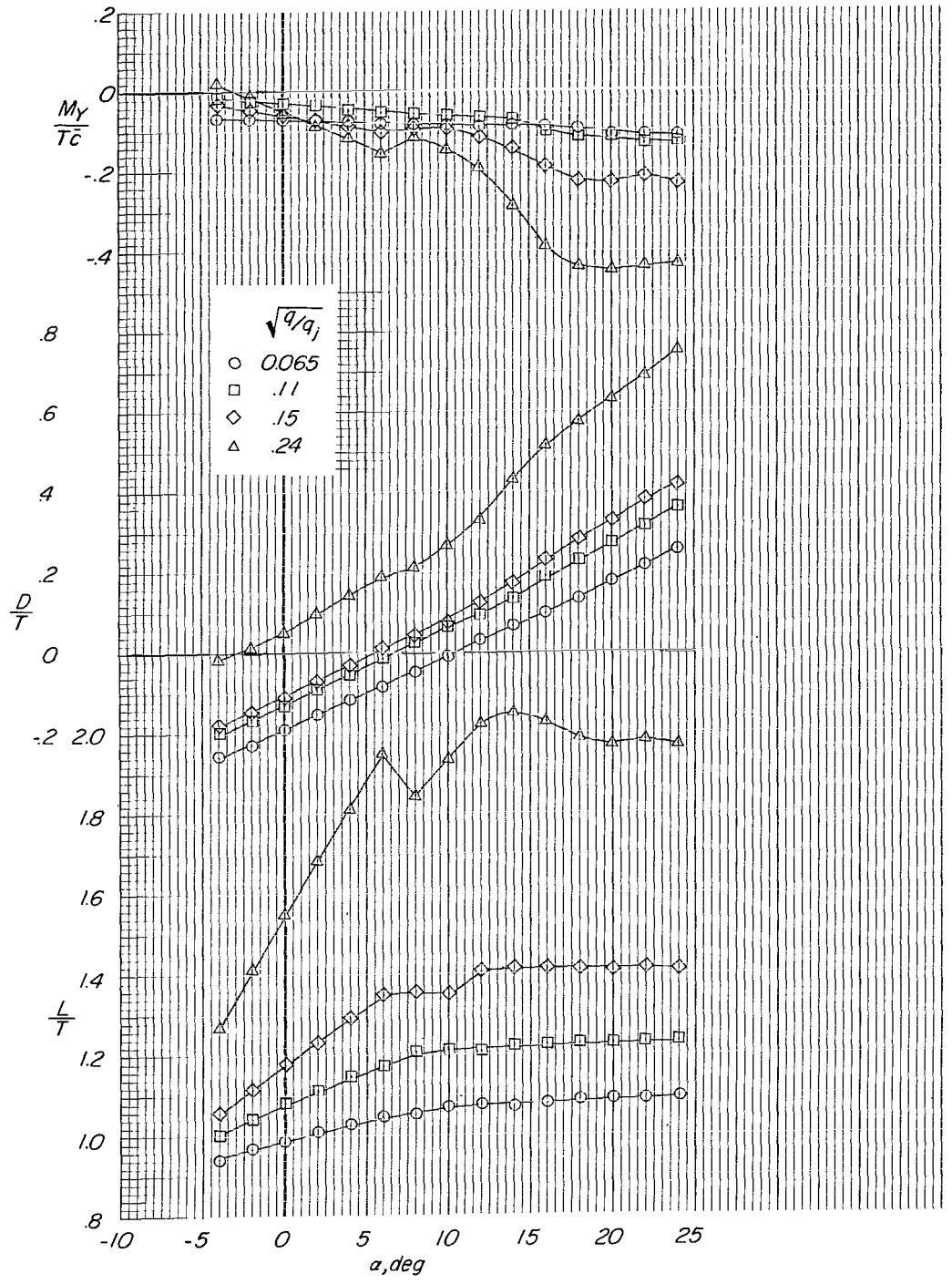

(c) Tail in high position.

Figure 20.- Continued.

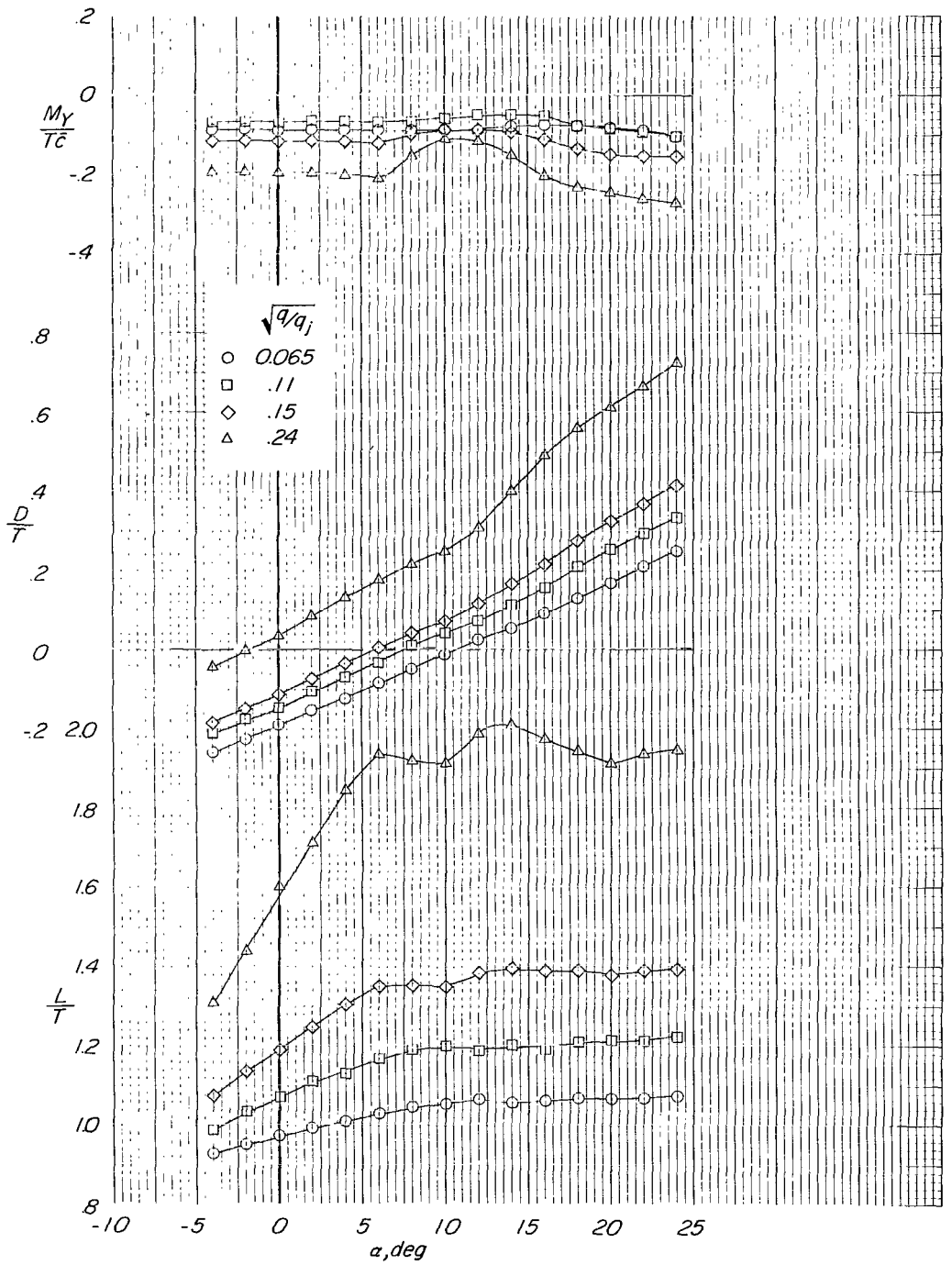

(d) Tail off.

Figure 20.- Concluded.

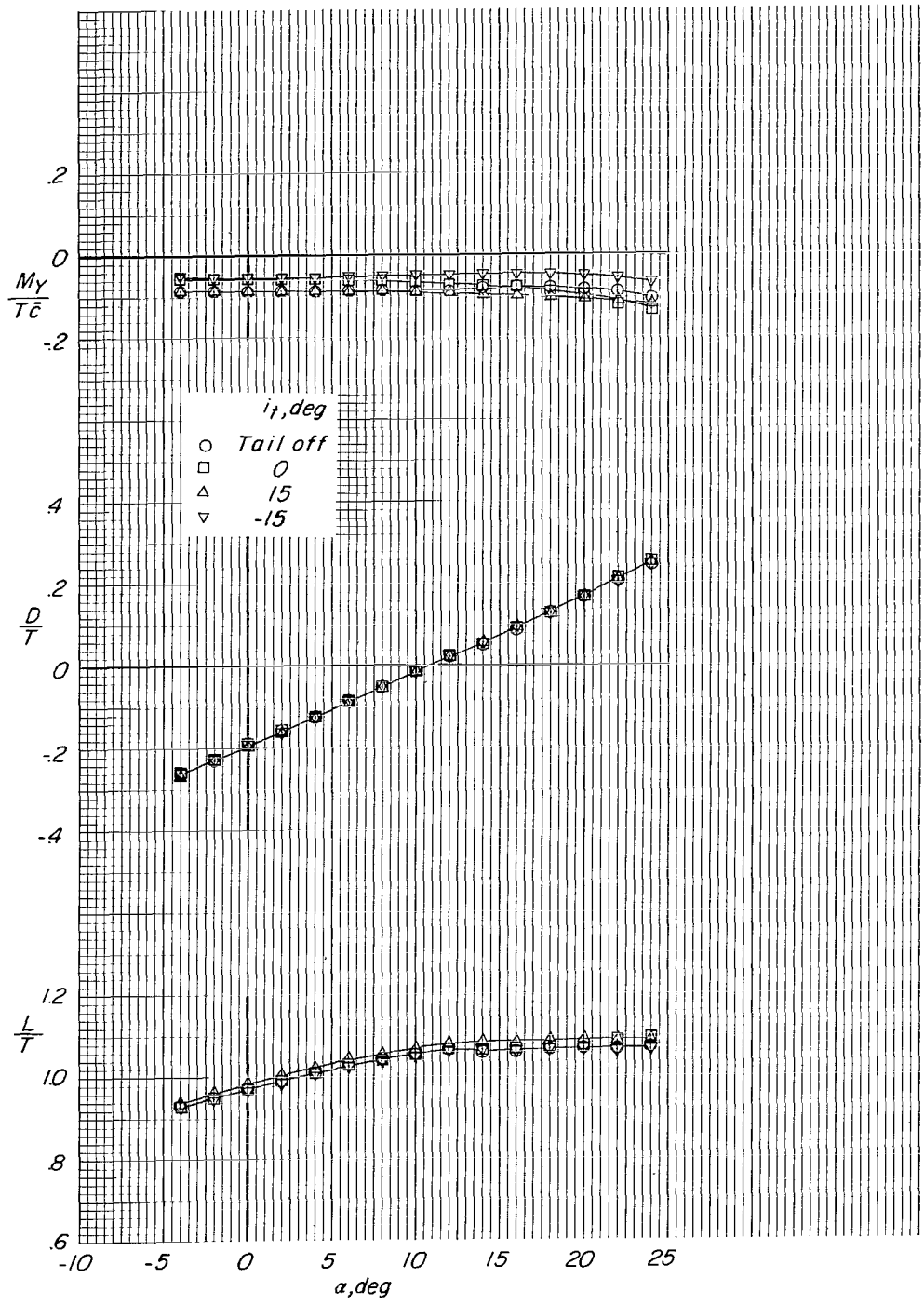

(a) $\sqrt{q/q_j}$ = 0.065.

Figure 21.- Effect of horizontal-tail incidence on longitudinal aerodynamic characteristics of model with large tail in low position. Flaps on; power on; engine pods at midspan.

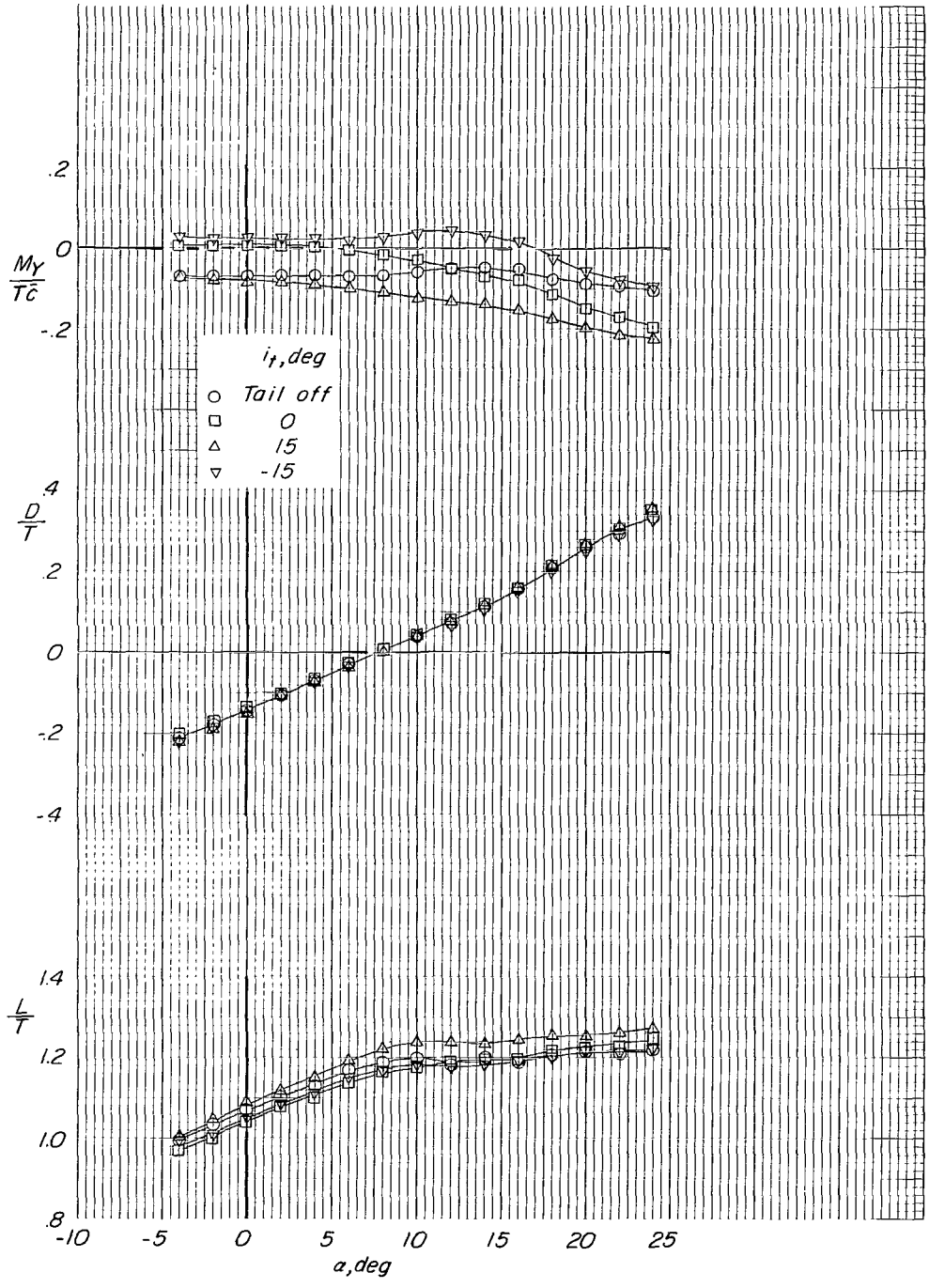

(b) $\sqrt{q/q_j} = 0.11$.

Figure 21.- Continued.

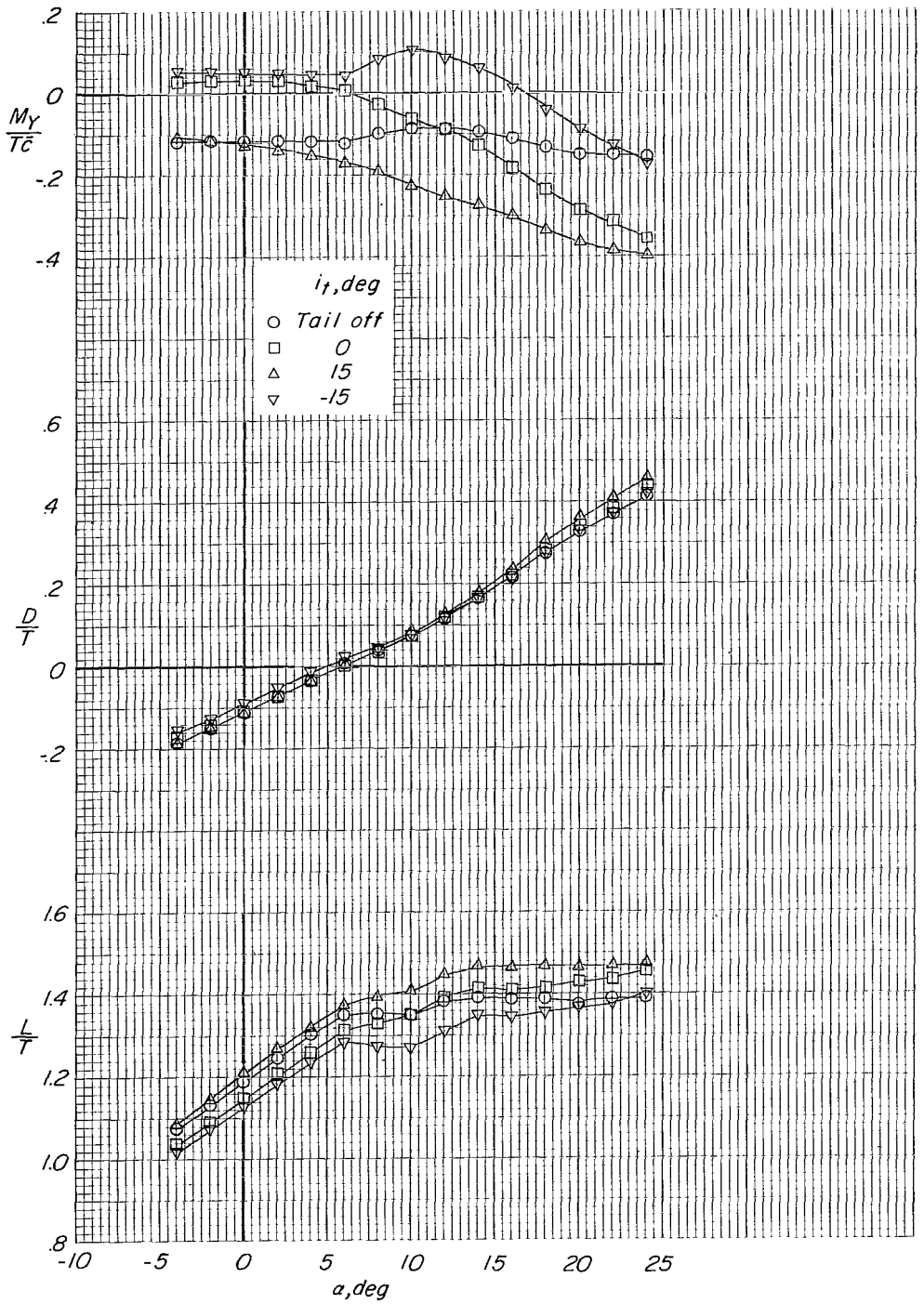

(c) $\sqrt{q/q_j}$ = 0.15.

Figure 21.- Continued.

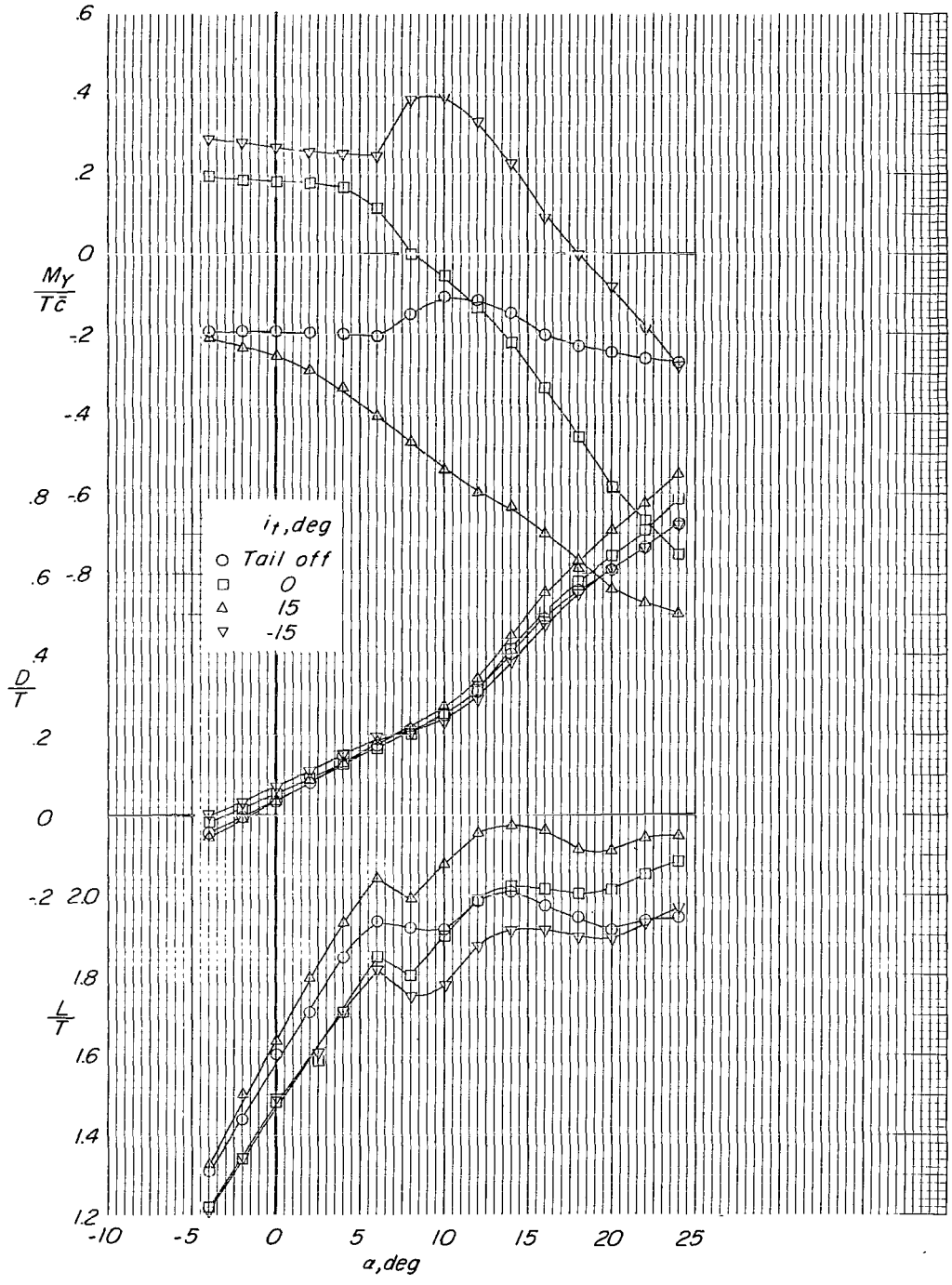

(d) $\sqrt{q/q_j} = 0.24$.

Figure 21.- Concluded.

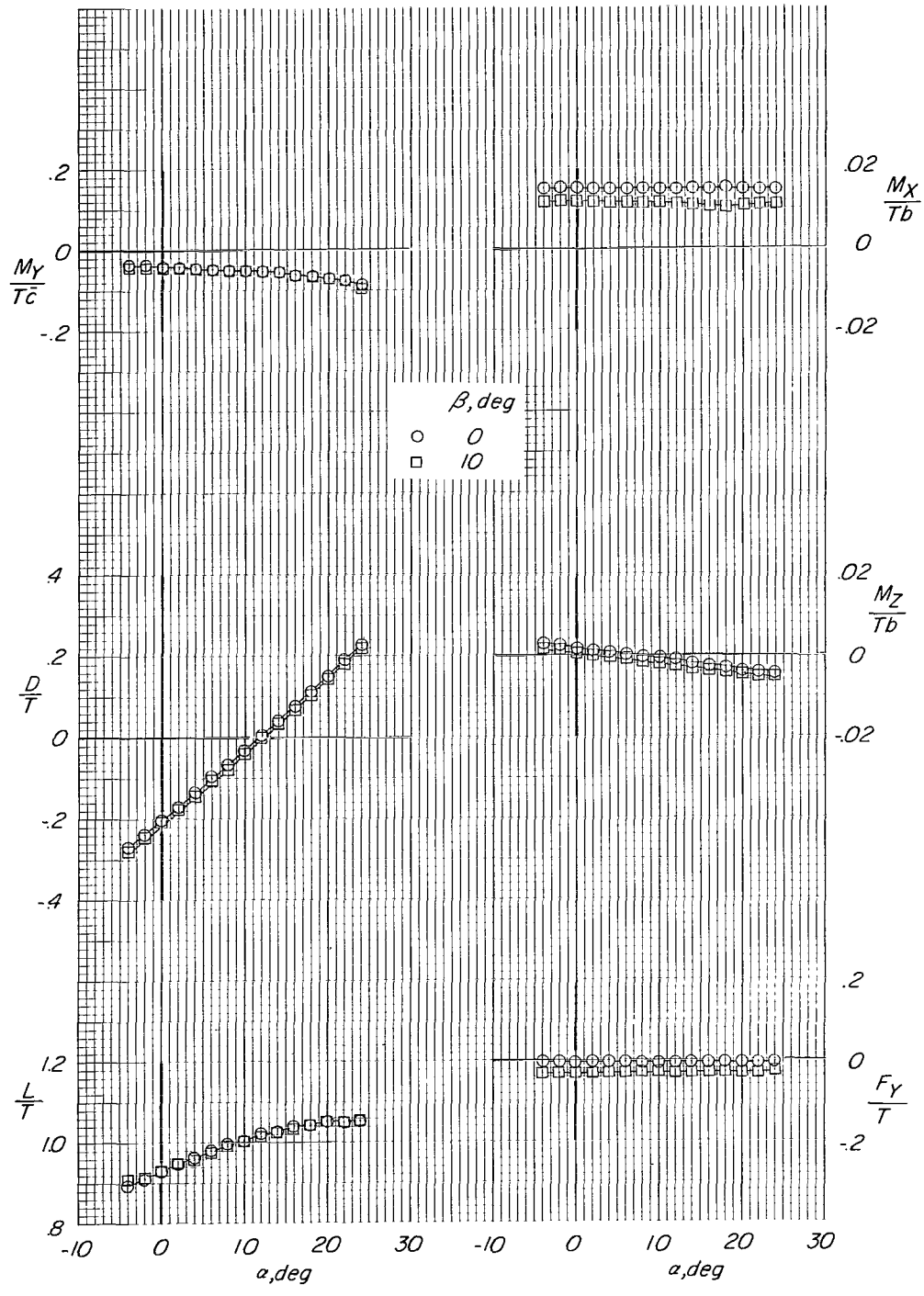

(a) $\sqrt{q/q_j} = 0.065$.

Figure 22.- Effect of 10^0 sideslip on aerodynamic characteristics of model with large tail in low position and with flaps off and vertical tail removed. Power on; $i_t = 0^0$; engine pods at midspan.

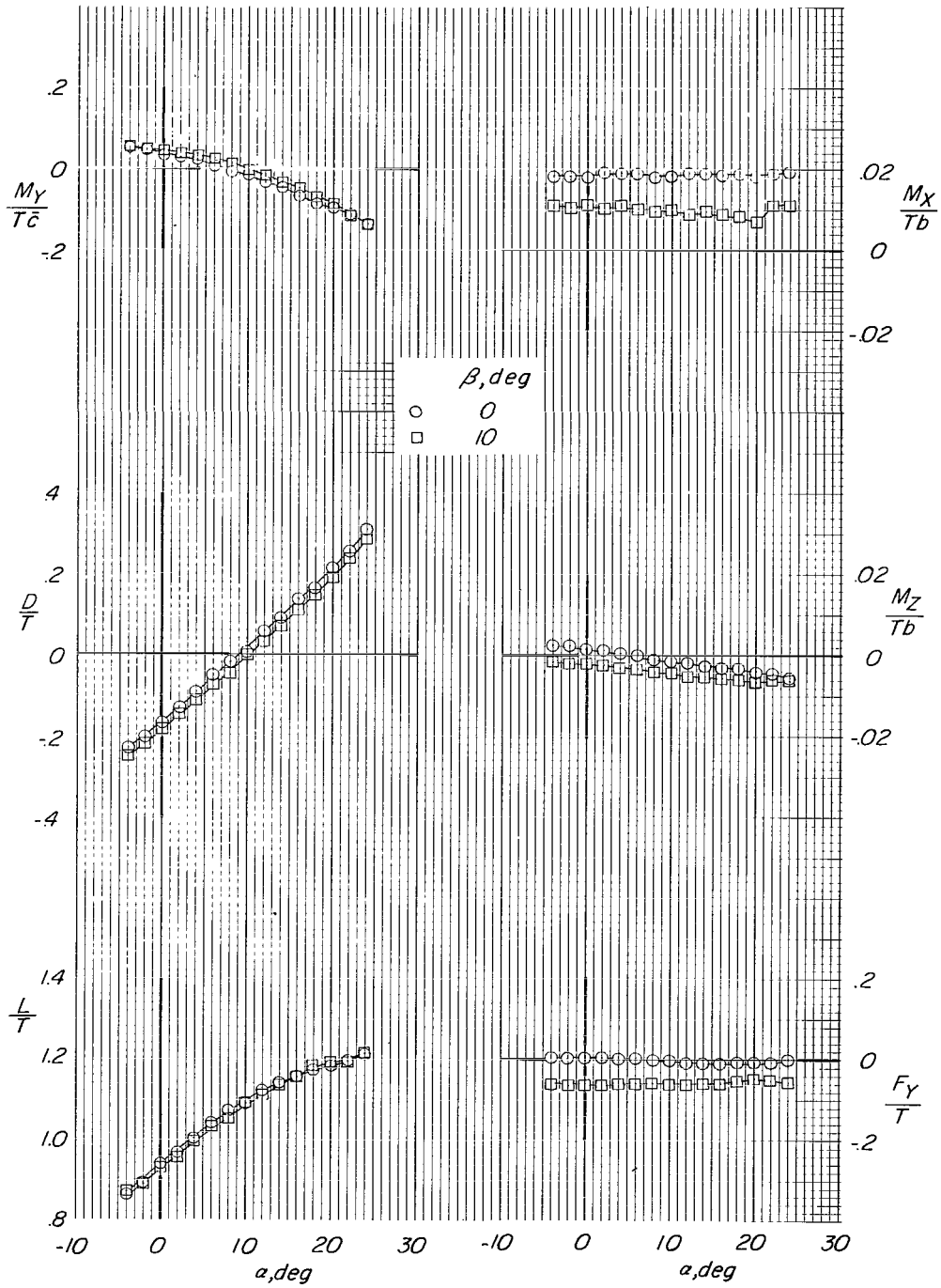

(b) $\sqrt{q/q_j} = 0.11$.

Figure 22.- Continued.

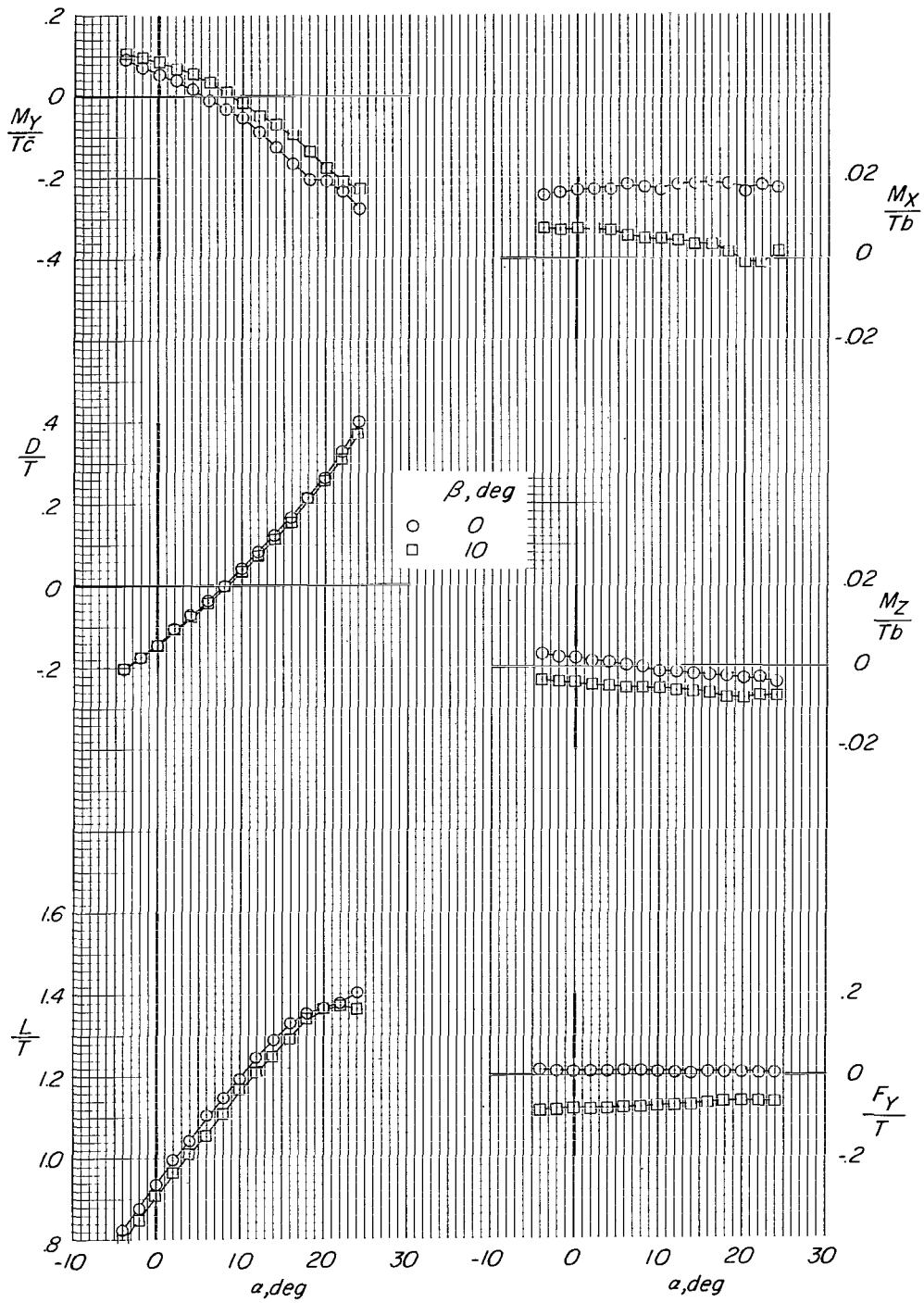

(c) $\sqrt{q/q_j}$ = 0.15.

Figure 22.- Continued.

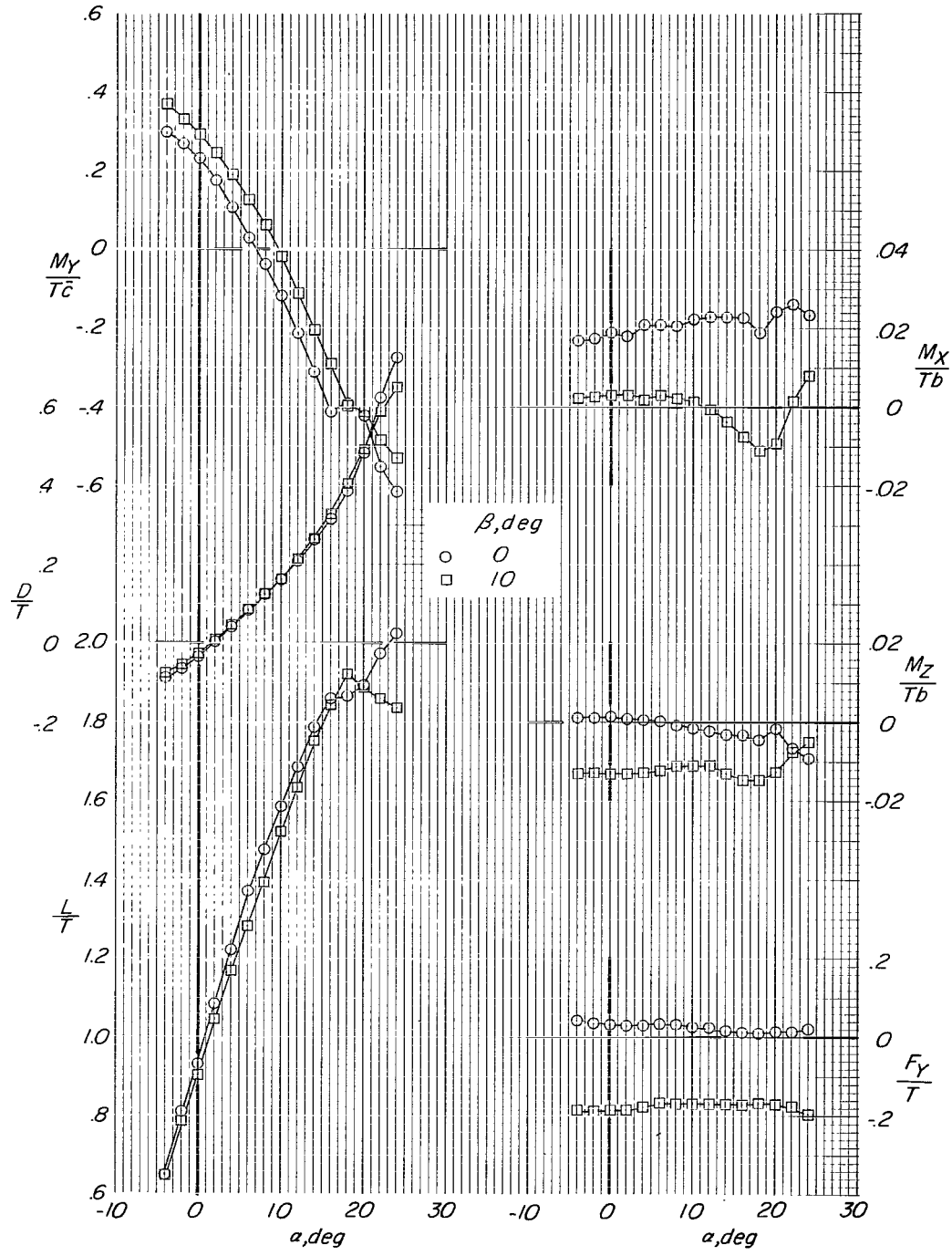

(d) $\sqrt{q/q_j}$ = 0.24.

Figure 22.- Concluded.

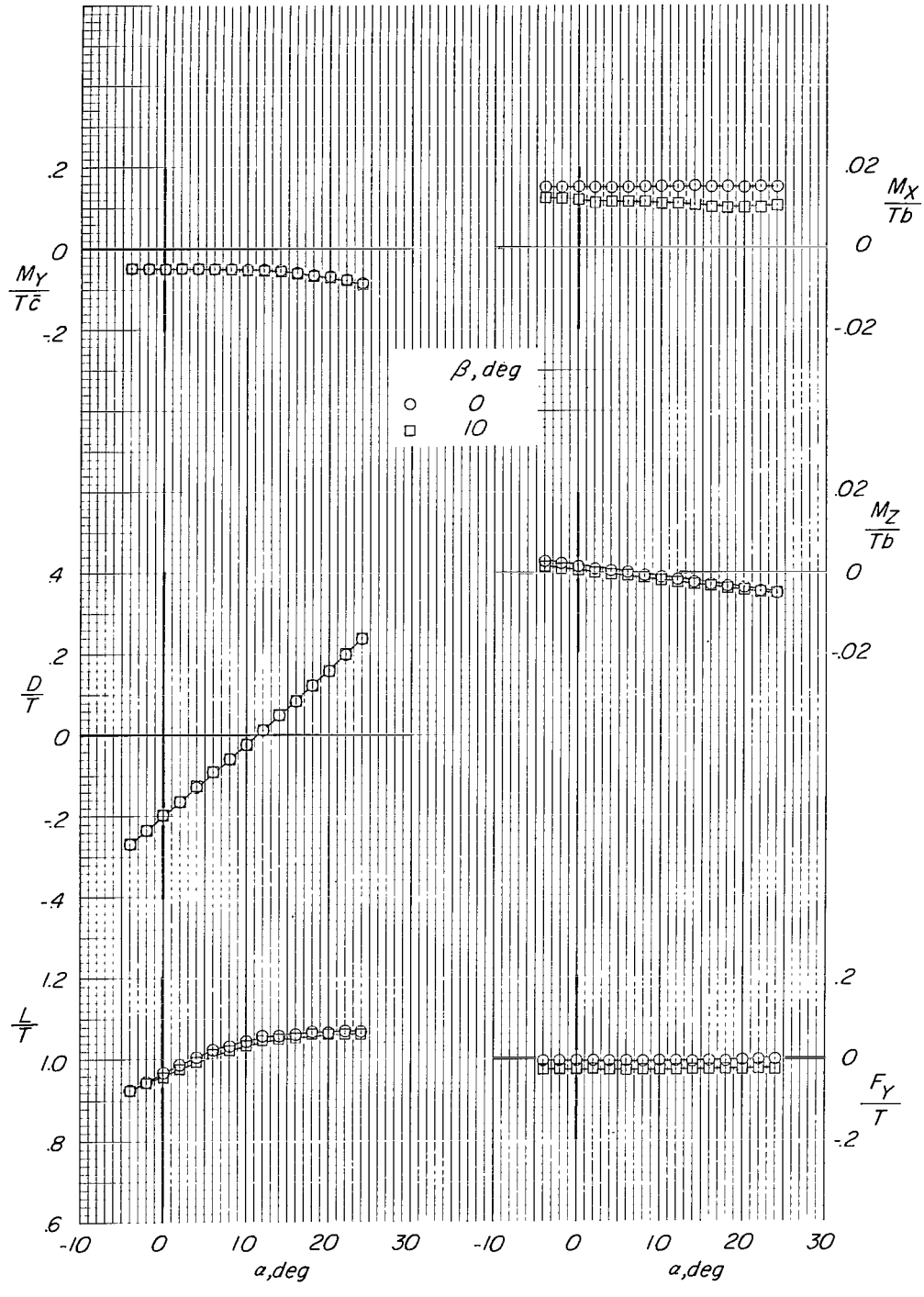

(a) $\sqrt{q/q_j} = 0.065$.

Figure 23.- Effect of 10^0 sideslip on aerodynamic characteristics of model with large tail in low position and with flaps on and vertical tail removed. Power on; $i_t = 0^0$; engine pods at midspan.

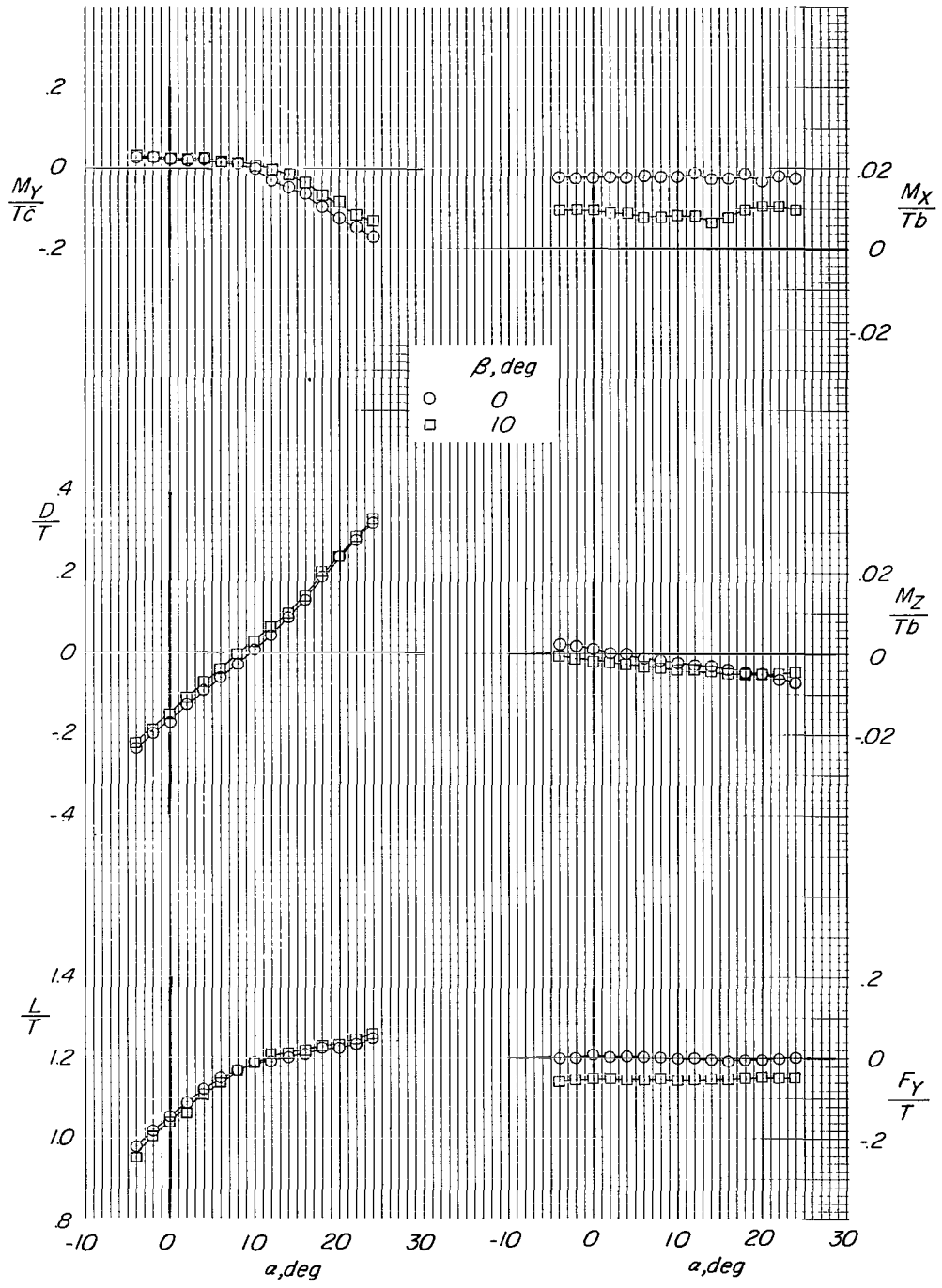

(b) $\sqrt{q/q_j} = 0.11$.

Figure 23.- Continued.

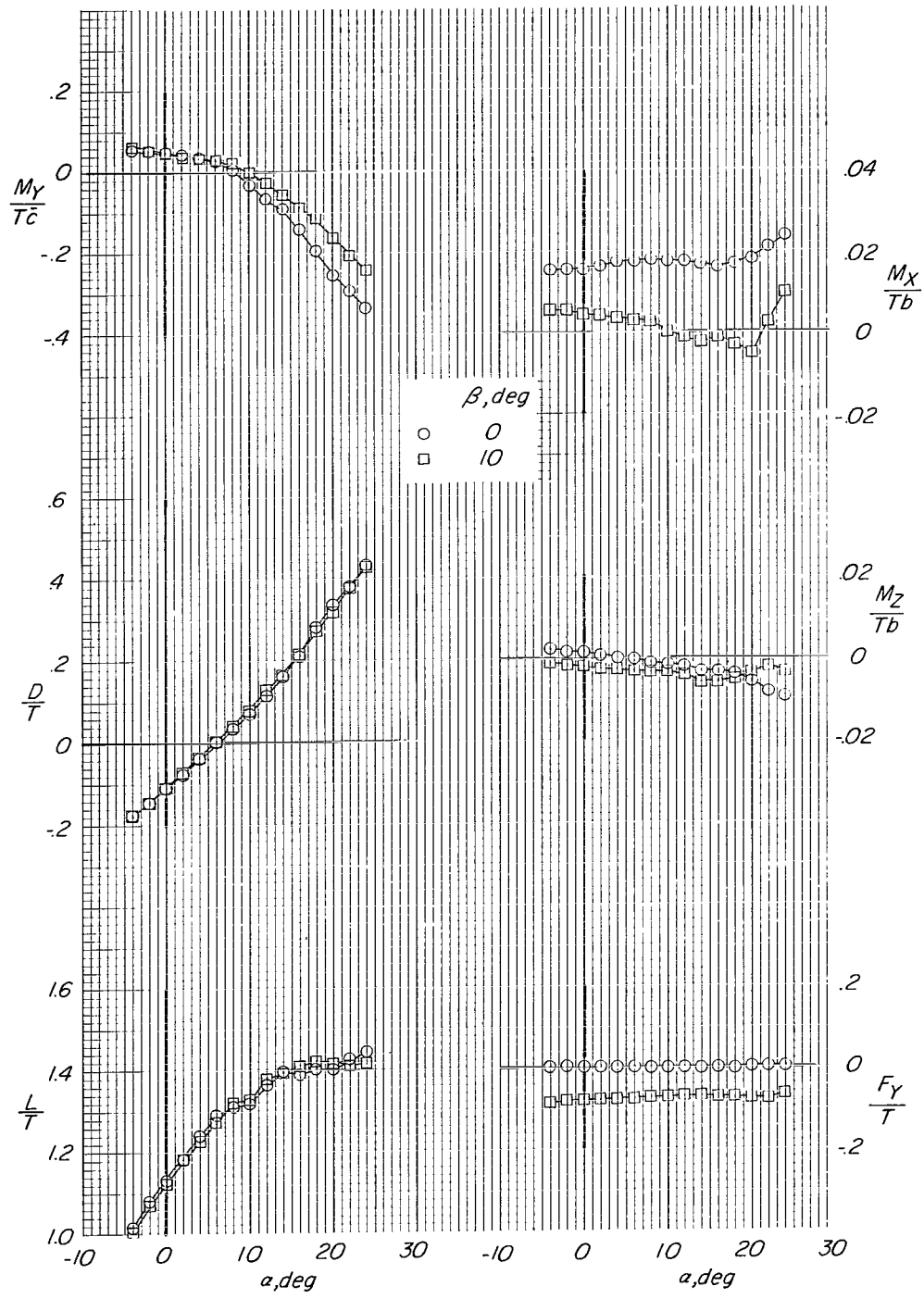

(c) $\sqrt{q/q_j}$ = 0.15.

Figure 23.- Continued.

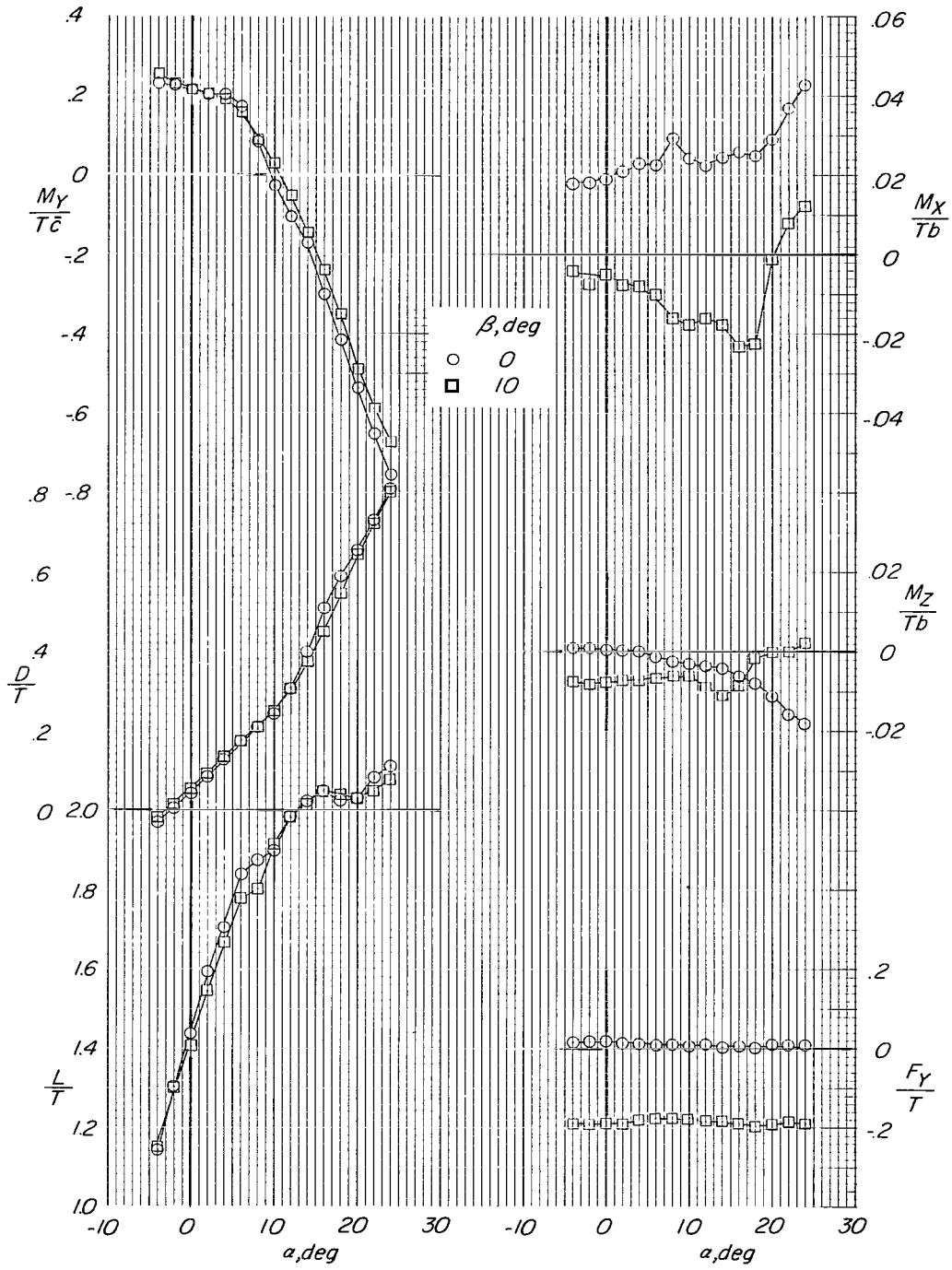

(d) $\sqrt{q/q_j} = 0.24$.

Figure 23.- Concluded.

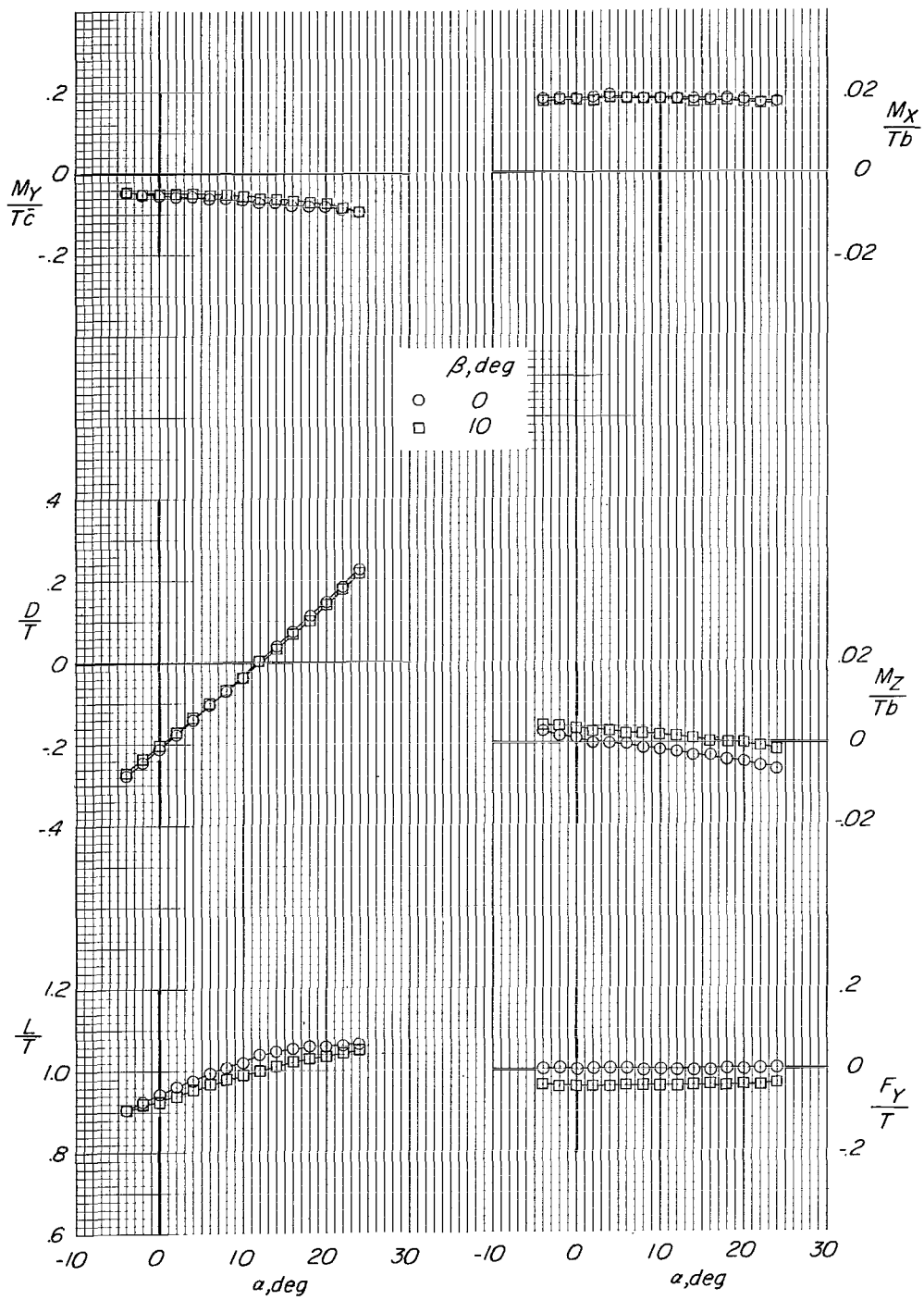

(a) $\sqrt{q/q_j} = 0.065$.

Figure 24.- Effect of 10^0 sideslip on aerodynamic characteristics of model with large tail in low position. Flaps off; power on; $i_t = 0^0$; engine pods at midspan.

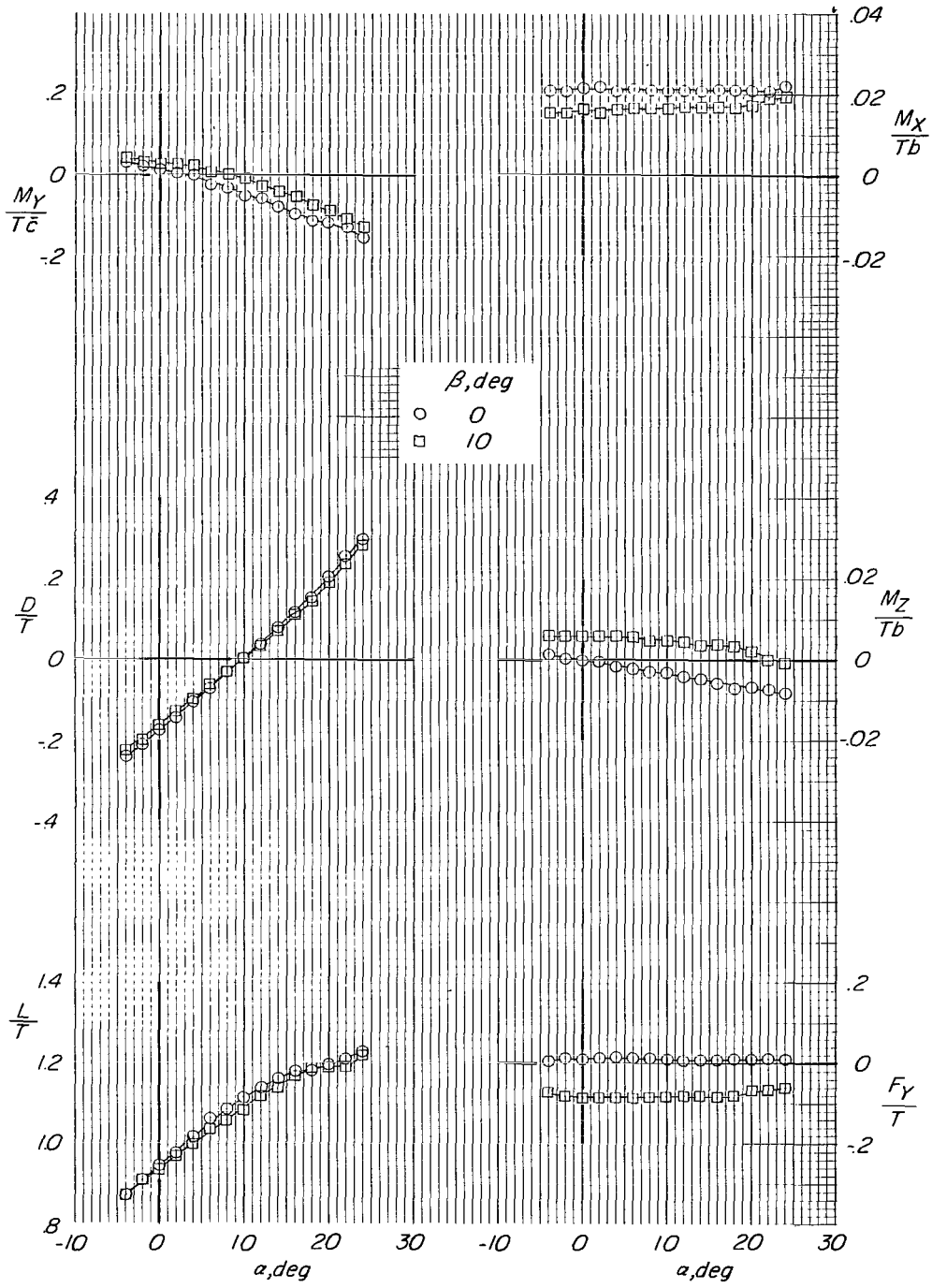

(b) $\sqrt{q/q_j} = 0.11$.

Figure 24.- Continued.

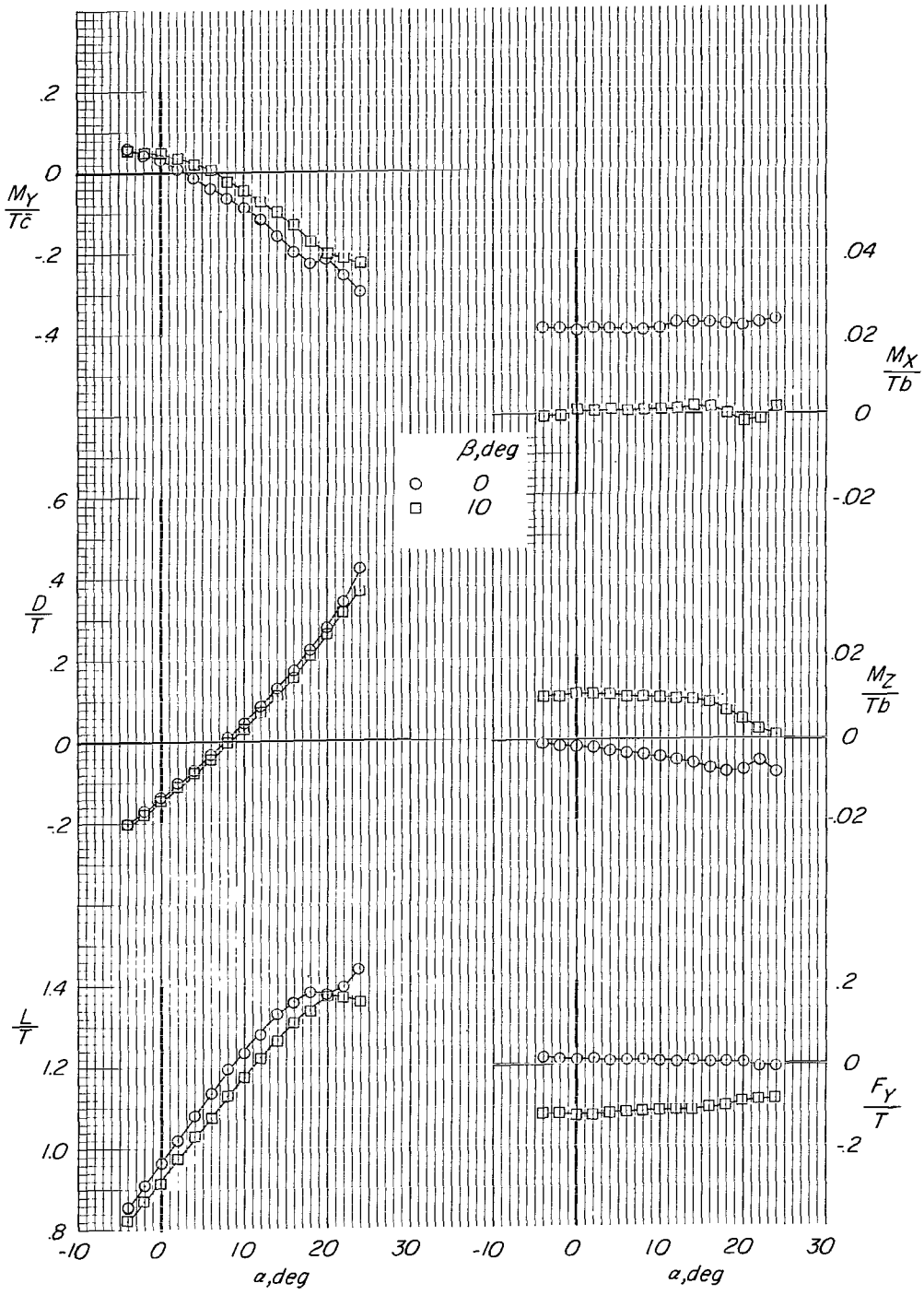

(c) $\sqrt{q/q_j} = 0.15$.

Figure 24.- Continued.

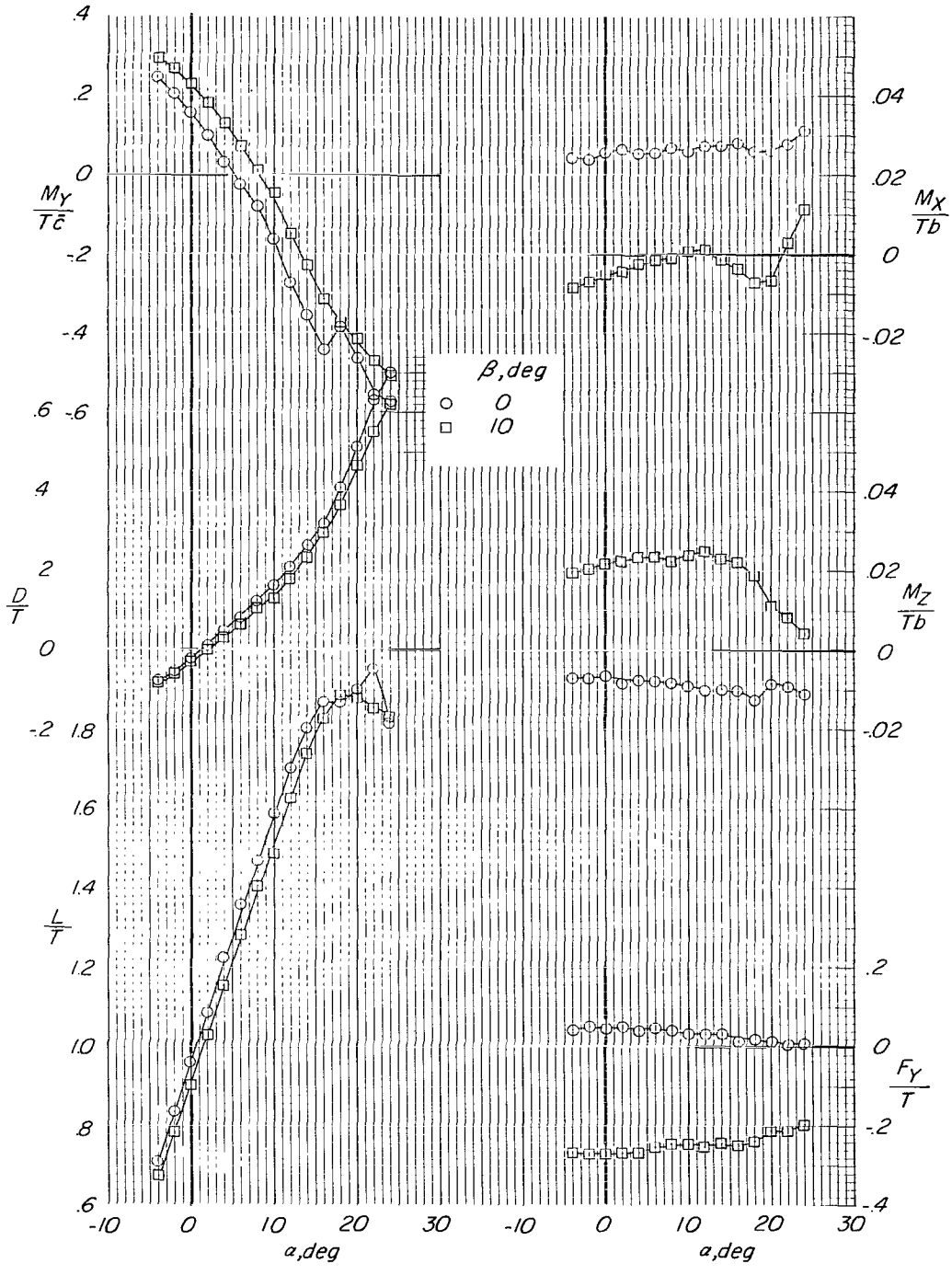

(d) $\sqrt{q/q_j} = 0.24$.

Figure 24.- Concluded.

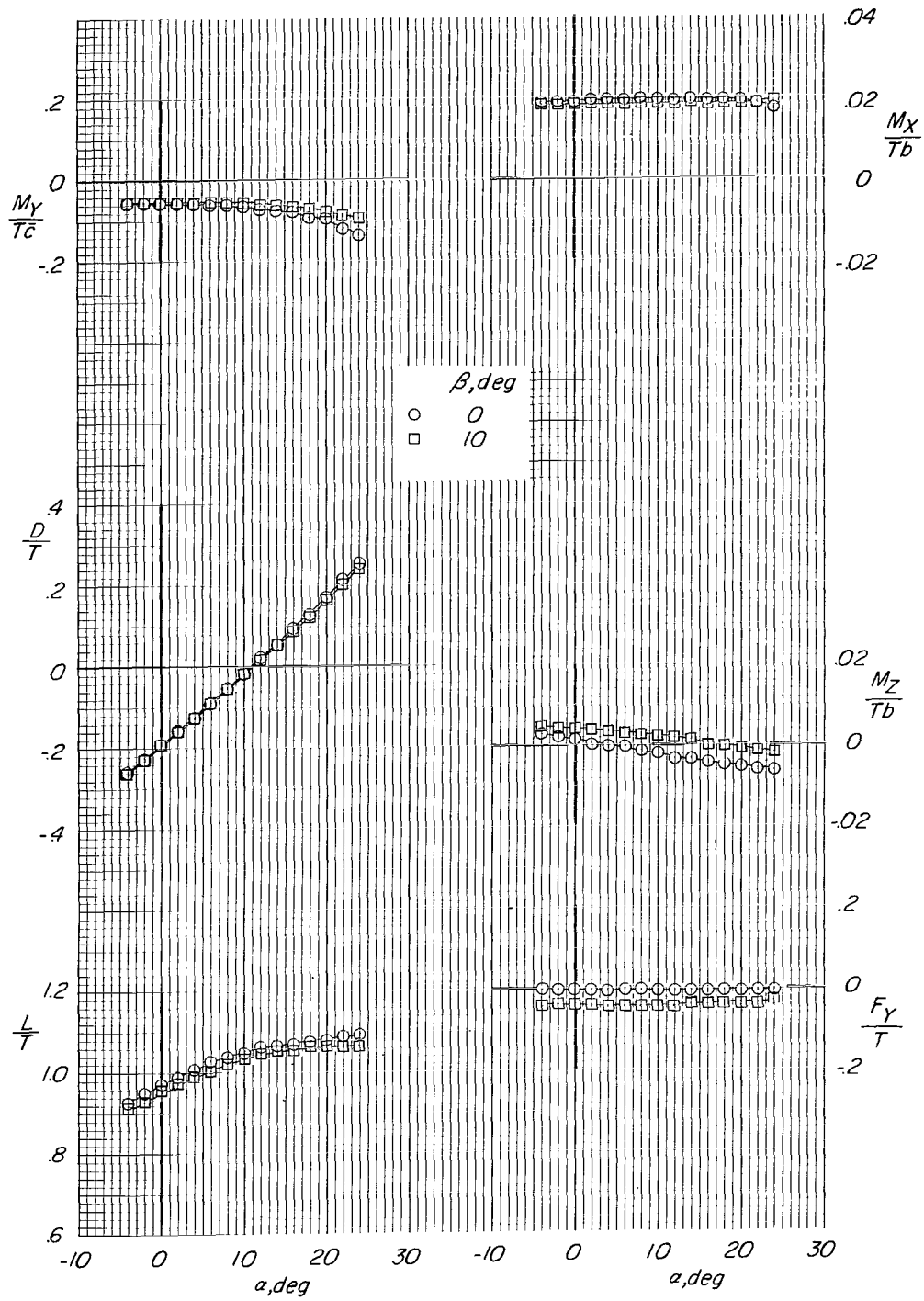

(a) $\sqrt{q/q_j} = 0.065$.

Figure 25.- Effect of 10^0 sideslip on model aerodynamic characteristics with large tail in low position. Flaps on; power on; $i_t = 0^0$; engine pods at midspan.

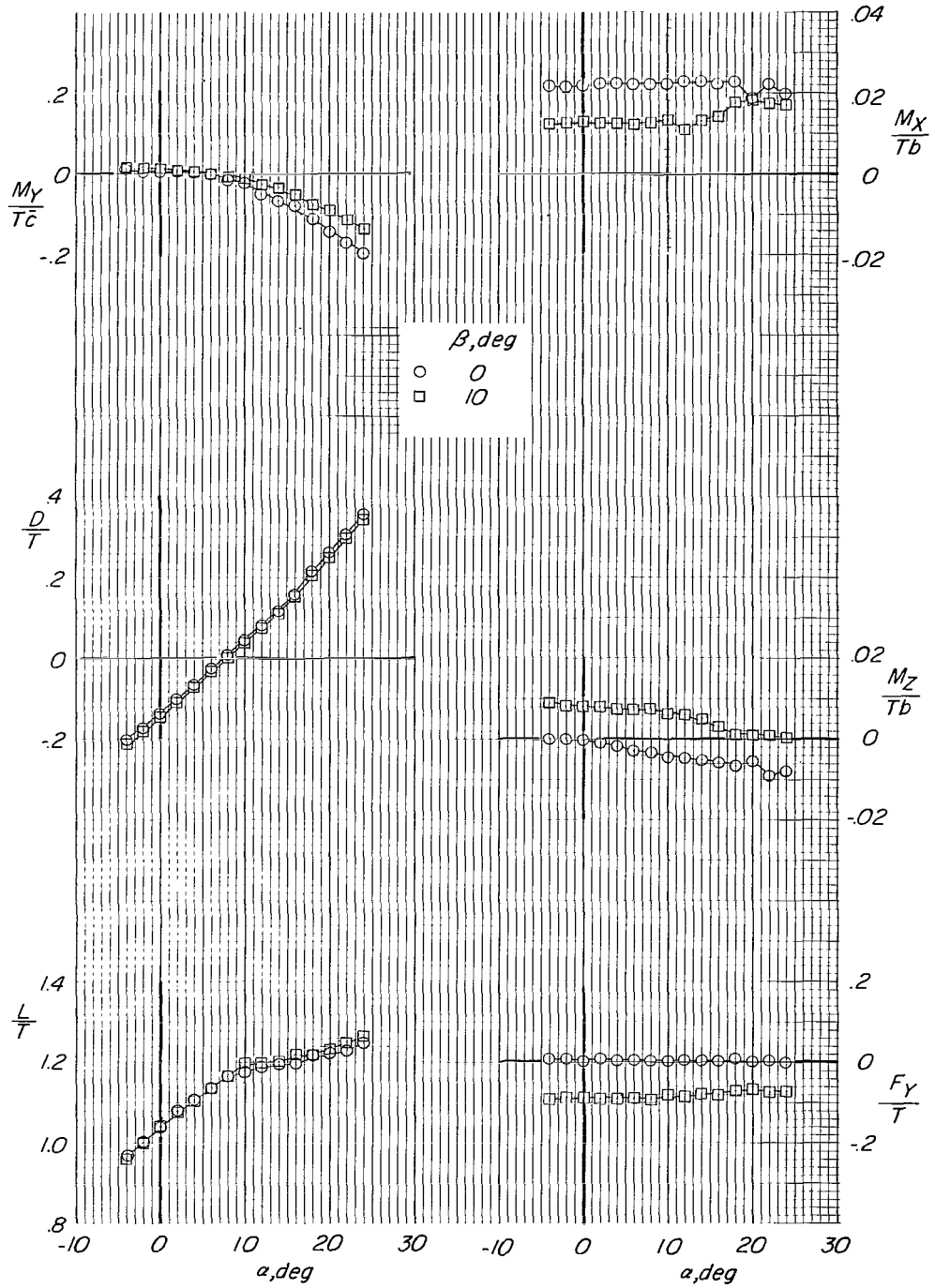

(b) $\sqrt{q/q_j} = 0.11$.

Figure 25.- Continued.

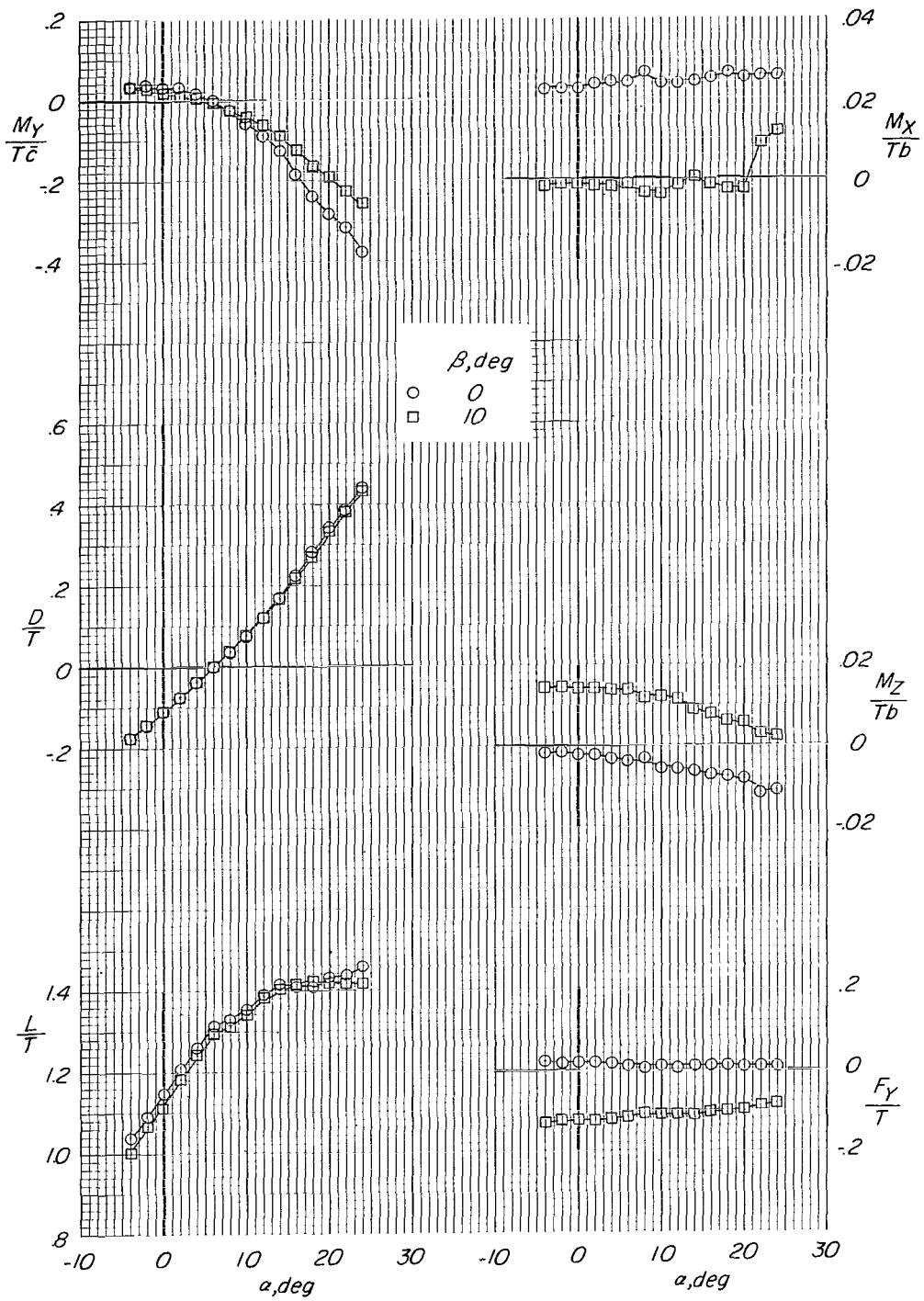

(c) $\sqrt{q/q_j} = 0.15$.

Figure 25.- Continued.

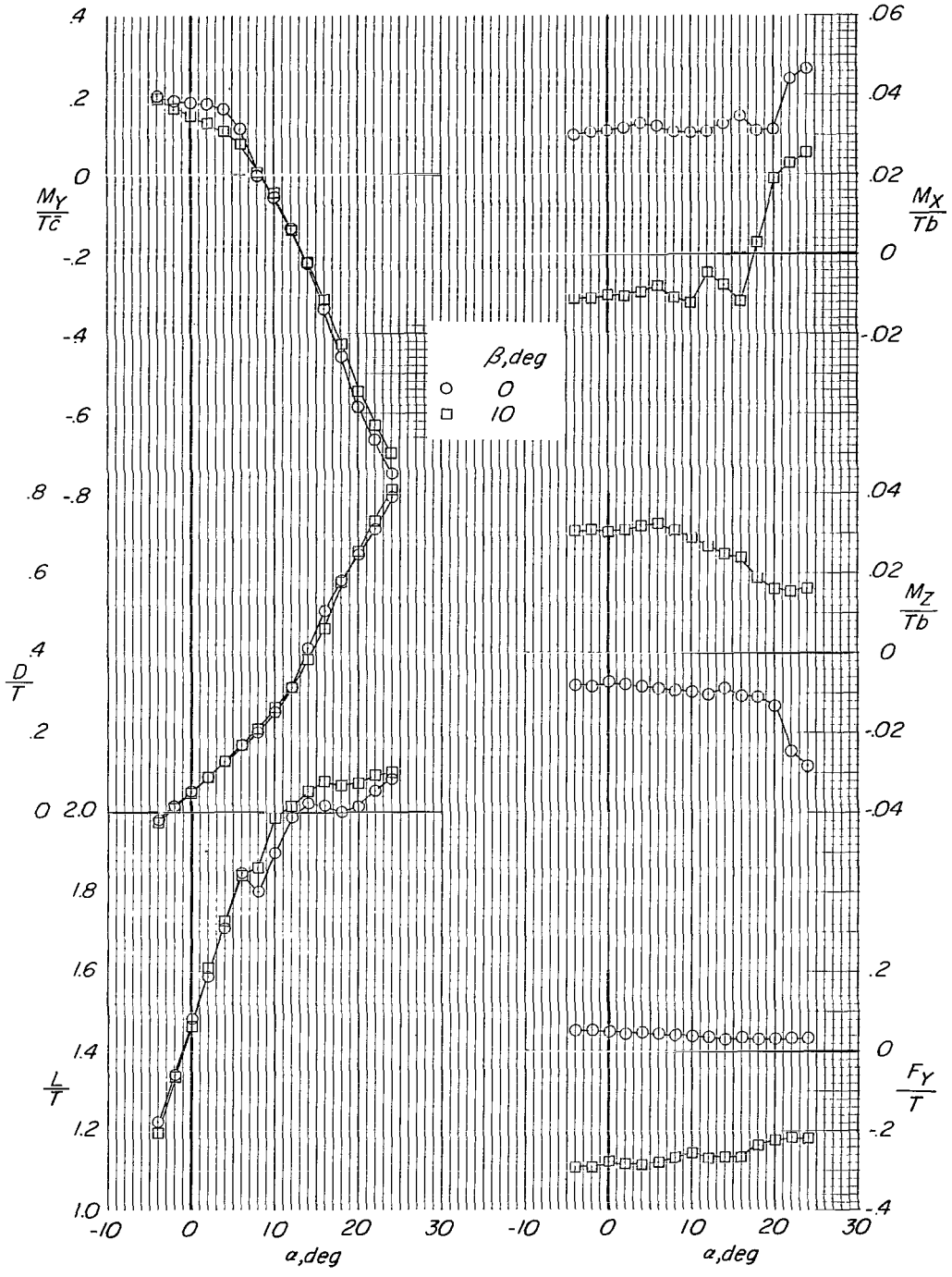

(d) $\sqrt{q/q_j}$ = 0.24.

Figure 25.- Concluded.

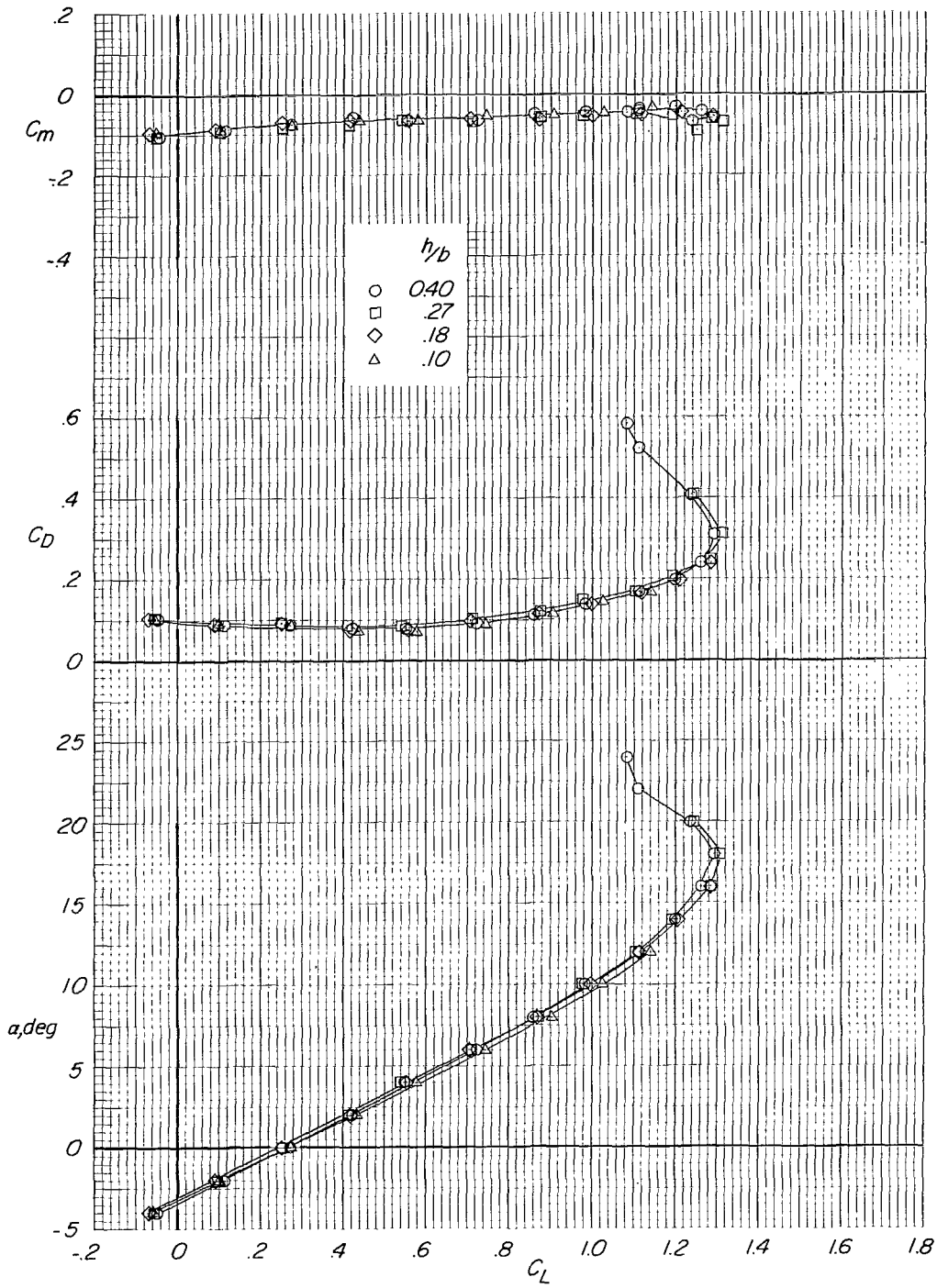

(a) Tail off.

Figure 26.- Longitudinal aerodynamic characteristics of model in ground effect with small horizontal tail off and in low position. Flaps off; power off; engine pods at midspan.

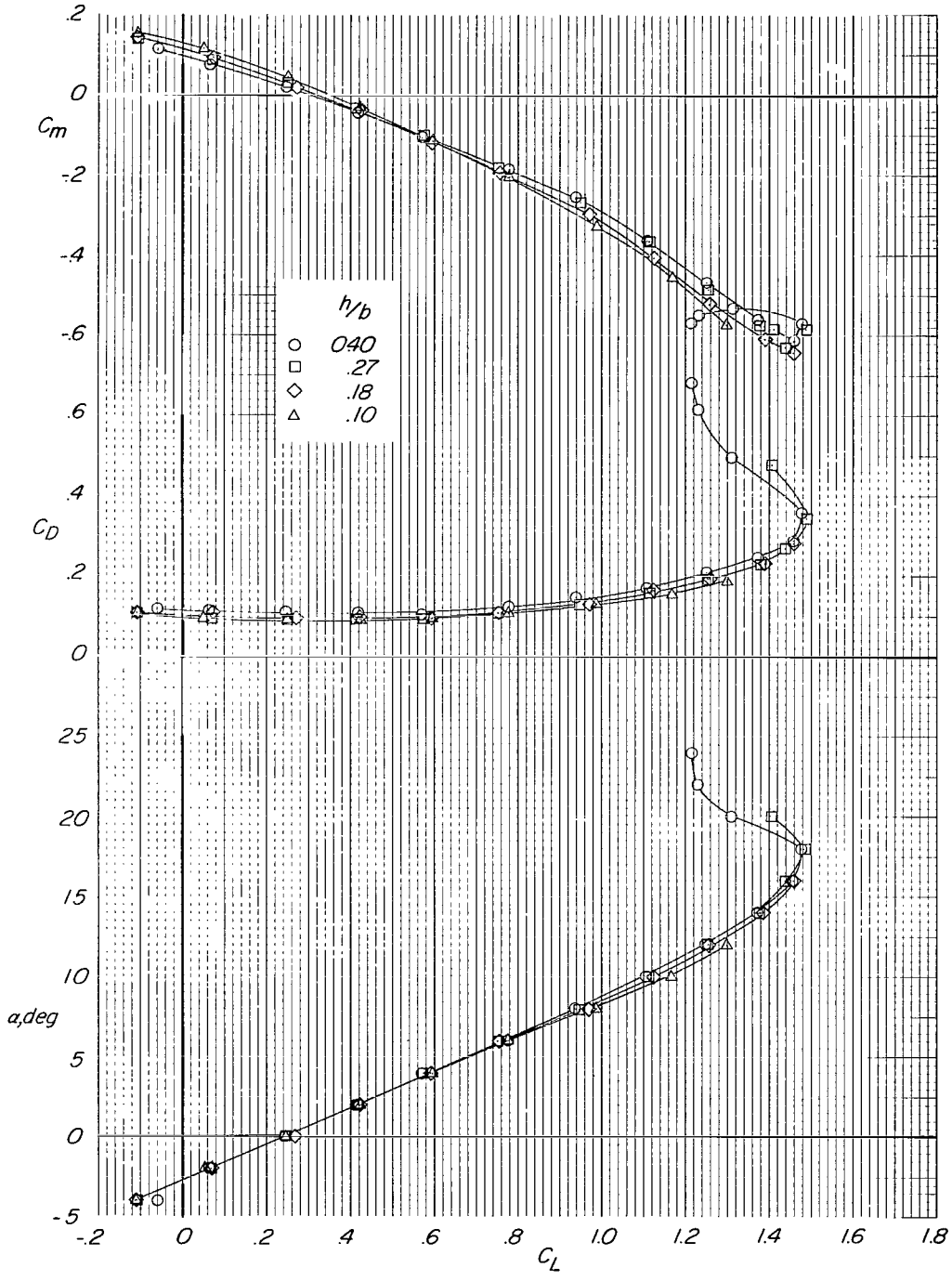

(b) $i_t = 0^0$.

Figure 26.- Continued.

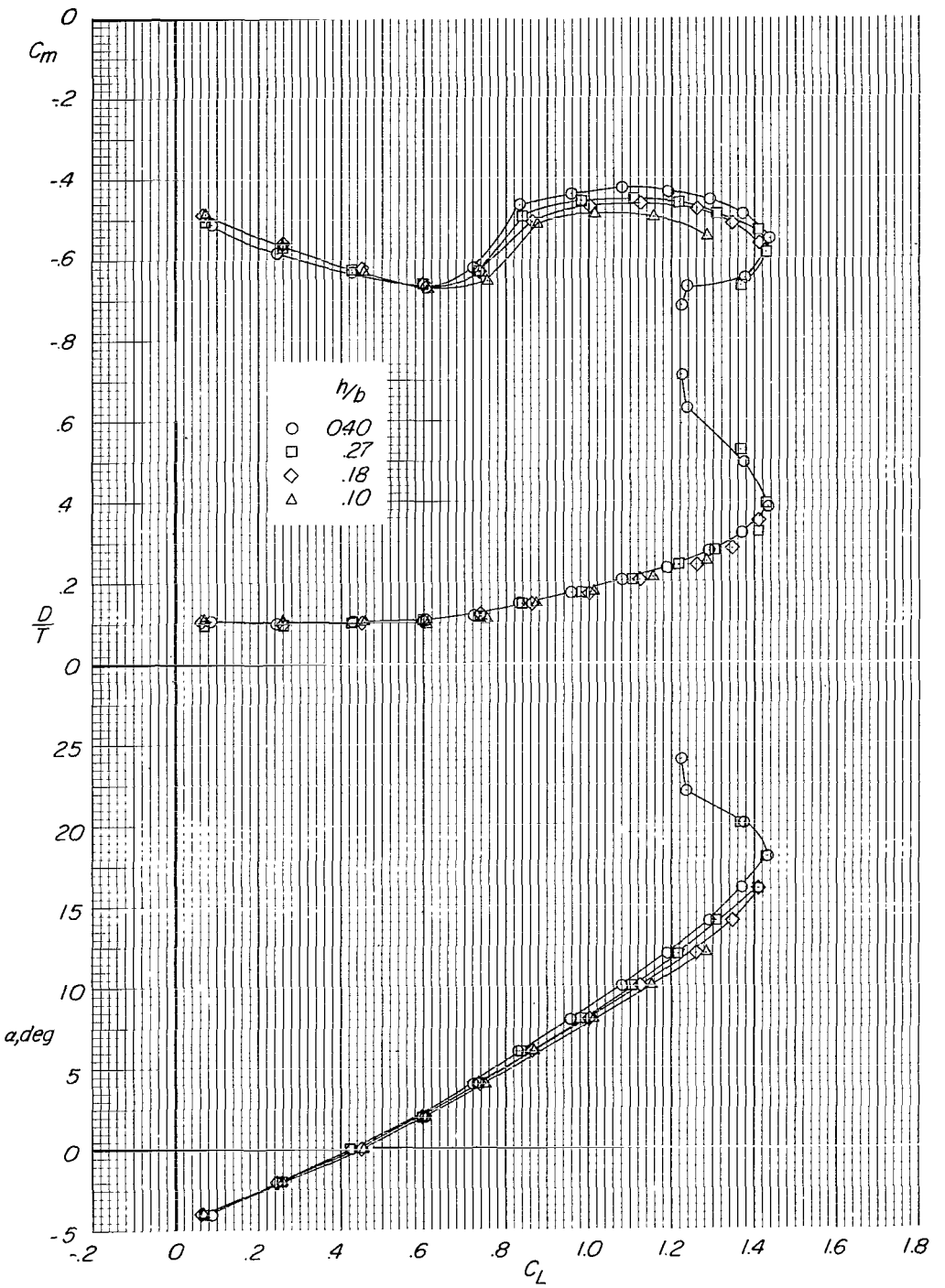

(c) $i_t = 15^0$.

Figure 26.- Concluded.

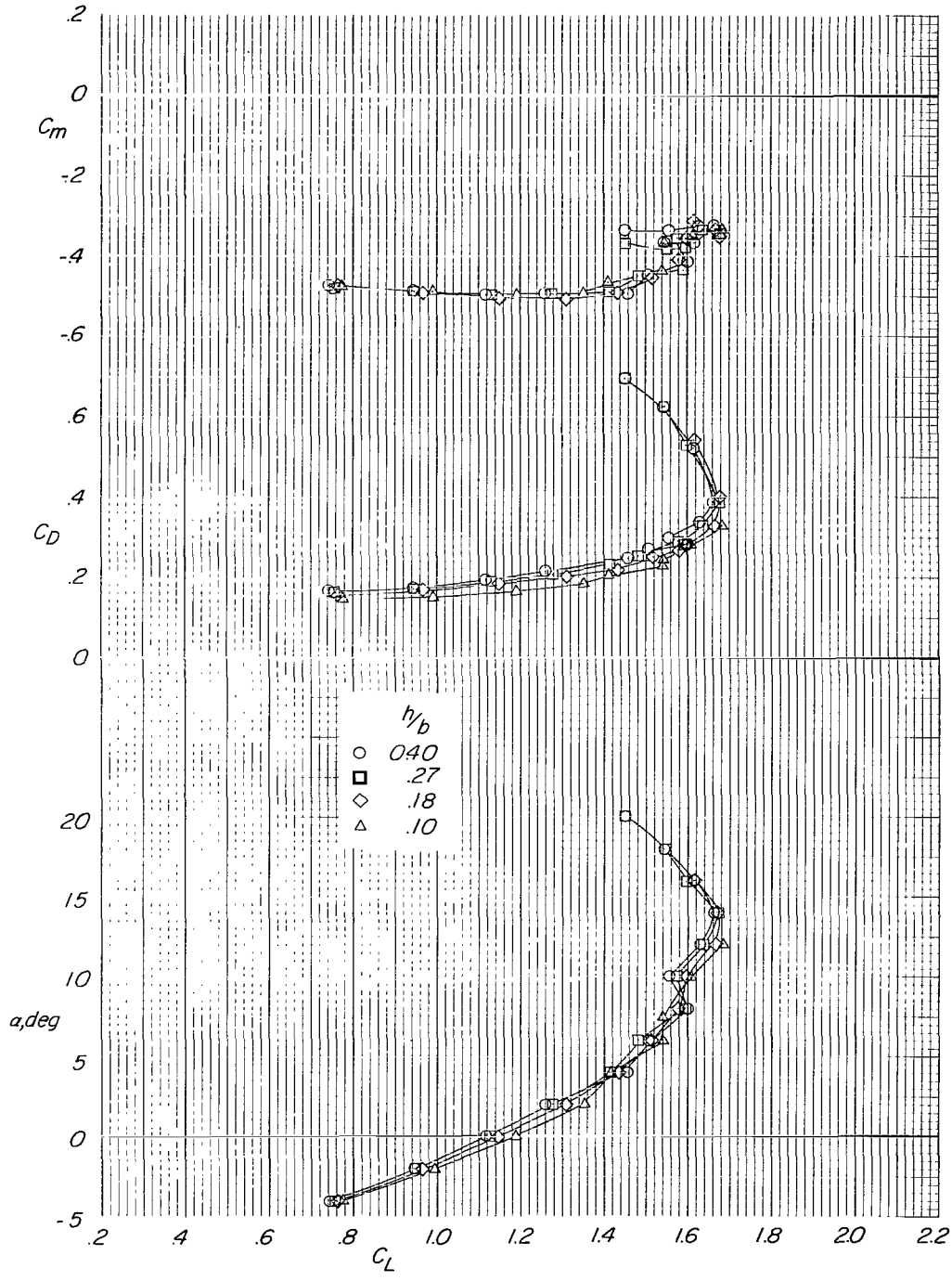

(a) Tail off.

Figure 27.- Longitudinal aerodynamic characteristics of model in ground effect with small horizontal tail off and in low position. Flaps on; power off; engine pods at midspan.

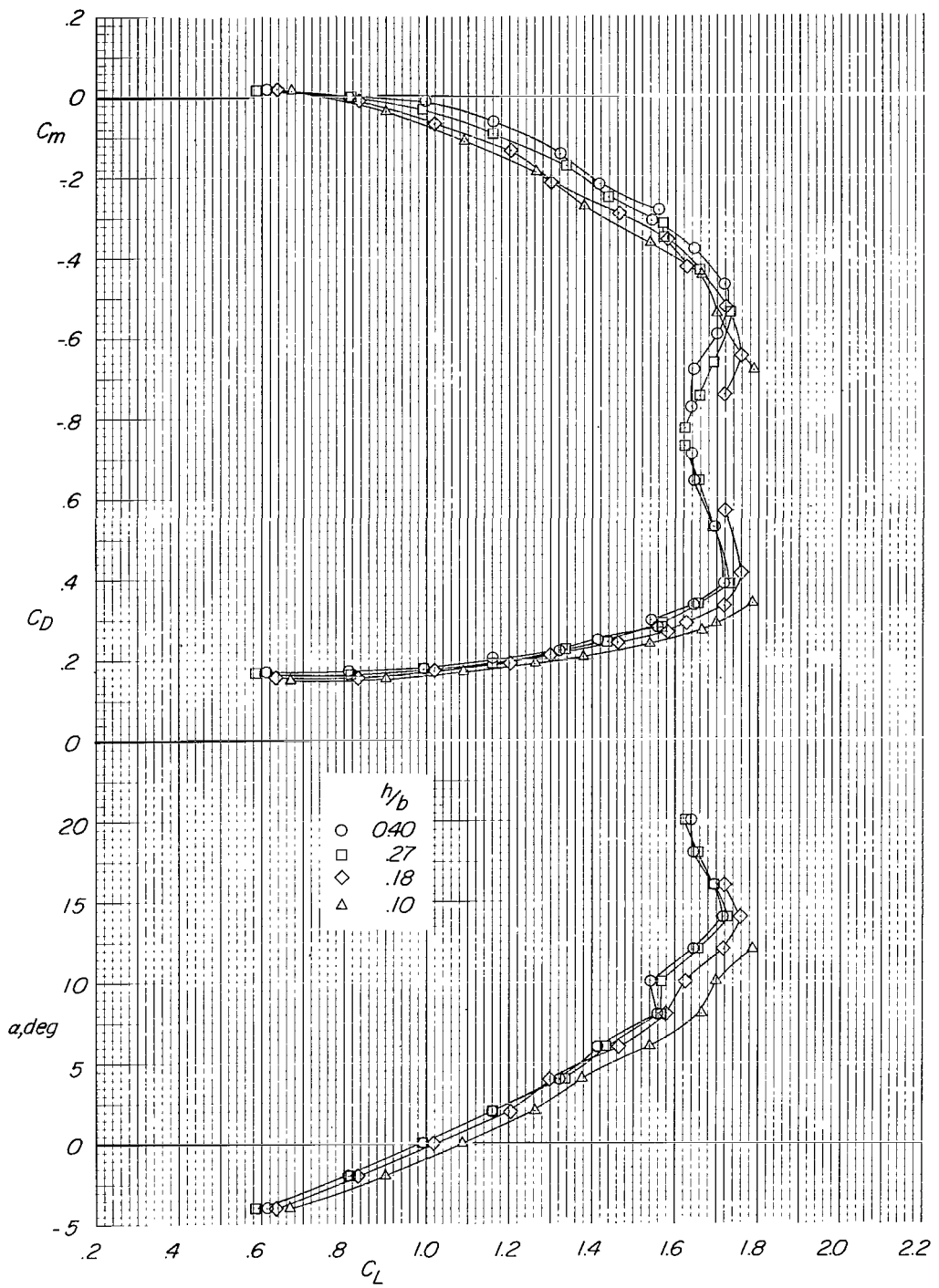

(b) $i_t = 0^0$.

Figure 27.- Continued.

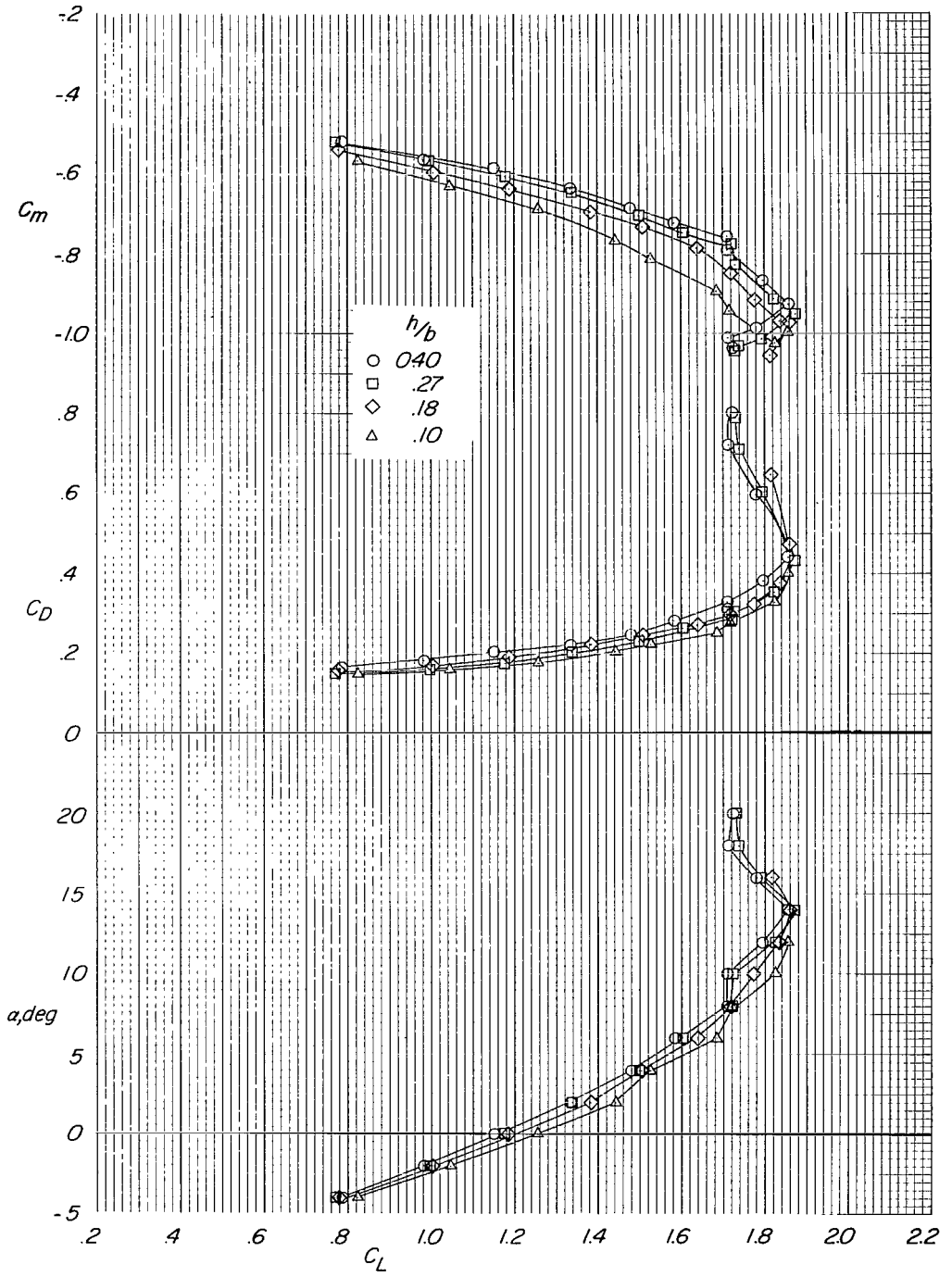

(c) $i_t = 15^0$.

Figure 27.- Concluded.

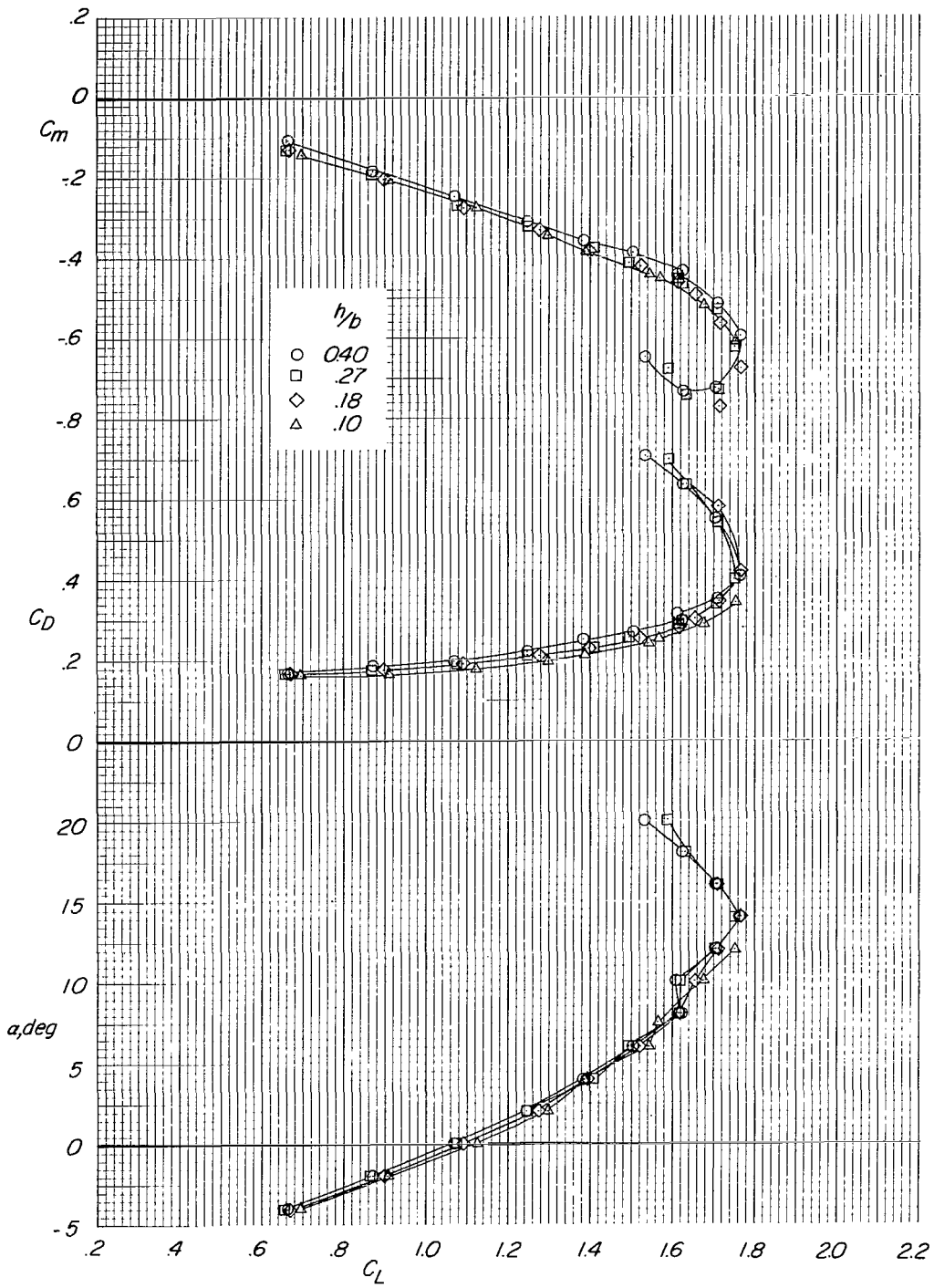

(a) $i_t = 0^o$.

Figure 28.- Longitudinal aerodynamic characteristics of model in ground effect with small horizontal tail in high position. Flaps on; power off; engine pods at midspan.

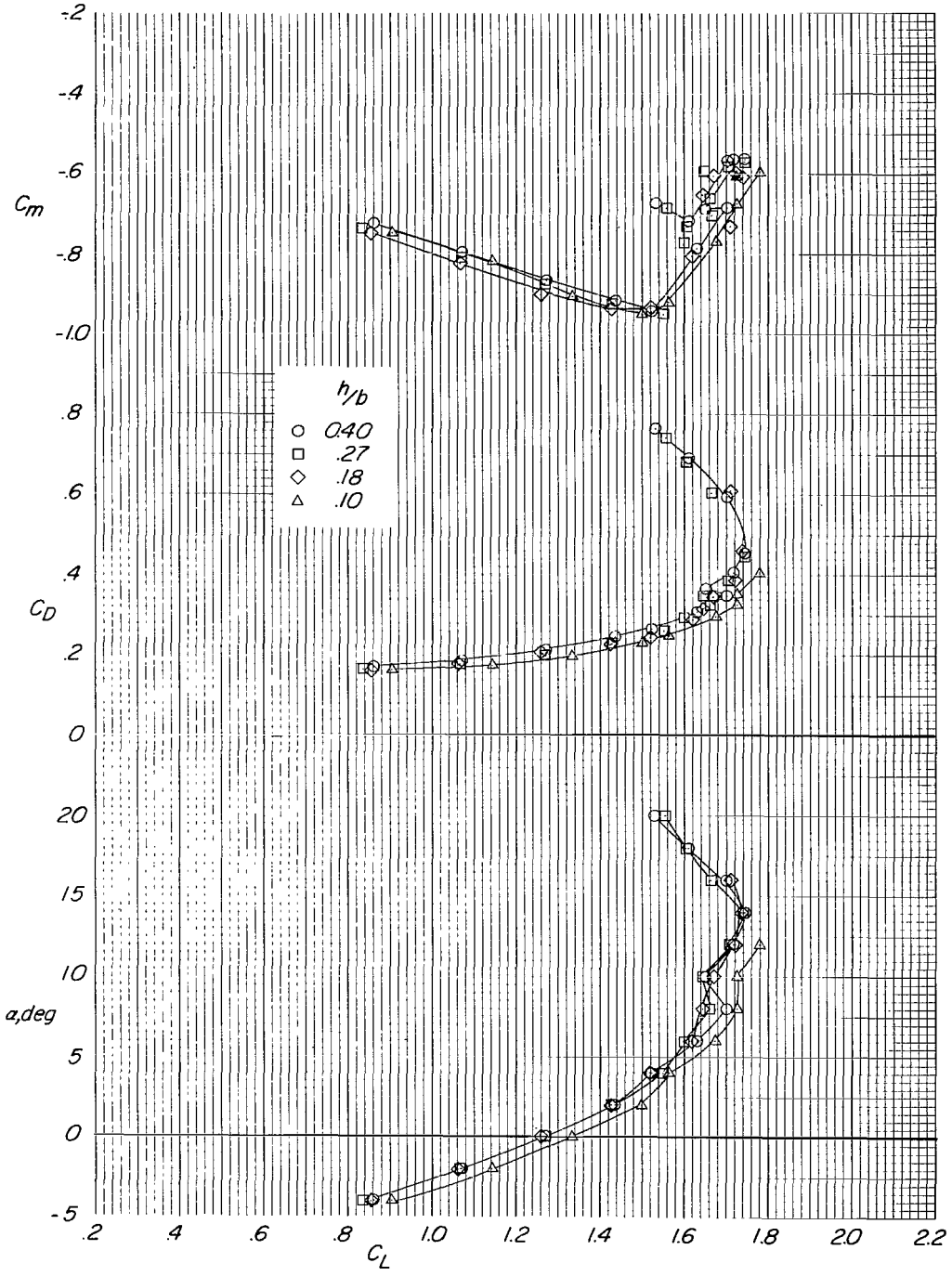

(b) $i_t = 15^0$.

Figure 28.- Concluded.

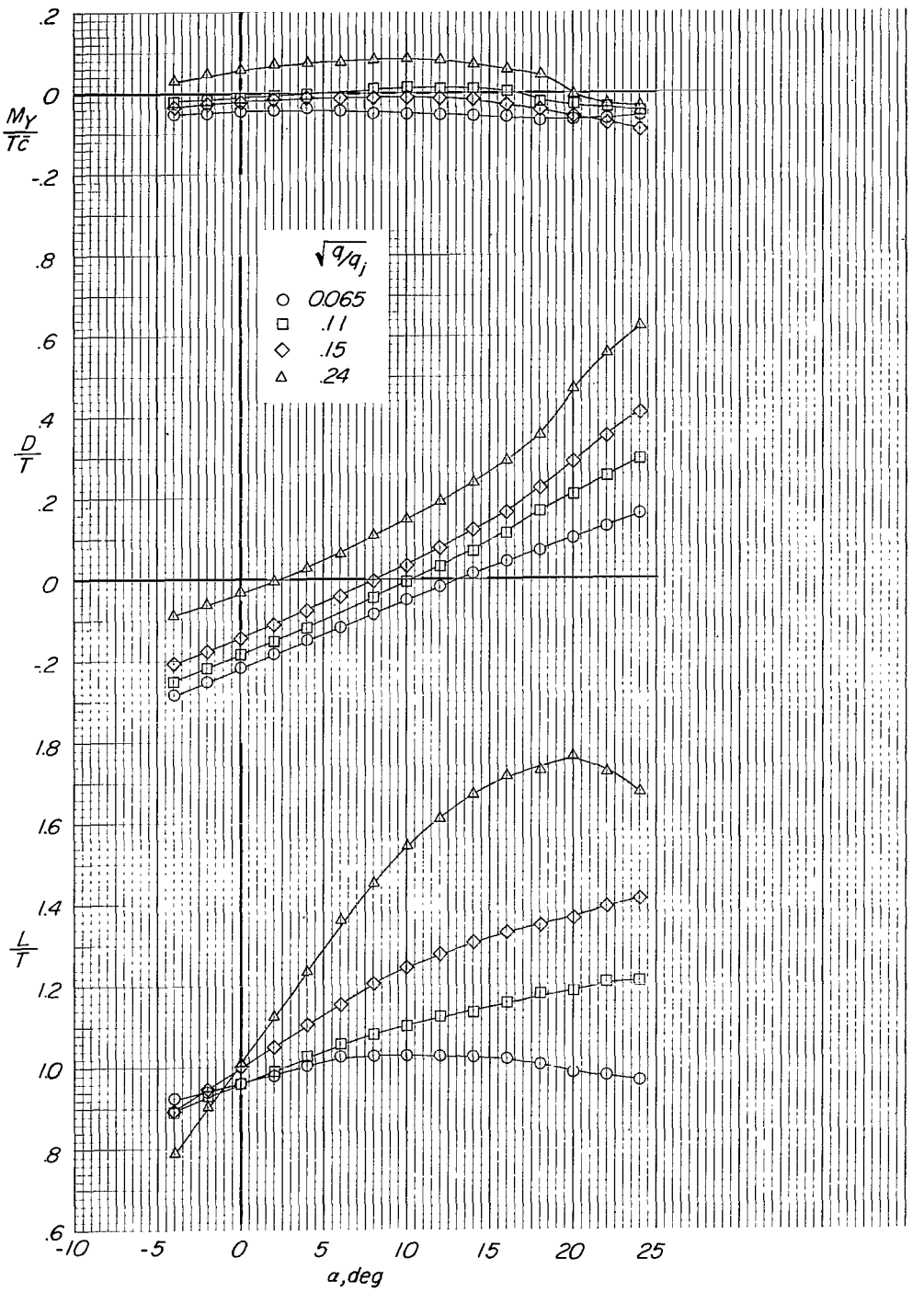

(a) h/b = 0.40.

Figure 29.- Longitudinal aerodynamic characteristics of model in ground effect. Flaps off; power on; tail off; engine pods at midspan.

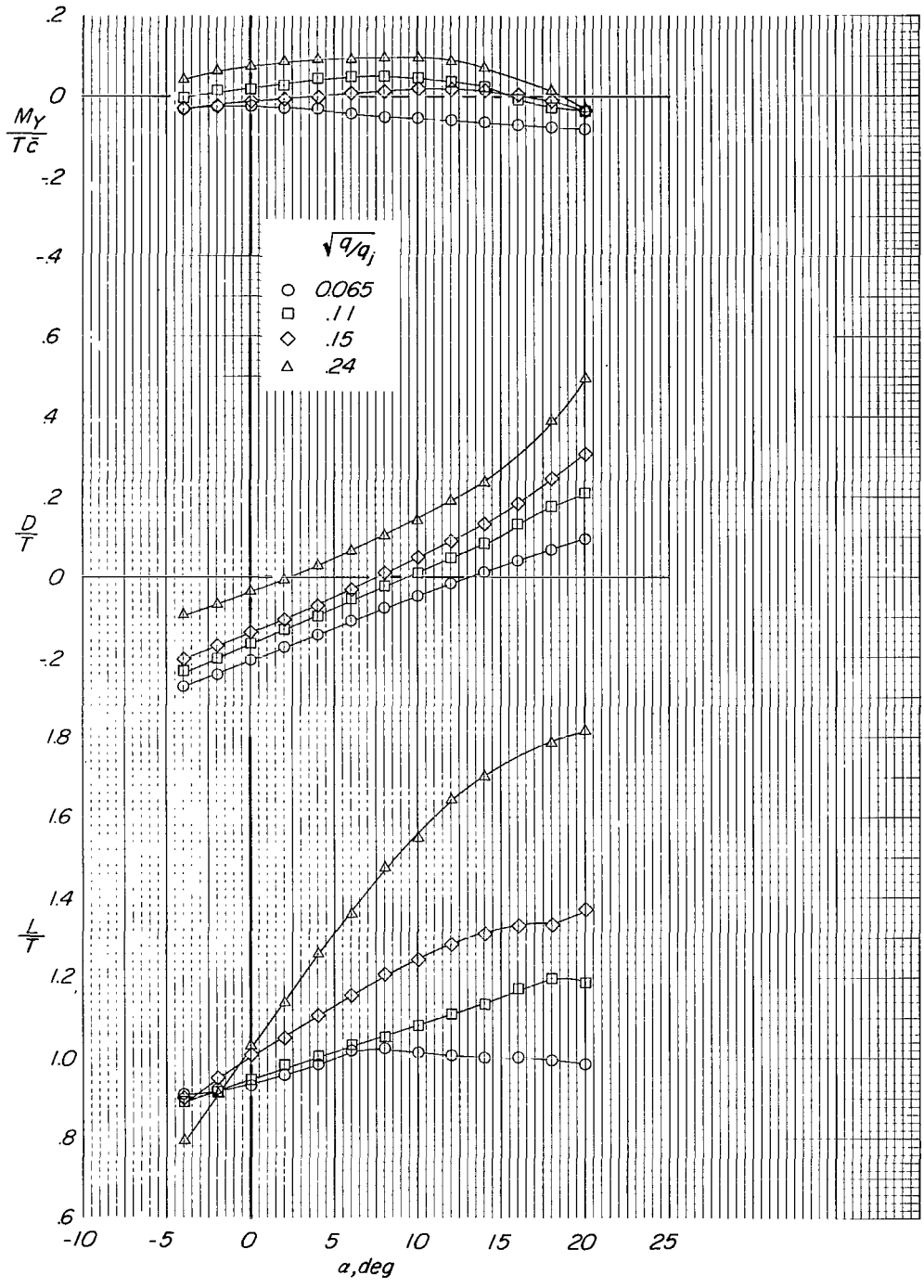

(b) h/b = 0.27.

Figure 29.- Continued.

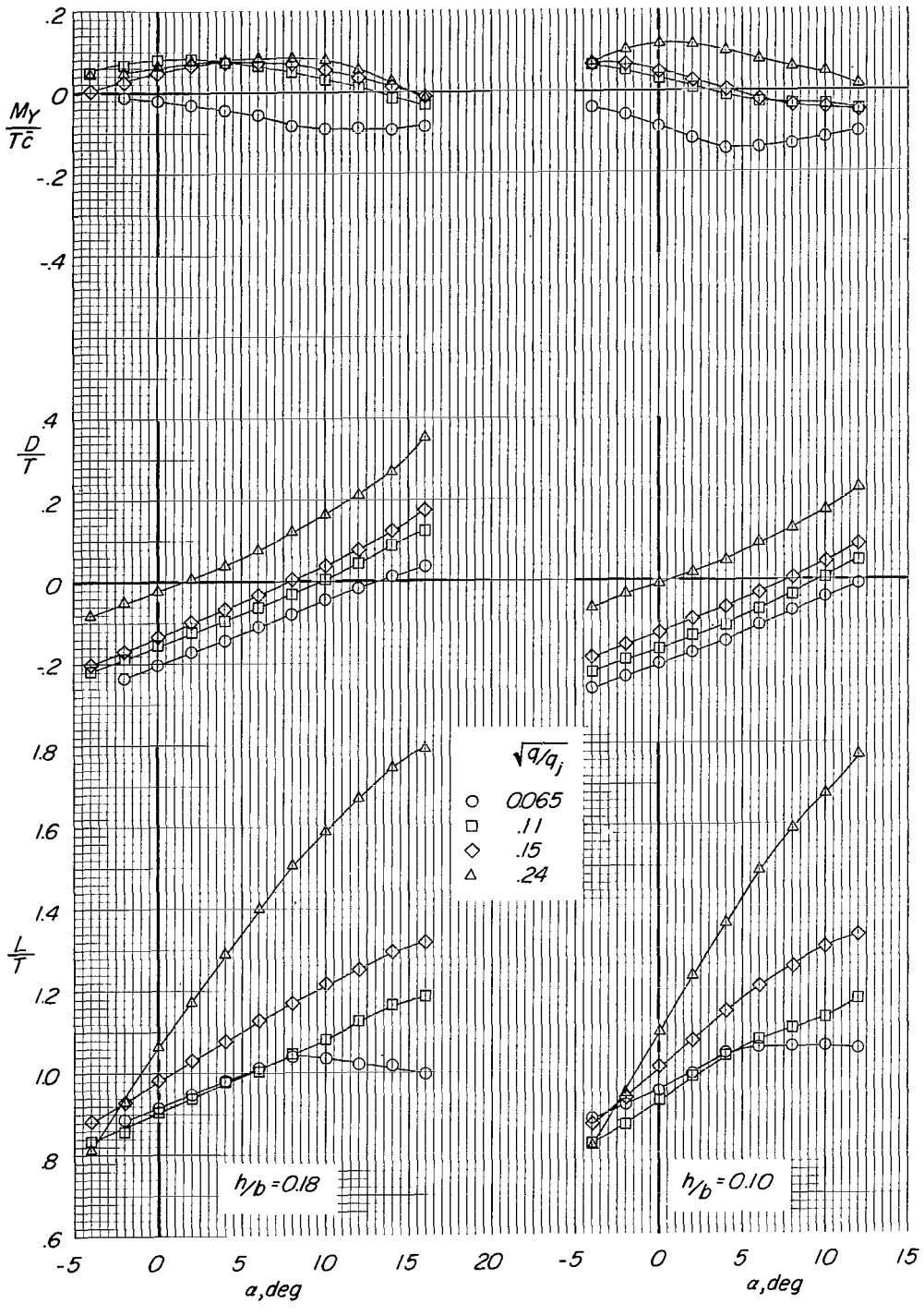

(c) h/b = 0.18 and 0.10.

Figure 29.- Concluded.

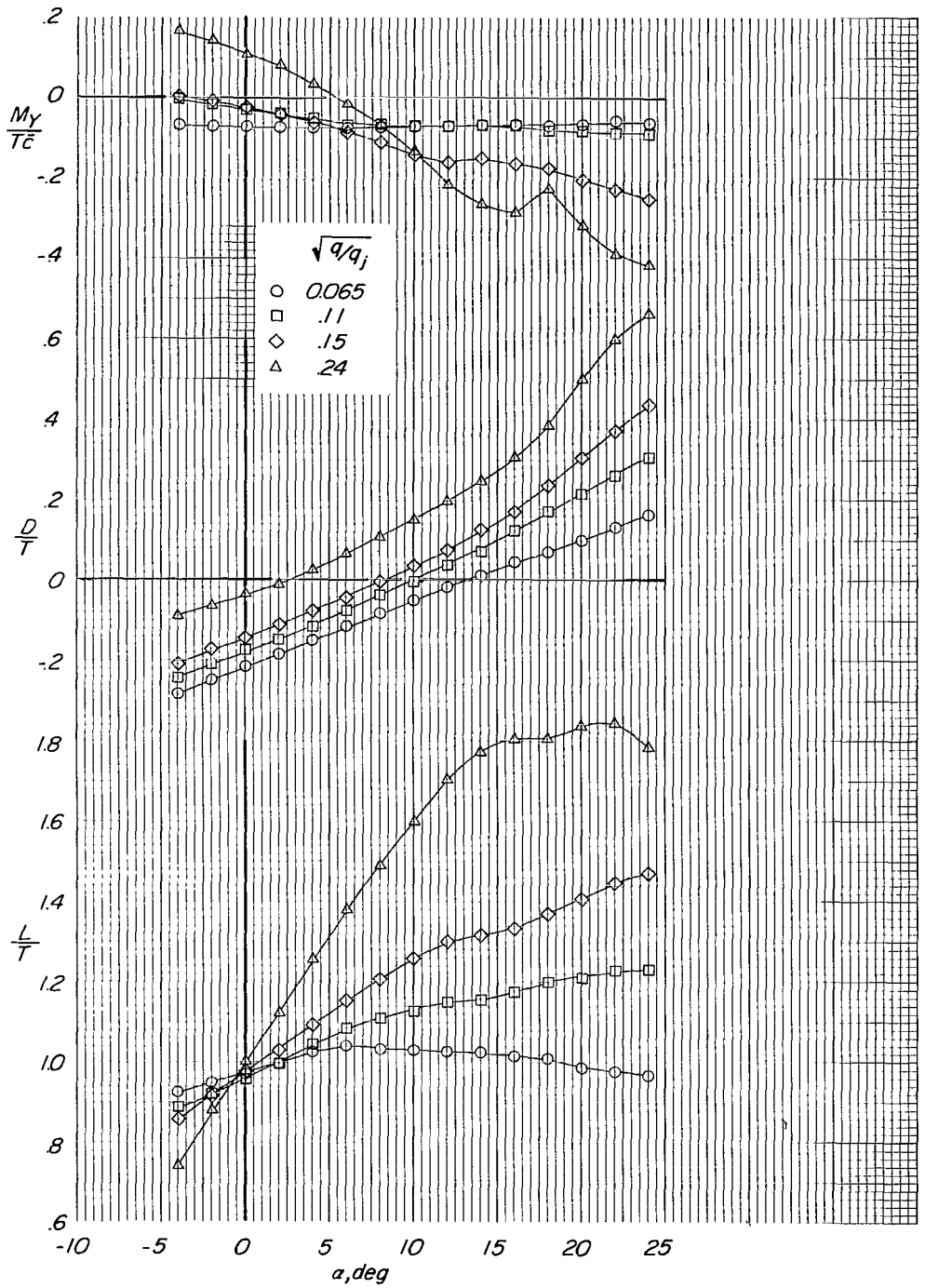

(a) $h/b = 0.40$.

Figure 30.- Longitudinal aerodynamic characteristics of model in ground effect with small tail in low position. Flaps off; power on; $i_t = 0^o$; engine pods at midspan.

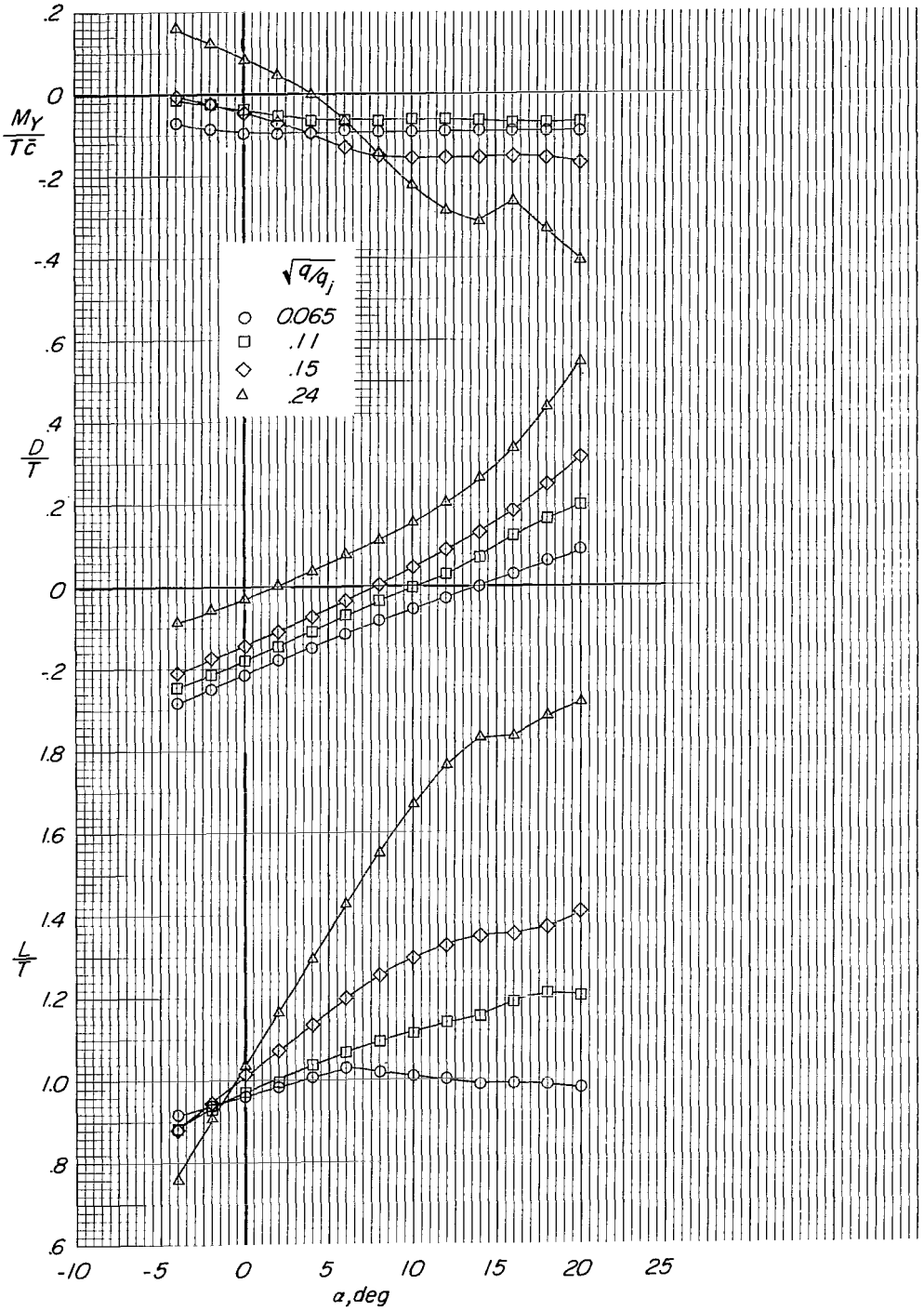

(b) h/b = 0.27.

Figure 30.- Continued.

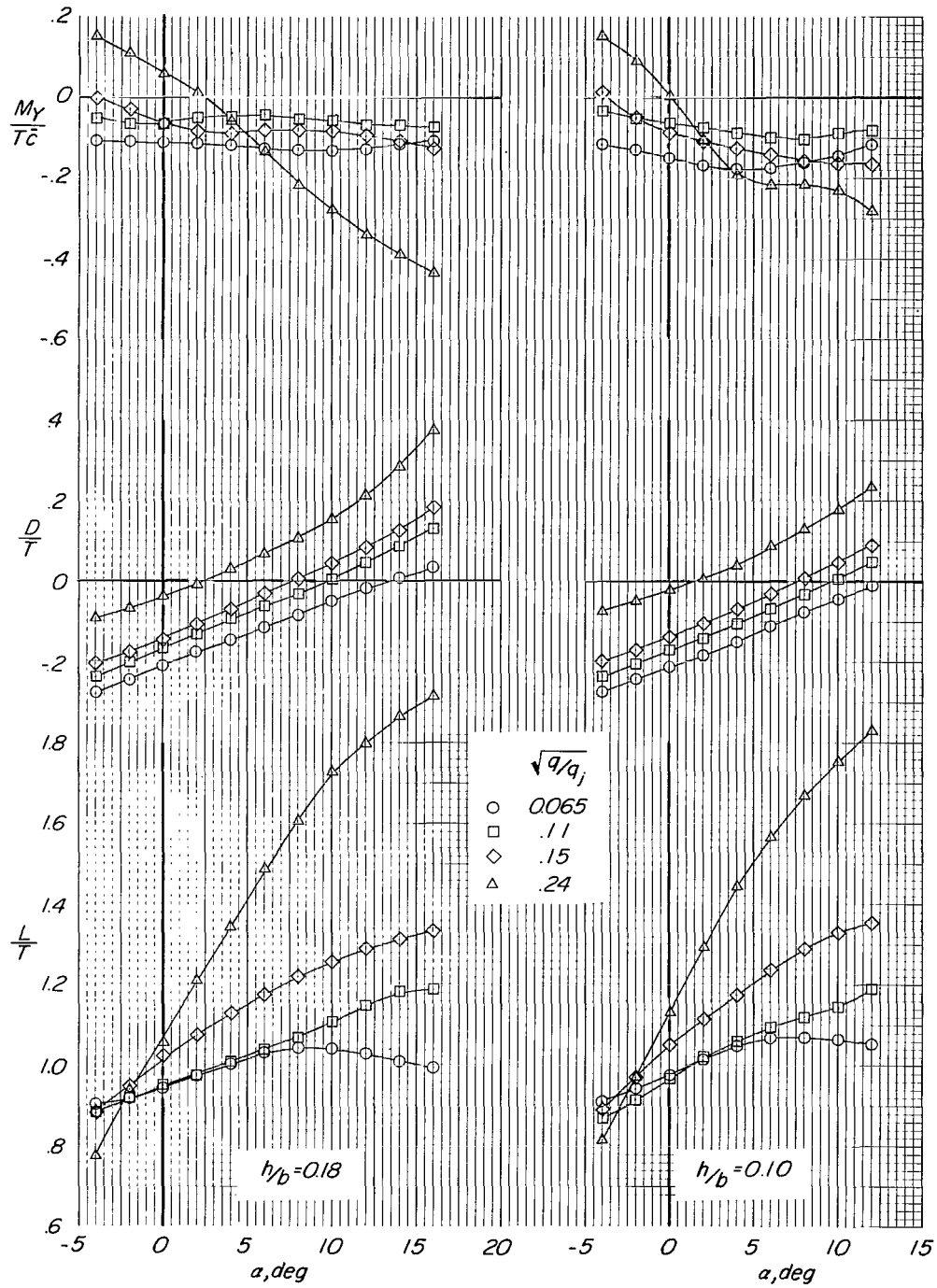

(c) h/b = 0.18 and 0.10.

Figure 30.- Concluded.

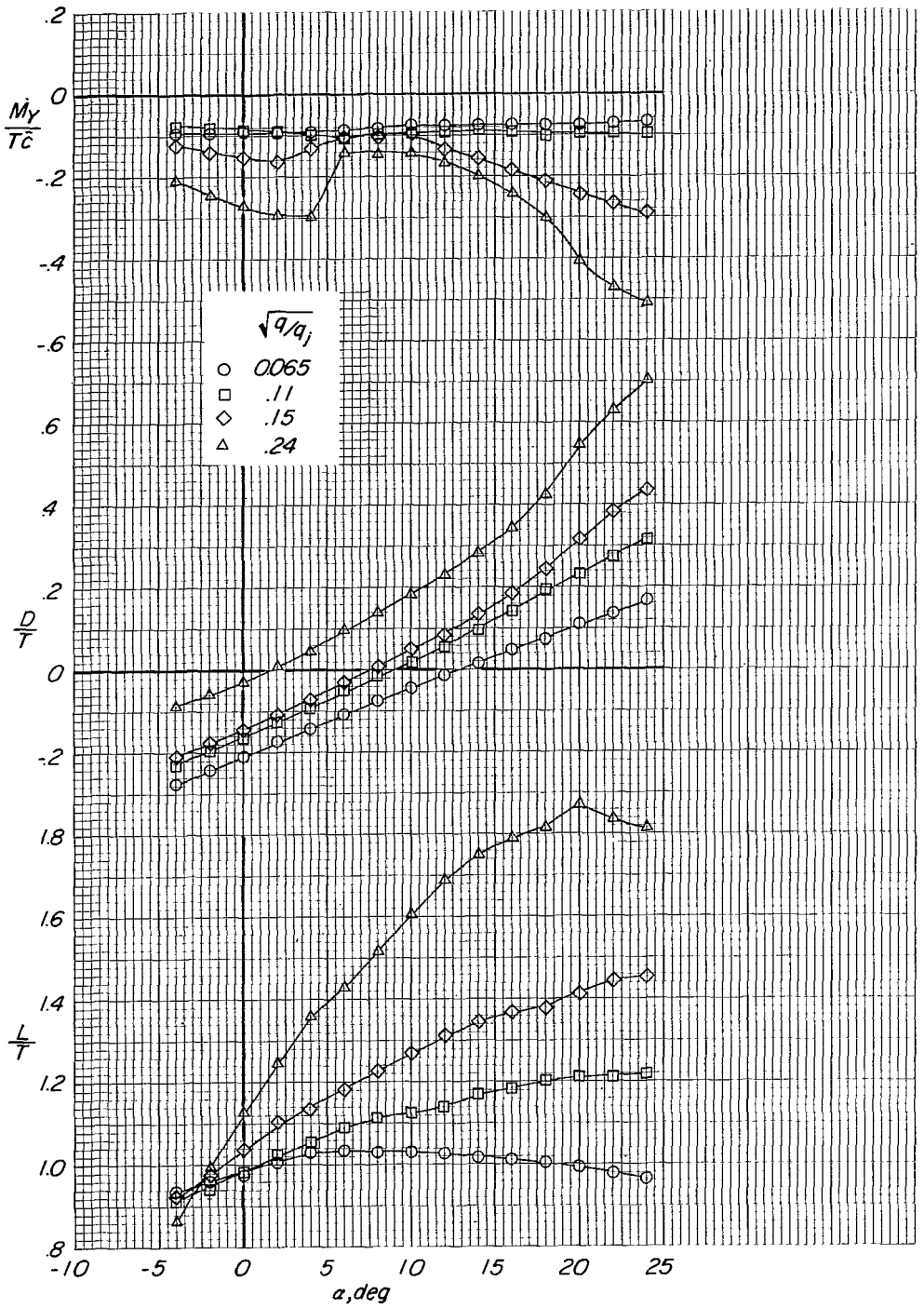

(a) h/b = 0.40.

Figure 31.- Longitudinal aerodynamic characteristics of model in ground effect with small tail in low position. Flaps off; power on; $i_t = 15^0$; engine pods at midspan.

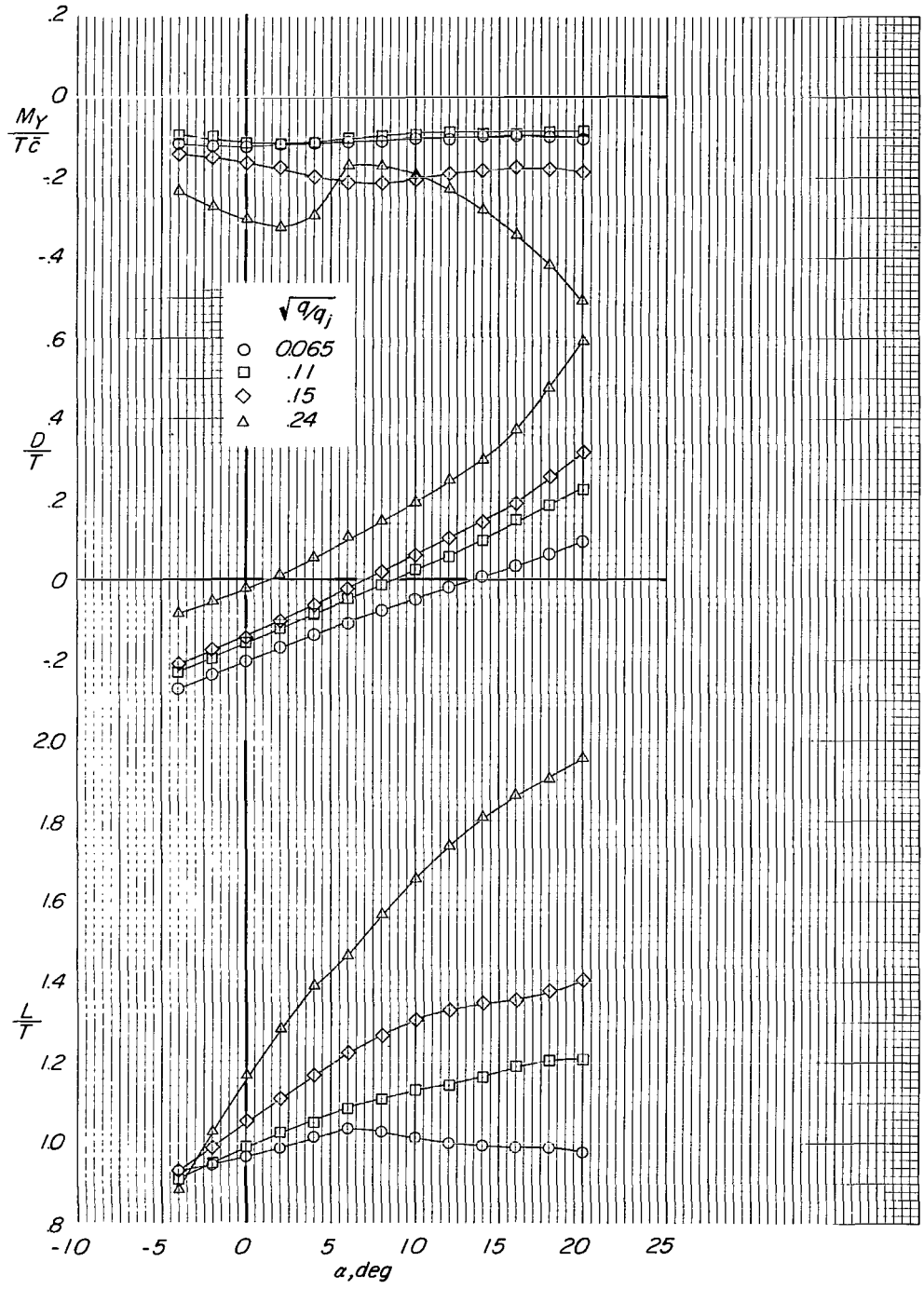

(b) h/b = 0.27.

Figure 31.- Continued.

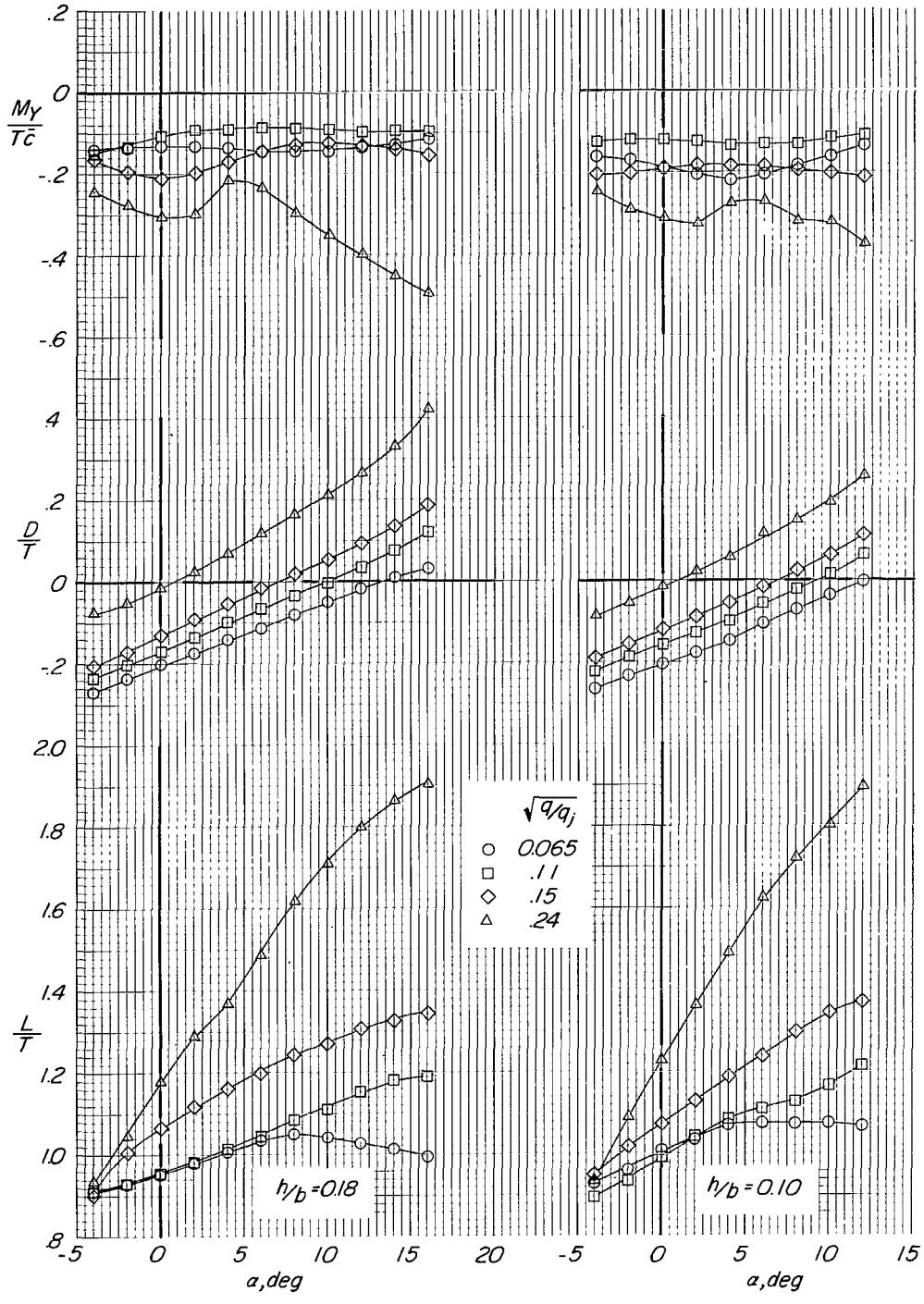

(c) h/b = 0.18 and 0.10.

Figure 31.- Concluded.

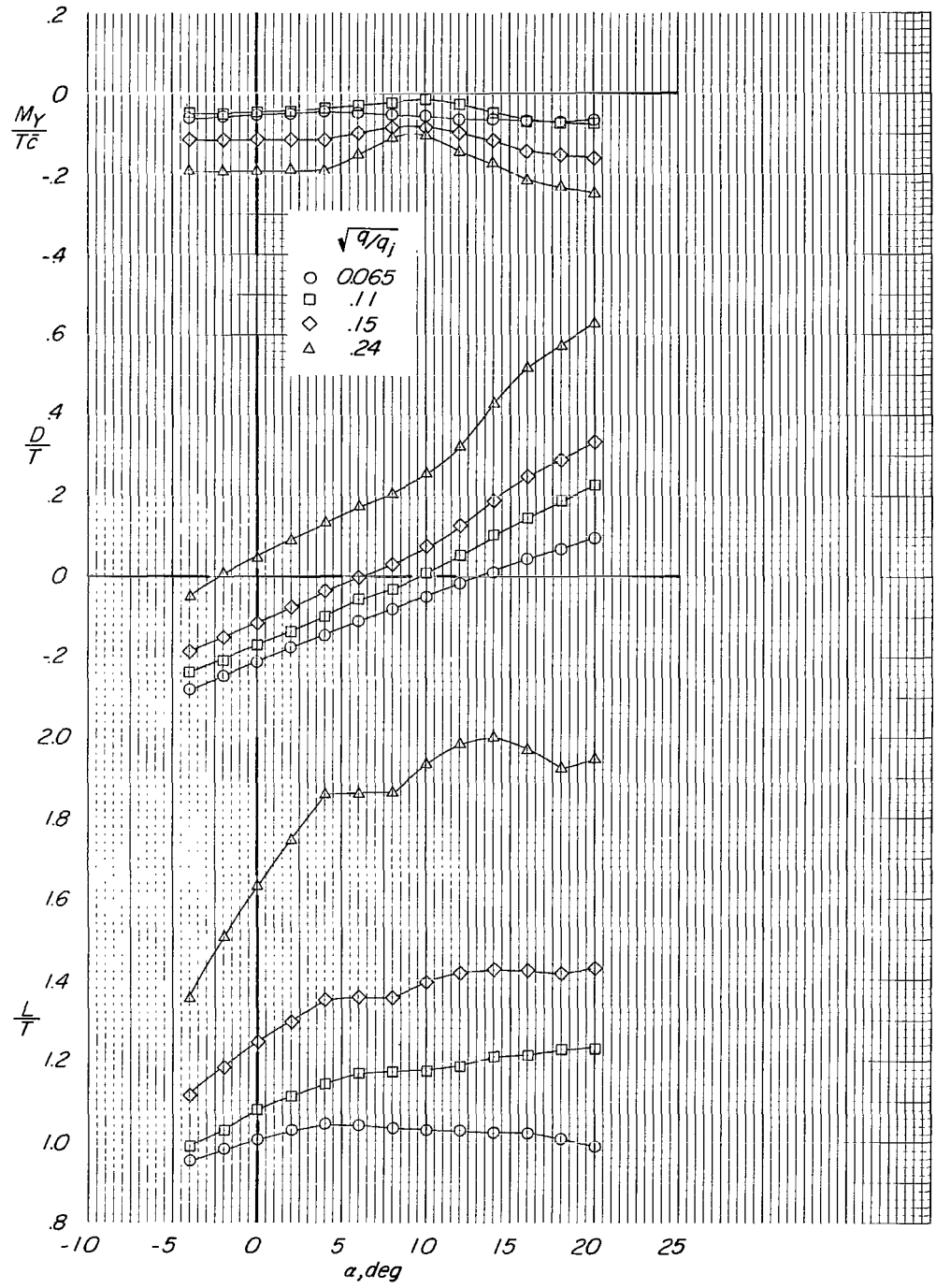

(a) h/b = 0.40.

Figure 32.- Longitudinal aerodynamic characteristics of model in ground effect. Flaps on; power on; tail off; engine pods at midspan.

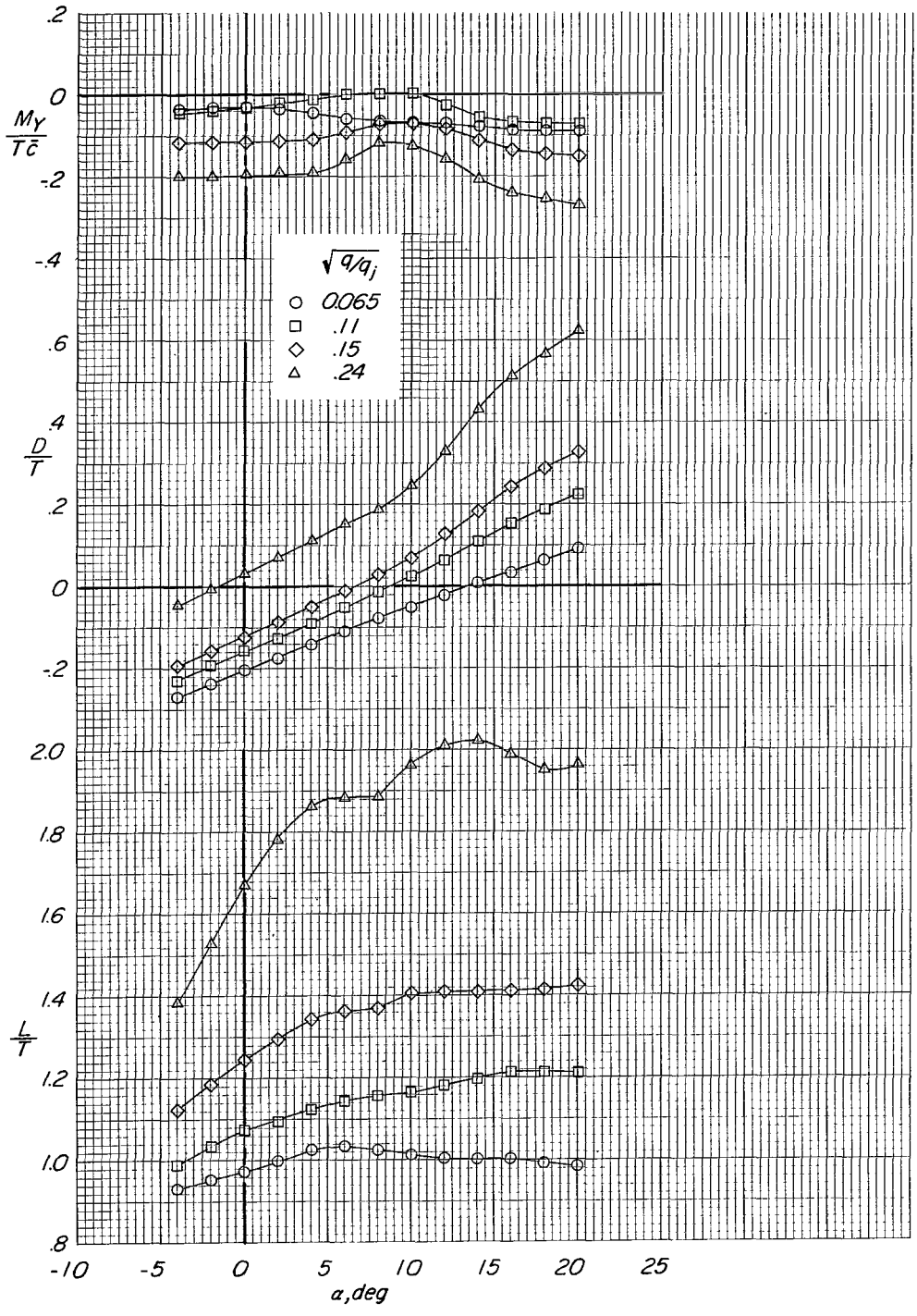

(b) h/b = 0.27.

Figure 32.- Continued.

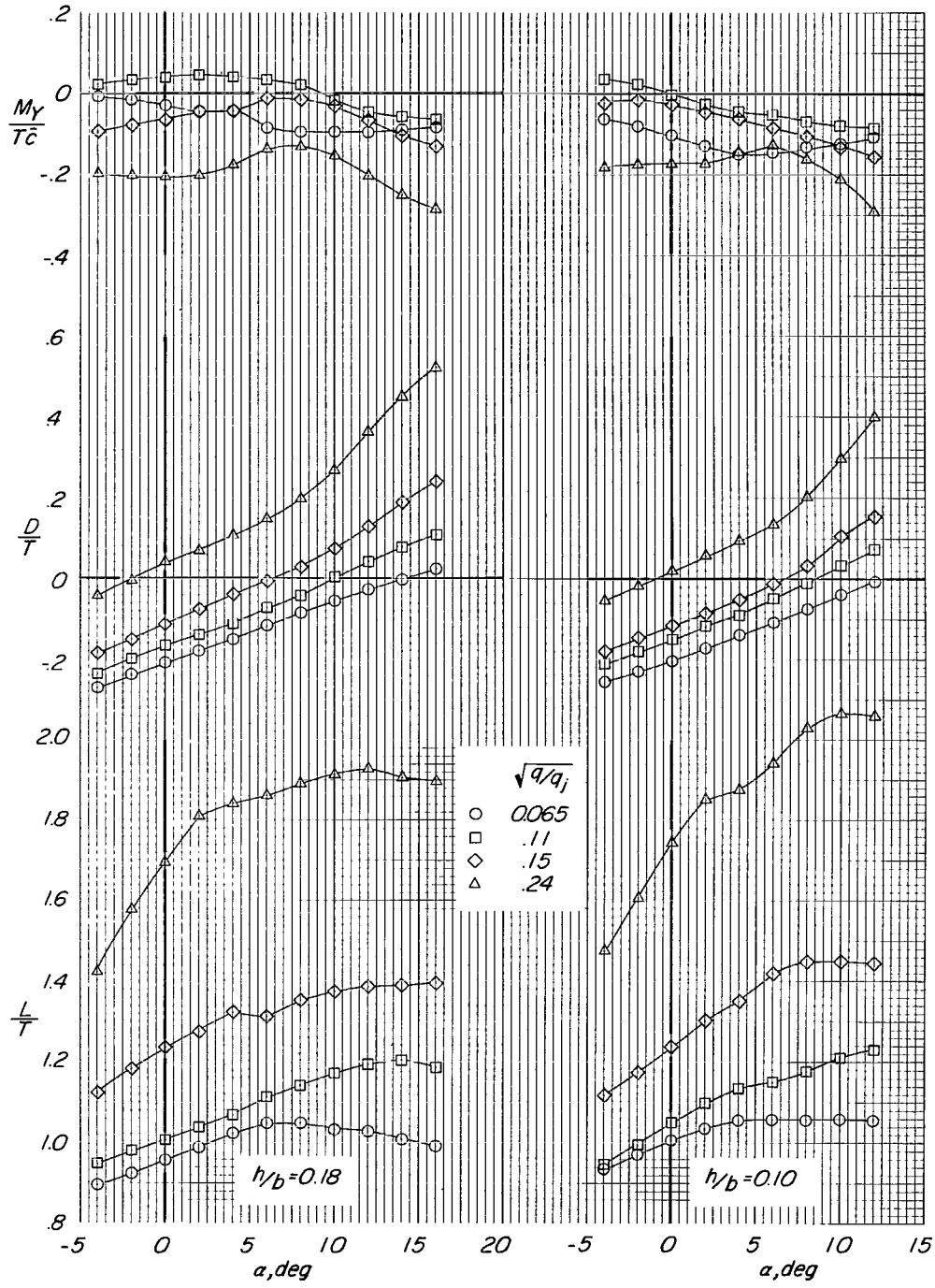

(c) h/b = 0.18 and 0.10.

Figure 32.- Concluded.

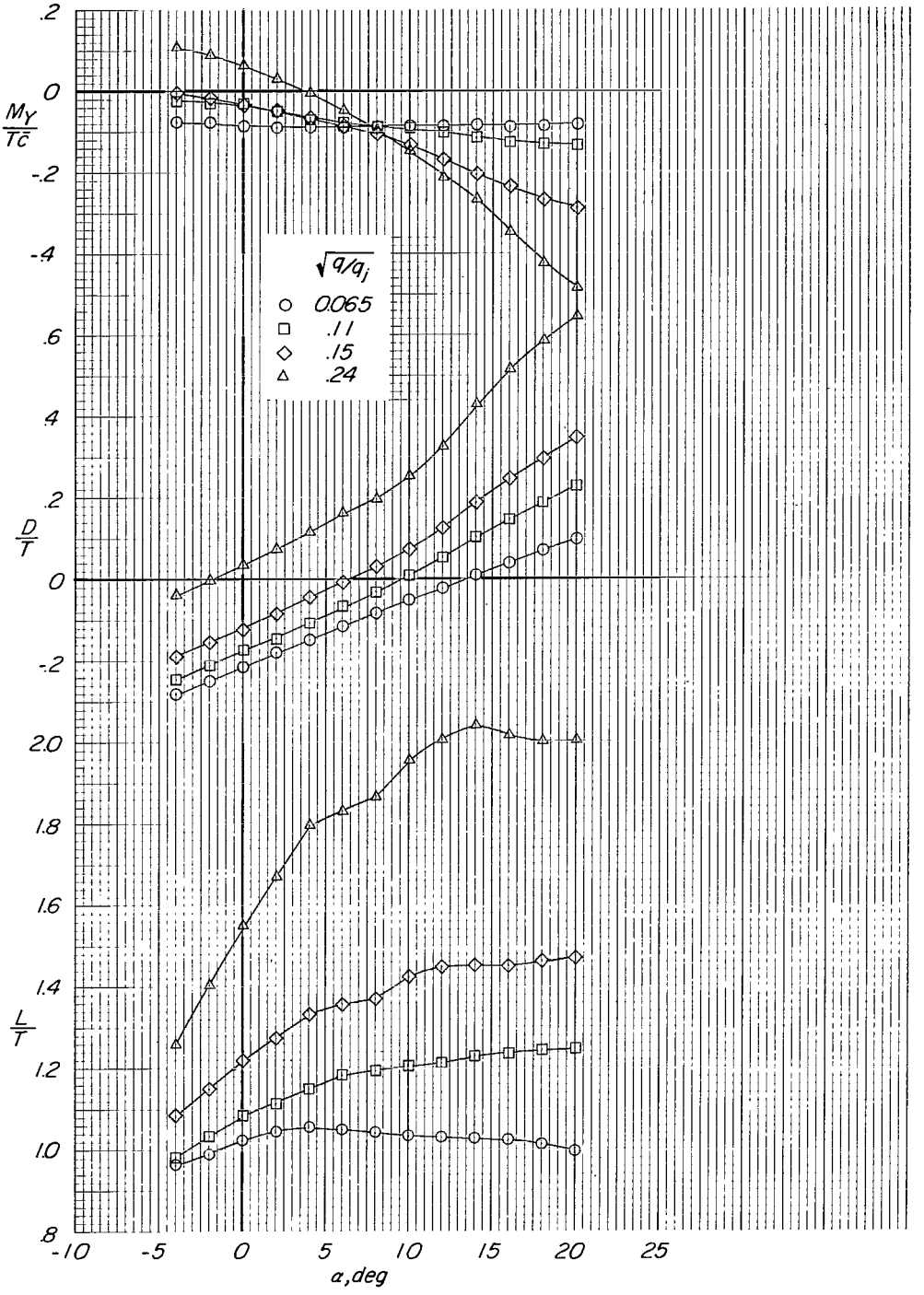

(a) h/b = 0.40.

Figure 33.- Longitudinal aerodynamic characteristics of model in ground effect with small tail in low position. Flaps on; power on; $i_t = 0^0$; engine pods at midspan.

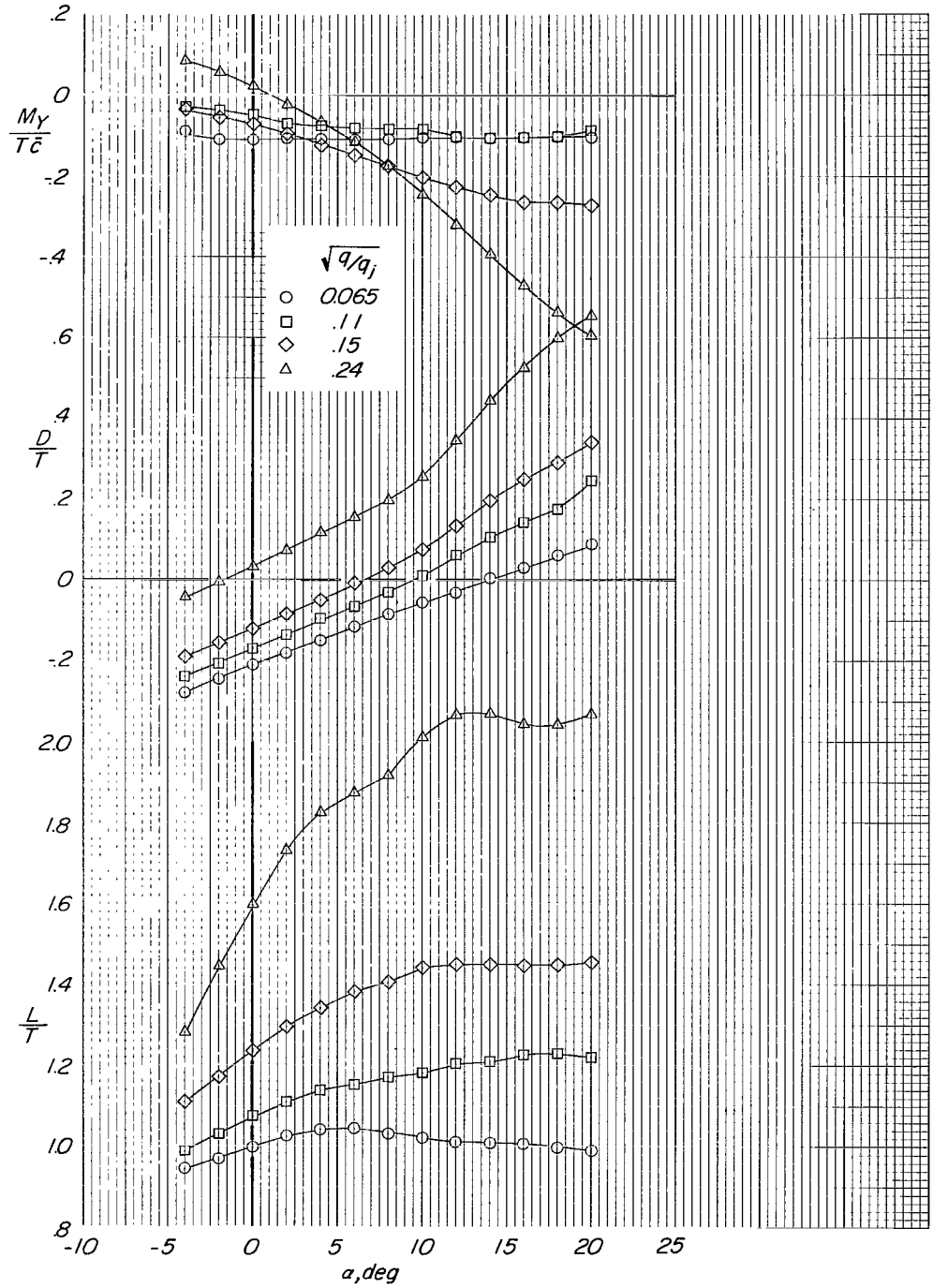

(b) h/b = 0.27.

Figure 33.- Continued.

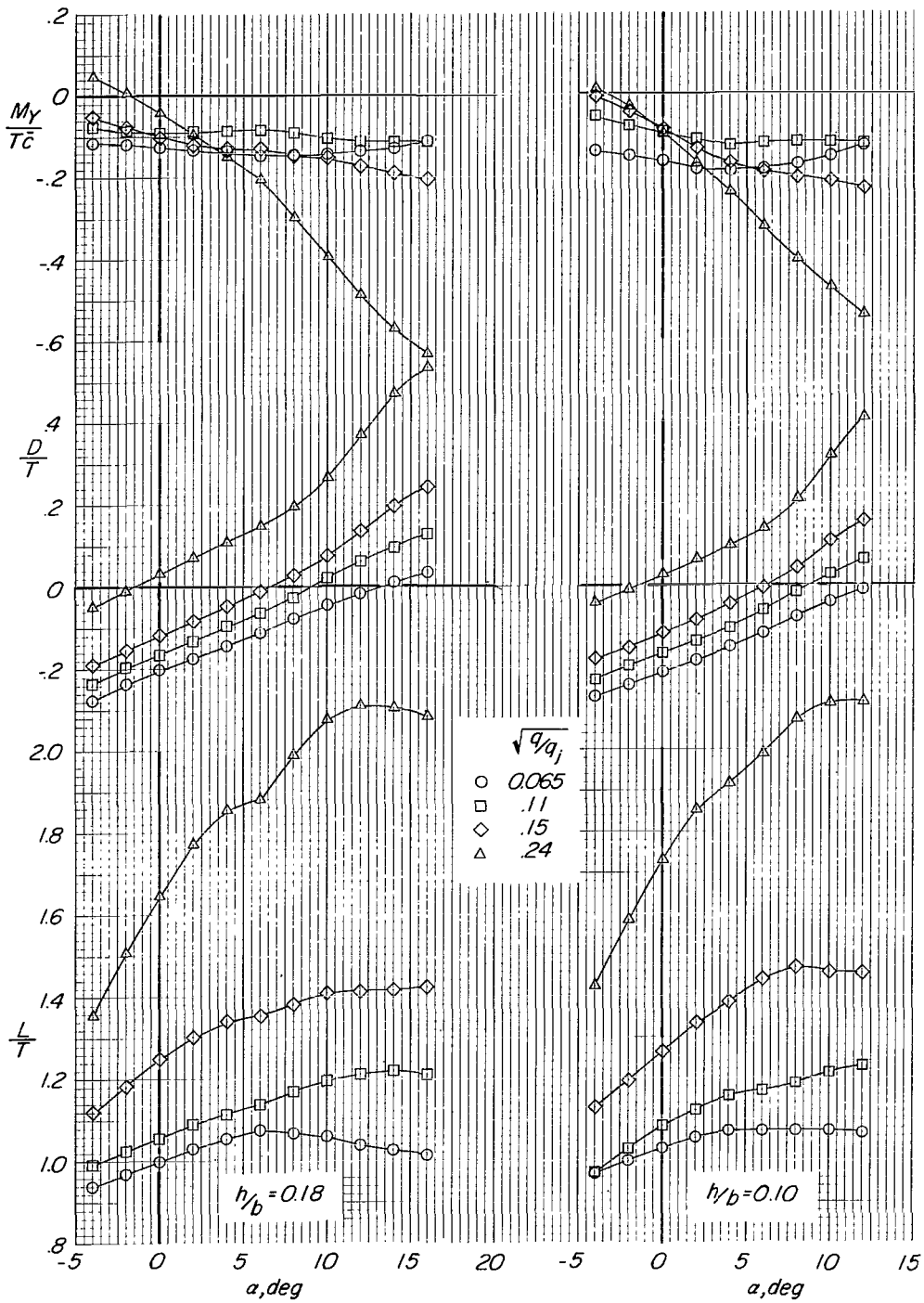

(c) h/b = 0.18 and 0.10.

Figure 33.- Concluded.

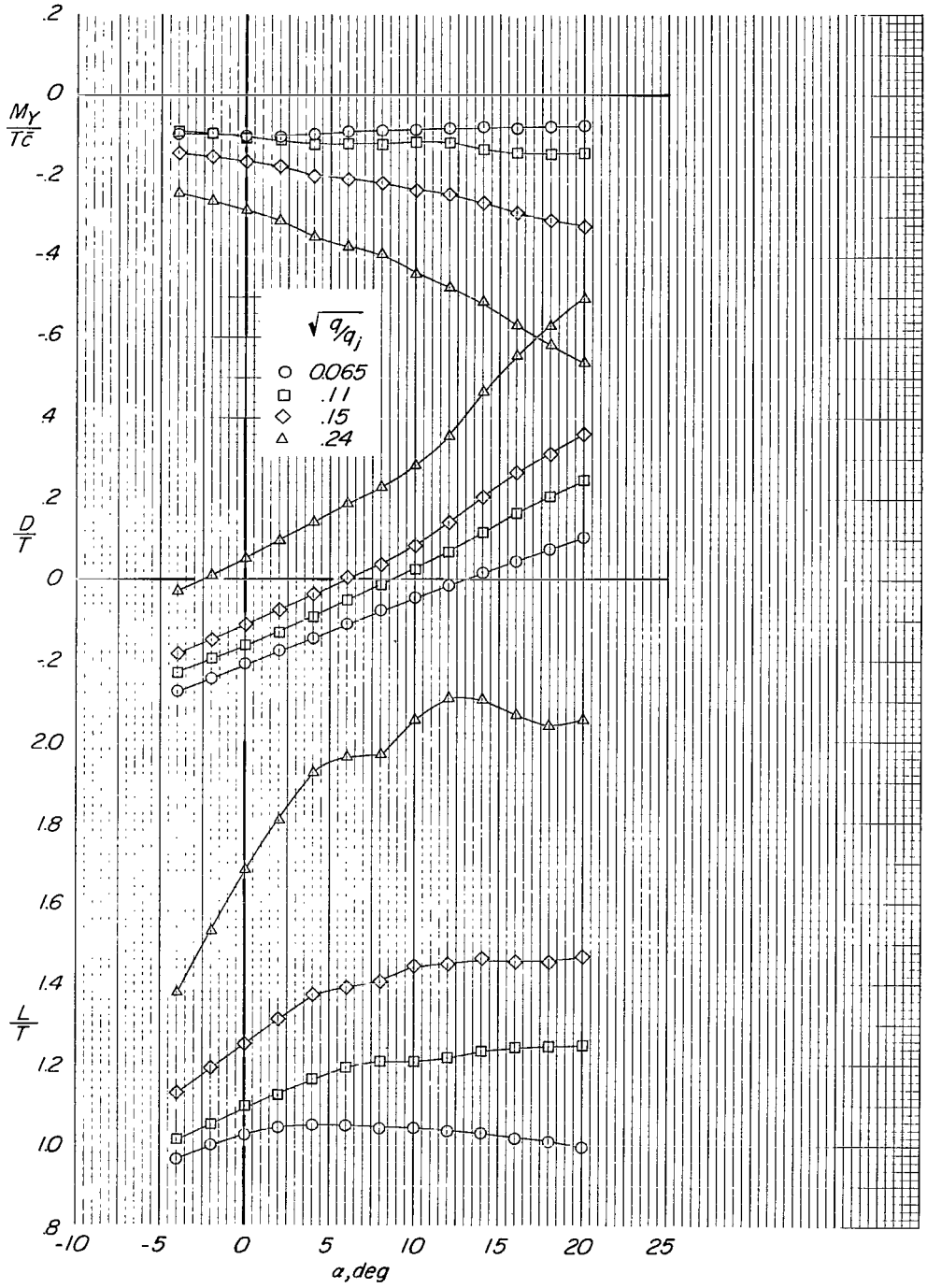

(a) h/b = 0.40.

Figure 34.- Longitudinal aerodynamic characteristics of model in ground effect with small tail in low position. Flaps on; power on; $i_t = 15^0$; engine pods at midspan.

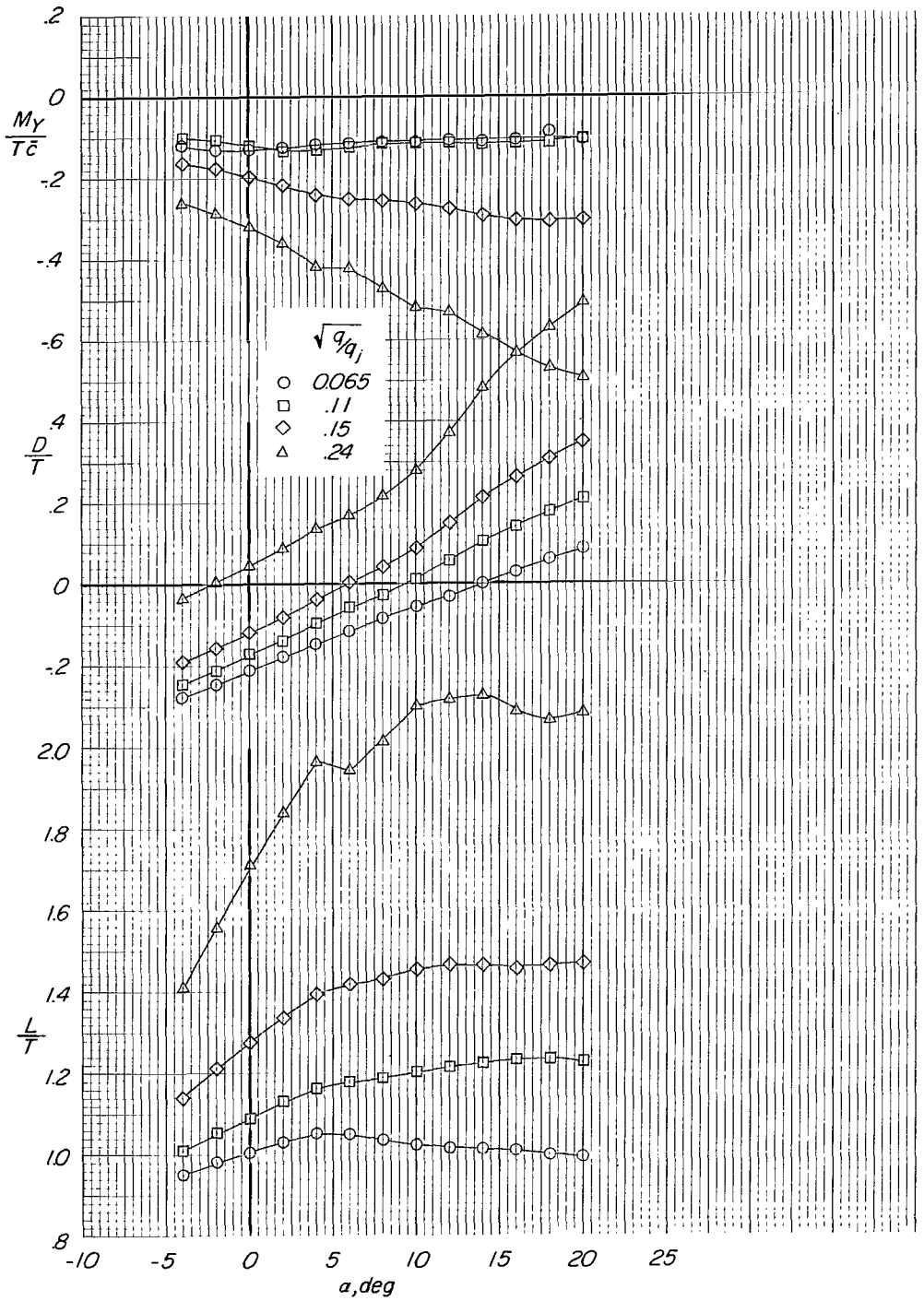

(b) h/b = 0.27.

Figure 34.- Continued.

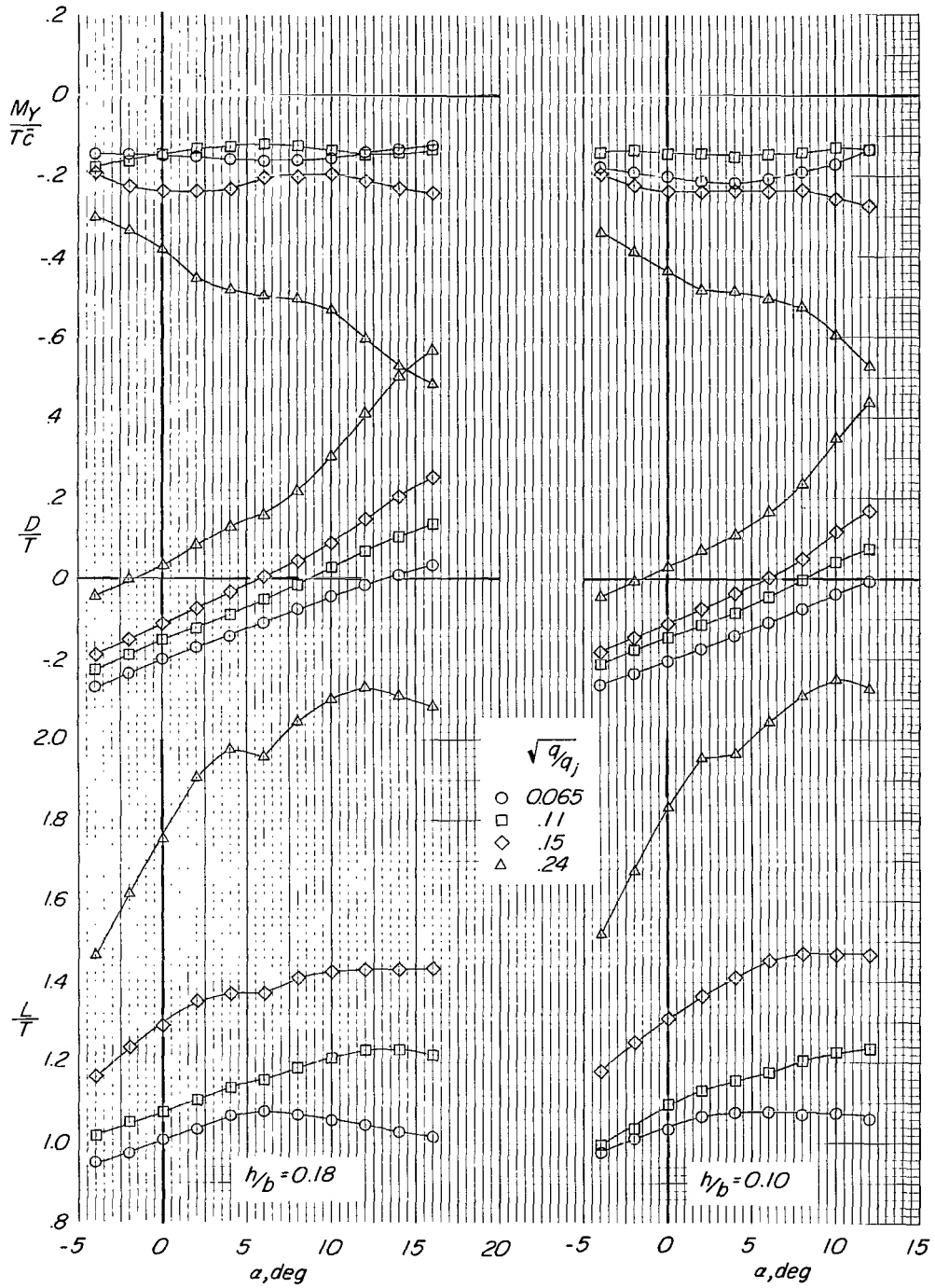

(c) h/b = 0.18 and 0.10.

Figure 34.- Concluded.

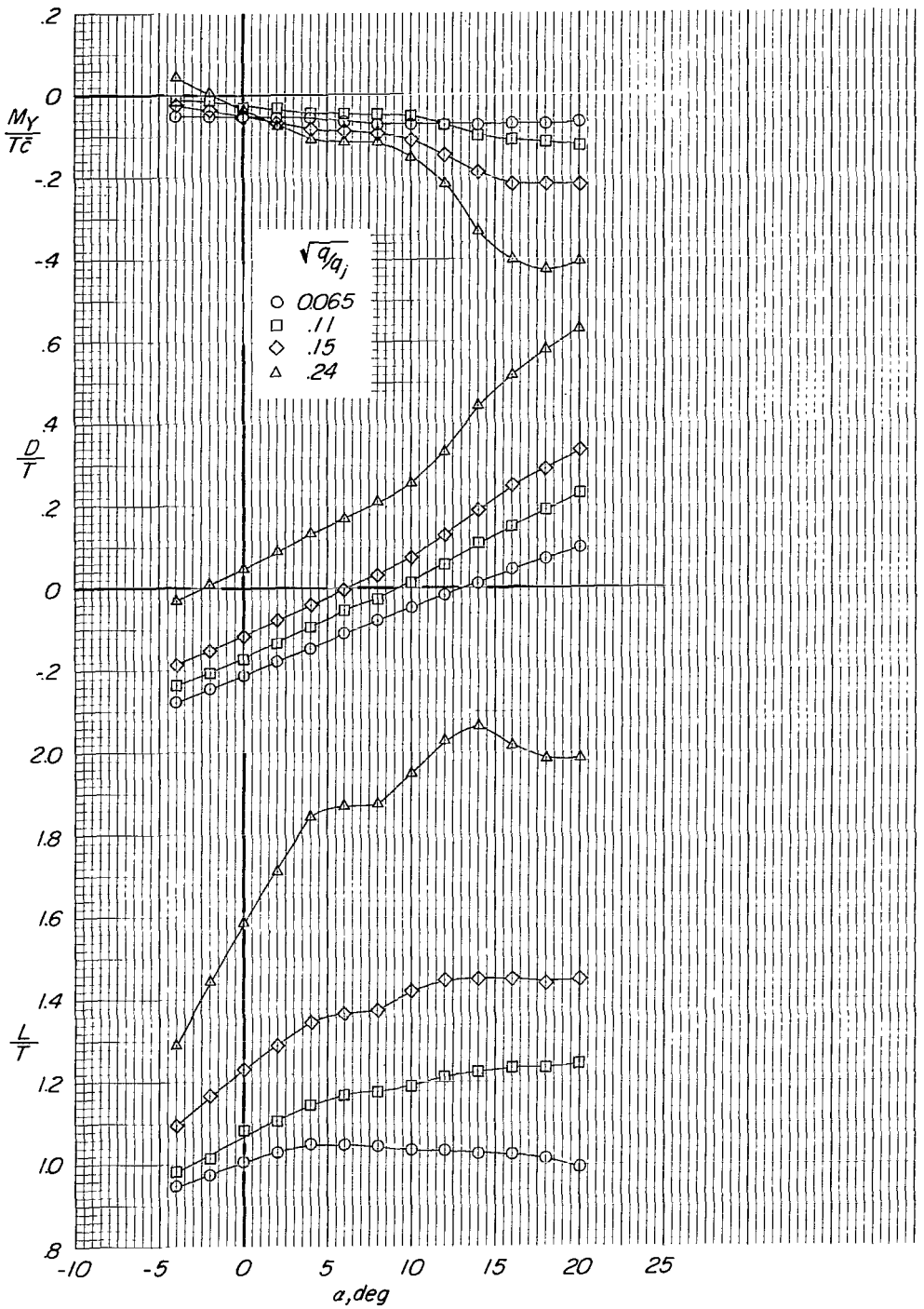

(a) h/b = 0.40.

Figure 35.- Longitudinal aerodynamic characteristics of model in ground effect with small horizontal tail in high position. Flaps on; power on; $i_t = 0^0$; engine pods at midspan.

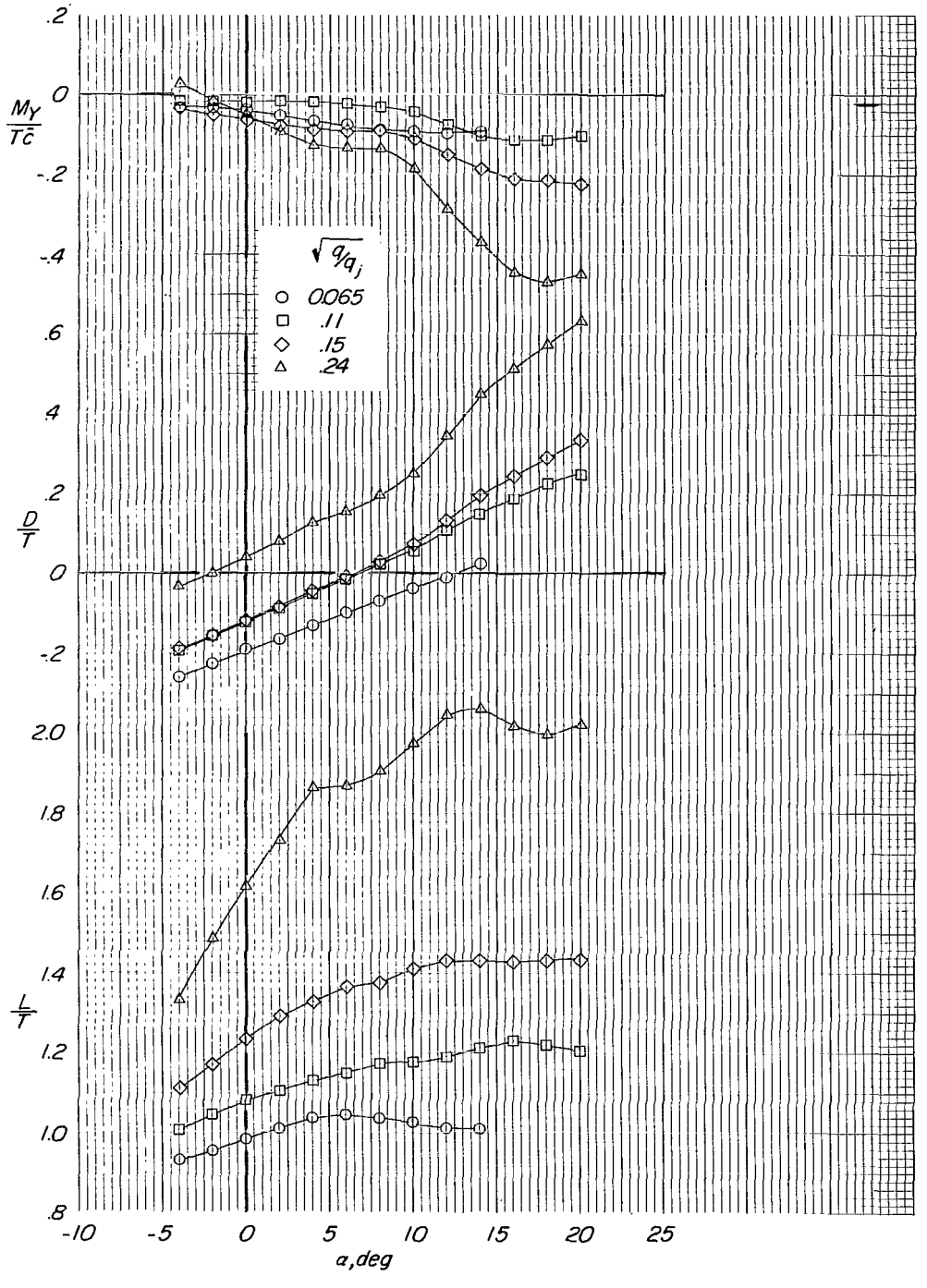

(b) h/b = 0.27.

Figure 35.- Continued.

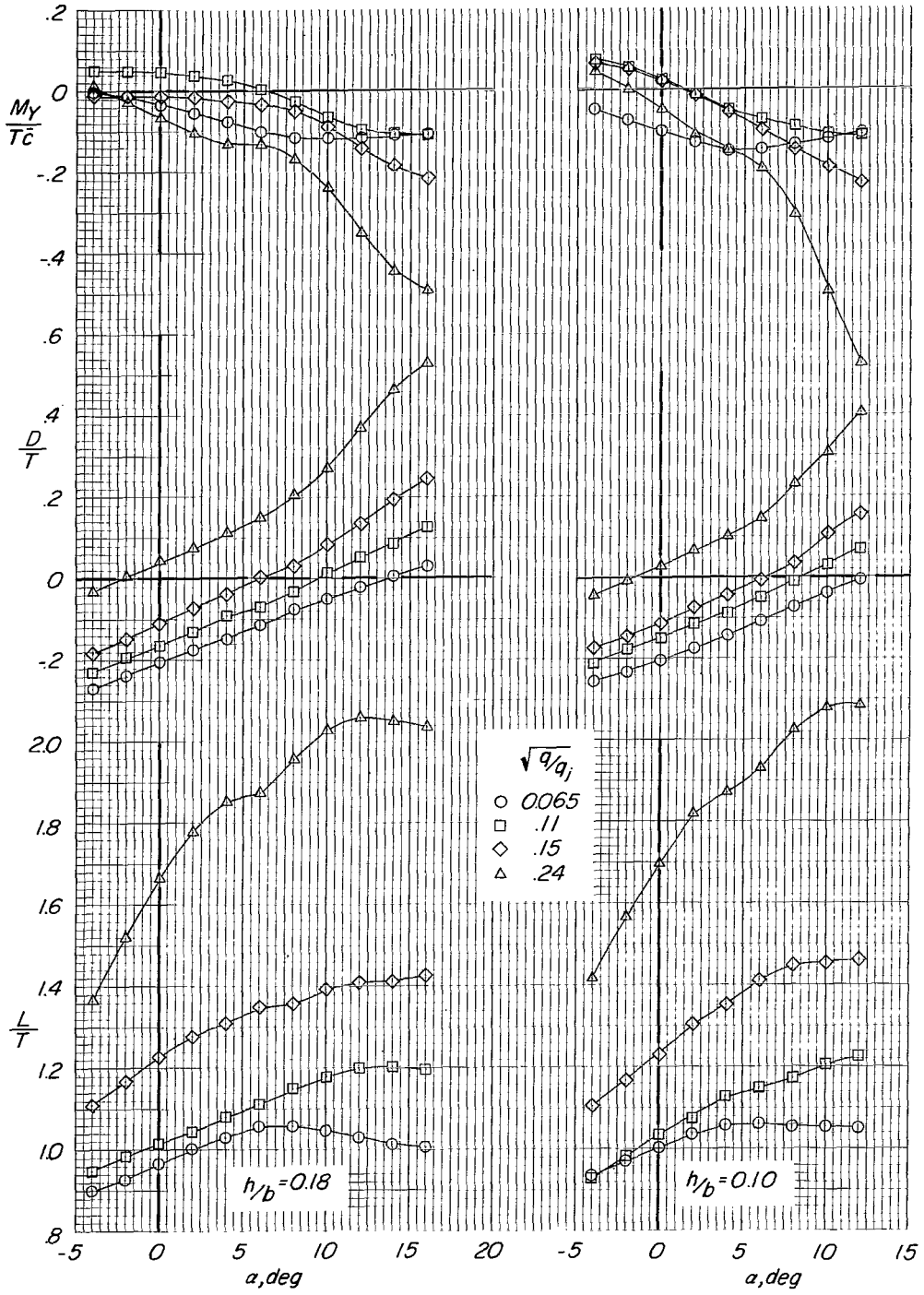

(c) h/b = 0.18 and 0.10.

Figure 35.- Concluded.

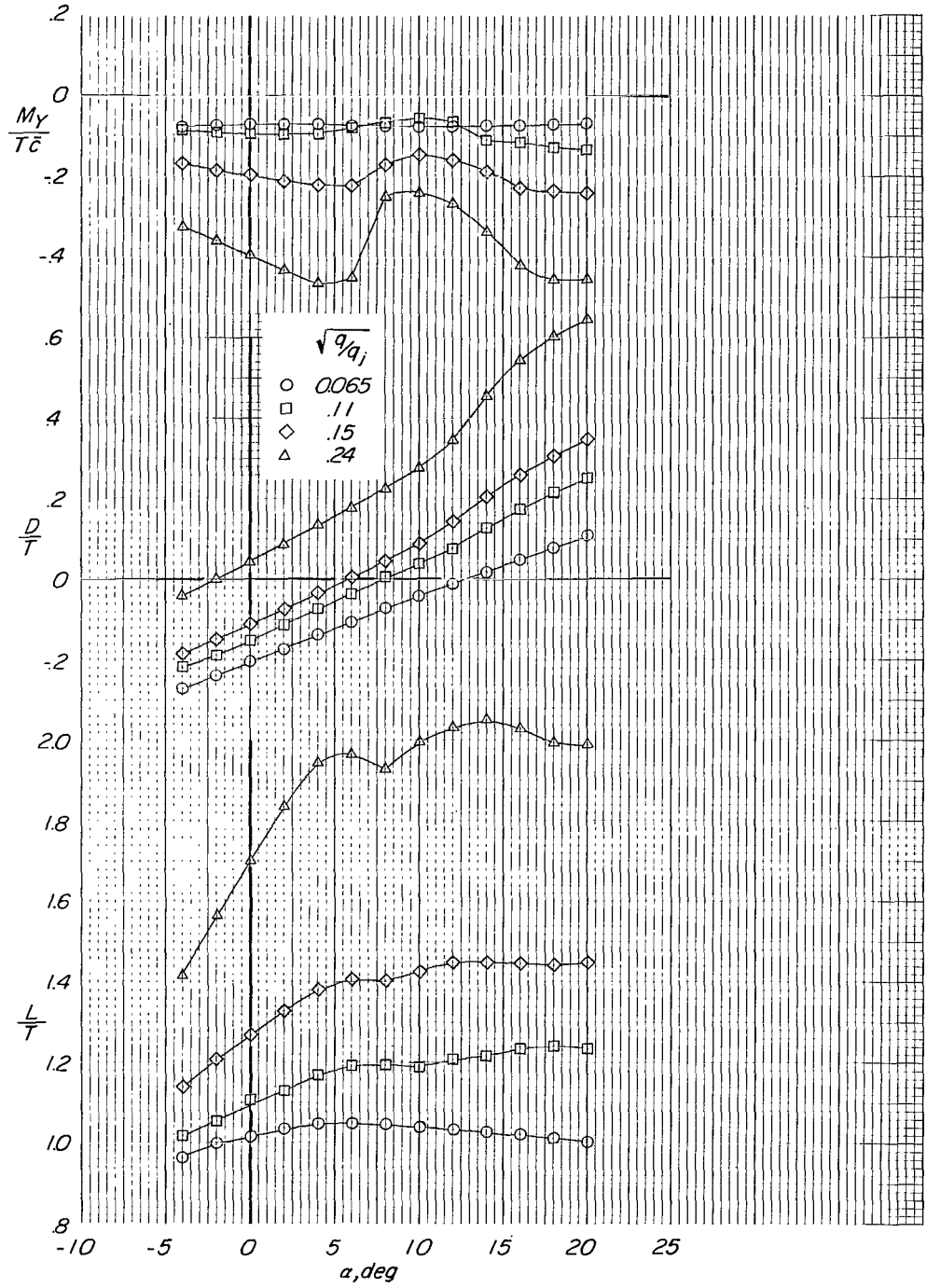

(a) h/b = 0.40.

Figure 36.- Longitudinal aerodynamic characteristics of model in ground effect with small horizontal tail in high position. Flaps on; power on; $i_t = 15^0$; engine pods at midspan.

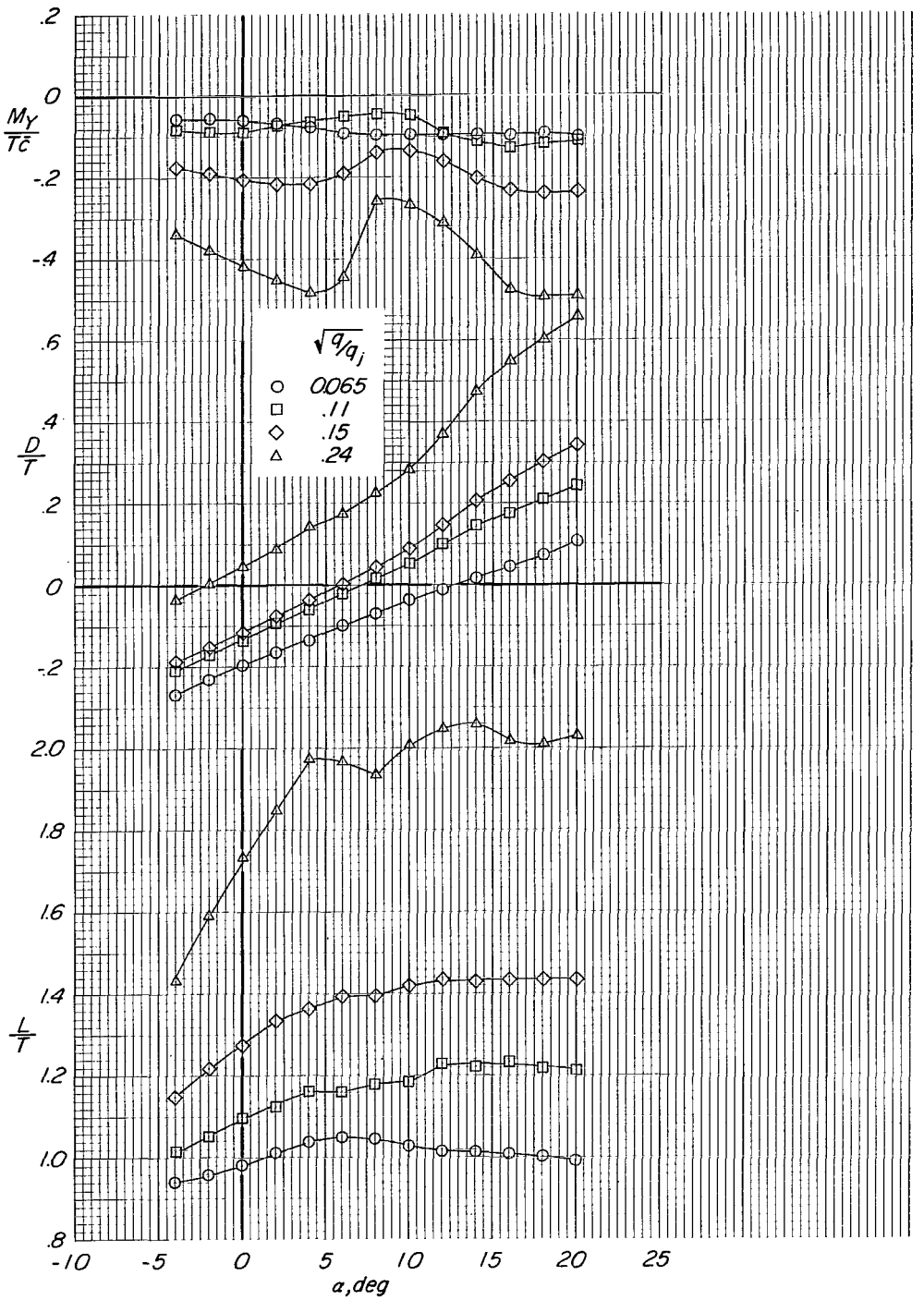

(b) h/b = 0.27.

Figure 36.- Continued.

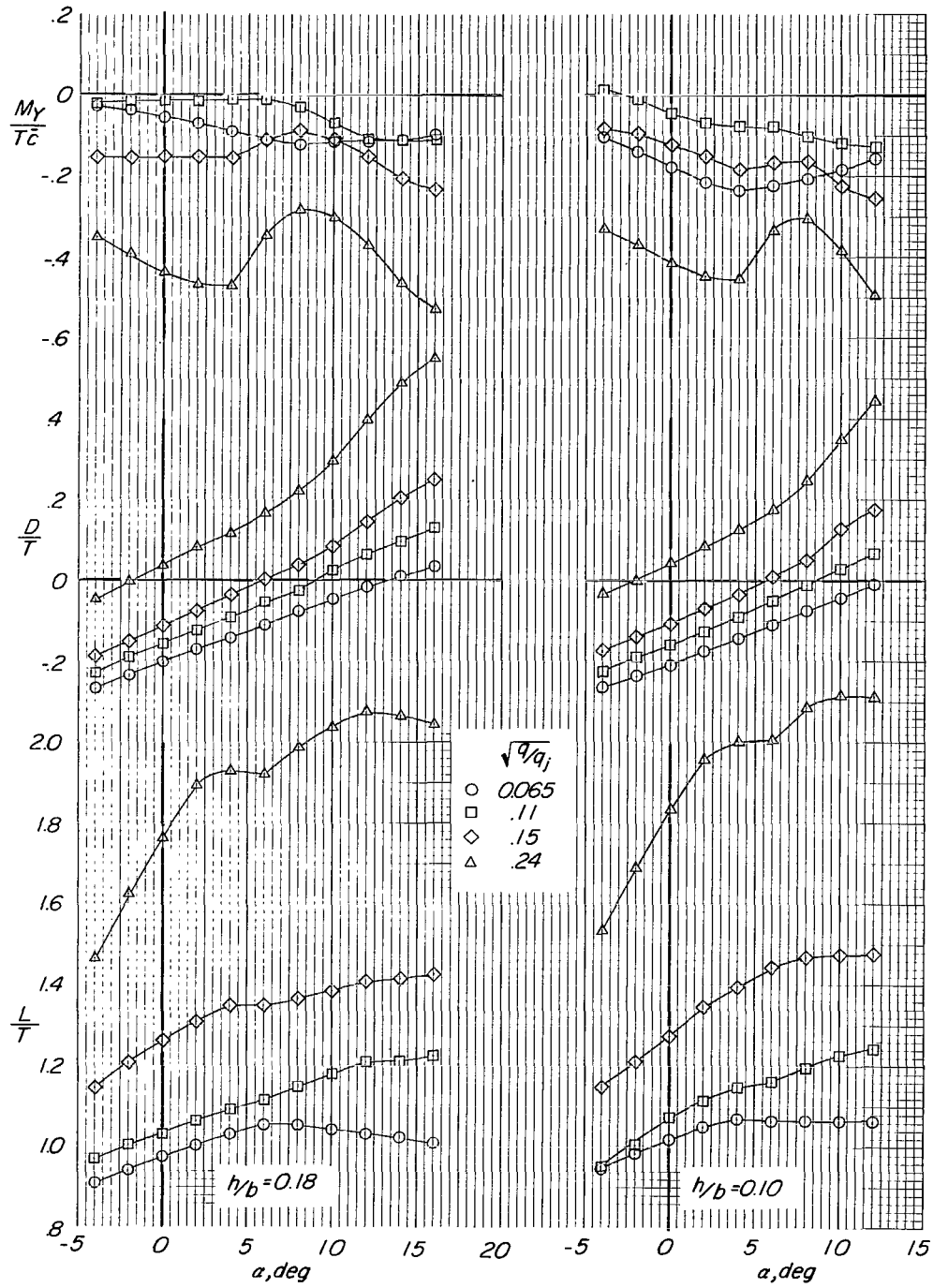

(c) h/b = 0.18 and 0.10.

Figure 36.- Concluded.

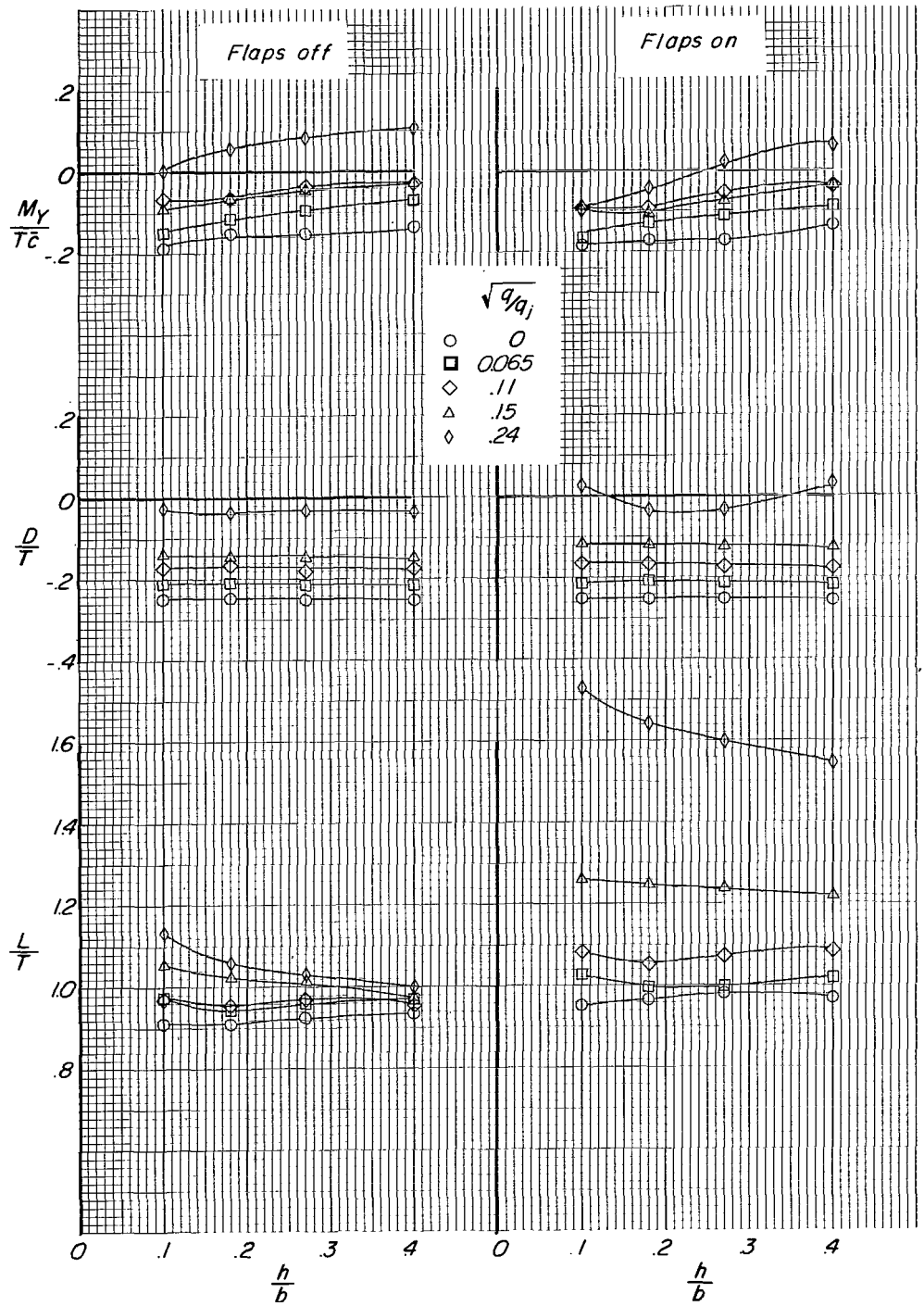

Figure 37.- Effect of model height and effective velocity ratio on longitudinal aerodynamic characteristics of model at $\alpha = 0^0$ over moving ground plane. Small tail in low position; flaps on and off; $i_t = 0^0$; engine pods at midspan.

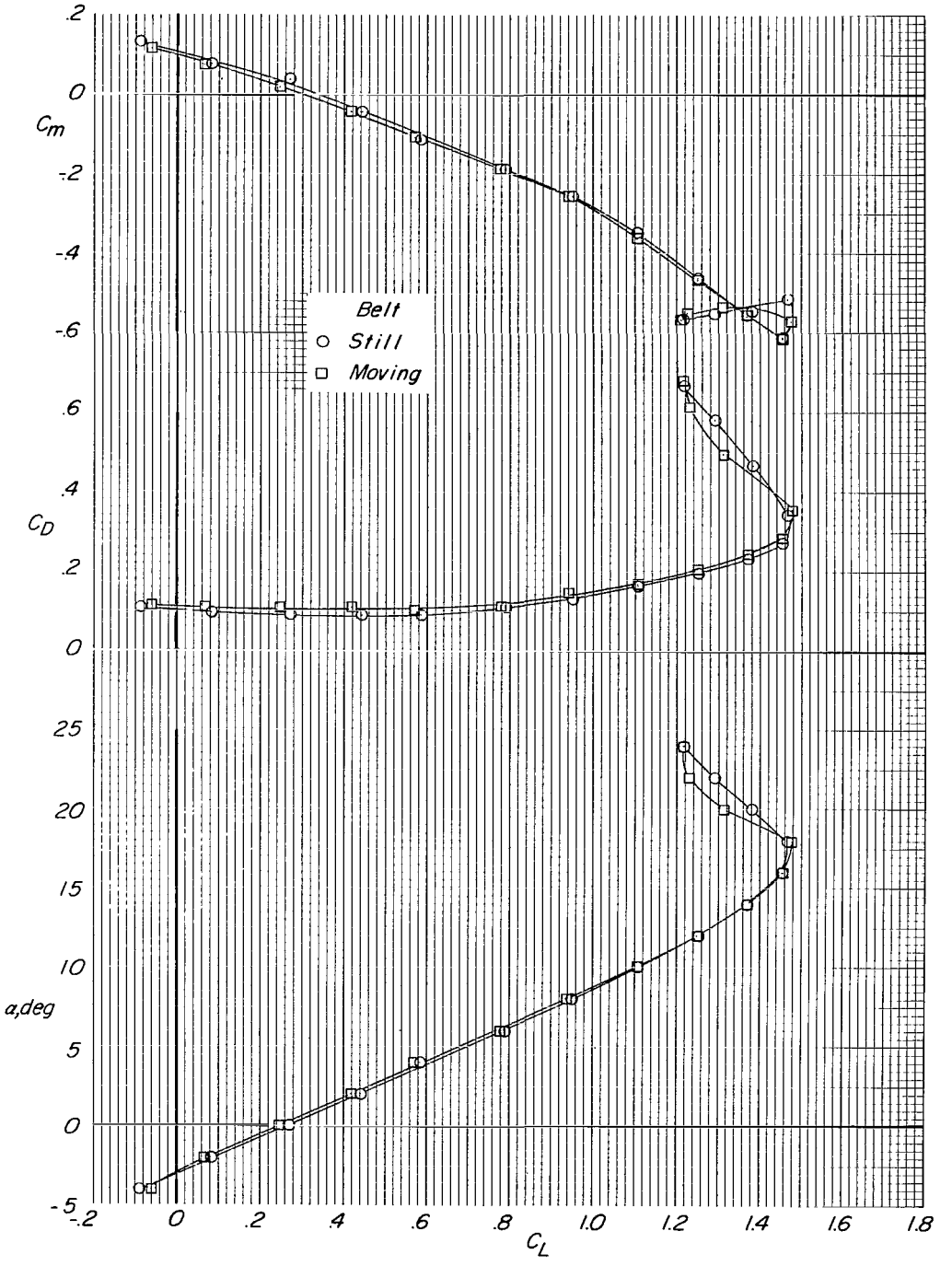

(a) h/b = 0.40.

Figure 38.- Comparison of longitudinal aerodynamic characteristics of model over still and over moving ground plane. Small tail in low position; $i_t = 0^0$; flaps off; power off; engine pods at midspan.

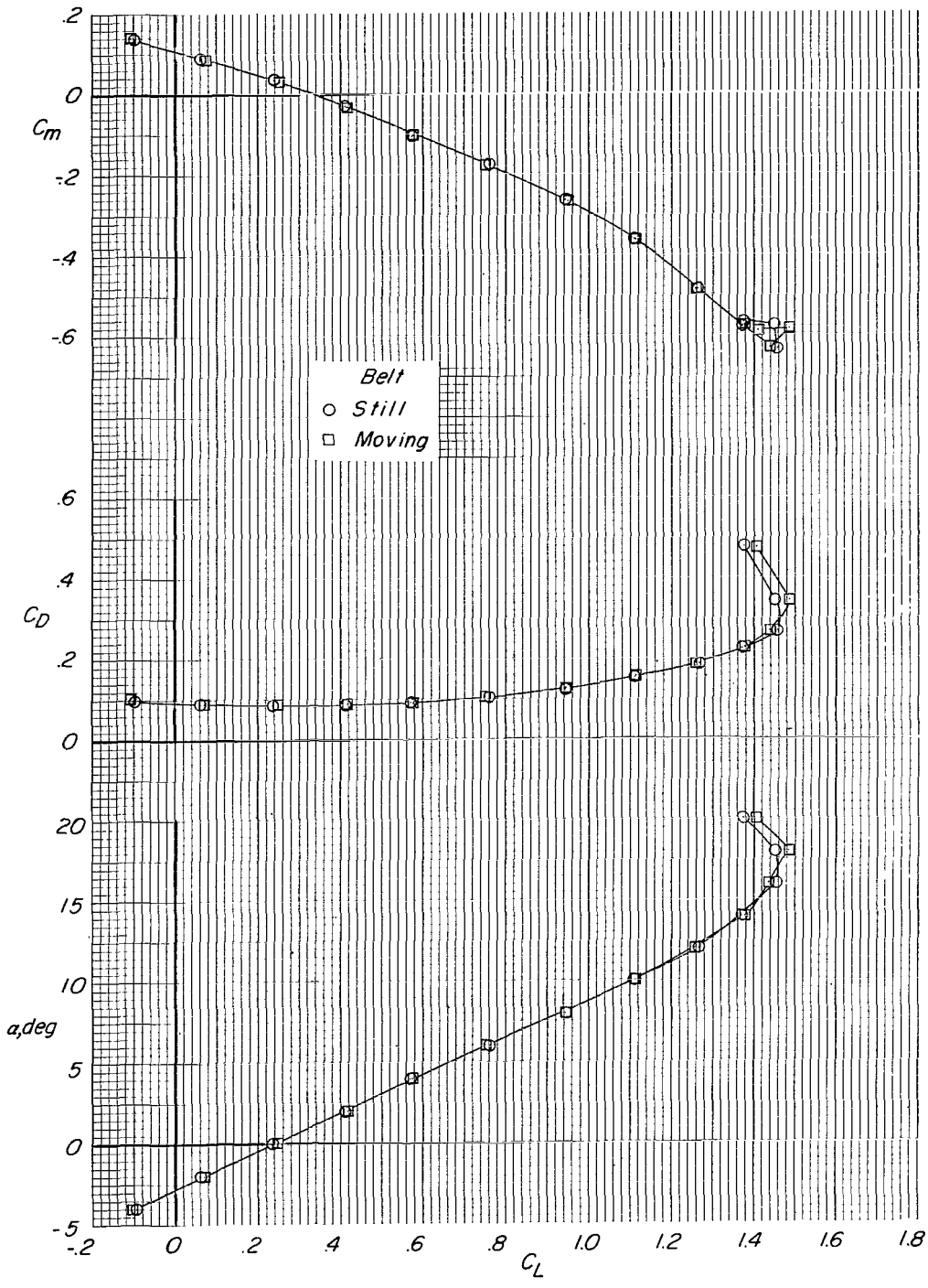

(b) h/b = 0.27.

Figure 38.- Continued.

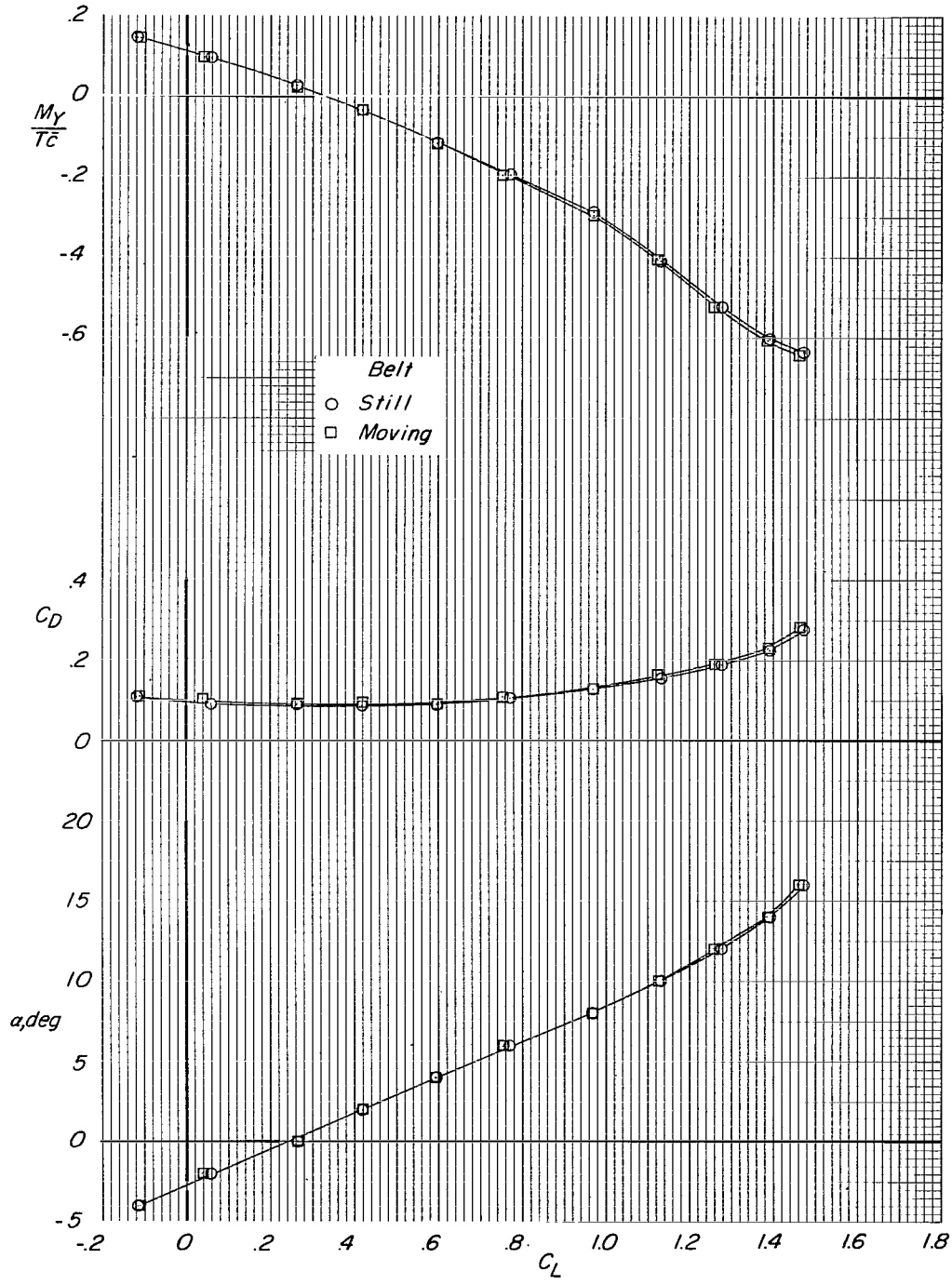

(c) h/b = 0.18.

Figure 38.- Continued.

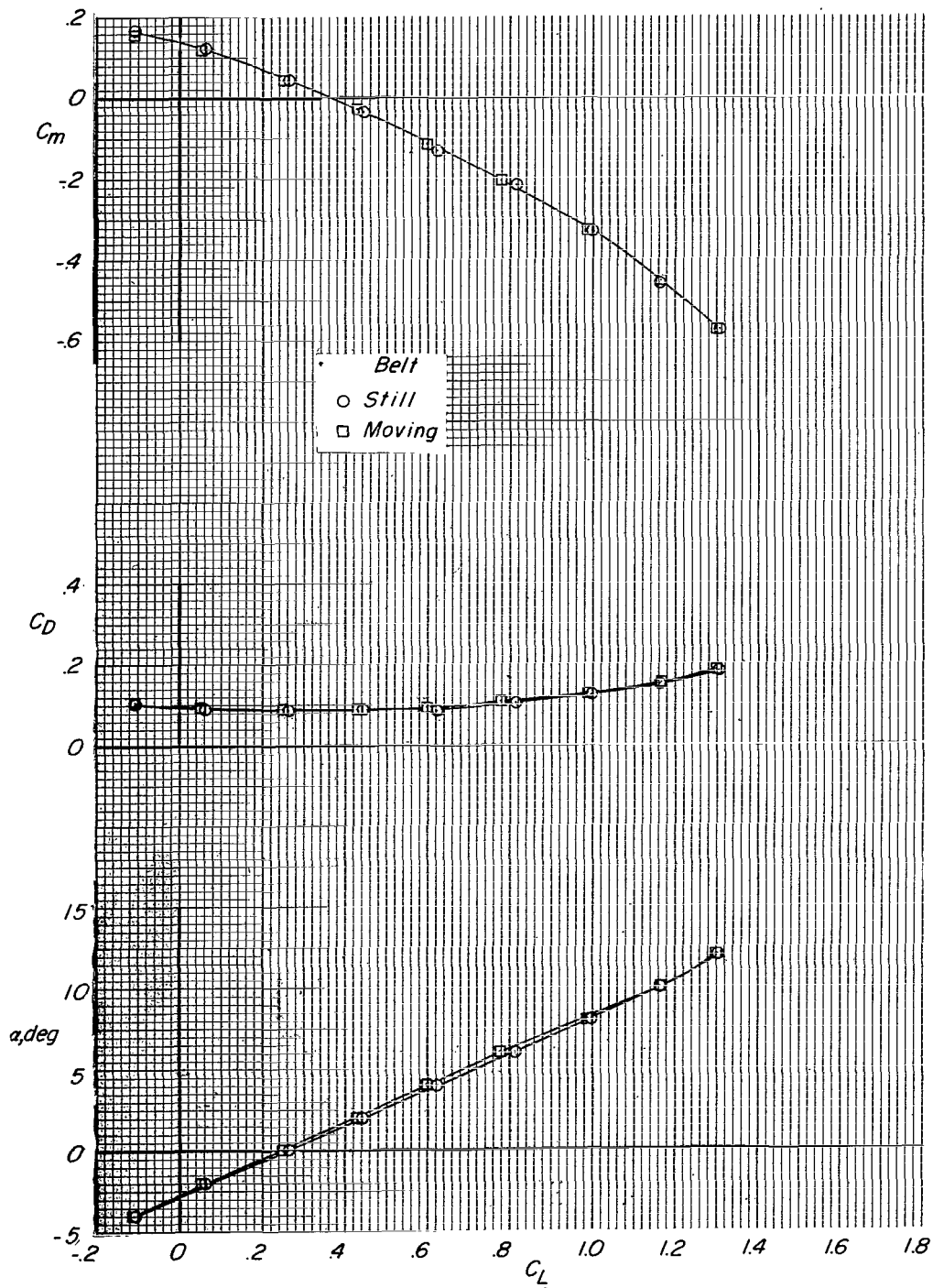

(d) h/b = 0.10.

Figure 38.- Concluded.

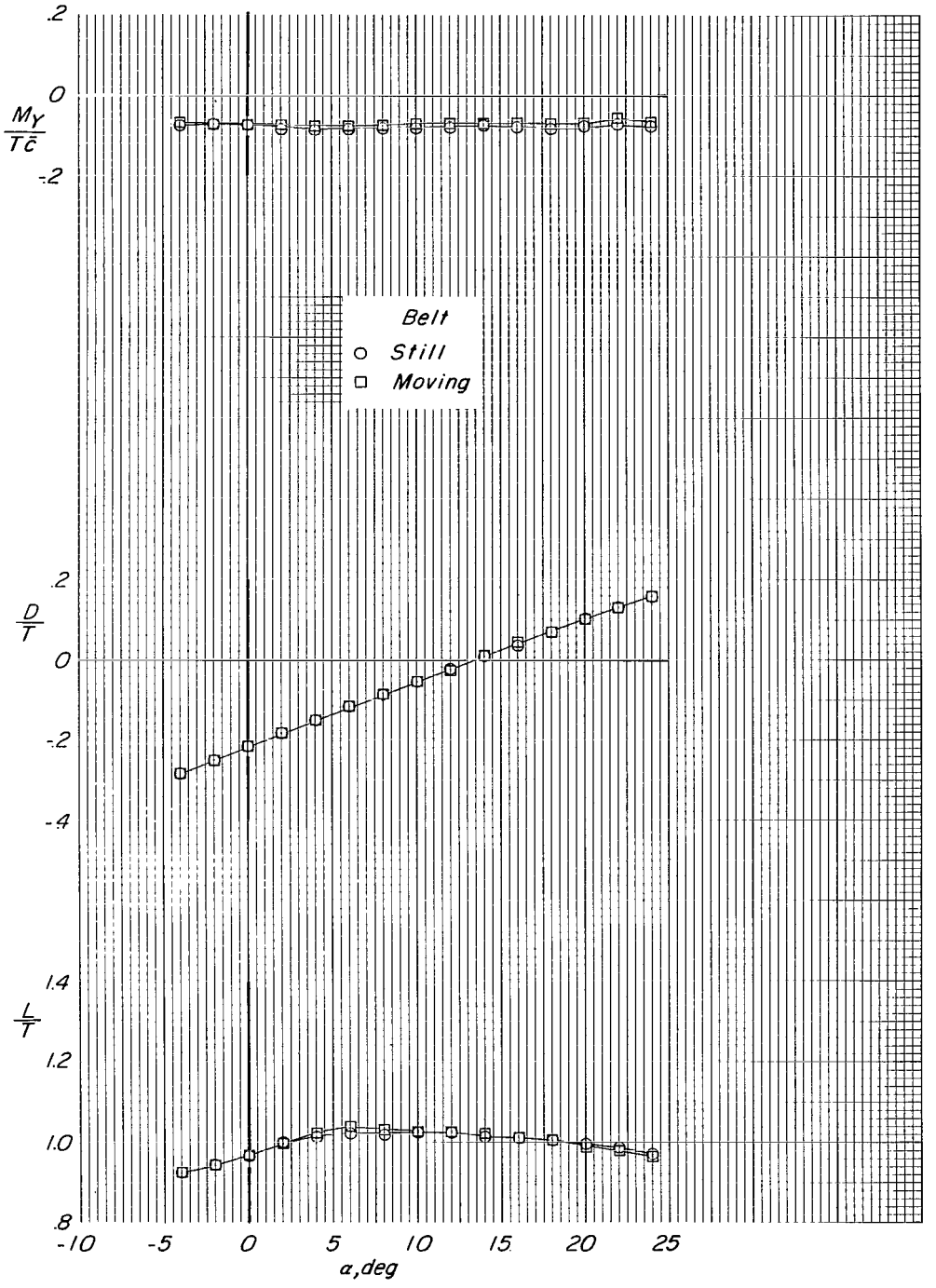

(a) h/b = 0.40; $\sqrt{q/q_j}$ = 0.065.

Figure 39.- Comparison of longitudinal aerodynamic characteristics of model over still and over moving ground plane. Small tail in low position; $i_t = 0^0$; flaps off; power on; engine pods at midspan.

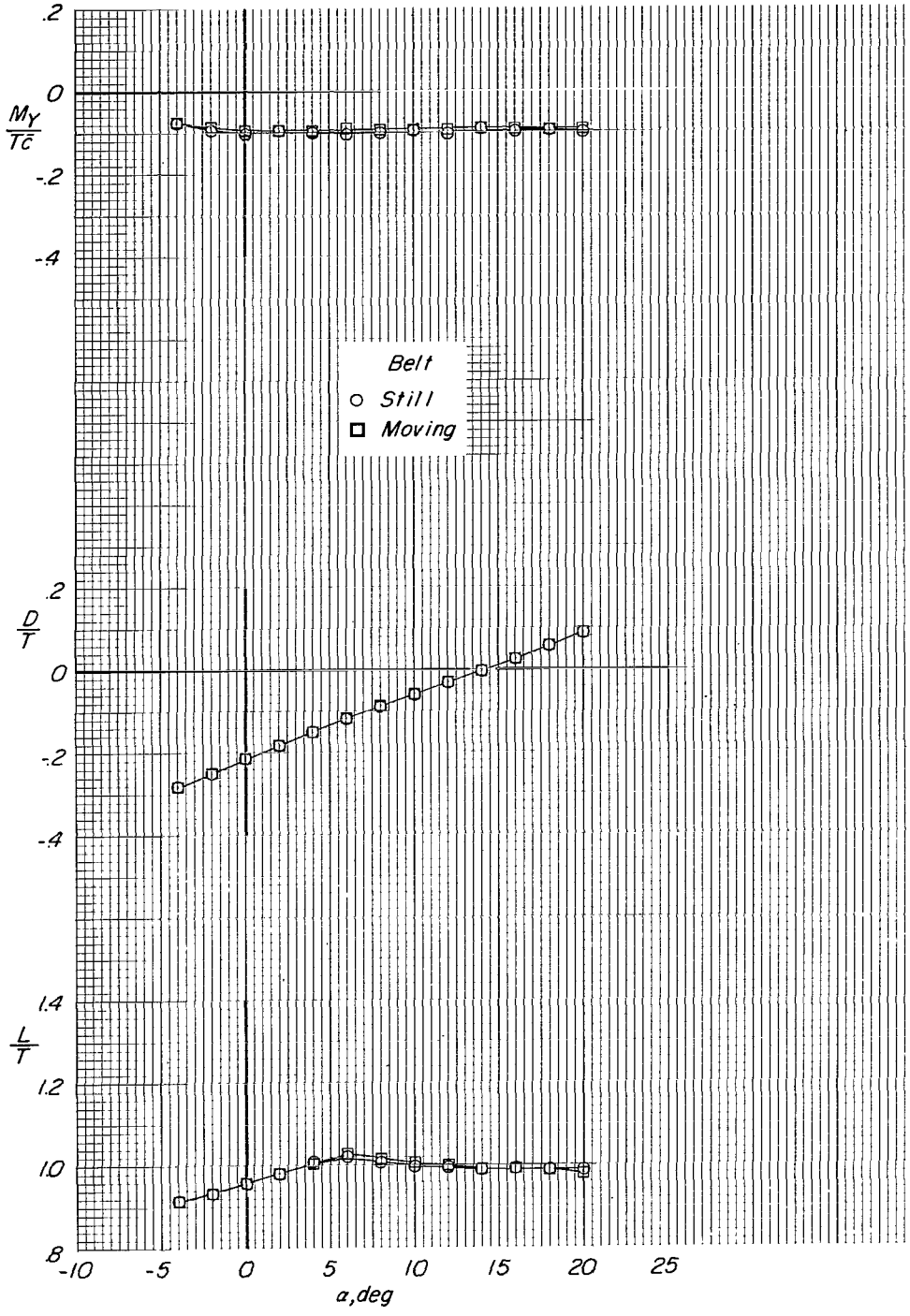

(b) h/b = 0.27; $\sqrt{q/q_j}$ = 0.065.

Figure 39.- Continued.

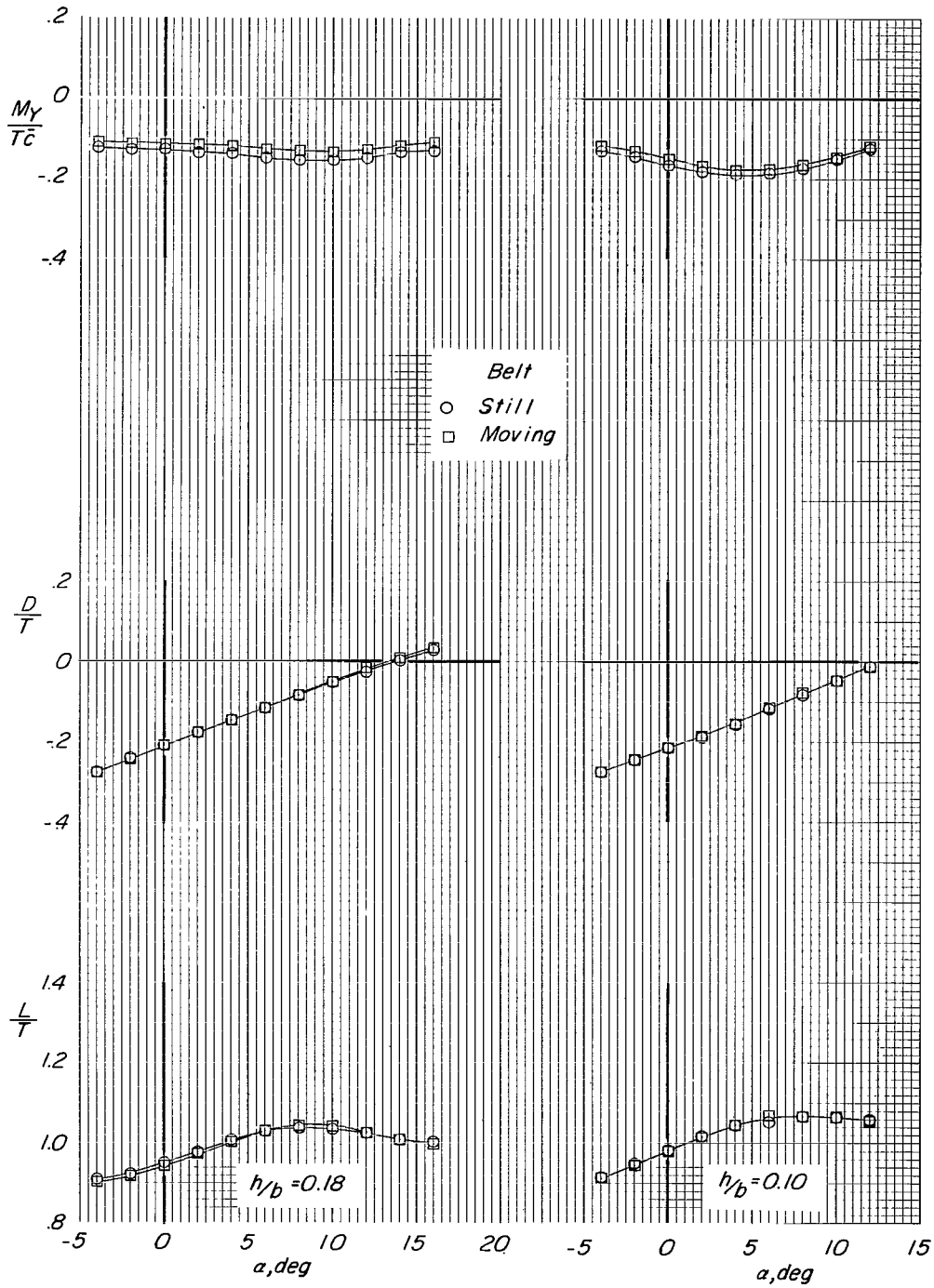

(c) h/b = 0.18 and 0.10; $\sqrt{q/q_j}$ = 0.065.

Figure 39.- Continued.

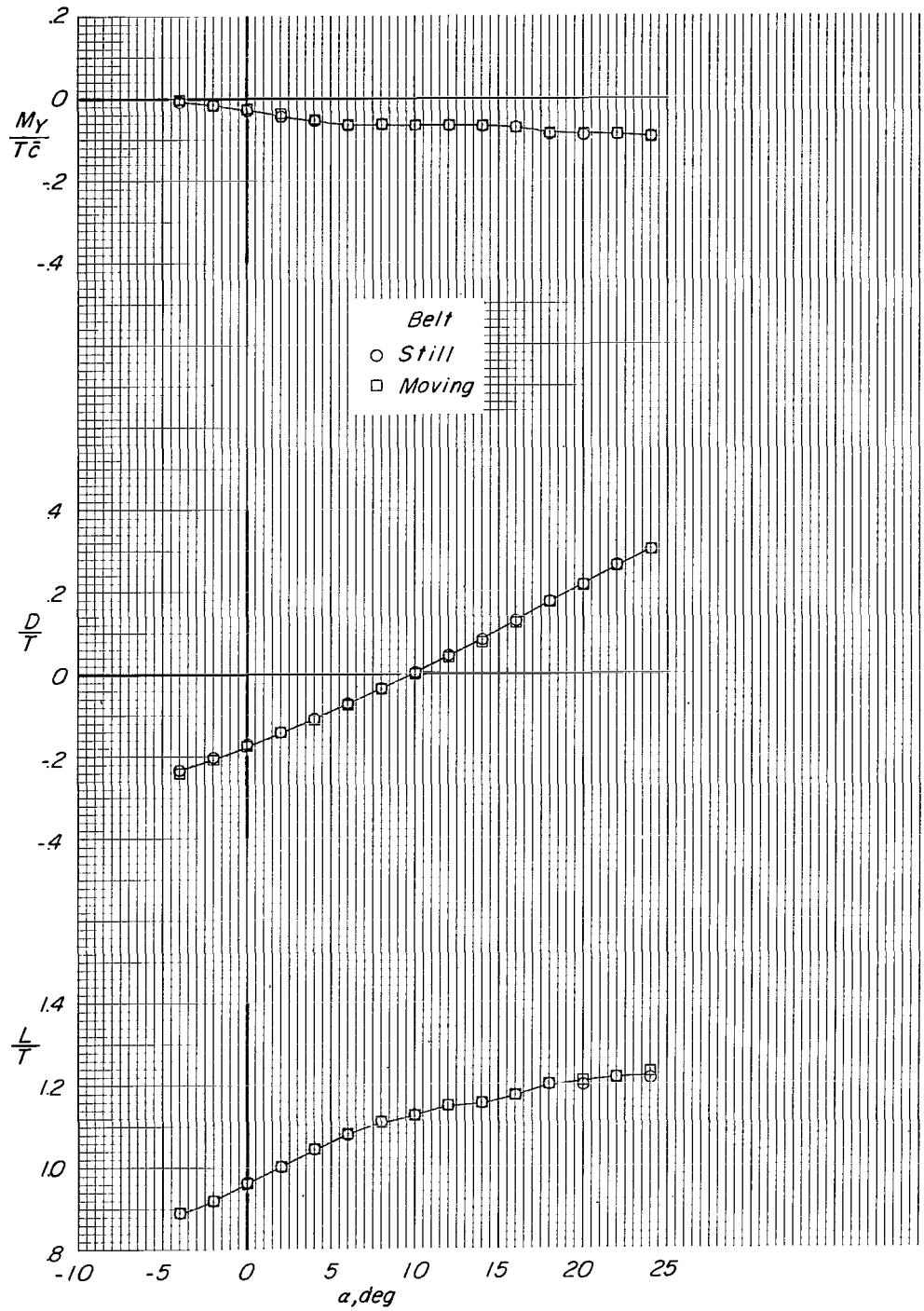

(d) $h/b = 0.40$; $\sqrt{q/q_j} = 0.11$.

Figure 39.- Continued.

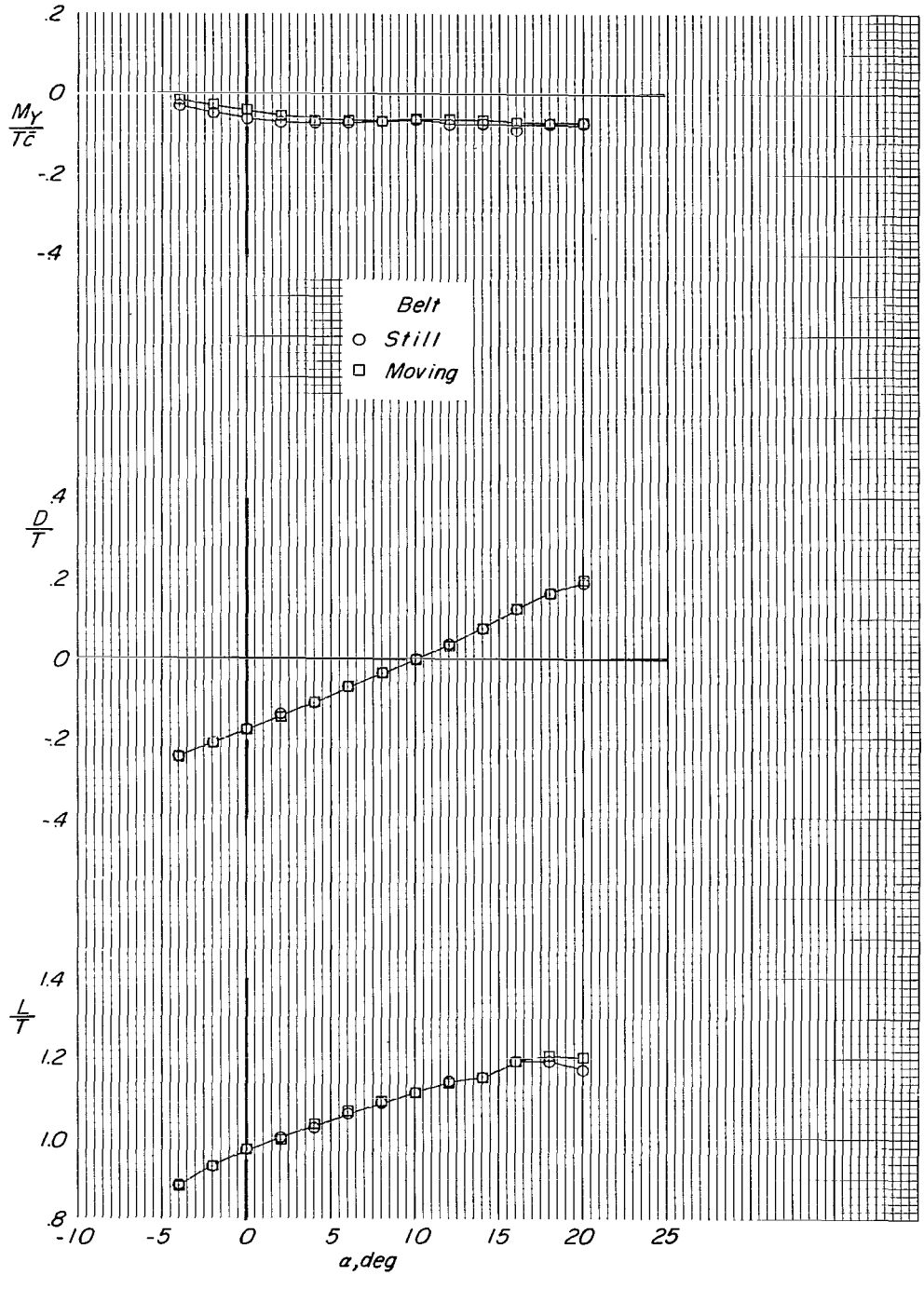

(e) h/b = 0.27; $\sqrt{q/q_j}$ = 0.11.

Figure 39.- Continued.

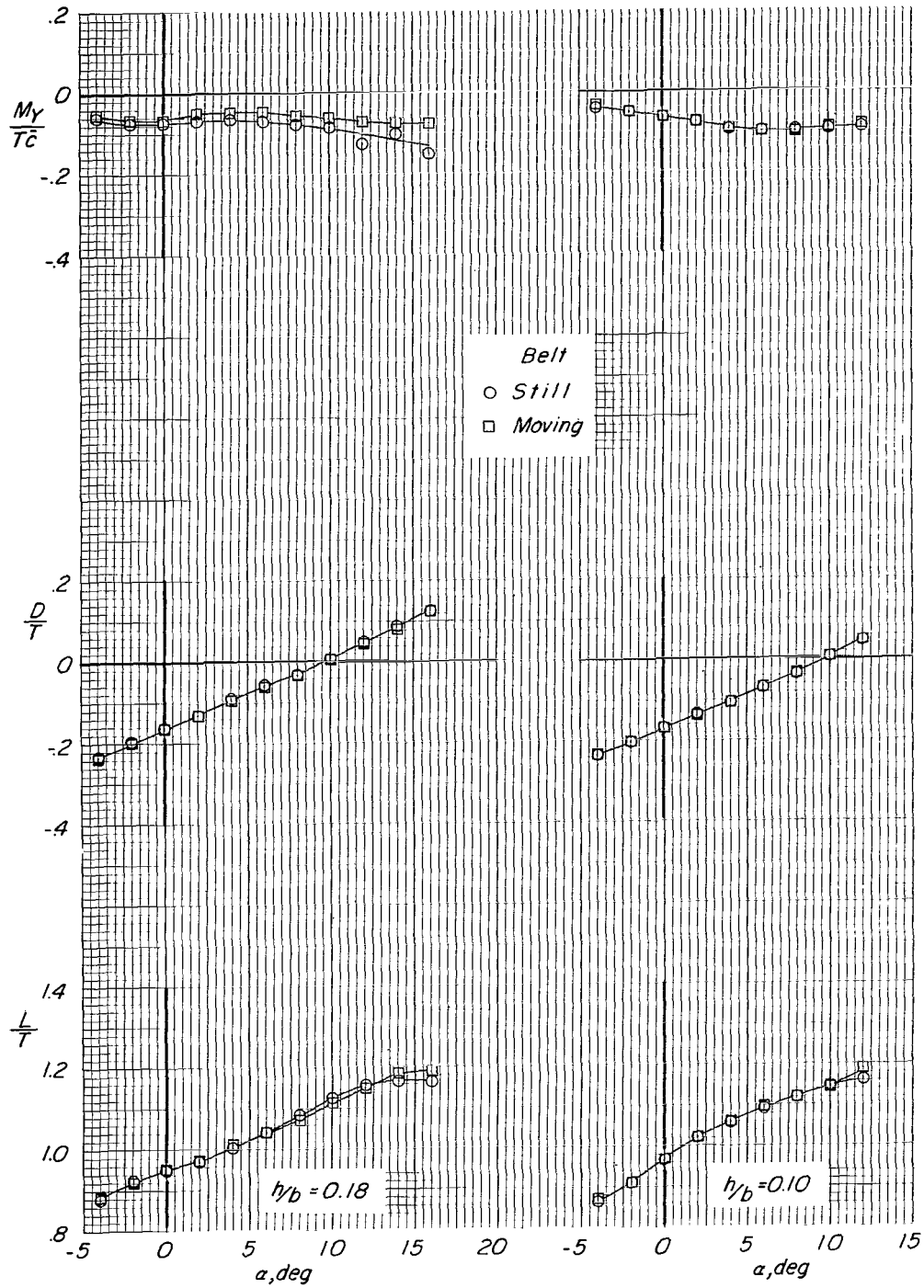

(f) h/b = 0.18 and 0.10; $\sqrt{q/q_j} = 0.11$.

Figure 39.- Continued.

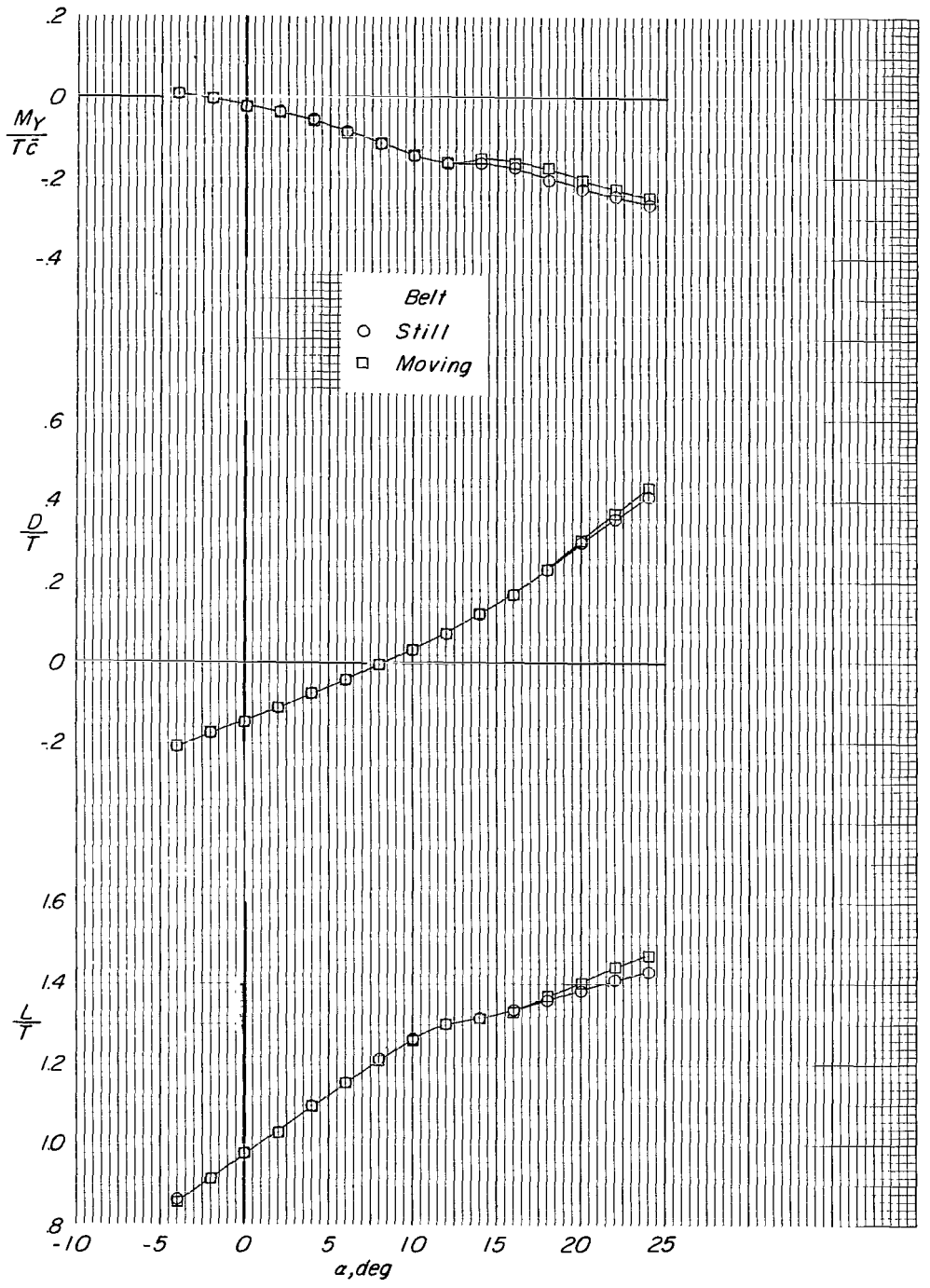

(g) h/b = 0.40; $\sqrt{q/q_j}$ = 0.15.

Figure 39.- Continued.

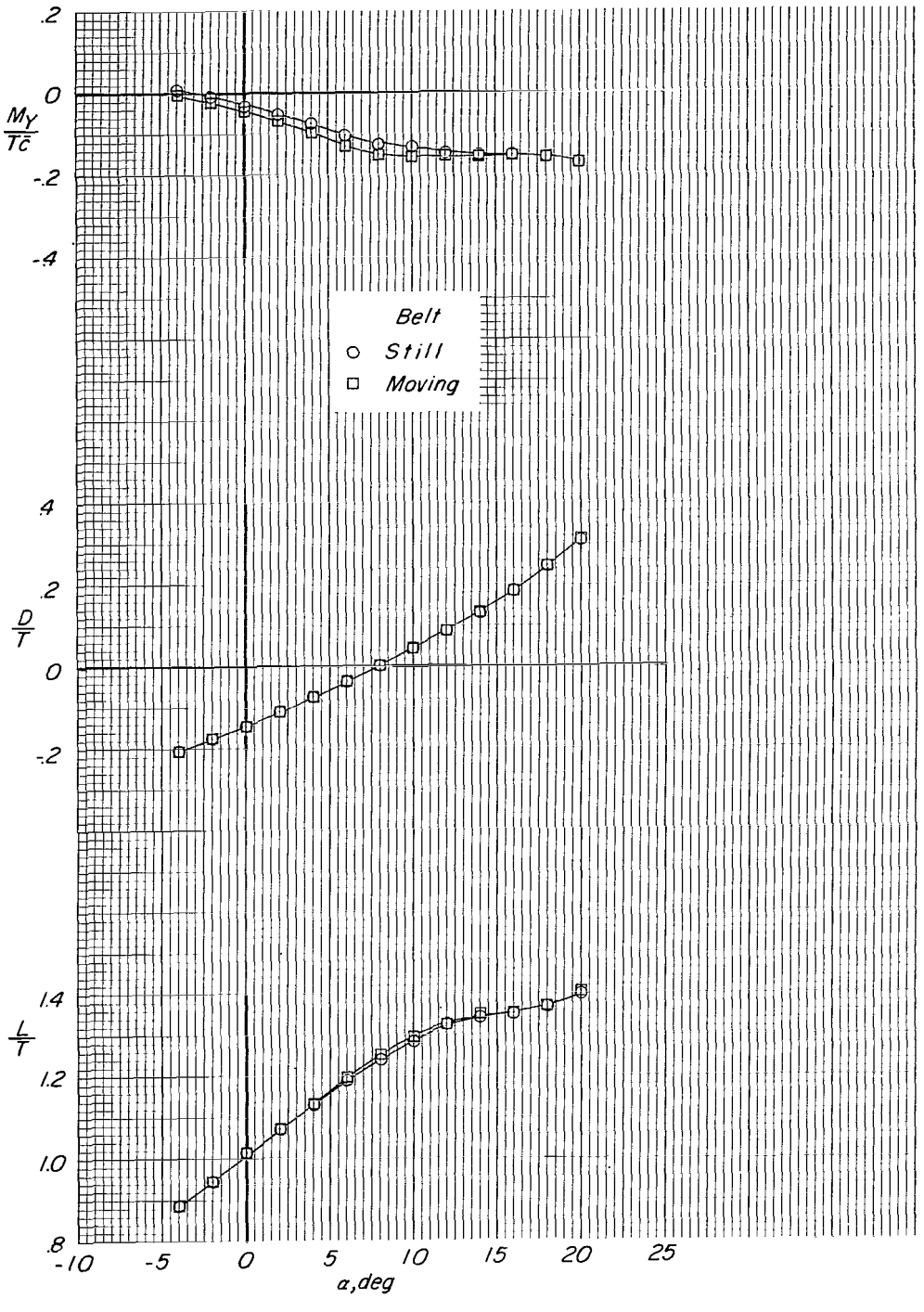

(h) h/b = 0.27; $\sqrt{q/q_j}$ = 0.15.

Figure 39.- Continued.

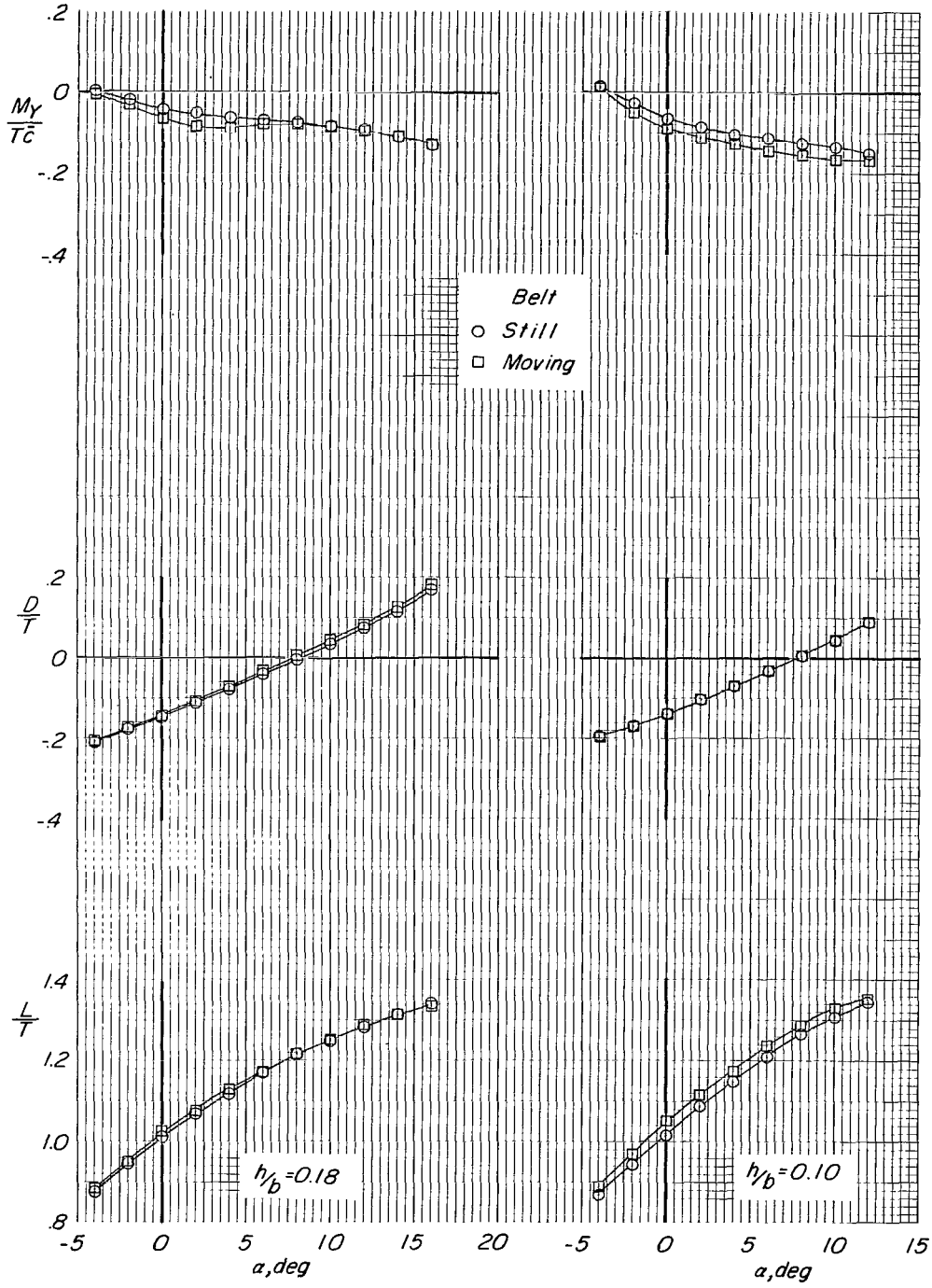

(i) h/b = 0.18 and 0.10; $\sqrt{q/q_j}$ = 0.15.

Figure 39.- Continued.

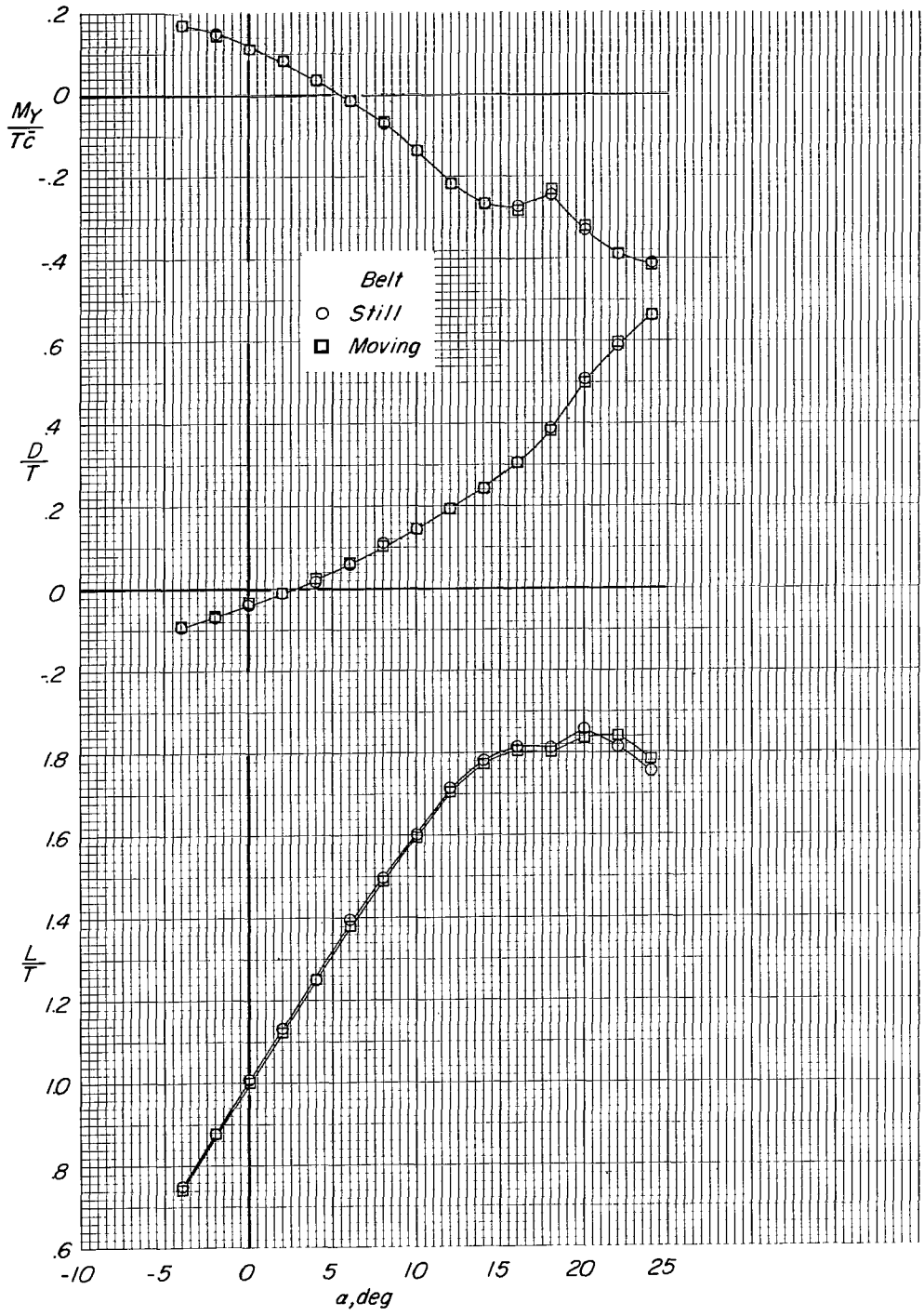

(j) h/b = 0.40; $\sqrt{q/q_j}$ = 0.24.

Figure 39.- Continued.

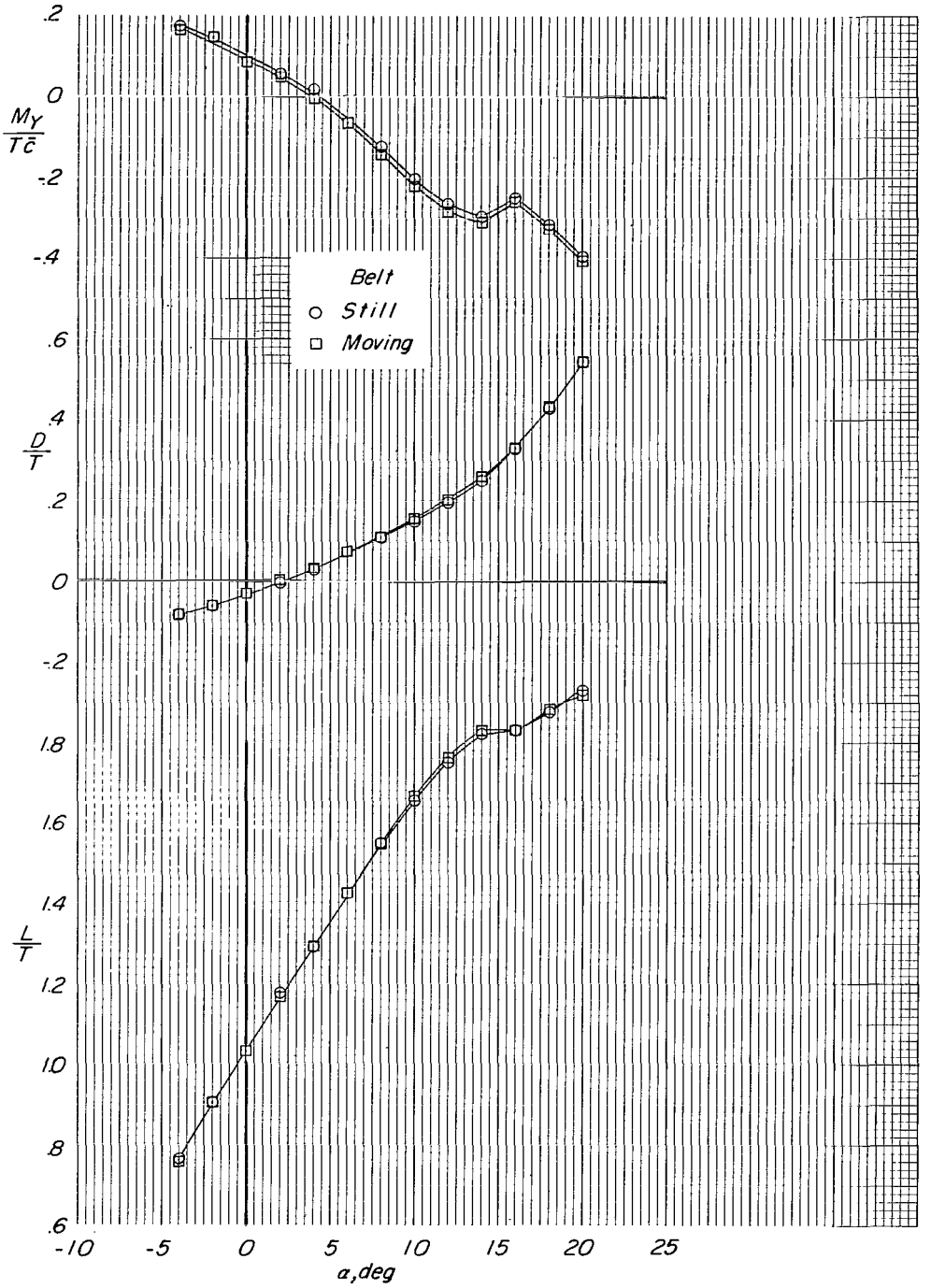

(k) h/b = 0.27; $\sqrt{q/q_j}$ = 0.24.

Figure 39.- Continued.

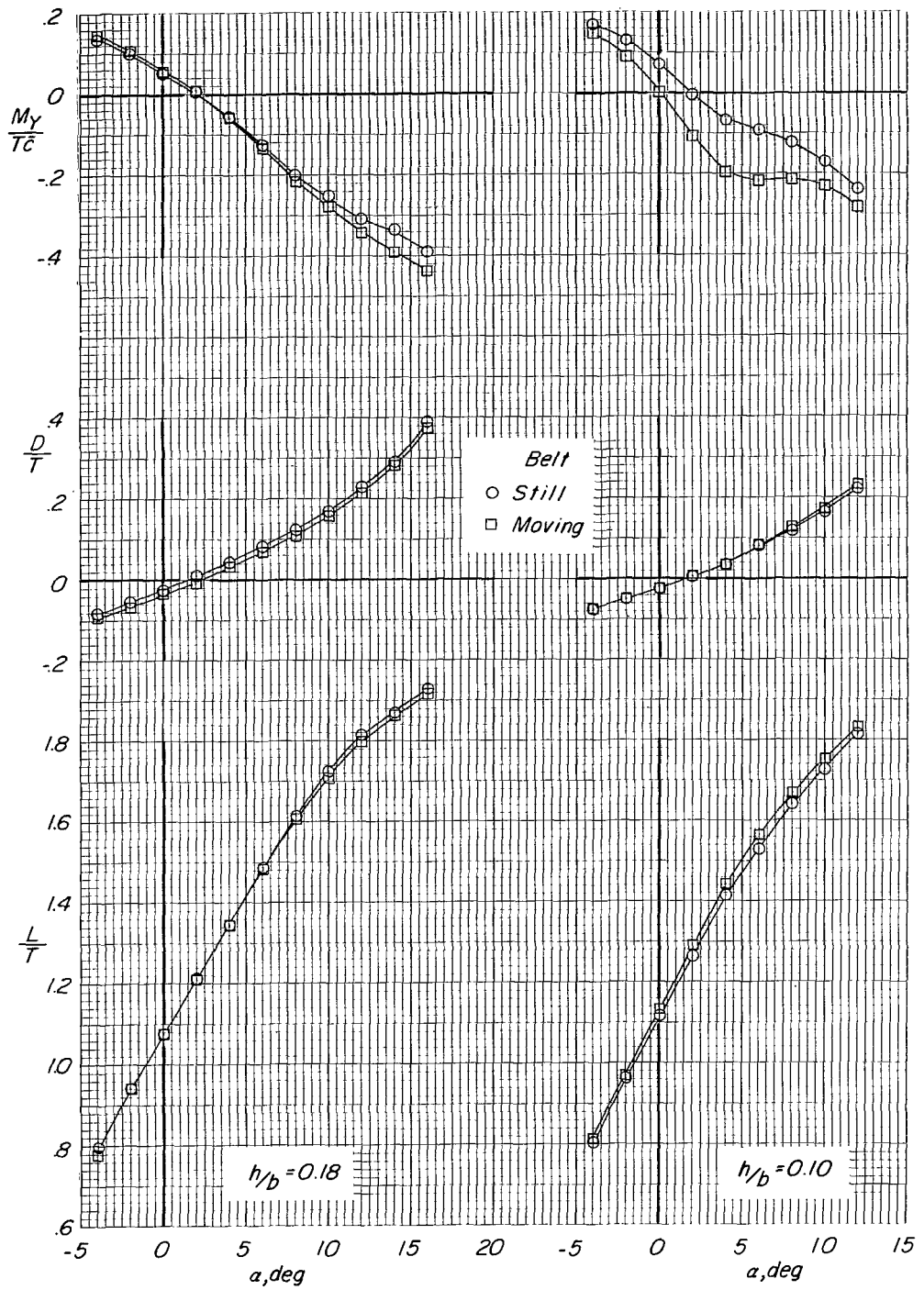

(l) h/b = 0.18 and 0.10; $\sqrt{q/q_j} = 0.24$.

Figure 39.- Concluded.

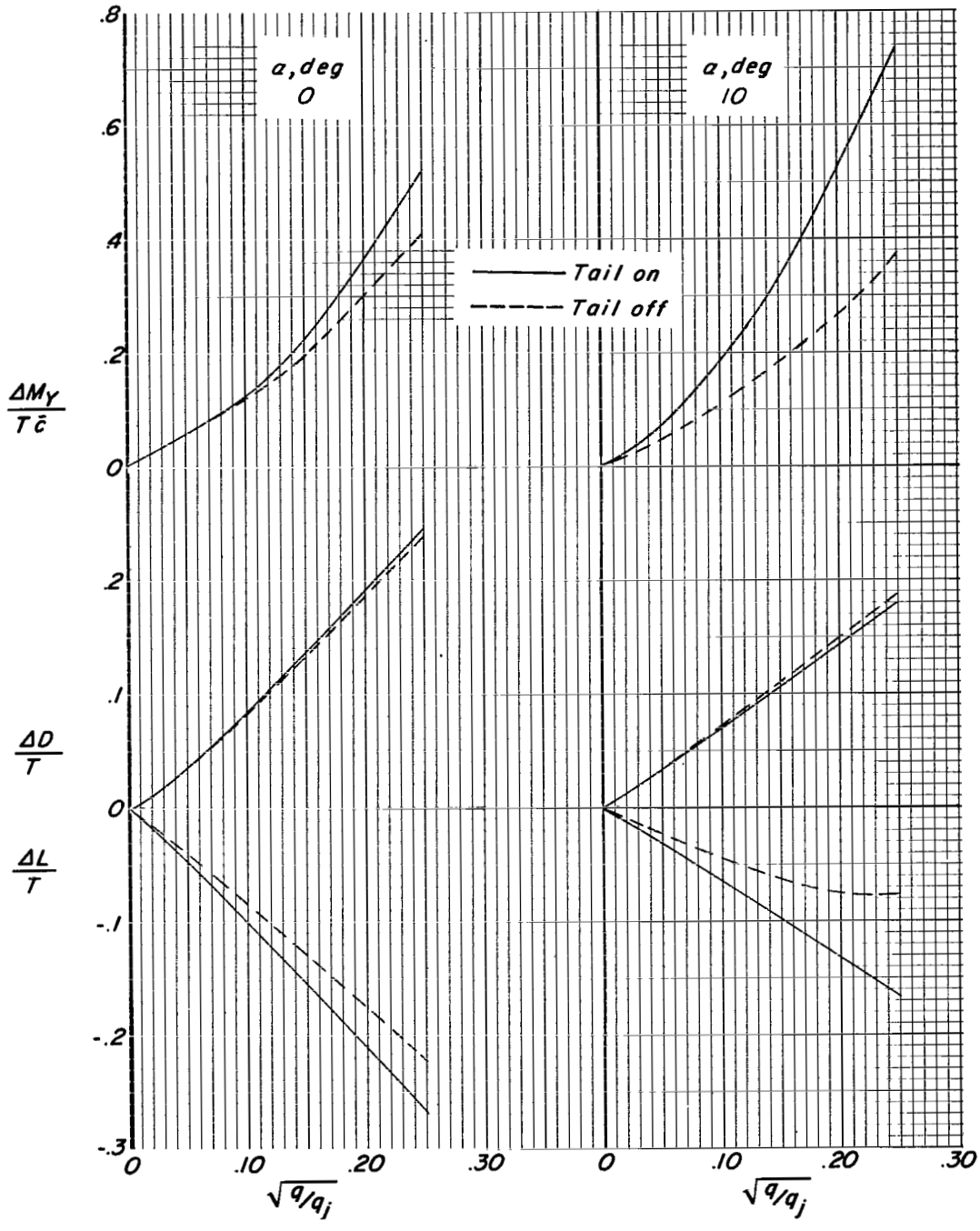

(a) Large tail in low position and tail off.

Figure 40.- Increments of lift, drag, and pitching-moment coefficients produced by interference. Flaps on; power on; $i_t = 0^0$ if tail on; engine pods inboard.

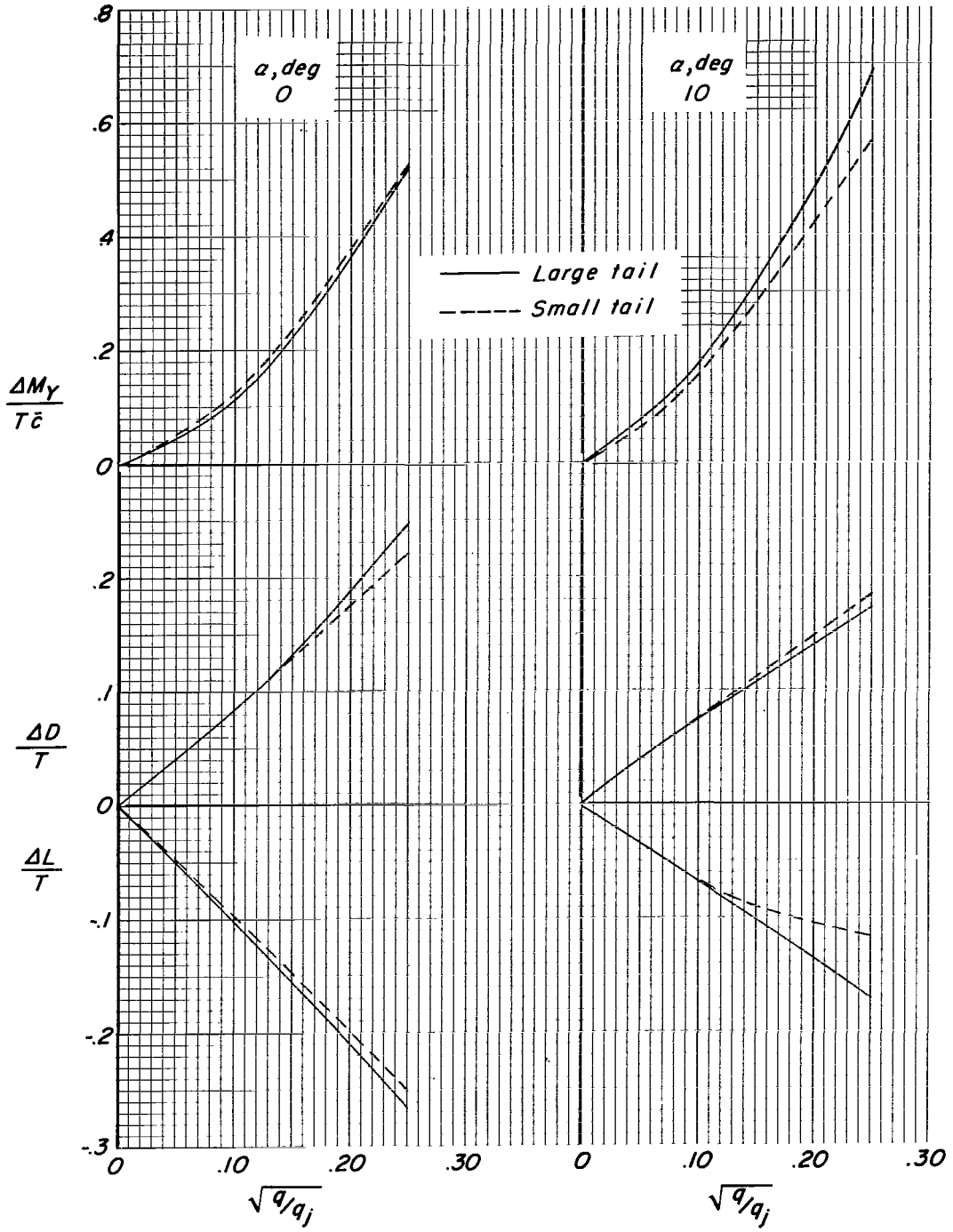

(b) Large tail and small tail; low position.

Figure 40.- Continued.

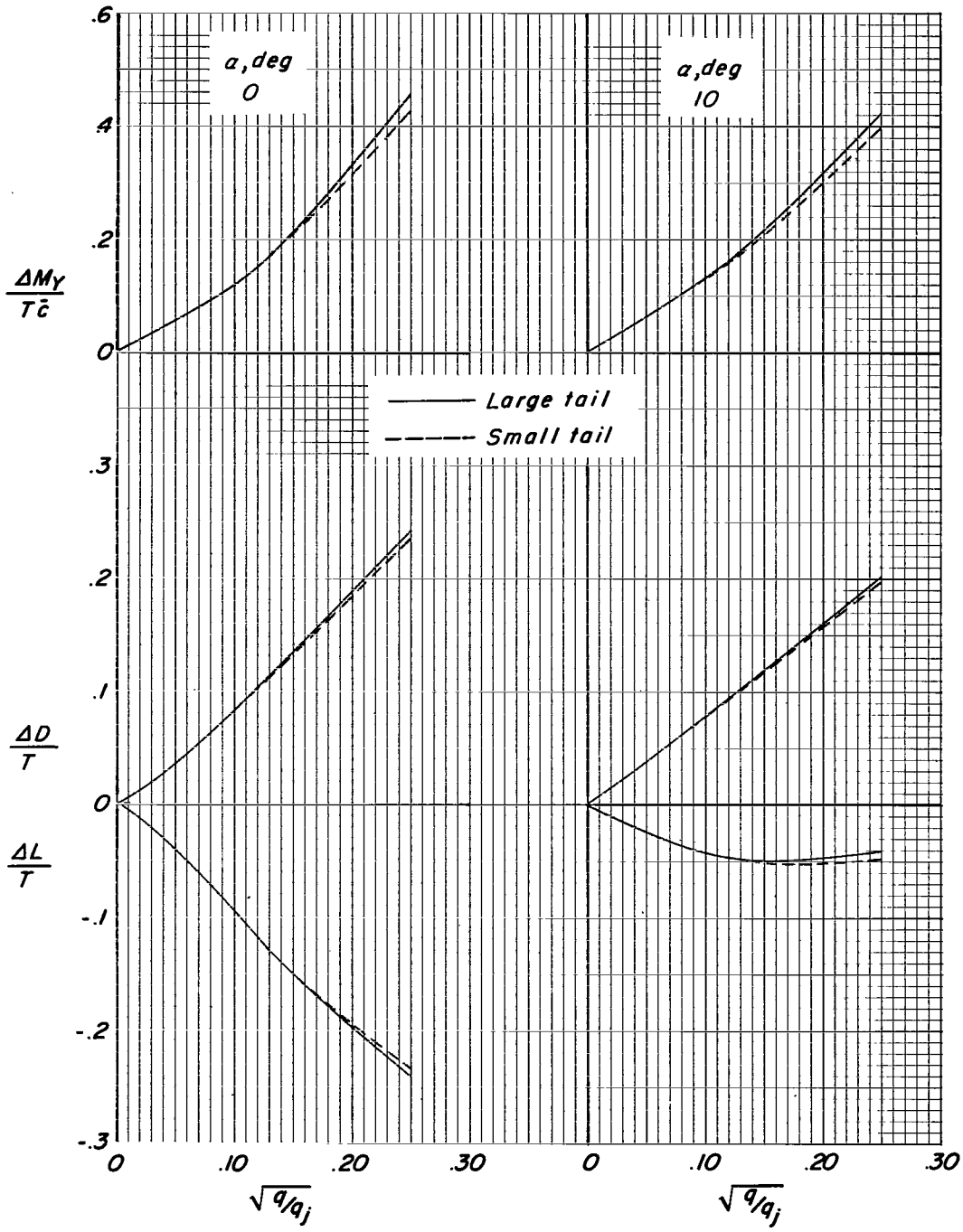

(c) Large tail and small tail; high position.

Figure 40.- Concluded.

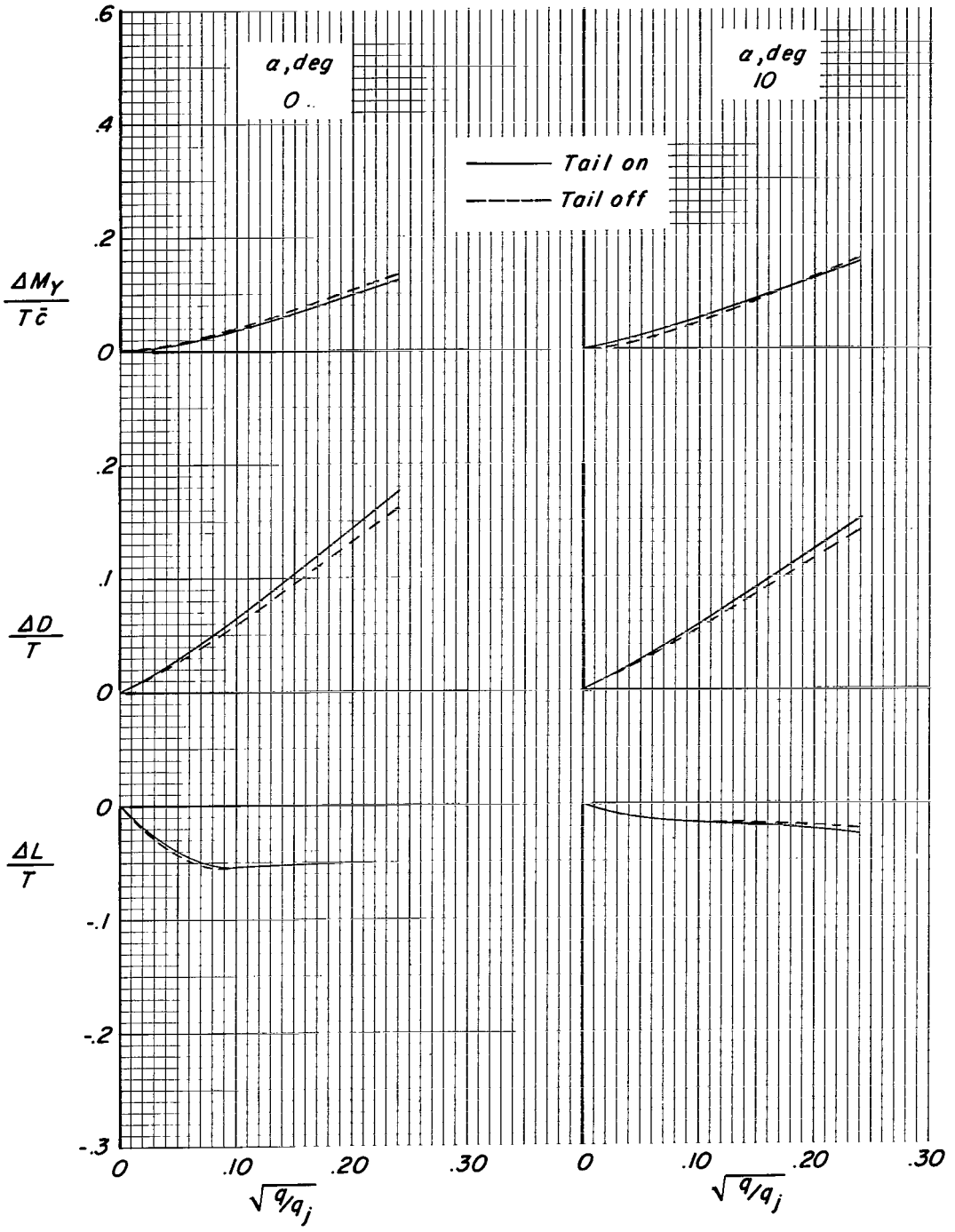

(a) Large tail in low position and tail off.

Figure 41.- Increments of lift, drag, and pitching-moment coefficients produced by interference. Flaps on; power on; $i_t = 0^0$ if tail on; engine pods at midspan.

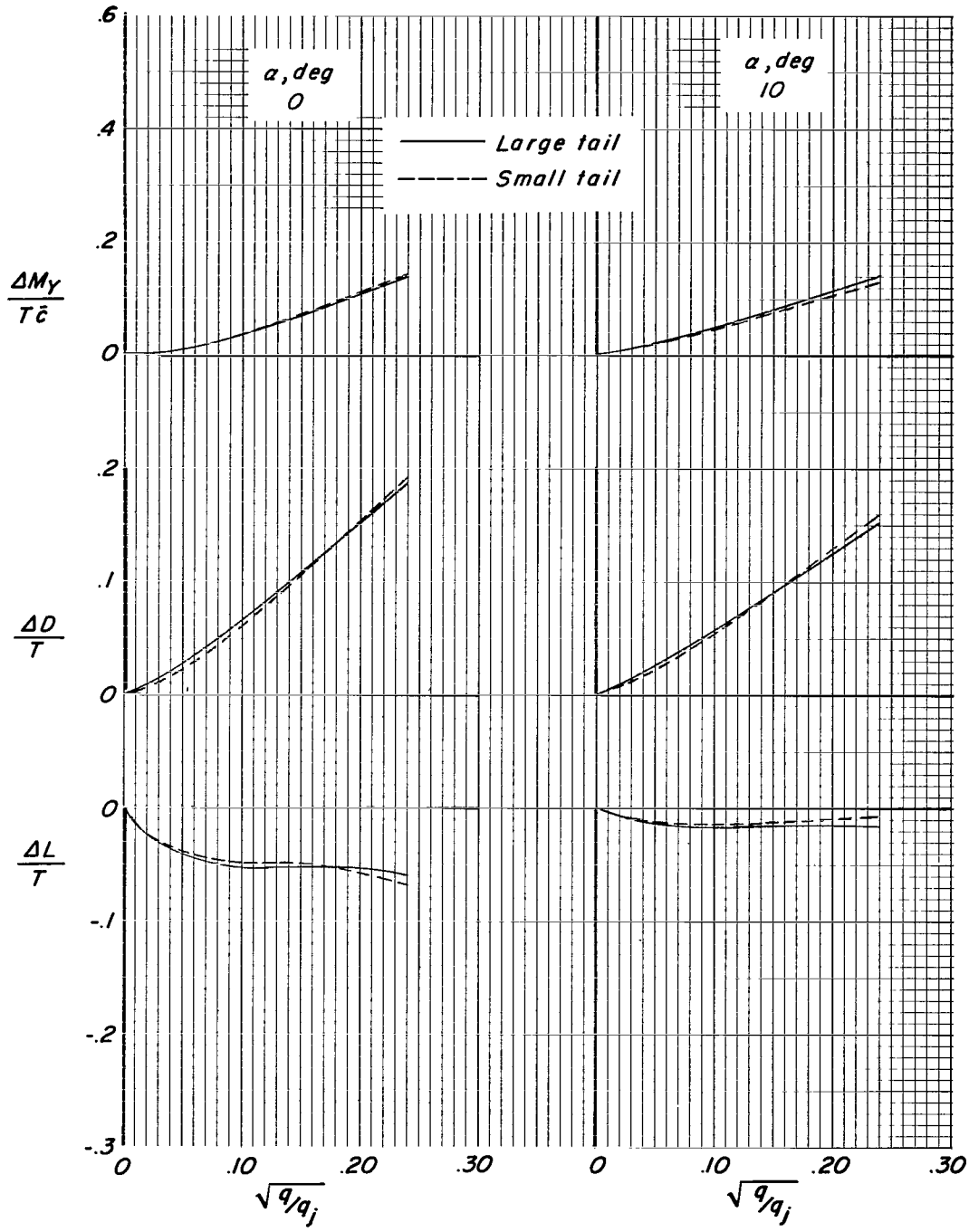

(b) Large tail and small tail; low position.

Figure 41.- Continued.

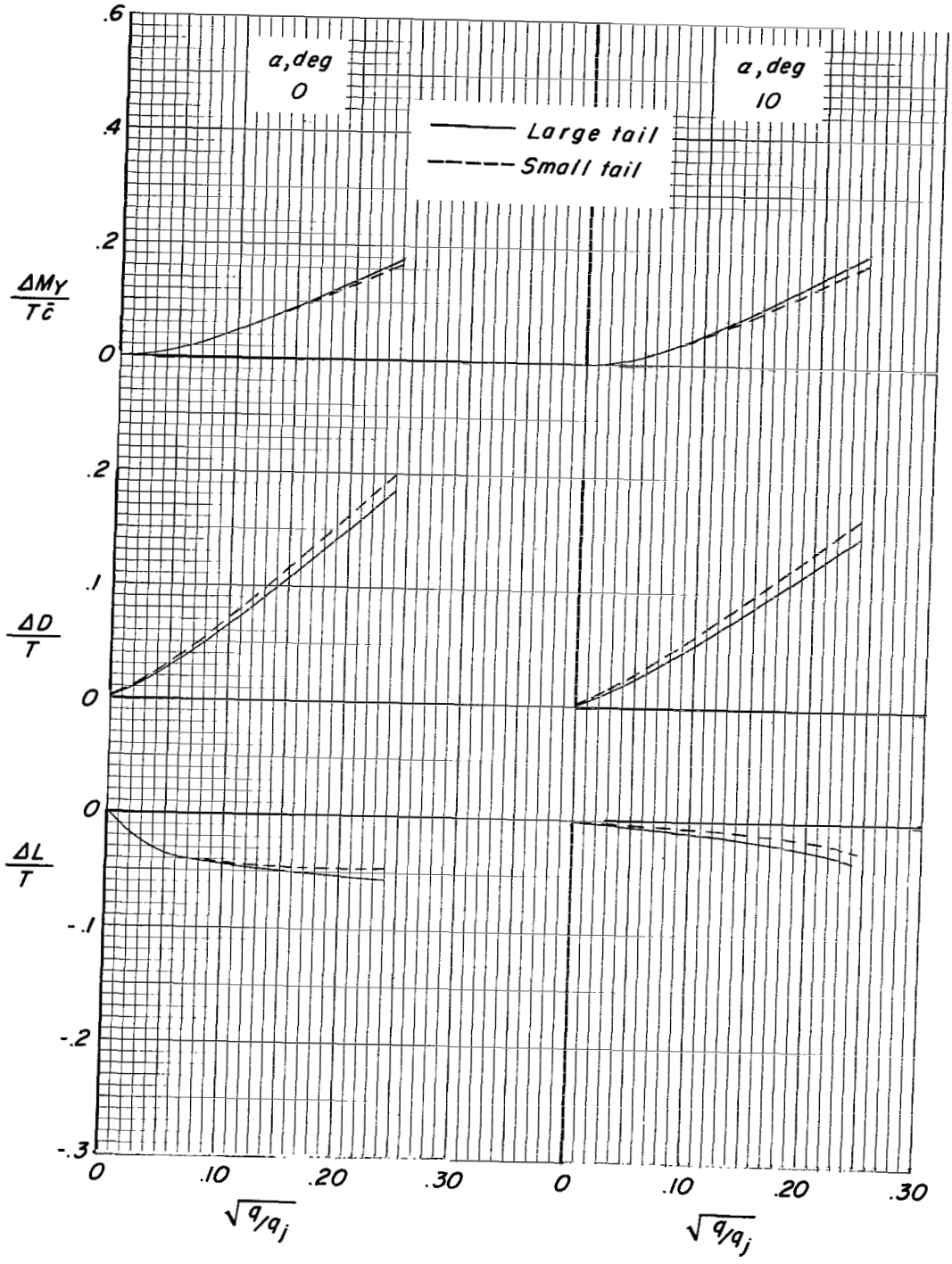

(c) Large tail and small tail; high position.

Figure 41.- Concluded.

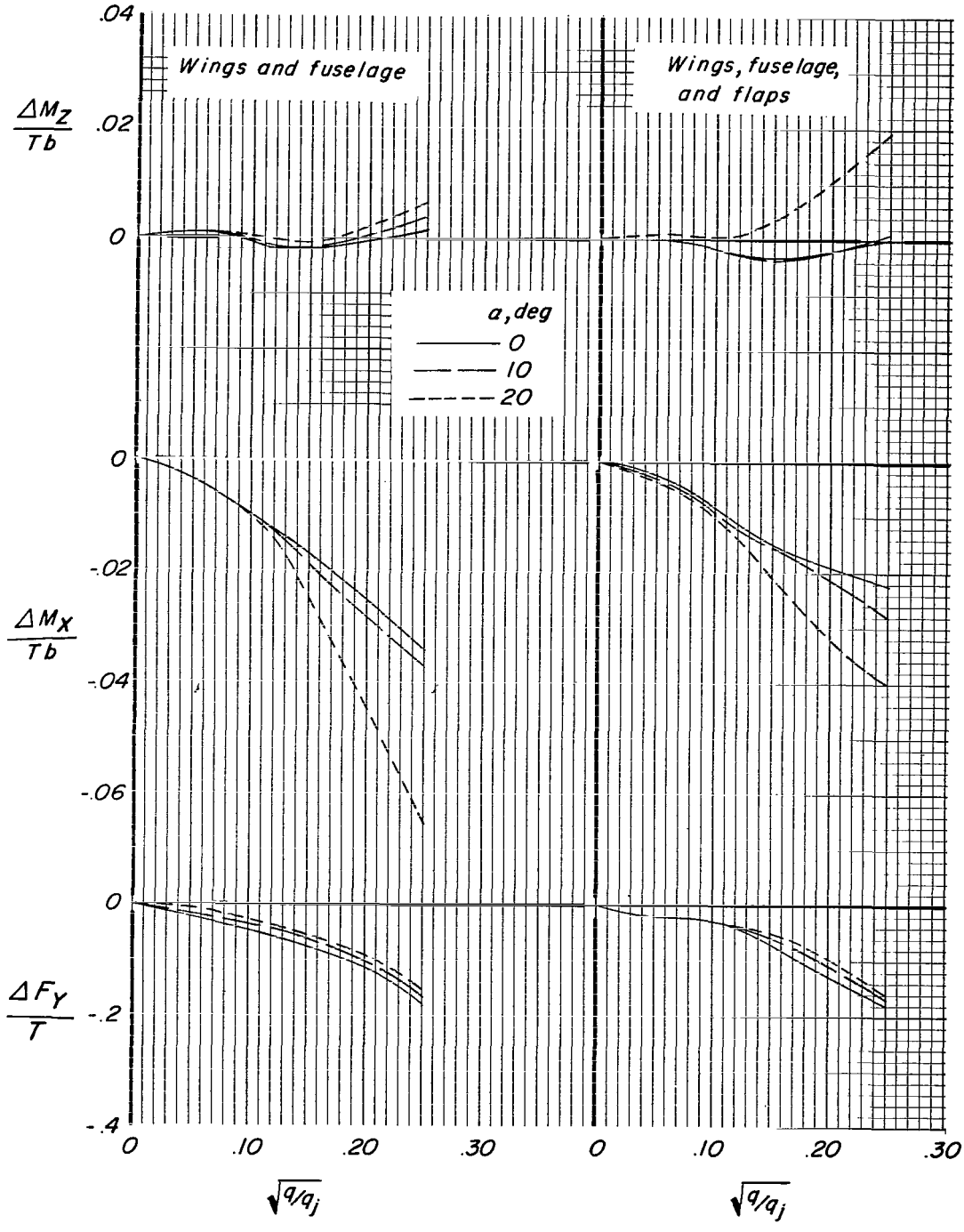

Figure 42.- Summary of lateral effects of 10^0 of sideslip produced by various components of model through effective-velocity-ratio range. Engine pods inboard.

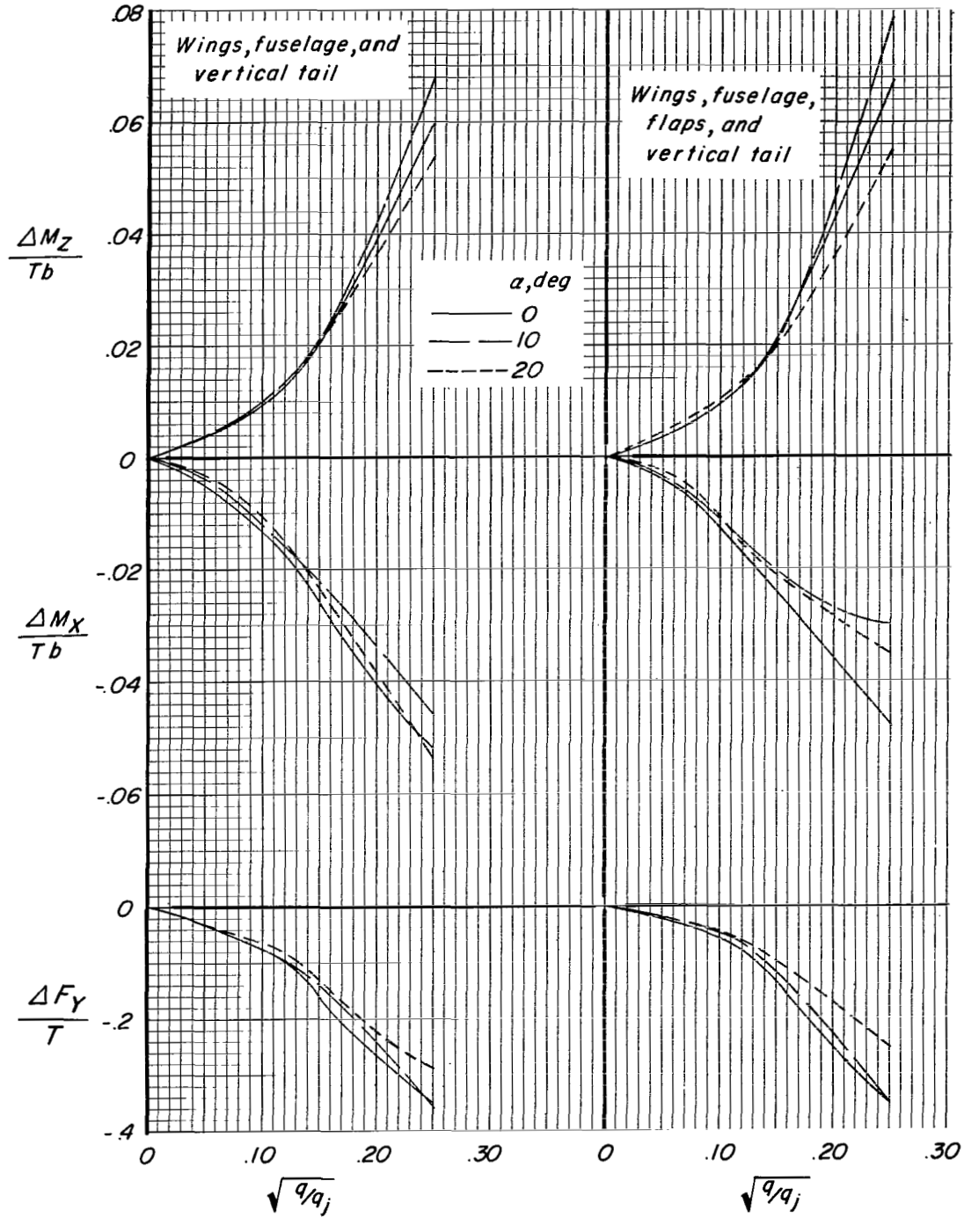

Figure 42.- Concluded.

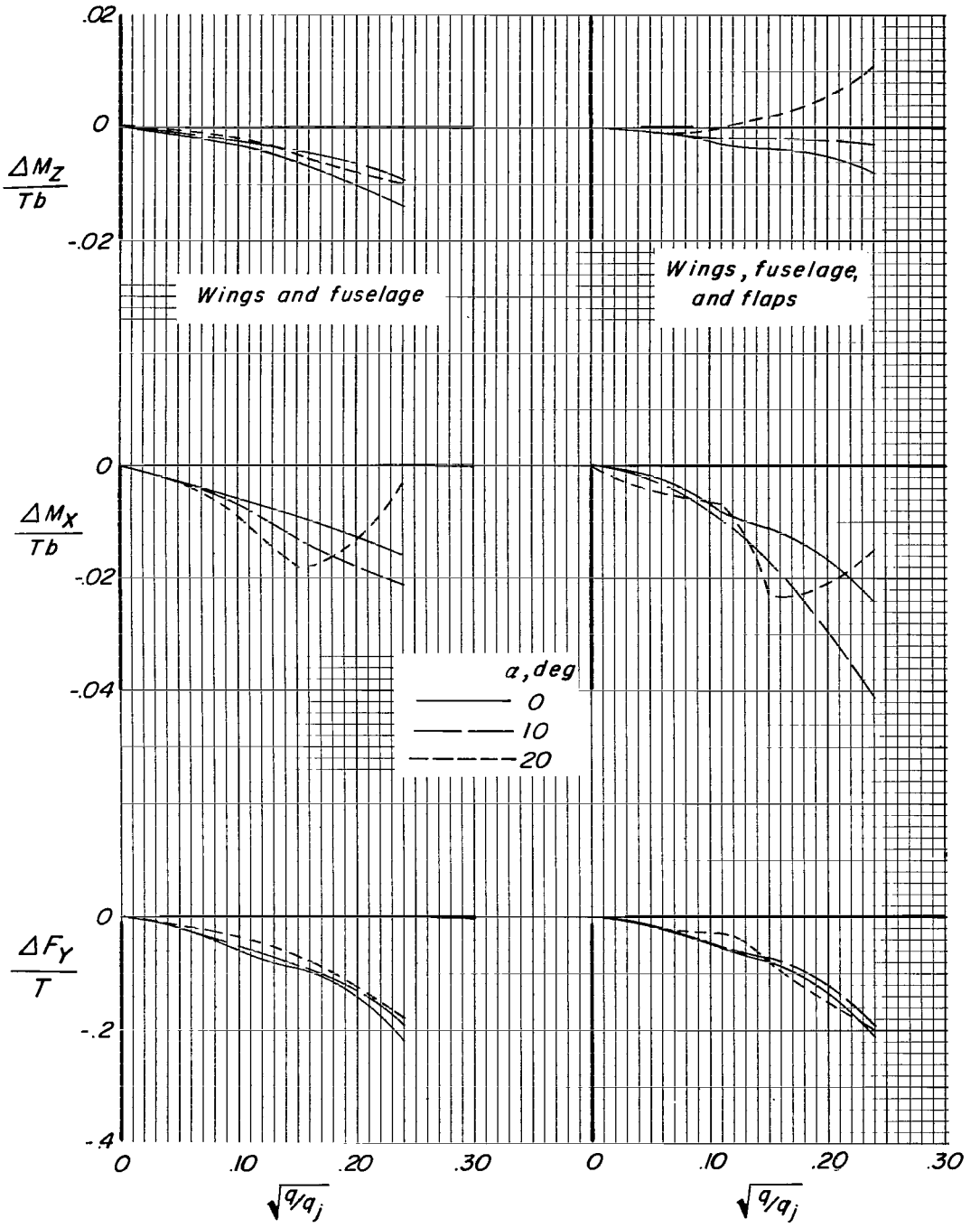

Figure 43.- Summary of lateral effects of 10^0 of sideslip produced by various components of model through effective-velocity-ratio range. Engine pods at midspan.

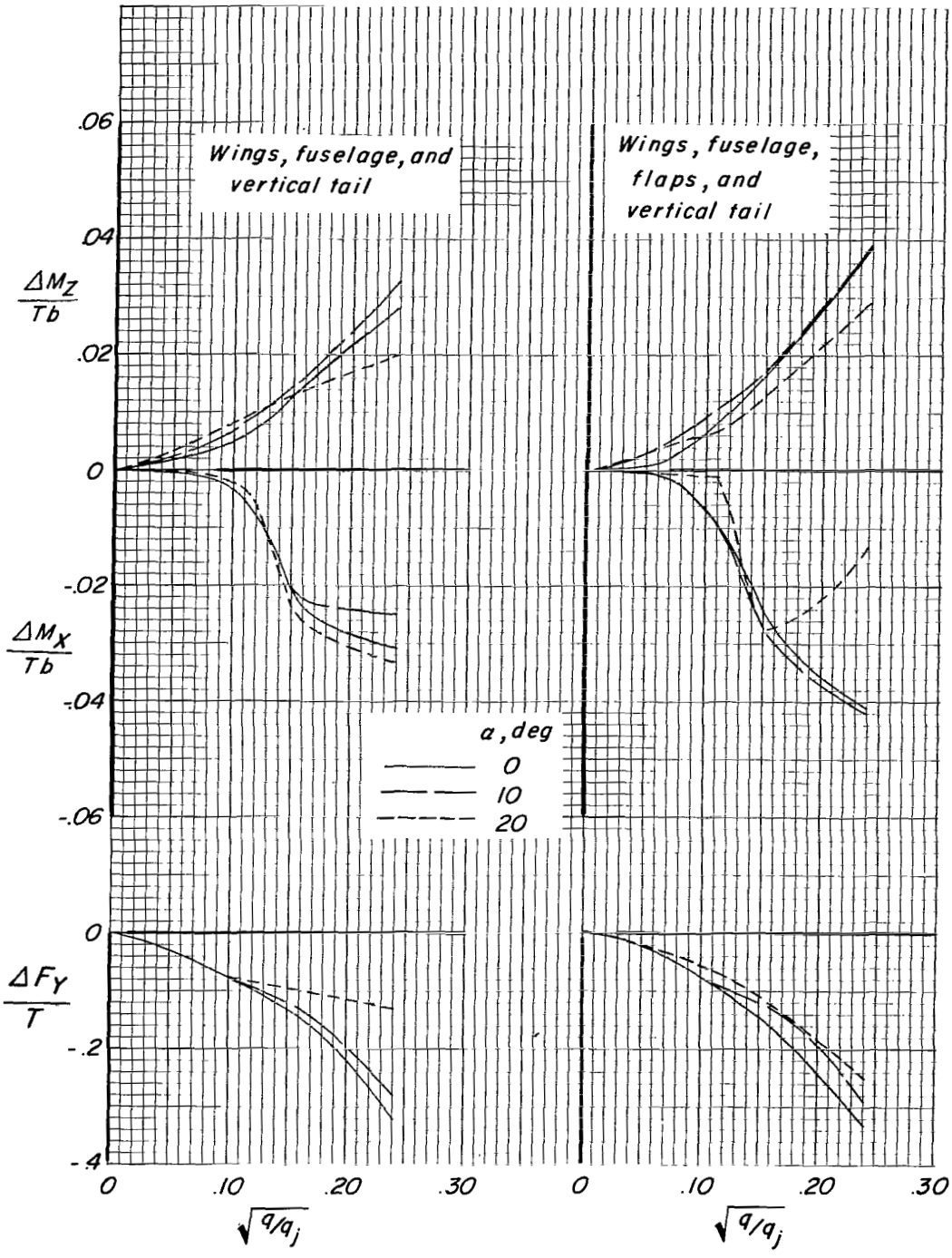

Figure 43.- Concluded.

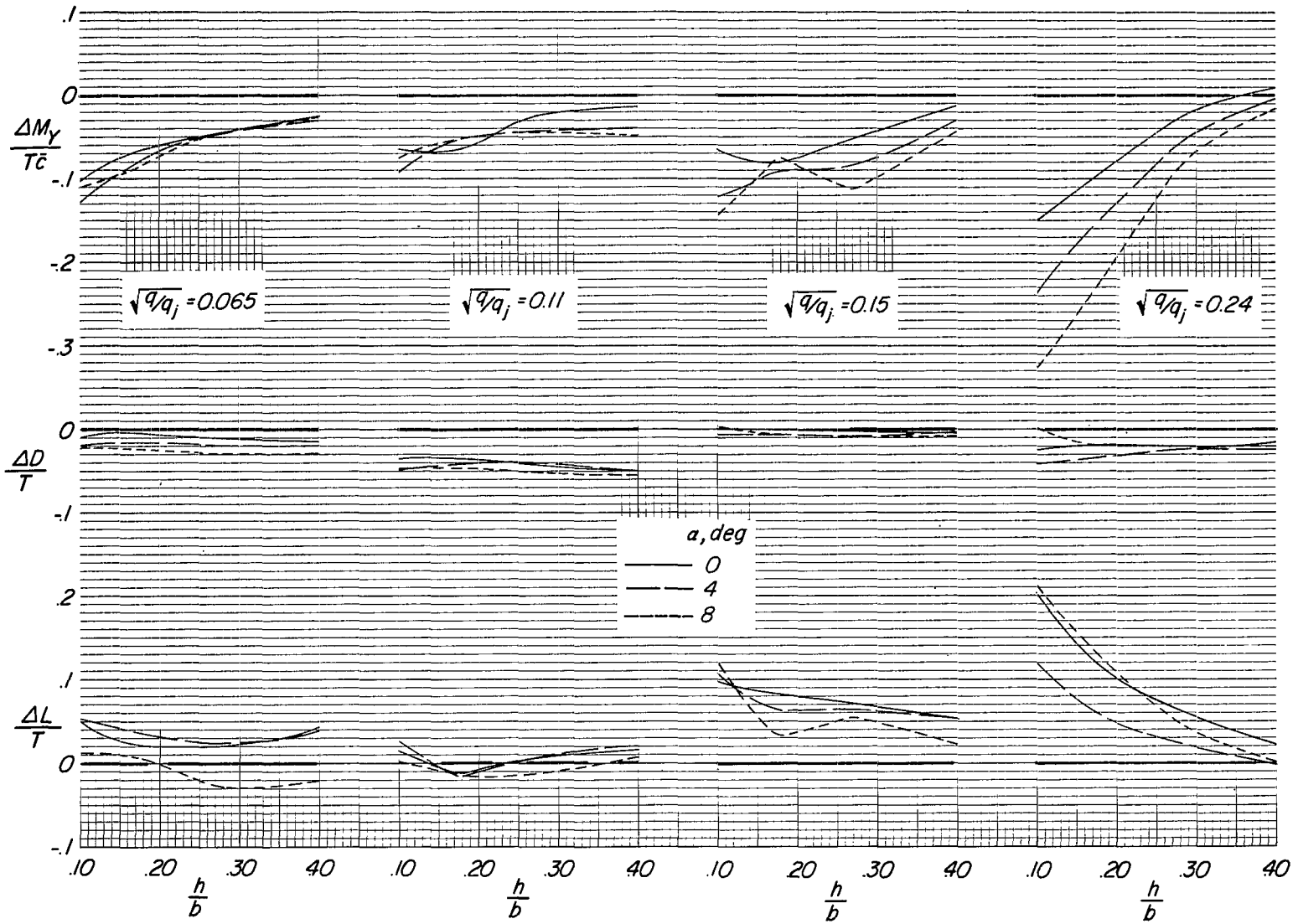

(a) Small tail in low position; $i_t = 0^o$.

Figure 44.- Incremental effects of ground proximity and effective velocity ratio on longitudinal aerodynamic characteristics of model over moving ground plane. Flaps on; power on engine pods at midspan.

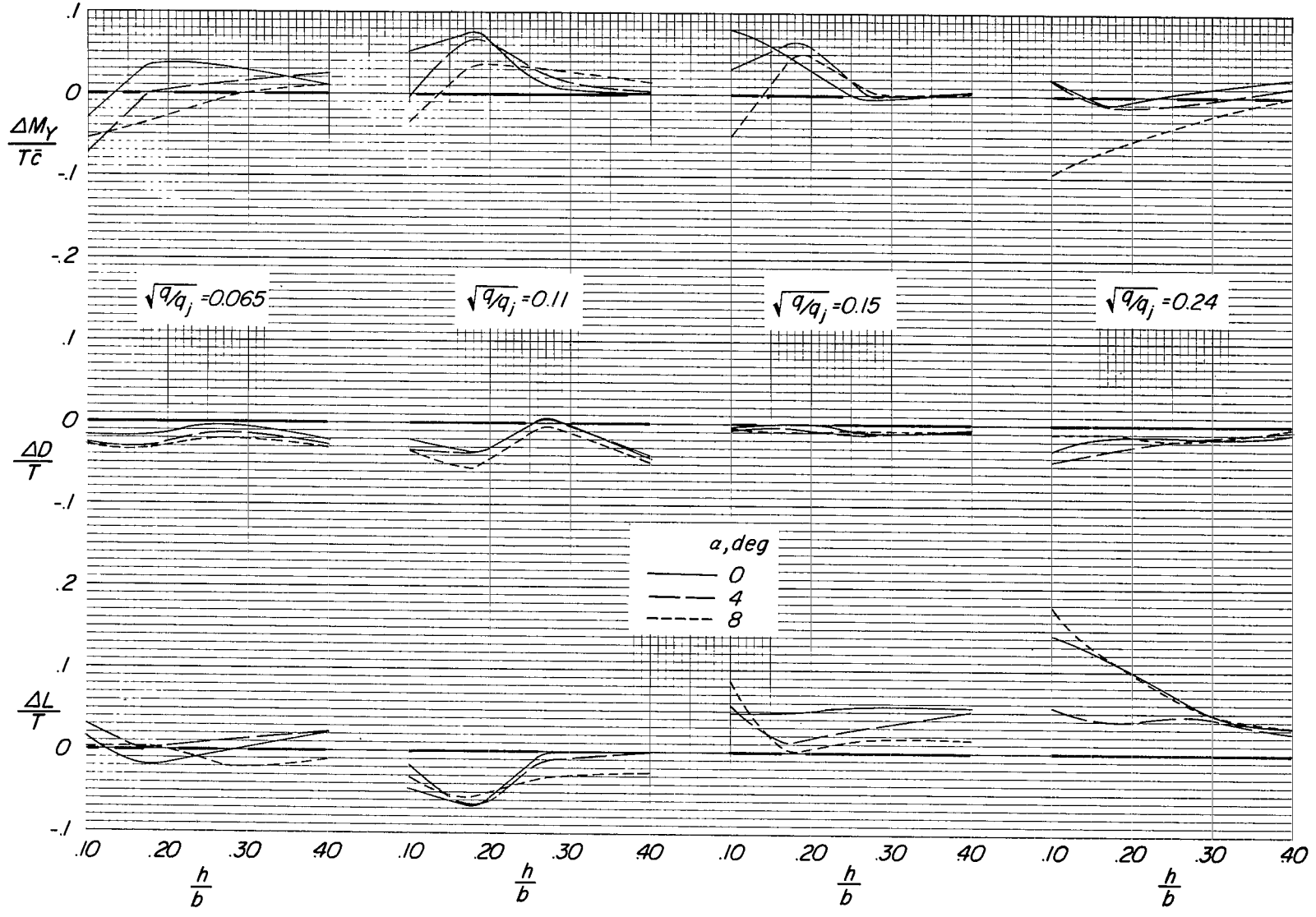

(b) Small tail in high position; $i_t = 0^0$.

Figure 44.- Continued.

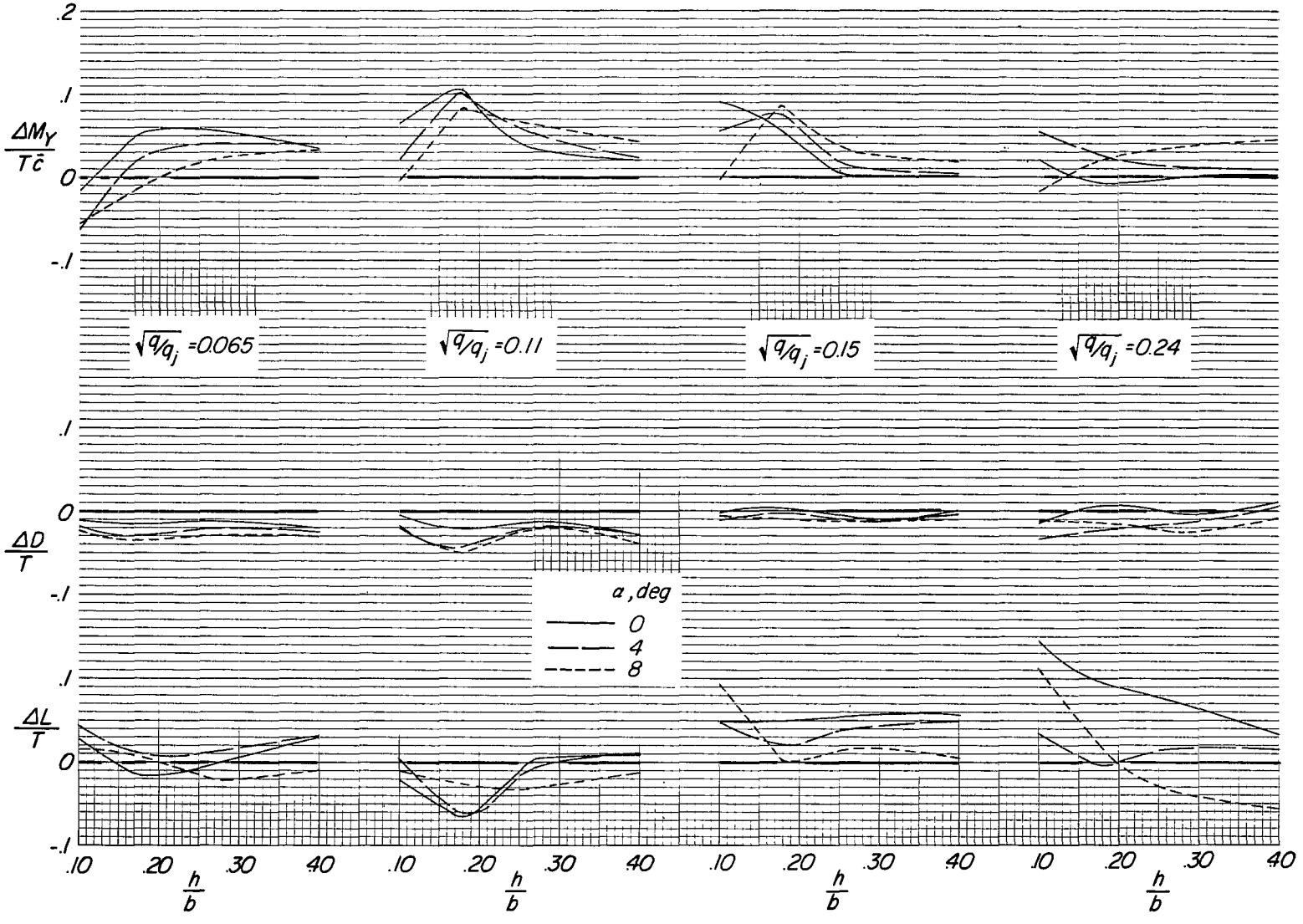

(c) Tail off.

Figure 44.- Concluded.

"The aeronautical and space activities of the United States shall be conducted so as to contribute . . . to the expansion of human knowledge of phenomena in the atmosphere and space. The Administration shall provide for the widest practicable and appropriate dissemination of information concerning its activities and the results thereof."

—NATIONAL AERONAUTICS AND SPACE ACT OF 1958

NASA SCIENTIFIC AND TECHNICAL PUBLICATIONS

TECHNICAL REPORTS: Scientific and technical information considered important, complete, and a lasting contribution to existing knowledge.

TECHNICAL NOTES: Information less broad in scope but nevertheless of importance as a contribution to existing knowledge.

TECHNICAL MEMORANDUMS: Information receiving limited distribution because of preliminary data, security classification, or other reasons.

CONTRACTOR REPORTS: Scientific and technical information generated under a NASA contract or grant and considered an important contribution to existing knowledge.

TECHNICAL TRANSLATIONS: Information published in a foreign language considered to merit NASA distribution in English.

SPECIAL PUBLICATIONS: Information derived from or of value to NASA activities. Publications include conference proceedings, monographs, data compilations, handbooks, sourcebooks, and special bibliographies.

TECHNOLOGY UTILIZATION PUBLICATIONS: Information on technology used by NASA that may be of particular interest in commercial and other non-aerospace applications. Publications include Tech Briefs, Technology Utilization Reports and Technology Surveys.

Details on the availability of these publications may be obtained from:

SCIENTIFIC AND TECHNICAL INFORMATION DIVISION

NATIONAL AERONAUTICS AND SPACE ADMINISTRATION

Washington, D.C. 20546